NUREG/CR-5709

Pitting, Galvanic, and Long-Term Corrosion Studies on Candidate Container Alloys for the Tuff Repository

Prepared by
J. A. Beavers, N. G. Thompson, C. L. Durr

Cortest Columbus Technologies, Inc.

Prepared for
U.S. Nuclear Regulatory Commission

AVAILABILITY NOTICE

Availability of Reference Materials Cited in NRC Publications

Most documents cited in NRC publications will be available from one of the following sources:

1. The NRC Public Document Room, 2120 L Street, NW., Lower Level, Washington, DC 20555

2. The Superintendent of Documents, U.S. Government Printing Office, P.O. Box 37082, Washington, DC 20013-7082

3. The National Technical Information Service, Springfield, VA 22161

Although the listing that follows represents the majority of documents cited in NRC publications, it is not intended to be exhaustive.

Referenced documents available for inspection and copying for a fee from the NRC Public Document Room include NRC correspondence and internal NRC memoranda; NRC bulletins, circulars, information notices, inspection and investigation notices; licensee event reports; vendor reports and correspondence; Commission papers; and applicant and licensee documents and correspondence.

The following documents in the NUREG series are available for purchase from the GPO Sales Program: formal NRC staff and contractor reports, NRC-sponsored conference proceedings, international agreement reports, grant publications, and NRC booklets and brochures. Also available are regulatory guides, NRC regulations in the *Code of Federal Regulations*, and *Nuclear Regulatory Commission Issuances*.

Documents available from the National Technical Information Service include NUREG-series reports and technical reports prepared by other Federal agencies and reports prepared by the Atomic Energy Commission, forerunner agency to the Nuclear Regulatory Commission.

Documents available from public and special technical libraries include all open literature items, such as books, journal articles, and transactions. *Federal Register* notices, Federal and State legislation, and congressional reports can usually be obtained from these libraries.

Documents such as theses, dissertations, foreign reports and translations, and non-NRC conference proceedings are available for purchase from the organization sponsoring the publication cited.

Single copies of NRC draft reports are available free, to the extent of supply, upon written request to the Office of Administration, Distribution and Mail Services Section, U.S. Nuclear Regulatory Commission, Washington, DC 20555.

Copies of industry codes and standards used in a substantive manner in the NRC regulatory process are maintained at the NRC Library, 7920 Norfolk Avenue, Bethesda, Maryland, for use by the public. Codes and standards are usually copyrighted and may be purchased from the originating organization or, if they are American National Standards, from the American National Standards Institute, 1430 Broadway, New York, NY 10018.

NUREG/CR-5709
RW

Pitting, Galvanic, and Long-Term Corrosion Studies on Candidate Container Alloys for the Tuff Repository

Manuscript Comp .ed: January 1992
Date Published: January 1992

Prepared by
J. A. Beavers, N. G. Thompson, C. L. Durr

Cortest Columbus Technologies, Inc.
2704 Sawbury Boulevard
Columbus, OH 43235

Prepared for
Division of Regulatory Applications
Office of Nuclear Regulatory Research
U.S. Nuclear Regulatory Commission
Washington, DC 20555
NRC FIN D1692

RELATED DOCUMENTS

The following is a listing of Topical Reports summarizing the research performed in the various tasks of the program issued to Cortest Columbus Technologies, Inc. (CC Technologies):

"Environmental Effects On Corrosion In The Tuff Repository." NUREG/CR-5435 published February, 1990.

"Potentiodynamic Polarization Studies On Candidate Container Alloys For The Tuff Repository." NUREG/CR-5708 to be published January, 1992.

"Immersion Studies On Candidate Container Alloys For The Tuff Repository." NUREG/CR-5598 published May, 1991.

ABSTRACT

Cortest Columbus Technologies, Inc. (CC Technologies) investigated the long-term performance of container materials for high-level radioactive waste packages as part of the information needed by the Nuclear Regulatory Commission to assess the Department of Energy's application to construct a geologic repository for the high-level radioactive waste. The scope of work focused on the Tuff Repository and employed short-term techniques, such as electrochemical and mechanical techniques to examine a wide range of possible failure modes. Long-term tests were used to verify and further examine specific failure modes identified as important by the short-term studies.

Two classes of alloys were evaluated for use as container materials for the Tuff Repository; Fe-Cr-Ni alloys and copper-base alloys. The candidate Fe-Cr-Ni alloys were Type 304L Stainless Steel (Alloy 304L) and Incoloy Alloy 825 (Alloy 825). The candidate copper-base alloys were CDA 102 Copper (Alloy CDA 102) and CDA 715 Copper-30 Nickel (Alloy CDA 715). The corrosion testing was performed in a simulated J-13 well water and in solutions selected from an experimental matrix from Task 2 of the program. This report summarizes the results of Task 4 (Pitting Studies), Task 6 (Other Failure Modes) and Task 7 (Long-Term Exposures) of the program.

Pit-initiation studies, performed in Task 4, focused on anomalous Cyclic Potentiodynamic Polarization (CPP) behavior of the copper-base alloys reported in Task 2 of the program; hysteresis in the CPP curve was, in many instances, associated with thick tarnish growth on the specimen and active attack beneath the tarnish, as opposed to pitting. The results of these pit initiation studies were consistent with the previously reported CPP behavior. It was confirmed that standard interpretations of CPP tests are not always appropriate in the presence of thick tarnish layers. On the other hand, pit-initiation studies performed on the Fe-Cr-Ni alloys confirmed that, in general, the standard interpretation of the CPP curves appears to be accurate.

Pit propagation studies were performed on Alloy CDA 102 in Task 4 of the program. The results of the experiments showed that the propagation rate of pits in Alloy CDA 102 may be limited in the absence of oxidizing species such as H_2O_2. However, H_2O_2 is a chemical species that has been shown to occur as a result of irradiation of the groundwater. Other oxidizing species also will be present. These oxidizing species, if present in sufficient concentrations, will promote pit propagation in Alloy CDA 102.

Two types of galvanic corrosion studies were performed in Task 6 of the program; thermogalvanic couples and borehole liner-container interactions. In the thermogalvanic couples tests, the effect of temperature variation on the surface of the container on acceleration of corrosion was evaluated for two alloys; Alloy CDA 102 and Alloy 304L. The results of these tests indicated that thermogalvanic corrosion may affect corrosion performance of the waste containers in the presence of oxidizing radiolysis products. However, the major effect still appears to be an increase in rates of attack (general or pitting corrosion) with increasing temperature as opposed to a thermogalvanic effect.

In Task 6, borehole liner-container interaction studies were conducted to evaluate the galvanic effects of metal-to-metal contact of the liner and container materials. Galvanic attack is normally considered to be the accelerated attack of the less noble member of a dissimilar-metal couple. However, evidence in the literature indicates that the less noble member of the couple can promote accelerated corrosion of the more noble member by creating an aggressive environment in the crevice between the two alloys. Two borehole liner-container combinations were evaluated; C1010 carbon steel/Alloy 304L and Alloy 304L/Alloy 825. In these tests, there was no evidence of accelerated corrosion of the more noble member of the galvanic couple: The less noble member of the couple consistently experienced galvanic corrosion. However, in the case of the Alloy 304L/Alloy 825 couple, the environment was not sufficiently aggressive to promote significant attack of Alloy 304L, which is necessary for the crevice corrosion mechanism to operate.

Long-term immersion tests were conducted in Task 7 of the program. The purpose of these tests was to provide long-term exposure data for evaluating the various modes of corrosion identified in other tasks of the program. The tests were designed to assess the performance of the candidate alloys at times when the temperature of the repository is near the boiling point of water and periodic intrusion of vadose water occurs. The tests were performed at 90°C for 80 weeks in simulated J-13 well water that was concentrated by evaporation. These tests differed from those performed in Task 3 of the program in that evaluation of the effects of concentration of salts in the groundwater on corrosion behavior was included. Results indicated negligible general corrosion rates for Alloys 825, 304L, and CDA 715 following eighty weeks of exposure. Alloy CDA 102 experienced a general corrosion rate of 0.45 µm/yr in this environment. No SCC of U-bend specimens of any of the four alloys occurred. Alloy 304L and Alloy 825 exhibited no evidence of localized corrosion (pitting or crevice corrosion). However, some localized corrosion was evident on specimens of Alloy CDA 102 and Alloy CDA 715. Comparison of the previous results of the Task 3 exposures with the above results suggests that uniform concentration of ionic species in simulated J-13 well water does not appear to be detrimental to the corrosion behavior of the candidate alloys. In the concentrated simulated groundwater, the corrosion rates of the alloys also decreased with time.

TABLE OF CONTENTS

TABLE OF CONTENTS (Continued)

LIST OF FIGURES

LIST OF FIGURES (Continued)

LIST OF FIGURES (Continued)

LIST OF FIGURES (Continued)

LIST OF FIGURES (Continued)

LIST OF FIGURES (Continued)

LIST OF FIGURES (Continued)

LIST OF FIGURES (Continued)

LIST OF TABLES

LIST OF TABLES (Continued)

LIST OF TABLES (Continued)

EXECUTIVE SUMMARY

Cortest Columbus Technologies, Inc. (CC Technologies) investigated the long-term performance of container materials for high-level radioactive waste packages as part of the information needed by the Nuclear Regulatory Commission to assess the Department of Energy's application to construct a geologic repository for the high-level radioactive waste. The scope of work focused on the Tuff Repository and employed short-term techniques, such as electrochemical and mechanical techniques to examine a wide range of possible failure modes. Long-term tests were used to verify and further examine specific failure modes identified as important by the short-term studies.

Two classes of alloys were evaluated for use as container materials for the Tuff Repository; Fe-Cr-Ni alloys and copper-base alloys. The candidate Fe-Cr-Ni alloys were Type 304L Stainless Steel (Alloy 304L) and Incoloy Alloy 825 (Alloy 825). The candidate copper-base alloys were CDA 102 Copper (Alloy CDA 102) and CDA 715 Copper-30 Nickel (Alloy CDA 715). The corrosion testing was performed in a simulated J-13 well water and in solutions selected from an experimental matrix from Task 2 of the program. This report summarizes the results of Task 4 (Pitting Studies), Task 6 (Other Failure Modes), and Task 7 (Long-Term Exposures) of the program.

Task 4 - Pitting Studies

The objectives of the pitting studies were (1) to study the relationship between pitting parameters derived from Cyclic Potentiodynamic Polarization (CPP) curves (the pitting potential (E_{pit}) and the protection potential (E_{prot})) and long-term pit initiation behavior, and (2) to evaluate pit-propagation behavior. The pit-initiation studies were focused on the copper-base alloys. Limited pit-initiation studies were also conducted with the Fe-Cr-Ni alloys.

The earlier CPP studies, performed in Task 2 of the program, suggested that the conventional interpretation of CPP curves is not appropriate for the copper-base alloys studied; Alloy CDA 102 and Alloy CDA 715. Hysteresis in the CPP curves was not always associated with classical pitting. In many instances, hysteresis in the CPP curves was associated with thick tarnish growth on the specimen and active attack beneath the tarnish.

In the Task 4 pit-initiation studies, the relationship between the long-term pitting behavior and the electrochemical parameters was assessed by potentiostatic-polarization tests. The tests were performed in simulated Tuff repository environments selected from a statistically based test solution matrix designed in Task 2 of the program. The specimens were polarized over a range of potentials between the free-corrosion potential (E_{cor}) and E_{pit} and the relationship between the corrosion morphology and potential was determined.

Results of the potentiostatic tests, performed on the copper-base alloys, were consistent with the behavior observed in the Task 2 CPP tests. When specimens were potentiostated for long periods of time at potentials within the hysteresis loop, the morphology of attack of the specimens was similar to that observed in the CPP tests. It also was generally observed that, in environments that promoted tarnish growth, the potentiostatic current decreased with time. On the other hand, in environments that promoted pitting, the potentiostatic currents generally remained at high values during the testing. This behavior is consistent with the morphologies

observed. The high stable potentiostatic currents are indicative of high rates of pitting or general attack while the decrease in currents with time is consistent with passivation or the growth of thick tarnish layers.

A limited number of pit-initiation studies was also conducted with Alloy 304L and Alloy 825. In general, the results of the Task 2 testing of the Fe-Cr-Ni alloys conformed with a conventional interpretation of the CPP curves; namely the occurrence of hysteresis in the CPP curves corresponded with localized corrosion (either pitting or crevice corrosion) on the specimens. Several instance were noted in the Task 2 studies where slight hysteresis in the CPP curves at noble potentials was associated with thin tarnish film growth as opposed to pitting.

The potentiostatic tests on the Fe-Cr-Ni alloys were performed in solutions that exhibited both types of behavior; namely hysteresis and pitting and hysteresis at noble potentials and tarnish growth. In some cases, pitting and crevice corrosion occurred in the potentiostatic tests where only tarnishing was evident in the CPP tests. Thus, the conventional interpretation of the CPP tests was accurate. However, there were a few instances where no localized corrosion occurred in the potentiostatic tests even though slight hysteresis was present in the CPP tests. These interpretation problems with the CPP curves for the Fe-Cr-Ni alloys may be only of academic interest since the slight hysteresis, which was associated with tarnishing, generally occurred at very noble potentials. This is in contrast to the copper-base alloys where the hysteresis occurs at potentials near the free corrosion potential.

In the pit-propagation studies, exposures of simulated pits were used to assess the rate of pit propagation as a function of pit depth. The results of previous studies have confirmed that pits readily initiate in the copper-base alloys in the Tuff Repository environments. Accordingly, for a copper container to provide adequate containment, it must be demonstrated that the rates of pit propagation are low in comparison to the thickness of the container wall.

Four pit-propagation experiments were performed with Alloy CDA 102 at 90°C in a solution (Solution Number 22) that was shown to promote pitting of that alloy in previous CPP tests. The propagation rate of pitting with this alloy-environment combination was assessed by electrochemical and gravimetric techniques. The pit-propagation experiments utilized a small pit specimen placed inside of a larger specimen (BES specimen) at a variable depth. The resulting pit cavity was filled with a corrosion product paste and the two specimens were galvanically coupled. Both 1:2 and 1:5 pit diameter-to-depth ratios were evaluated in these experiments. Hydrogen peroxide (H_2O_2) and potentiostatic polarization were used to stimulate pit propagation in several of the tests.

The results of the experiments indicated that the propagation rate of pits in Alloy CDA 102 may be limited in the absence of oxidizing species such as H_2O_2. However, H_2O_2 is a chemical species that has been shown to occur as a result of irradiation of groundwater. Other oxidizing species also will be present. These oxidizing species, if present in sufficient concentrations, will promote pit propagation in Alloy CDA 102. Sufficient testing was not performed to well characterize the kinetics of propagation but the limited testing performed suggests that rates will decrease with depth.

Task 6 - Other Failure Modes

Galvanic corrosion studies were conducted in Task 6 of the overall program. The purpose of Task 6 was to explore failure modes that are likely to produce accelerated attack and lead to premature failure of the waste container. Two possible galvanic corrosion modes were investigated in this task: Thermogalvanic couples and borehole liner-container interactions.

For a single container, it is likely that a temperature differential will exist from one portion of the surface to another. This temperature differential will produce a potential distribution on the container surface that can result in a differential cell couple similar to a galvanic couple of dissimilar metals. This "thermogalvanic couple" may accelerate the corrosion rate of that portion of the container having the more negative potential. The focus of this subtask was to estimate the accelerating effect of thermogalvanic couples on the corrosion rate of Alloy CDA 102 and Alloy 304L.

In the experiments, an unheated (isothermal) specimen was electrically coupled to an internally heated (heat-transfer) specimen. The galvanic current flow between the two was monitored as a function of time. Periodically, the specimens were uncoupled and the free corrosion potential and polarization resistance of each specimen were measured.

The results of these tests indicated that thermogalvanic corrosion may affect corrosion performance of the waste containers in the presence of oxidizing radiolysis products. The direction of the galvanic effect may be different, depending on the alloy-environment system examined. Considering the two alloys evaluated; the corrosion attack of the cooler (isothermal) specimen of Alloy CDA 102 was consistently accelerated by the thermogalvanic effect. On the other hand, for Alloy 304L, the heat-transfer specimen generally experienced accelerated attack as a result of thermogalvanic corrosion. However, the major effect still appears to be an increase in rates of attack (general or pitting corrosion) with increasing temperature, as opposed to a thermogalvanic effect.

Borehole liner-container interaction studies were conducted to evaluate the effects of metal-to-metal contact of the liner and container materials. The initial designs for the Tuff Repository proposed Alloy 304L and carbon (or low alloy) steel as the container and liner materials, respectively. The focus was later shifted to Alloy 825 and Alloy 304L as the container and liner materials. The purpose of these liners is to facilitate retrieval of the waste containers over a 50-year period following their emplacement. For the current repository design, it is probable that the liners and containers will be in direct contact, resulting in possible galvanic attack.

Galvanic attack is normally considered to be the accelerated attack of the less noble member of a dissimilar-metal couple. However, evidence in the literature indicates that the less noble member of the couple can promote accelerated corrosion of the more noble member by creating an aggressive environment in the crevice between the two alloys.

The actual experimental procedure was similar to that used in the thermogalvanic experiments. Sandwich-like specimens of the coupled materials were used; the specimens were electrically isolated using PTFE spacers. The coupled potential and galvanic current flow between the two specimens was monitored as a function of time. Periodically, the specimens were uncoupled and the free-corrosion potentials and polarization resistance of each specimen were measured.

Galvanic experiments were performed with the C1010 carbon steel/Alloy 304L couple in simulated J-13 well water at 90°C with and without the addition of 1000 ppm Cl. Galvanic experiments also were performed with the Alloy 304L/Alloy 825 couple in simulated J-13 well water and in Solution Number 10 at 90°C. Solution Number 10 was chosen from the experimental test matrix based on CPP behavior. These CPP curves showed a large hysteresis loop, and pitting, for Alloy 304L while no hysteresis or pitting attack occurred for Alloy 825.

In these borehole liner-container interaction tests, there was no evidence of accelerated corrosion of the more noble member of the galvanic couple: the less noble member of the couple consistently experienced galvanic corrosion. However, in the case of the Alloy 304L/Alloy 825 couple, the environment was not sufficiently aggressive to promote significant attack of Alloy 304L, which is necessary for the crevice corrosion mechanism to operate.

Task 7 - Long-Term Exposures

Long-term immersion tests were conducted in Task 7 of the program. The purpose of these tests was to provide long-term exposure data for evaluating the various modes of corrosion identified in other tasks of the program. The tests were designed to assess the performance of the candidate alloys at times when the temperature of the repository is near the boiling point of water and periodic intrusion of vadose water occurs. These tests differ from those performed in Task 3 of the program in that evaluation of the effects of concentration of salts in the groundwater on corrosion behavior were included. The tests were performed on the four candidate alloys in simulated J-13 well water at 90°C over a period of 80 weeks. During the exposures, the solutions were allowed to evaporate and new solution was added on a weekly basis. The experiments included constant strain (U-bend) specimens to evaluate SCC, weight-loss specimens, and non-destructive electrochemical techniques. The electrochemical techniques included periodic potential and polarization resistance measurements.

Corrosion rates, calculated from weight-loss measurements, after 23.8 weeks (4000 hours) of exposure, were less than 0.2 µm/yr for each of the alloys except Alloy CDA 102, which had a corrosion rate of 1.11 µm/yr. After 80 weeks, Alloys CDA 715, 304L and 825 all exhibited corrosion rates of less than 0.005 µm/yr; whereas, Alloy CDA 102 exhibited a corrosion rate of 0.45 µm/yr. No SCC was evident on any of the U-bend specimens of the four alloys. Alloy 304L and Alloy 825 also exhibited no evidence of localized corrosion (pitting or crevice corrosion) in the exposure tests. However, some localized corrosion was evident on specimens of Alloy CDA 102 and Alloy CDA 715. The latter alloy experienced shallow etching while Alloy CDA 102 experienced deep etching, up to 32 µm, and shallow pitting, 10 µm in depth.

Comparison of the previous results of the Task 3 exposures with the above results suggests that uniform concentration of ionic species in simulated J-13 well water does not appear to be detrimental to the corrosion behavior of the candidate alloys. In fact, the more concentrated groundwater appears to be less aggressive, from the standpoint of general corrosion, than the dilute simulated J-13 well water. These data also indicate that corrosion rates decreased with time. Although very low corrosion rates were obtained, these tests do not fully simulate actual repository conditions because factors such as of rock-water interactions, radiolysis, and interaction of the groundwater with species from failed containers were not considered.

1. INTRODUCTION

The Department of Energy (DOE) is conducting a program for the disposal of high-level radioactive waste in a deep-mined geologic repository. The Nuclear Regulatory Commission (NRC), which is responsible for regulating high-level radioactive waste disposal, will review DOE's application for the construction and operation of the repository. To assist in evaluating DOE's application, the NRC's Office of Nuclear Regulatory Research is developing an understanding of the long-term performance of the geologic repository. As part of this effort, CC Technologies was awarded a contract to investigate the long-term performance of container materials used for high-level waste packages. At the direction of the NRC, the program focused on the Tuff Repository. The scope of work consisted of employing relatively short-term electrochemical techniques to examine a wide range of possible failure modes. Long-term tests (1-2 years) were used to verify the short-term studies.

This report summarizes the results of pitting, galvanic, and long-term corrosion studies on two copper-base alloys (Alloy CDA 102 and Alloy CDA 715) and two Fe-Cr-Ni alloys (Alloy 304L and Incoloy Alloy 825) in simulated J-13 groundwater and other simulated solutions for the Tuff Repository. These other solutions were designed to simulate the chemical effects resulting from boiling and irradiation of the well water.

The primary focus of the pitting studies was to characterize pit initiation and pit propogation of the copper-base alloys. Limited pit-initiation studies were also conducted with the Fe-Cr-Ni alloys. The galvanic corrosion studies examined the effects of temperature differentials, which will exist along the canister after emplacement, on corrosion behavior. Other galvanic studies investigated the corrosion behavior resulting from borehole-liner container interactions. The long-term immersion studies explored the effects of weekly boiling and concentration of species in simulated J-13 well water at 90°C over a period of 80 weeks on corrosion behavior of each of the four alloys.

2. BACKGROUND - THE TUFF REPOSITORY ENVIRONMENT

2.1 Nominal Environment

The Tuff repository will be located in the Topopah Spring Member of the Paintbrush Tuff under Yucca Mountain, 100 miles northwest of Las Vegas, Nevada in the Nevada Test Site (NTS). The site is located in an extremely arid zone with about 15 cm/year annual precipitation. The evaporation-transpiration rates also are very high so the net water percolating down from the surface is of the order of a few millimeters per year (Montazer - 1984).

Tuff is an igneous rock of volcanic origin and is composed of volcanic rock fragments (shards) and ash. The structure of the tuff deposits depends on the cooling rate and degree of compaction after the volcanic eruption. The rock shards weld together and the compacted material may remain glassy or may devitrify. A layered structure develops; a densely welded core surrounded above and below by zones of material decreasing in density and strength. In the post-depositional period, alteration of the tuff layers occurs. Crystallization transforms the glassy material to feldspar plus quartz or cristobalite. Zeolitization produces hydrous silicates by reaction of the glassy material with groundwater. A typical stratigraphy of the tuff at the NTS is shown in Figure 2.1. A more detailed description of these tuff layers is found in Johnstone-1981.

The potential repository horizon is in the lower, densely welded and devitrified portion of the Topopah Spring Member located 700 to 1400 feet above the static water table. The bulk rock at the horizon is composed of rhyolite with a small range in composition as shown in Table 2.1. This small variation in geochemistry demonstrates that the host rock may be considered uniform, according to Glassley-1986.

A reference water used in many repository studies has been taken from Well J-13. That well is located near the repository site and produces water which has flowed through the Topopah Spring Member, where it lies at a lower elevation and is in the saturated zone. The J-13 well water is the best available source of water from the Topopah Spring Member, but may not be a good approximation of the actual water that will be present in the repository.

The location of the repository above the static water table has a major impact on the anticipated environment. First of all, the environment will be aerated; the J-13 well water contains 5.7 ppm dissolved oxygen which probably represents a lower limit for oxygen. This condition is unique in that the plans for all other repositories, either in the United States or elsewhere, have called for locations below the static water table where conditions are deaerated (anoxic).

A second feature of the location of the repository above the water table is the elimination of the hydrostatic head on the waste container. At the repository elevation, the boiling point for water is about 95°C, and thus the environment at the waste package surface will be steam and air during the early life of the repository.

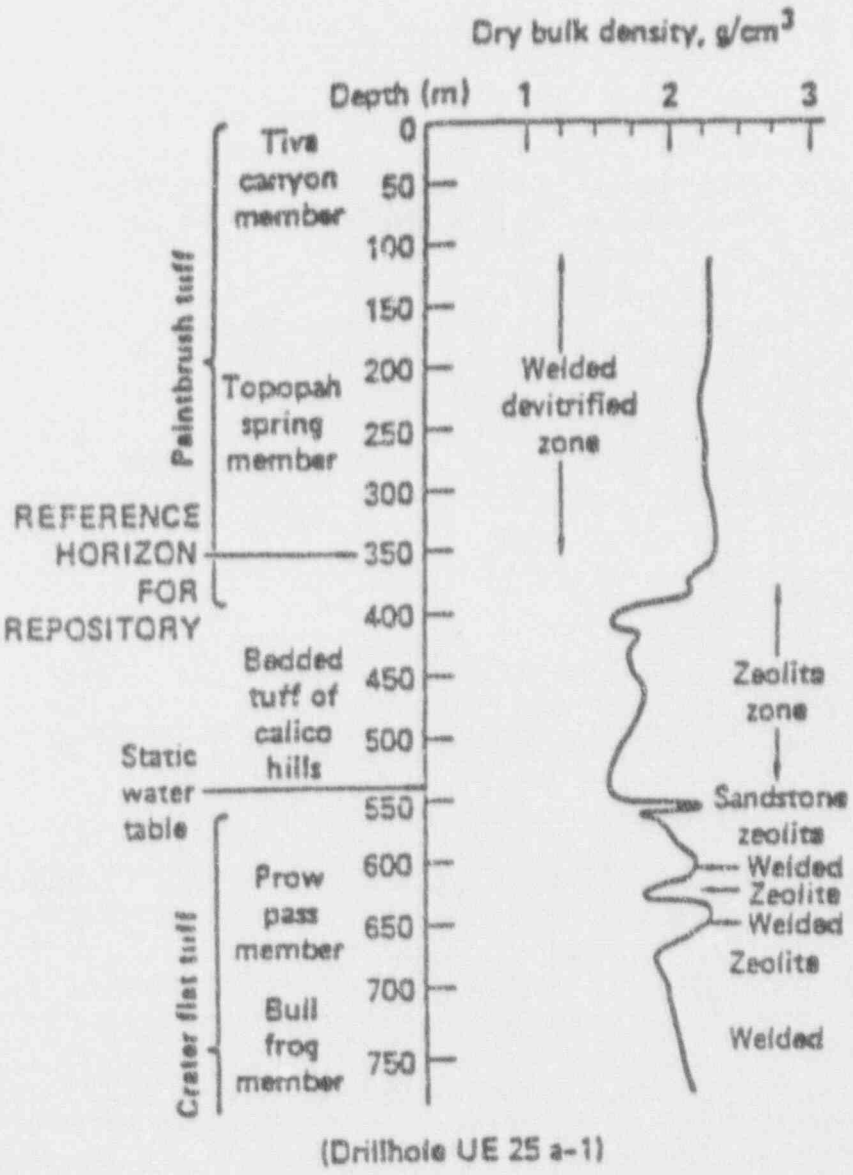

Figure 2.1 Representative Stratigraphic Section In Nevada Tuff (Drillhole UE25 a-1) (McCright-1984).

Table 2.1 Percentages Of Major Constituents In Topopah Springs Tuff, Drill Core USW GU-3, Samples 60, 61 And 62. Fe_2O_3 Represents Total Iron (Schuraytz-1985).

Constituent	60	61	62	Average	Std Dev
SiO_2	78.4	78.9	78.9	78.73	0.24
Al_2O_3	12.0	12.3	12.2	12.17	0.12
Fe_2O_3	1.016	0.973	1.000	0.996	0.018
CaO	0.492	0.451	0.480	0.474	0.017
MgO	0.1271	0.1281	0.1126	0.123	0.007
TiO_2	0.1108	0.0927	0.0964	0.101	0.008
Na_2O	4.07	3.92	4.25	4.08	0.13
K_2O	3.71	3.18	2.94	3.28	0.32
P_2O_2	0.01	0.01	0.03	0.02	0.01
MnO	0.0624	0.0455	0.0488	0.052	0.007

2.1.1 Thermal Effects

The repository is being designed for two types of waste packages; spent fuel and processed defense high level waste in the form of borosilicate glass. The spent fuel will have the highest thermal output of between 1.3 and 3.3 Kw per container, while the glass will have an output of 0.25 to 0.47 Kw per container. The temperature histories of the waste packages are sensitive functions of the thermal properties of the near-field rock, the specific configuration of boreholes and emplacement drifts, heat transfer mode as well as container output power; none of these factors has been precisely defined. Comparative canister surface temperatures as a function of time are shown in Figure 2.2 for one set of conditions. Note that the canister surface for spent fuel remains above the boiling temperature over at least a 300 year period following emplacement.

These elevated temperatures should exclude liquid water from the near field of the repository for several hundred years, although liquid water may be present in the pores in the rock up to 140°C. It is also possible that vadose water may come in contact with some of the waste packages during periods of liquid water movement through the repository.

A consequence of the elevated temperature in the repository will be the interaction of groundwater with the host rock in the vicinity of the waste package. A number of interaction studies has been performed over temperatures ranging from 90-250°C with core wafers, crushed core wafers in gold-bags and PTFE-lined (polytetrafluoroethylene) autoclaves. Rapid shifts in chemistry occurred with crushed rock as opposed to wafers because of the higher surface area with the former. Changes in solution concentration at 90°C were minor; whereas, more pronounced shifts occurred at 150°C. Results obtained by Knauss-1985 for crushed core material at 150°C are given in Figures 2.3 and 2.4. These data show that the silicon (Si) concentrations increased from about 30 ppm to around 150 ppm within 60 days, while the sodium (Na) concentration only increased slightly over the test period. The concentrations of aluminum[1] (Al), magnesium (Mg) and calcium (Ca) decreased with time while that of potassium[1] (K) was not greatly affected by thermal interaction; the pH decreased very slightly.

Another consequence of the elevated temperature in the repository will be the boiling of groundwater in the vicinity of the waste package. This will lead to the concentration of the species, both beneficial and deleterious, in the groundwater. Abraham (1986) has performed some solution analyses on boiling J-13 groundwaters at Brookhaven National Laboratory. The solutions were boiled in the presence of tuff rock and specimens of several stainless steels. The results are summarized in Table 2.2. These data show that the composition of J-13 well water changed quite dramatically as a result of boiling. The stable concentrations of most species after one year were more than an order of magnitude higher than those in the J-13 well water. Some species, such as SO_4^{2-}, NO^{3-}, Ca^{2+} and K^+ exhibited a maximum in concentration after only a few months which suggests the precipitation of compounds such as $CaSO_4$, etc.

The concentration of the species in the 10X J-13 well water also increased with exposure time in these tests. Although the magnitudes of the increases were smaller than those observed for

---

[1]Both aluminum and potassium exhibited initial transient increases in concentrations.

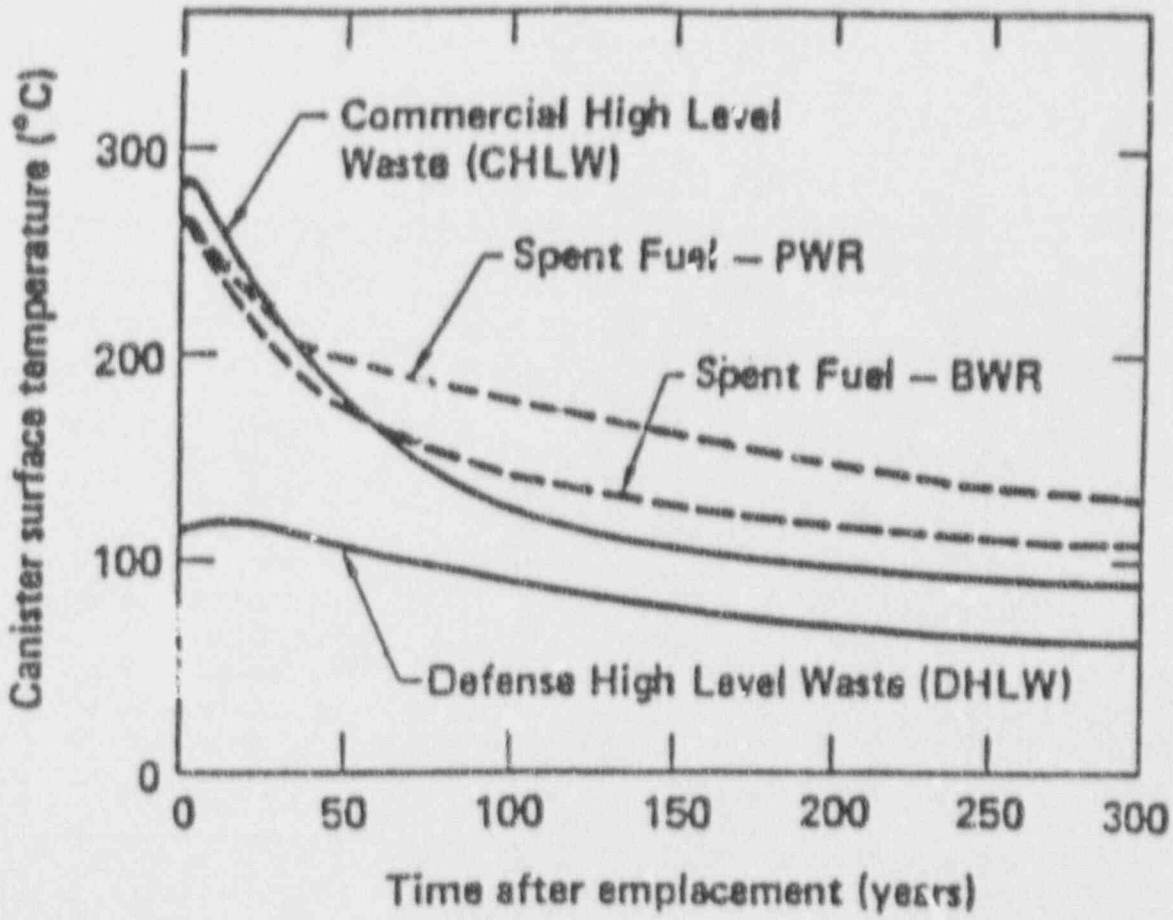

Figure 2.2 Comparative Canister Surface Temperature-Time Profiles For Different Waste Packages In A Tuff Repository (Vertical Emplacement, 50 kW/acre Areal Loading) (McCright-1984).

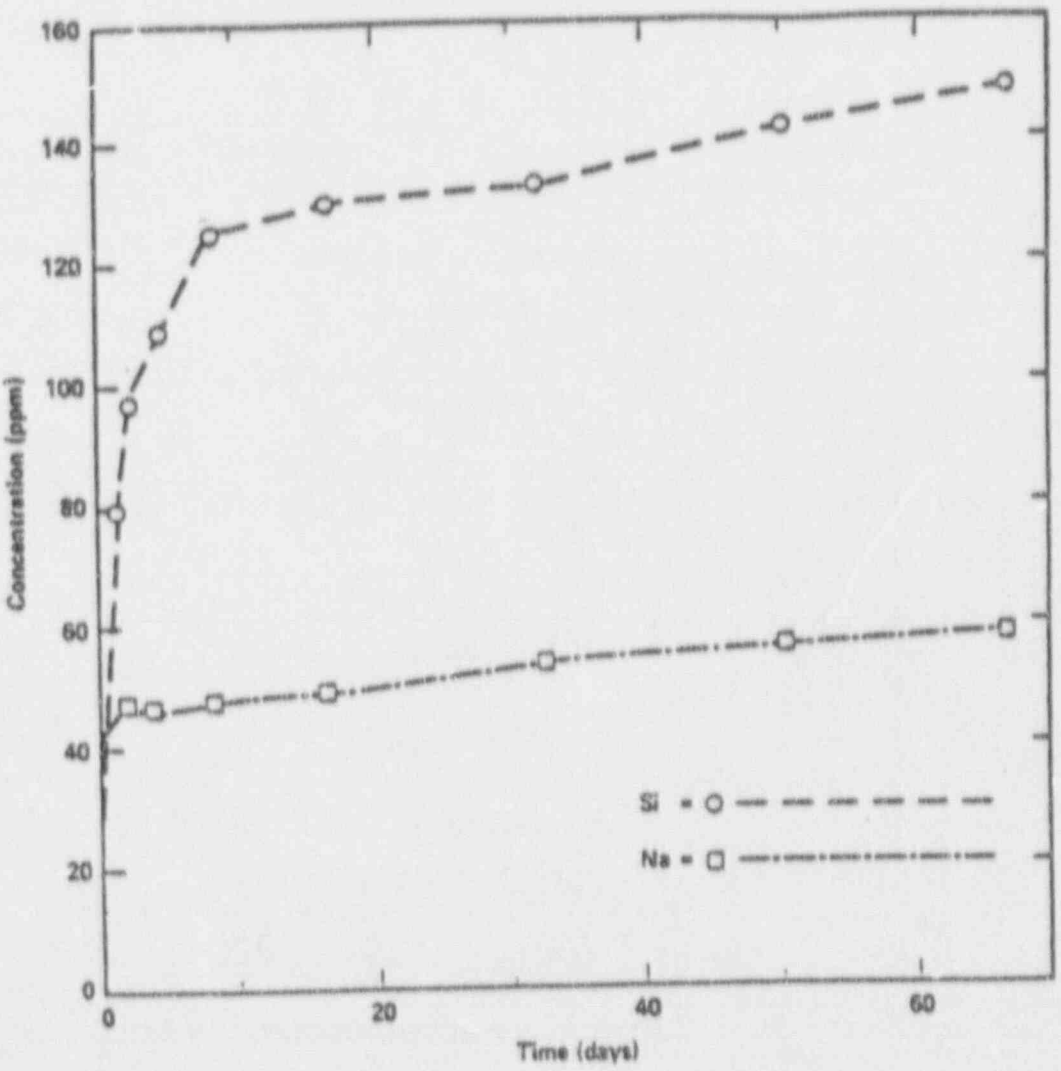

Figure 2.3 Silicon And Sodium Concentrations In J-13 Well Water Reacted With Crushed G-1 Material At 150°C As A Function Of Time In Days (Knauss-1985a).

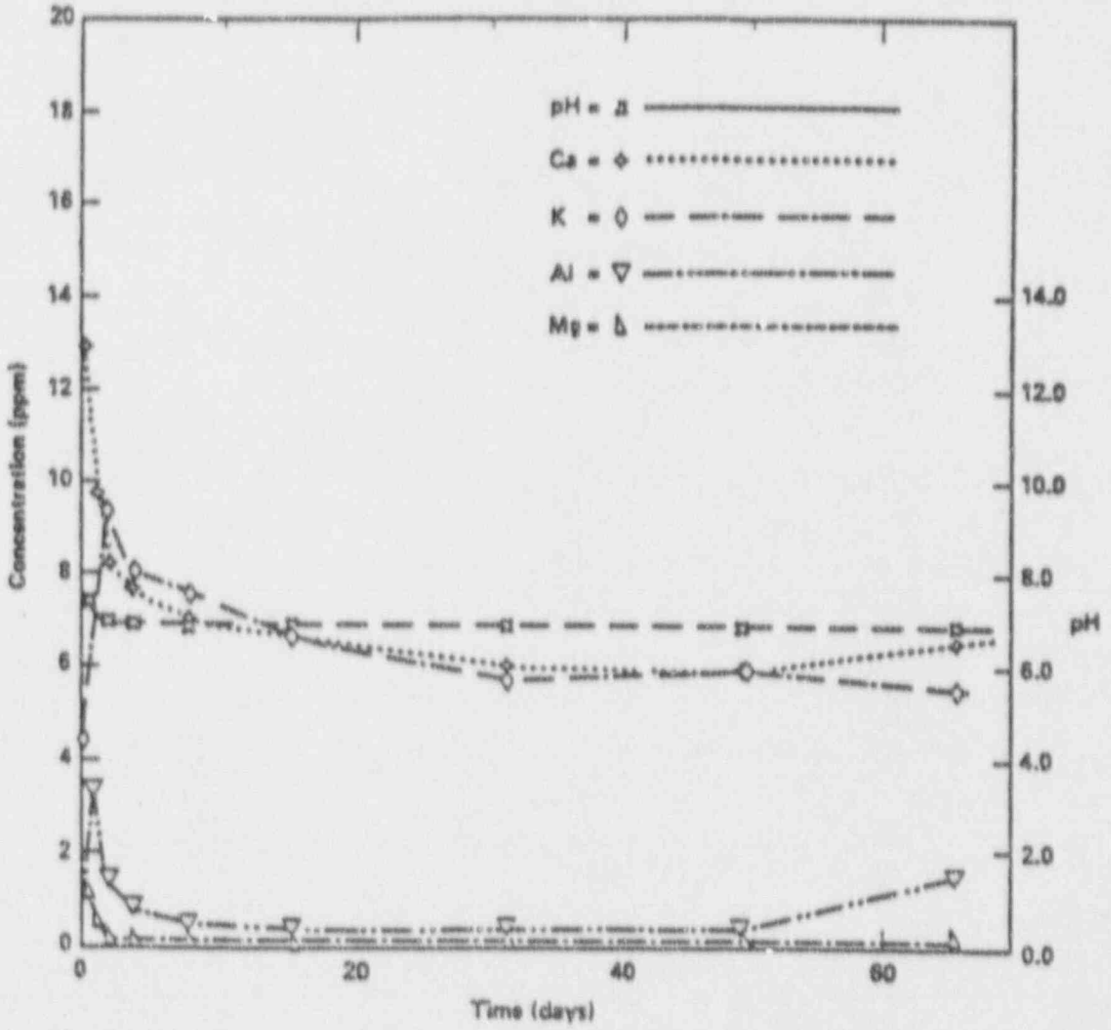

Figure 2.4 Aluminum, Potassium, Calcium, Magnesium, And pH Analyses From J-13 Well Water Reacted With Crushed G-1 Material At 150°C As A Function Of Time In Days (Knauss-1985a).

Table 2.2 Chemical Composition Of Test Solutions At The End Of Corrosion Tests (µg/ml) (Undiluted And Filtered Solution) (Abraham-1986).

	Reference	Synthetic J-13 Water			10-Times Conc. J-13 Water		
	J-13 Groundwater	3-Mo. Test	6-Mo. Test	1-Yr. Test	3-Mo. Test	6-Mo. Test	1-Yr. Test
Na^+	45	N.D.*	464	510	867	738	908
K^+	4.9	238	244	106	244	214	139
Ca^{2+}	14	308	161	104	301	164	129
Sn^{2+}	N.D.	3.4	0.4	1.0	4.4	0.5	1.2
F^-	2.2	12.1	4	6.31	14	5	21.1
Cl^-	7.5	130	236	161	330	211	260
NO_3^-	5.6	460	750	482	—	522	672
SO_4^{2-}	22	820	552	588	1300	1260	976
SiO_2	61	414	451	458	408	486	406
pH at room temperature	8.5	8.4	9.0	9.3	8.4	8.9	9.3

*N.D. = Not determined

the J-13 well water, the actual final concentrations of the species in the tests with the 10X J-13 well water were higher than those in the standard J-13 well water. As in the J-13 well water, maximum concentrations were observed for some species in the boiling 10X J-13 well water after a few months.

2.1.2 Radiation Effects

Relatively little research has been performed on the influence of the radiation field on the environment in the Tuff repository. On the other hand, a number of articles discuss, in general terms, the anticipated role of radiation in altering the repository environment while research on the effects of radiation on water and dilute aqueous solutions is much more extensive. As described by McCright-1984, the highest levels of radiation will occur on emplacement and the levels will begin to decay. The radiation of interest with regard to container corrosion will be gamma radiation. Interaction of the gamma radiation with either the container or the host rock is also expected to be minimal. Thus, the primary problem is the interaction of the gamma radiation field with the liquid and gas phases in the repository. Although most of the fission products responsible for gamma radiation decay rapidly, the repository environment will consist of air and water vapor during the time period when radiation levels will be high.

Radiolysis products expected in the moist-air system are not well established. Some experimental research regarding the temperature effects on radiolysis products has been performed by Van Konynenburg (1986) and others. Their research indicates that, above 135°C, the dominant species are NO, N_2O, and O_3. Between 120° and 135°C, NO_2, N_2O_4, H_2O, and O_3 are the dominant products, while below 120°C, the most abundant products are HNO_3 and H_2O with small amounts of O_3.

In liquid water at high radiation levels, small amounts of nitrates and nitrites will also be produced. However, the simultaneous presence of liquid water and high radiation fields are possible only intermittently during periods of liquid water movement through the repository.

Glass (1985 and 1986) reviewed the literature and performed electrochemical studies in irradiated J-13 well water. These studies concluded that the primary effect of radiation of J-13 well water is to produce the dominant oxidizing species O_2 and H_2O_2 with smaller concentrations of O^-_2 and still smaller concentrations of HO_2. Irradiation of water containing CO_2 or HCO_3 with O_2 was found to produce carboxylic acids (formic and oxalic).

Studies focused on the effects of radiation on water and dilute aqueous solutions concluded that a host of transient radicals, ions, and stable molecular species is created by gamma radiation. Some of these species are as follows: $H^\cdot$, $OH^\cdot$, e^-_{aq}, H_3O^+, OH^-, H_2, H_2O_2, O_2, O^-_2 and $HO_2^\cdot$. While these species only consider the breakdown of the water molecule, many other species are generated by reactions with other species in the groundwater.

2.2 Simulated Environments

2.2.1 Simulated J-13 Well Water

In Task 2 of this program, Cyclic-Potentiodynamic-Polarization (CPP) tests were performed in simulated and actual J-13 well water (Tuff groundwater). The purpose of these tests was to reproduce and verify the polarization behavior observed by McCright at Lawrence Livermore National Laboratory and to establish that the simulated J-13 well water produced similar corrosion behavior to the actual Tuff groundwater. To reproduce the behavior observed by McCright (Figure 2.5), the following test conditions were used: Actual J-13 well water, a scan rate of 3.6 V/hr, temperature of 80°C, aerated conditions, and an initial exposure of 1-2 hours prior to performing the CPP test. The potentiodynamic polarization technique is discussed in more detailed in Appendix A. The J-13 well water used in this subtask of the NRC program initially was obtained from Oak Ridge National Laboratories. Due to the difficulty in obtaining actual J-13 well water required over the duration of the program, a simulated J-13 well water was used in most other tasks. This simulated J-13 well water was previously developed by Battelle Memorial Institute. The composition of the simulated J-13 well water is given in Table 2.3.

The results of experiments performed for Alloy CDA 102 under the above conditions in simulated J-13 well water and actual in J-13 well water are shown in Table 2.4 and Figures 2.6 and 2.7, respectively. The curves are similar, with slight differences in the polarization parameters of E_b, E_{rp}, and i_{cor} (corrosion current). Repetition of these experiments verified the similarities. Although the passive current density is lower for the curves produced in this study, as compared to McCright's data, the polarization behavior reasonably reproduces the behavior shown by McCright in Figure 2.5. The above results produce two important findings that are critical to the remaining work performed in this project:

(1) Prepared solutions can reasonably simulate actual well waters extracted from the Tuff site, and

(2) The experimental procedures used for the NRC project are capable of reproducing the polarization behavior observed at Lawrence Livermore National Laboratory under similar test conditions.

2.2.2 Selected Simulated Environments

In Task 2 of the program, a statistically based experimental test matrix was formulated in an effort to evaluate the influence on corrosion of the possible range of environmental variables that may occur over the life of the canister. The major difficulty encountered in designing these synthetic test solutions is in defining the geochemistry and the actual environments to which the canister will be exposed. The J-13 well water is probably the most dilute environment that can be expected within the Tuff Repository since boiling of the groundwater and its interaction with the host rock at elevated temperatures will tend to concentrate most species. The presence of the radiation field will generate new species, such as nitrates, carboxylic acids and hydrogen

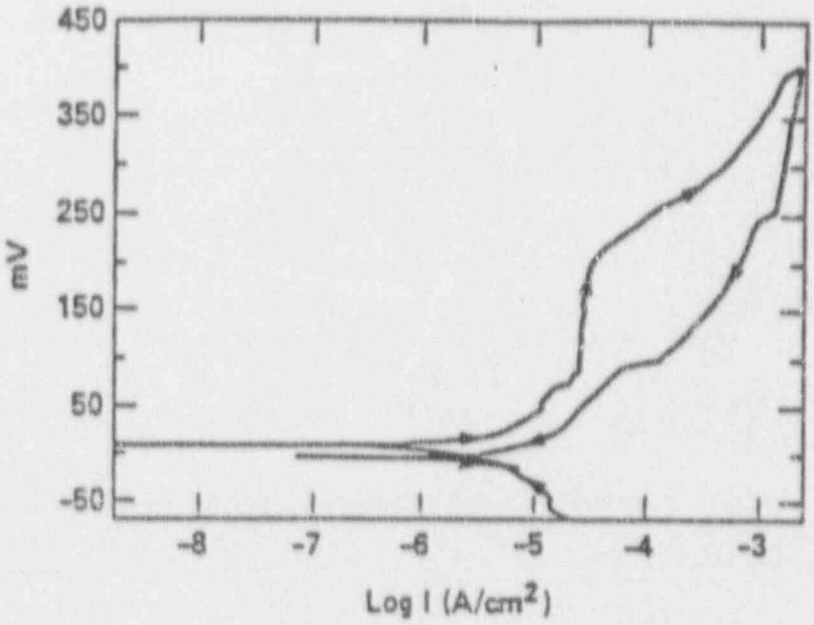

Figure 2.5 CPP Curve For Alloy CDA 102 In Actual J-13 Well Water At 80°C (Scan Rate: 1 mV/s) Produced By McCright (McCright-1985).

Table 2.3 Chemical Composition Of Simulated Tuff Groundwater And J-13 Well Water From Yucca Mountain, Nevada (For Comparison).

Environmental Variable	Actual Chemical Used	J-13* ppm	Simulated J-13‡ ppm
Na^+	$NaHCO_3$	44.0	46.0
K^+	KCl, KF	5.1	5.5
Mg^{2+}	$MgCl_2 \cdot 6H_2O$	1.9	1.7
Ca^{2+}	$Ca(NO_3)_2 \cdot 4H_2O$, $CaSO_4 \cdot \frac{1}{2}H_2O$	12.5	12.0
SiO_2	H_2SiO_3	58.	64.2
F^-	KF	2.2	1.7
Cl^-	KCl, $MgCl_2 \cdot 6H_2O$	6.9	6.4
HCO_3^-	$NaHCO_3$	125.	121.
NO_3^-	$Ca(NO_3)_2 \cdot 4H_2O$	9.6	12.4
SO_4^{2-}	$CaSO_4 \cdot \frac{1}{2}H_2O$	18.7	19.2
pH		7.6	7.0 ± 0.2
TDS		291.5	290.3

*Knauss, 1985

‡Beavers, 1987

The pH adjustment was accomplished by bubbling carbon dioxide through the solution.

Table 2.4 Polarization Parameters For The Candidate Alloys In Actual And Simulated J-13 Well Water.

Alloy	J-13 Well Water	Temperature °C	Initial Exposure Hours	Scan Rate V/hr	E_{corr} V, SCE	I_{corr} µA/cm²	E_{pit}/E_b V, SCE	E_{prot}/E_{rp} V, SCE
CDA 102	Actual *	80	1 - 2	3.6	-0.011	5.78	+0.201	+0.092
CDA 102	Simulated	80	1	3.6	-0.015	0.13	+0.161	-0.140
CDA 102	Actual	80	1	3.6	+0.004	0.31	+0.212	-0.179

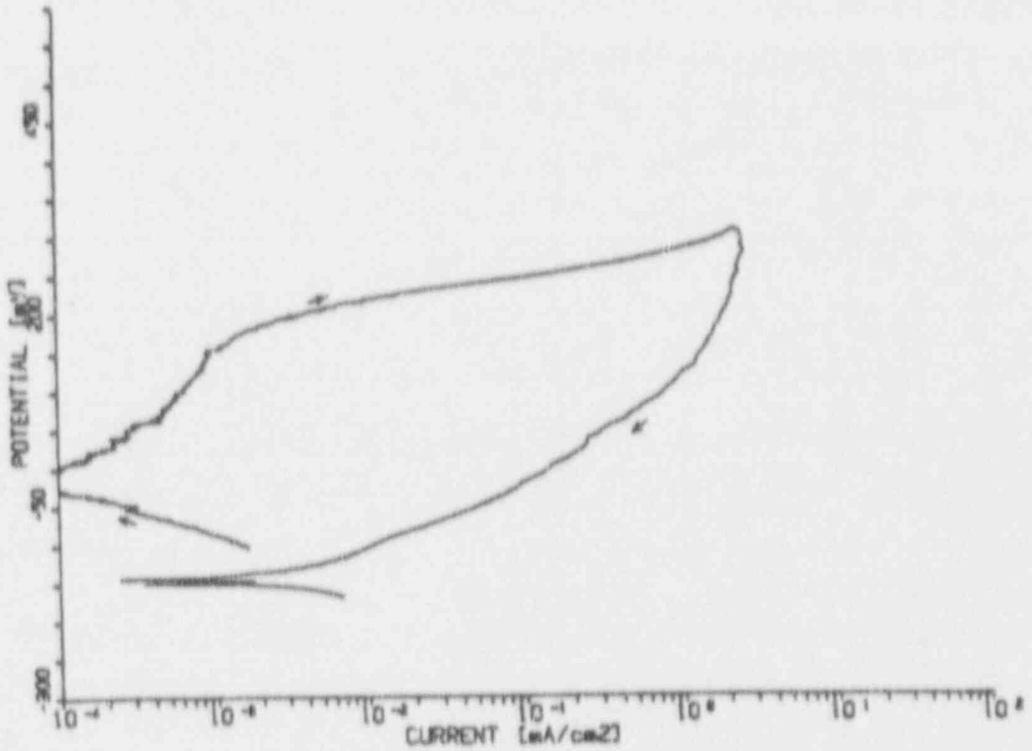

Figure 2.6 Polarization Curve For Alloy CDA 102 In Simulated J-13 Well Water At 80°C Following A One Hour Initial Exposure (Beavers-1988)

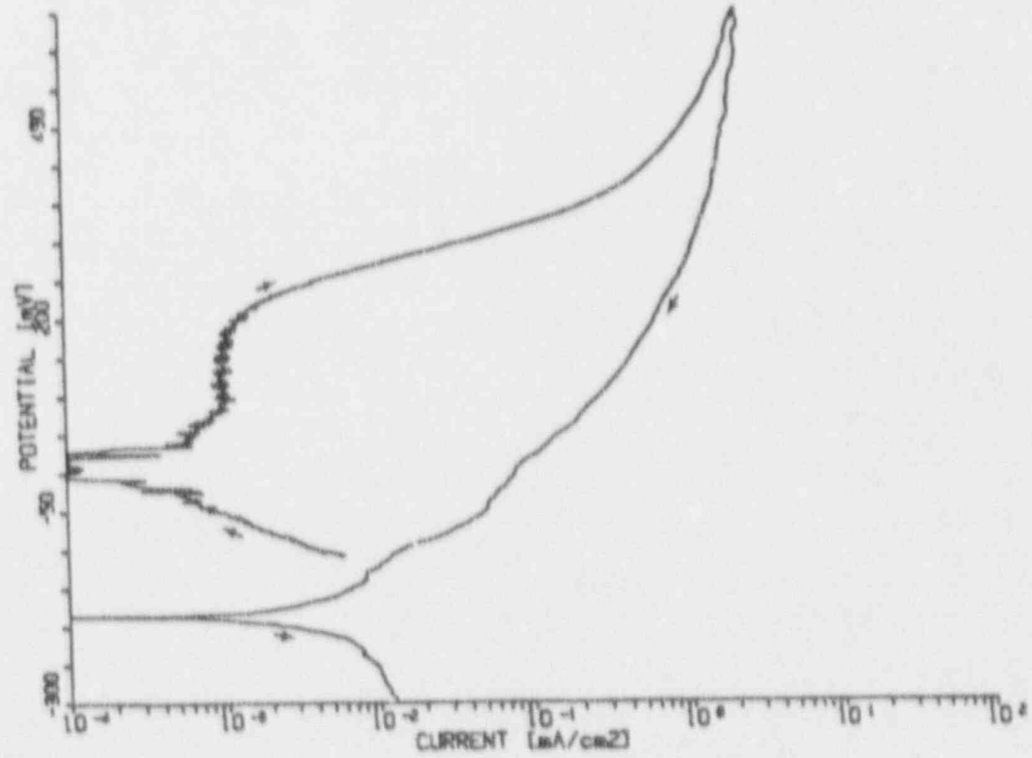

Figure 2.7 Polarization Curve For Alloy CDA 102 In Actual J-13 Well Water At 80°C Following A One Hour Initial Exposure (Beavers-1988).

peroxide. Those species that are not volatile also may concentrate at the surface of the canister as a result of the combination of boiling and radiation.

The test matrix of simulated environments was designed as a screening matrix to identify important species, or regions of the environmental factor space, with respect to corrosion of the container materials, where additional research is needed. Each individual test solution represents individual points within the factor space. While it is not known whether these specific environments will be encountered, the maximum concentrations of the majority of the species within the solutions are thought to be reasonable, based on a thorough review of the literature (Beavers-1990). Further details of the Task 2 studies are given in Appendix B.

Table 2.5 gives the compositions of the synthetic test solutions used in the Task 2 studies. Several of these solutions were used in the Task 4, 6, and 7 studies summarized in this report. The selection of a specific composition was based primarily on the CPP behavior observed in Task 2 as opposed to the constituents in the solution or the likelihood that a specific composition would exist in the repository.

Table 2.5 Compositions Of Solutions In The Experimental Test Matrix From Task 2 (Beavers - 1989).

Test No.	SiO_2	HCO_3^-	F^-	Cl^-	NO_3^-	NO_2^-	H_2O_2	Ca^{2+}	Mg^{2+}	Al^{3+}	PO_4^{3-}	Oxalic Acid	O_2	Temp °C	pH
1	2.2	0.4	200	1000	1000	200	200	0.8	0.004	0.0004	0.01	0	5	90	5
2	2.2	2000	200	1000	1000	0	0	0.004	0.004	0.8	2.0	172	5	50	5
3	215	0.4	0.04	0.2	1000	200	0	0.8	0.004	0.8	2.0	0	30	50	5
4	215	2000	0.04	0.2	1000	0	200	0.004	0.004	0.0004	0.01	172	30	90	5
5	2.2	0.4	200	0.2	0.2	0	200	0.8	0.8	0.8	0.01	172	30	50	5
6	2.2	2000	200	0.2	0.2	200	0	0.004	0.8	0.0004	2.0	0	30	90	5
7	215	0.4	0.04	1000	0.2	0	0	0.8	0.8	0.0004	2.0	172	5	90	5
8	215	2000	0.04	1000	0.2	200	200	0.004	0.8	0.8	0.01	0	5	50	5
9	2.2	0.4	0.04	1000	0.2	200	200	0.004	0.004	0.0004	2.0	172	30	50	10
10	2.2	2000	0.04	1000	0.2	0	0	0.8	0.004	0.8	0.01	0	30	90	10
11	215	0.4	200	0.2	0.2	200	0	0.004	0.004	0.8	0.01	172	5	90	10
12	215	2000	200	0.2	0.2	0	200	0.8	0.004	0.0004	2.0	0	5	50	10
13	2.2	0.4	0.04	0.2	1000	0	200	0.004	0.8	0.8	2.0	0	5	90	10
14	2.2	2000	0.04	0.2	1000	200	0	0.8	0.8	0.0004	0.01	172	5	50	10
15	215	0.4	200	1000	1000	0	0	0.004	0.8	0.0004	0.01	0	30	50	10
16	215	2000	200	1000	1000	200	200	0.8	0.8	0.8	2.0	172	30	90	10
17	215	2000	0.04	0.2	0.2	0	0	0.004	0.8	0.8	2.0	172	30	50	10
18	215	0.4	0.04	0.2	0.2	200	200	0.8	0.8	0.0004	0.01	0	30	90	10
19	2.2	2000	200	1000	0.2	0	200	0.004	0.8	.004	0.01	172	5	90	10
20	2.2	0.4	200	1000	0.2	200	0	0.8	0.8	0.8	2.0	0	5	50	10
21	215	2000	0.04	1000	1000	200	0	0.004	0.004	0.0004	2.0	0	5	90	10
22	215	0.4	0.04	1000	1000	0	200	0.8	0.004	0.8	0.01	172	5	50	10
23	2.2	2000	200	0.2	1000	200	200	0.004	0.004	0.8	0.01	0	30	50	10
24	2.2	0.4	200	0.2	1000	0	0	0.8	0.004	0.0004	2.0	172	30	90	10
25	215	2000	200	0.2	1000	0	0	0.8	0.8	0.8	0.01	0	5	90	5
26	2.2	0.4	200	0.2	1000	200	200	0.004	0.8	0.0004	2.0	172	5	50	5
27	2.2	2000	0.04	1000	1000	0	200	0.8	0.8	0.0004	2.0	0	30	50	5
28	2.2	0.4	0.04	1000	1000	200	0	0.004	0.8	0.8	0.01	172	30	90	5
29	215	2000	200	1000	0.2	200	0	0.8	0.004	0.0004	0.01	172	30	50	5
30	215	0.4	200	1000	0.2	0	200	0.004	0.004	0.8	2.0	0	30	90	5
31	2.2	2000	0.04	0.2	0.2	200	200	0.8	0.004	0.8	2.0	172	5	90	5
32	2.2	0.4	0.04	0.2	0.2	0	0	0.004	0.8	0.0004	0.01	0	5	50	5
33*	108	500	50	250	250	50	50	0.2	0.2	0.2	1.3	43	15	70	7.5
34*	108	500	50	250	250	50	50	0.2	0.2	0.2	1.3	43	15	70	7.5
35*	108	500	50	250	250	50	50	0.2	0.2	0.2	1.3	43	15	70	7.5
36*	108	500	50	250	250	50	50	0.2	0.2	0.2	1.3	43	15	70	7.5
37±	64.2	121	1.7	6.4	12.4	0	0	12	1.7	0	0	0	0	90	7.0
38+	64.2	121	1.7	1000	12.4	0	0	12	1.7	0	0	0	0	90	7.0
39	108	500	50	250	250	50	50	0.1	0.1	0.5	1.3	50	15	70	5
40	108	500	50	250	250	50	50	20	20	0.5	1.3	50	15	70	5
41	108	500	50	250	250	50	50	20	0.1	0.5	1.3	50	15	70	10
42	108	500	50	250	250	50	50	0.1	20	0.5	1.3	50	15	70	10

* Tests 33 through 36 are quadruplicate midpoint tests which help to establish the degree of reproducibility of the CPP Tests.

± Simulated J-13 well water.

\+ Simulated J-13 well vater containing 1000 ppm Cl^-.

3. PITTING-CORROSION STUDIES

Pitting-corrosion studies were conducted in Task 4 of the program. The purposes of these studies were (1) to study the relationships between the pitting parameters E_{pit} and E_{prot} and long-term pit initiation behavior, and (2) to evaluate pit-propagation behavior. The focus of the pit initiation studies was to verify the CPP technique used in Task 2 of the program. DOE also utilized a potentiodynamic-polarization technique to assess the likelihood of pit initiation in simulated Tuff repository environments. It was assumed that, if E_{cor} is far away from E_{prot} and E_{pit}, pitting is unlikely to initiate in a given environment.

The relationship between long-term pitting behavior and the electrochemical parameters was assessed by means of potentiostatic-polarization tests. Specimens were polarized over a range of potentials between E_{cor} and E_{pit} and the relationship between the time to pit initiation and potential was determined. These tests were performed on the candidate container materials at 90°C in simulated Tuff environments selected from Task 2.

In the pit-propagation studies, the propagation rates of pits in Alloy CDA 102 were assessed by means of electrochemical and gravimetric techniques. The results of previous studies have confirmed that pits readily initiate on the copper-base alloys in Tuff repository environments (Beavers-1991b, McCright-1985). Accordingly, for a copper container to provide adequate containment, it must be demonstrated that the rates of pit propagation are low in comparison to the container wall thickness. In this subtask, pit-propagation experiments were performed on Alloy CDA 102 in Solution Number 22, an environment identified by CPP tests in earlier studies as likely to promote pitting. The pit-propagation experiments involved exposures of simulated pit specimens which permitted electrochemical and gravimetric measurements of the rate of pit propagation as a function of pit depth.

3.1 Pit-Initiation Studies

The pit-initiation studies were conducted with all four of the candidate alloys in several synthetic solutions selected from the Task 2 studies. The focus of this research, however, was primarily orientated toward the copper-base alloys. In the research on copper, the various forms of localized corrosion observed after CPP tests were compared with the morphology of the attack observed over longer periods of time at a constant potential. These earlier CPP studies, performed in Task 2 of the program, suggested that conventional methods of interpretation could not be used to analyze the polarization behavior of either Alloy CDA 102 or Alloy CDA 715. Hysteresis in the CPP tests of these alloys was not always associated with classical pitting. Repetition of several of these tests confirmed the anomalous behavior. As a consequence, the term pitting potential and protection potential were replaced by the term breakdown (E_b) and repassivation (E_{rp}) potentials, respectively.

A limited number of pit-initiation studies were also conducted with the Fe-Cr-Ni alloys utilizing the potentiostatic-polarization technique. Current waste package designs for the Tuff Repository specify relatively thin-walled containers (Site Characterization Plan, 1988). Thus, if pits initiate,

container failure by pitting corrosion may occur within a relatively short period of time. Accordingly, the resistance to pit initiation is critical for the adequate performance of an Fe-Cr-Ni container. The DOE is utilizing electrochemical techniques to assess the probability of pit initiation for stainless steels in simulated Tuff Repository environments. The critical polarization parameters used in the evaluation are E_{cor}, E_{pit}, and E_{prot}. The assumption is that if E_{cor} is far away from E_{prot} and E_{pit}, pitting is unlikely to initiate in a given environment.

3.1.1 Experimental Approach

In the potentiostatic-polarization studies, the experimental equipment, test cells, and specimen geometry were identical to those used in the cyclic-potentiodynamic-polarization experiments performed in Task 2 of the program and outlined in Appendix A. In the potentiostatic testing, the specimen was polarized to a preselected potential by starting at the free-corrosion potential and polarizing it in approximately 50 mV increments and allowing 30 to 60 seconds between each step. This procedure provided a fairly rapid polarization up to the selected potential, at which point this selected potential was maintained constant for some period of time, up to a maximum of 72 hours. In several of the tests, the specimens were potentiostated after scanning to a higher potential on the forward scan and then reversing the scan to a lower potential. The selected potential on the reverse scan was then held constant for some period of time. The current was monitored as a function of time and the weight loss of the specimen was measured at the end of the experiment. The data were then plotted and superimposed on the previously determined CPP curve as shown in the example in Figure 3.1. Actual data for the potentiostatic experiments are presented as a horizontal line drawn at the constant potential maintained throughout the experiment. The current density is noted at the start of the experiment by a black dot, and at the end of the experiment by the tip of the horizontal arrow. The duration of the potentiostatic-polarization test is also noted on each plot. The current density based on the post-examination weight-loss measurement is indicated by a vertical arrow. A current density, based on weight loss, which falls within the range of currents measured during the potentiostatic test indicates qualitative agreement between weight loss and the electrochemical current measured for the specimen.

3.1.2 Copper-Base Alloys

Potentiostatic testing was performed with Alloy CDA 102 in seven different synthetic solutions selected from the experimental matrix (Solutions 1, 9, 10, 13, 20, 23, and 30 from Table 2.5). In all of these solutions, the CPP curves exhibited hysteresis, but optical examination revealed the absence of pitting. Five other synthetic solutions were evaluated with Alloy CDA 715 in which the CPP tests resulted in either pitting or active attack in the absence of pitting (Solutions 14, 15, 24, 28, and 38 from Table 2.5). The results of the potentiostatic tests superimposed on the CPP curves of the copper-base alloys are given in Appendix C. The results of the testing is also presented in tabular form in Tables 3.1 and 3.2 for Alloy CDA 102 and Alloy CDA 715, respectively.

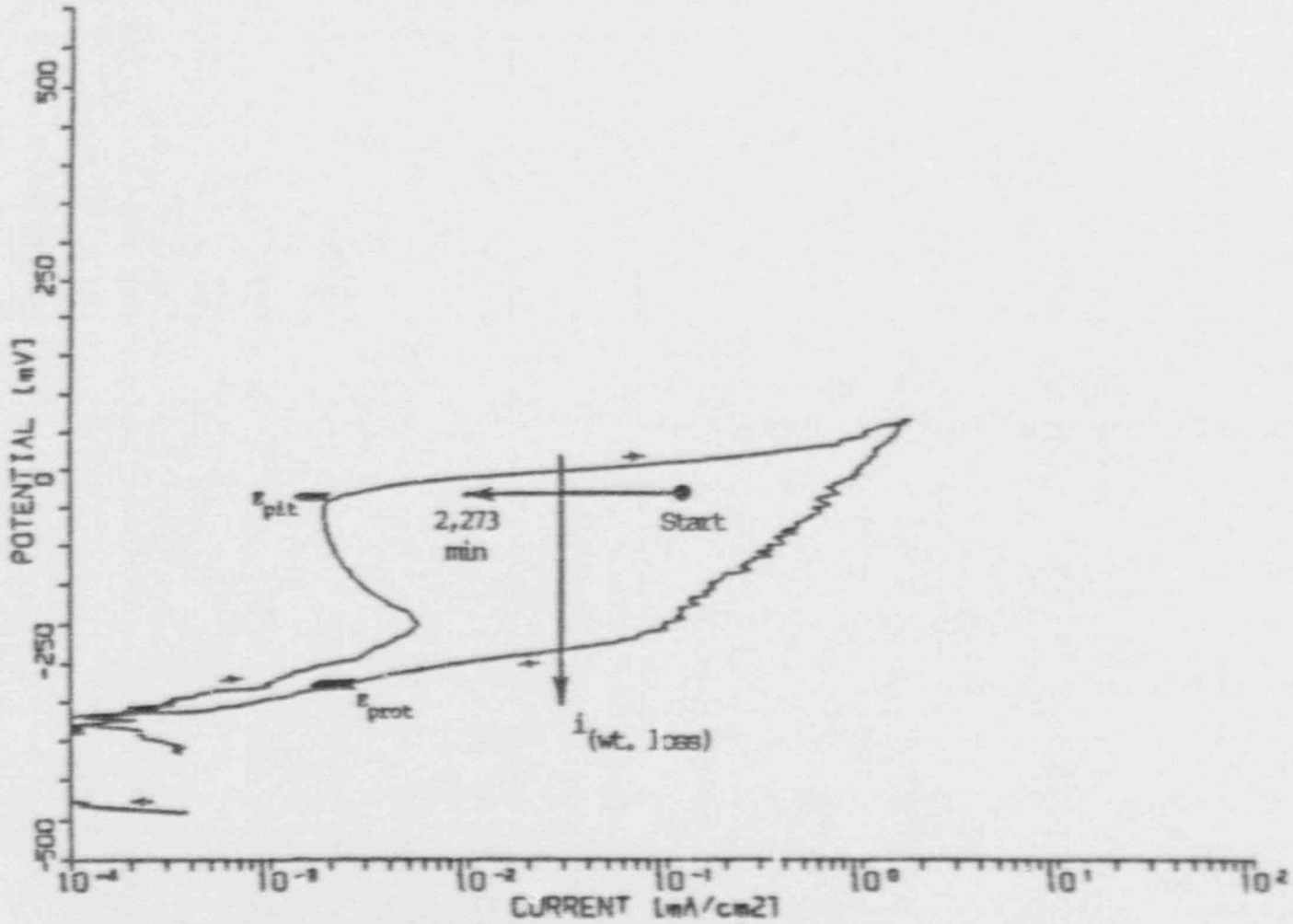

Figure 3.1 Cyclic Potentiodynamic Polarization And Potentiostatic Data For Alloy CDA 715 In 90°C Simulated J-13 Well Water Containing 1000 mg/l Chloride (As NaCl) At 90°C Potentiostated To -40 mV (SCE) (No Pitting, Local Active Attack In Potentiostatic Test).

Table 3.1 Cyclic Potentiodynamic Polarization Data And Data For Potentiostatic Tests Of Alloy CDA 102 In Selected Synthetic Environments.

Solution №	CPP PARAMETERS			POTENTIOSTATIC TEST PARAMETERS						
	E_{oc} V, SCE	E_b V, SCE	E_{rp} V, SCE	E_{oc} V, SCE	Polarized Potential V, SCE	Initial Current mA/cm^2	Final Current mA/cm^2	Current* mA/cm^2	Total Time hours	Comments
1	+0.005	+0.160	0.000	—	—	—	—	—	—	CPP: No pitting, oxide growth.
	—	—	—	-0.020	+0.125	5.08×10^{-1}	7.20×10^{-2}	2.45×10^{-1}	14.5	PSP: Active corrosion beneath black oxide.
9	+0.045	+0.050	+0.030	—	—	—	—	—	—	CPP: No pitting, local oxide growth.
	—	—	—	-0.007	+0.120	1.27×10^{-1}	2.27×10^{-3}	4.59×10^{-4}	44.9	PSP: Active corrosion beneath red oxide.
10A	-0.115	+0.330	-0.070	—	—	—	—	—	—	CPP: No pitting, local oxide growth and active areas.
	—	—	—	-0.146	+0.151	2.22×10^{-3}	2.22×10^{-5}	6.8×10^{-5}	66.2	PSP: Slightly tarnished, very little corrosion.
10B	—	—	—	-0.150	+0.150®	8.22×10^{-3}	4.44×10^{-4}	8.2×10^{-3}	65.4	PSP: Local active attack beneath oxide.
10C	—	—	—	-0.128	+0.350®	3.33×10^{-1}	5.80×10^{-1}	9.28×10^{-1}	15.7	PSP: Large areas of local active attack beneath green oxide.
13A	-0.035	+0.120	0.000	—	—	—	—	—	—	CPP: No pitting.
	—	—	—	+0.060	+0.110	3.31×10^{-2}	2.22×10^{-3}	1.16×10^{-4}	39.8	PSP: No pitting. Shallow local active attack.
13B	—	—	—	+0.016	+0.376®	9.49×10^{-1}	1.07×10^{0}	5.72×10^{-1}	14.7	PSP: No pitting. Severe active attack beneath oxide.
20	-0.085	-0.035	-0.015	—	—	—	—	—	—	CPP: No pitting, active areas.
	—	—	—	-0.140	-0.021	1.59×10^{-3}	2.27×10^{-4}	3.11×10^{-4}	37.9	PSP: No pitting, very few small active sites.
23	-0.075	+0.275	+0.075	—	—	—	—	—	—	CPP: No pitting.
	—	—	—	+0.103	+0.325	1.10×10^{0}	2.38×10^{-2}	2.41×10^{-1}	64.6	PSP: Pitting, severe active attack.
30	-0.150	+0.150	+0.150	—	—	—	—	—	—	CPP: No pitting.
	—	—	—	-0.102	0.000	8.58×10^{-2}	4.90×10^{-2}	6.24×10^{-3}	67.0	PSP: No pitting, severe active corrosion.

* Current calculated from actual weight loss. ® Polarized on the reverse scan.
CPP: Description following cyclic-potentiodynamic-polarization. PSP: Description following potentiodynamic-polarization.

Table 3.2 Cyclic Potentiodynamic Polarization Data And Data For Potentiostatic Tests Of Alloy CDA 715 In Selected Synthetic Environments.

Solution №	CPP PARAMETERS			POTENTIOSTATIC TEST PARAMETERS						
	E_{corr} V, SCE	E_b V, SCE	E_{rp} V, SCE	E_{corr} V, SCE	Polarized Potential V, SCE	Initial Current mA/cm^2	Final Current mA/cm^2	Current* mA/cm^2	Total Time hours	Comments
14A	+0.240	+0.240	+0.020	—	—	—	—	—	—	CPP: Pitting and oxide growth.
	—	—	—	-0.112	+0.349	3.10×10^{-3}	5.35×10^{-1}	4.19×10^{-1}	15.7	PSP: No pitting, locally severe active attack.
14B	—	—	—	-0.208	+0.399®	5.12×10^{0}	5.80×10^{-6}	3.52×10^{0}	6.1	PSP: Pitting, severe local corrosion.
15	-0.160	+0.200	-0.200	—	—	—	—	—	—	CPP: No pitting, active areas.
	—	—	—	-0.130	+0.125®	1.24×10^{-1}	9.03×10^{-2}	1.04×10^{-1}	41.8	PSP: Pitting, severe active corrosion.
24	-0.100	+0.140	-0.180	—	—	—	—	—	—	CPP: Pitting, tarnished.
	—	—	—	+0.112	+0.226	5.31×10^{-1}	$<1.0 \times 10^{-2}$	8.04×10^{-3}	41.7	PSP: Few pits, active attack.
28A	-0.050	+0.200	-0.020	—	—	—	—	—	—	CPP: No pitting, active attack.
	—	—	—	-0.159	+0.200	1.21×10^{-1}	3.45×10^{-3}	1.28×10^{-3}	41.0	PSP: Pitting, active attack.
28B	—	—	—	-0.153	+0.200®	8.97×10^{-3}	1.10×10^{-2}	7.89×10^{-4}	41.2	PSP: No pitting, active attack.
38A	-0.400	-0.040	-0.280	—	—	—	—	—	—	CPP: Local changes in oxide, local active attack.
	—	—	—	-0.132	-0.040	4.45×10^{-2}	1.14×10^{-2}	2.96×10^{-3}	37.9	PSP: No pitting, local active attack.
38B	—	—	—	-0.173	-0.040®	1.28×10^{-1}	6.90×10^{-3}	6.55×10^{-3}	37.5	PSP: No pitting, severe active attack.

* Current calculated from actual weight loss. ® Polarized on the reverse scan.
CPP: Description following cyclic-potentiodynamic-polarization. PSP: Description following potentiodynamic-polarization.

These figures and data indicate that a wide range of behavior was observed for both of the copper-base alloys. An interesting series of curves is shown for Alloy CDA 102 in Solution Number 10 in Figures 3.2 through 3.4. Figure 3.2 shows Alloy CDA 102 in Solution Number 10 potentiostated to 150 mV (SCE) on the forward scan. The current at the start of the potentiostatic test is similar to that observed in the CPP test, but decreases with time to very small values. This behavior is not unusual for a passive alloy in which the passive current decreases with time. Figure 3.3 shows Alloy CDA 102 in Solution Number 10 potentiostated on the reverse scan to 150 mV (SCE). The current is relatively high at the start of the potentiostatic test, but decreases significantly over time to a current value similar to that measured in Figure 3.2 for Alloy CDA 102 potentiostated on the forward scan. From conventional interpretation of the CPP curve, which shows a repassivation potential of about -70 mV (SCE), it would be predicted that the current on the reverse scan at +150 mV (SCE) would remain high and pits would propagate. However, the decrease in current of the specimen whose data are shown in Figure 3.3 is contrary to this conventional interpretation. In effect, the repassivation potential must be more positive than the +150 mV (SCE) potential used in this test.

Figure 3.4 shows the data for Alloy CDA 102 in Solution Number 10 potentiostated on the reverse scan to +350 mV (SCE) (200 mV more positive than the potential used in Figure 3.3). In this case, the current remained relatively high and severe locally active corrosion occurred on the specimen. The short time period used in the potentiostatic test shown in Figure 3.4 as compared to those data previously shown in Figures 3.2 and 3.3 does not alter this finding, since the current in all cases was permitted to stabilize. In conclusion, the CPP curve for Alloy CDA 102 in Solution Number 10 predicted classical passivation and pitting corrosion. In reality, no pitting was observed, only severe locally active attack. This same behavior was observed with Alloy CDA 102 in all of the other synthetic solutions that were evaluated, with the exception of Solution Number 23. In the case of Solution Number 23, the specimen was potentiostated 50 mV above the breakdown potential and optical examination revealed pitting and severe active attack following the potentiostatic test. No pitting was observed following the original CPP test.

Five synthetic solutions were evaluated with Alloy CDA 715 and their data are presented in Appendix C. Two of the five environments evaluated, Solution Number 14 and Solution Number 38 (simulated J-13 well water containing 1000 ppm chloride as sodium chloride), exhibited rather unusual behavior, and are discussed in more detail below.

Figures 3.5 and 3.6 show the data for specimens of Alloy CDA 715 potentiostated to 349 mV (SCE) and 399 mV (SCE) in Solution Number 14 on the forward and reverse scans, respectively. For the case of the specimen potentiostated during the forward scan (Figure 3.5), the current significantly increased with time. An overall increase of the current with time was also observed for the specimen potentiostated on the reverse scan. In Figure 3.6, the horizontal arrow indicates an increase in current during the first 159 minutes of exposure followed by a decrease in current to the point when the specimen was removed at 392 minutes. Severe attack occurred on both of the specimens potentiostated in Solution Number 14.

Although no pitting was observed on the specimen potentiostated on the forward scan, pitting was observed on the specimen potentiostated on the reverse scan. It would appear that the actual breakdown potential for this alloy-environment system lies above 350 mV (SCE), which is 110 mV (SCE) higher than the breakdown potential predicted by the CPP curve

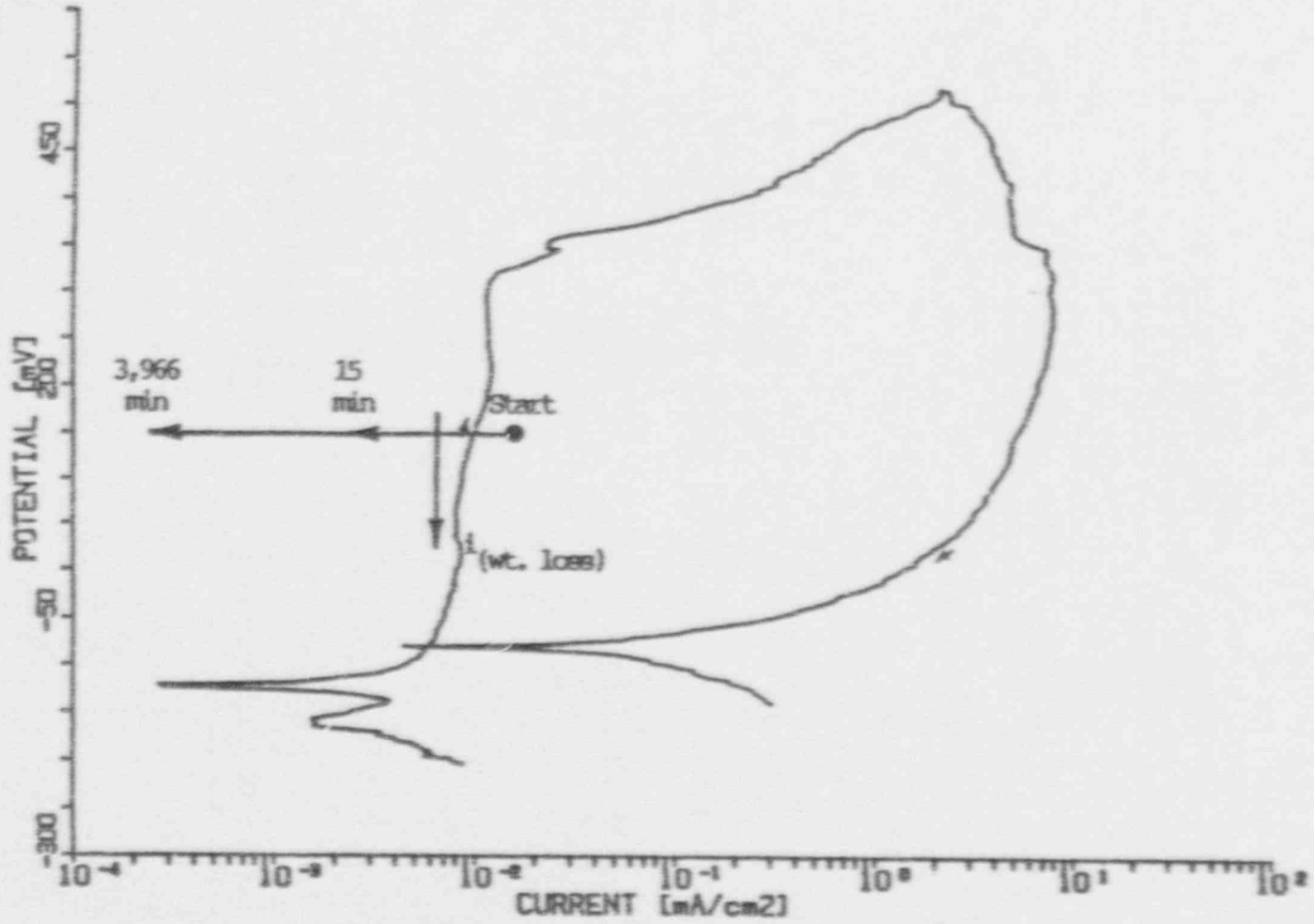

Figure 3.2 Cyclic Potentiodynamic Polarization And Potentiostatic Data For Alloy CDA 102 In Solution No. 10 At 90°C Potentiostated On The Forward Scan To +150 mV (SCE) (No Pitting, Slightly Tarnished In Potentiostatic Test).

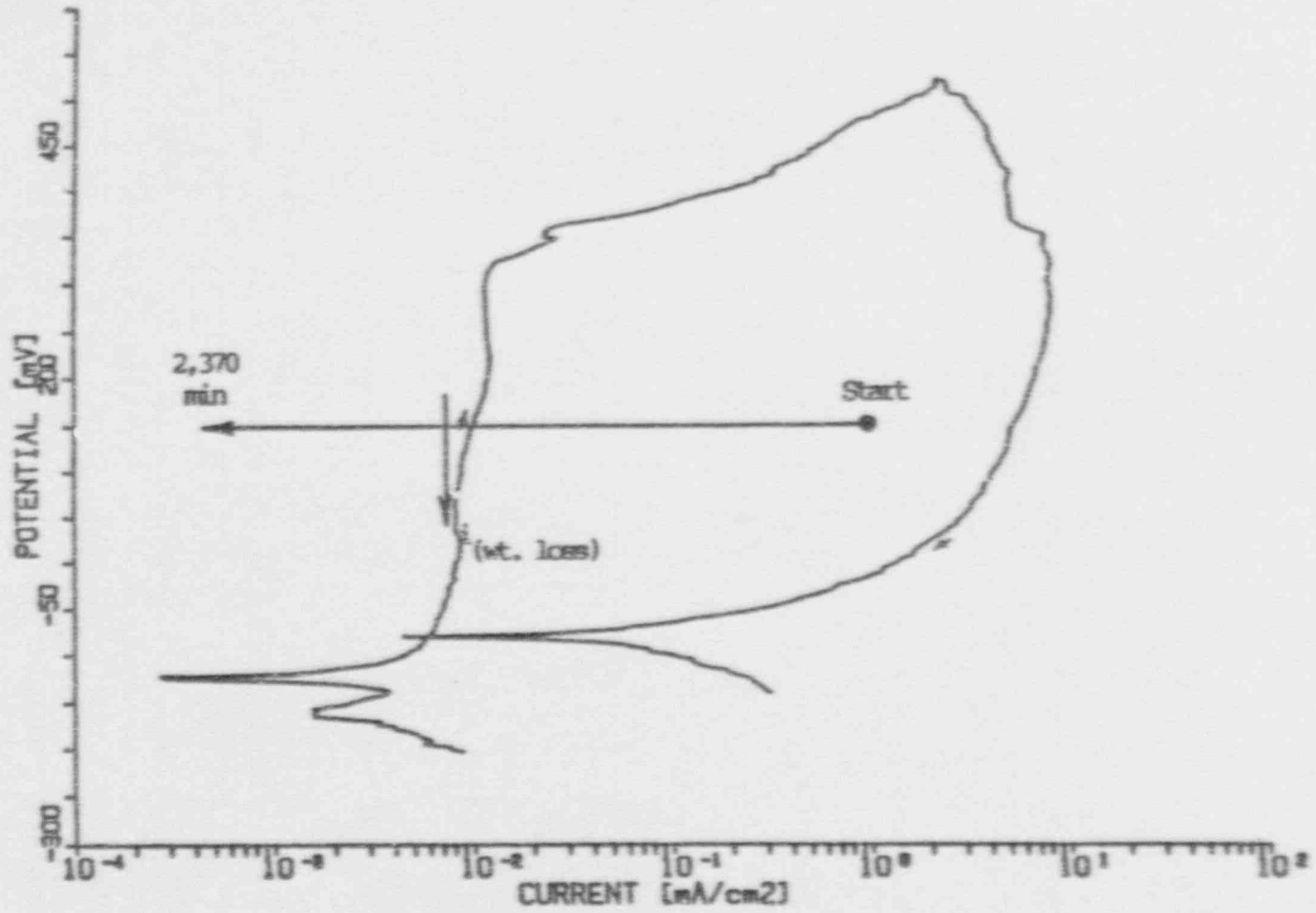

Figure 3.3 Cyclic Potentiodynamic Polarization And Potentiostatic Data For Alloy CDA 102 In Solution No. 10 At 90°C Potentiostated On The Reverse Scan To +150 mV (SCE) (No Pitting, Locally Active Attack Beneath Oxide In Potentiostatic Test).

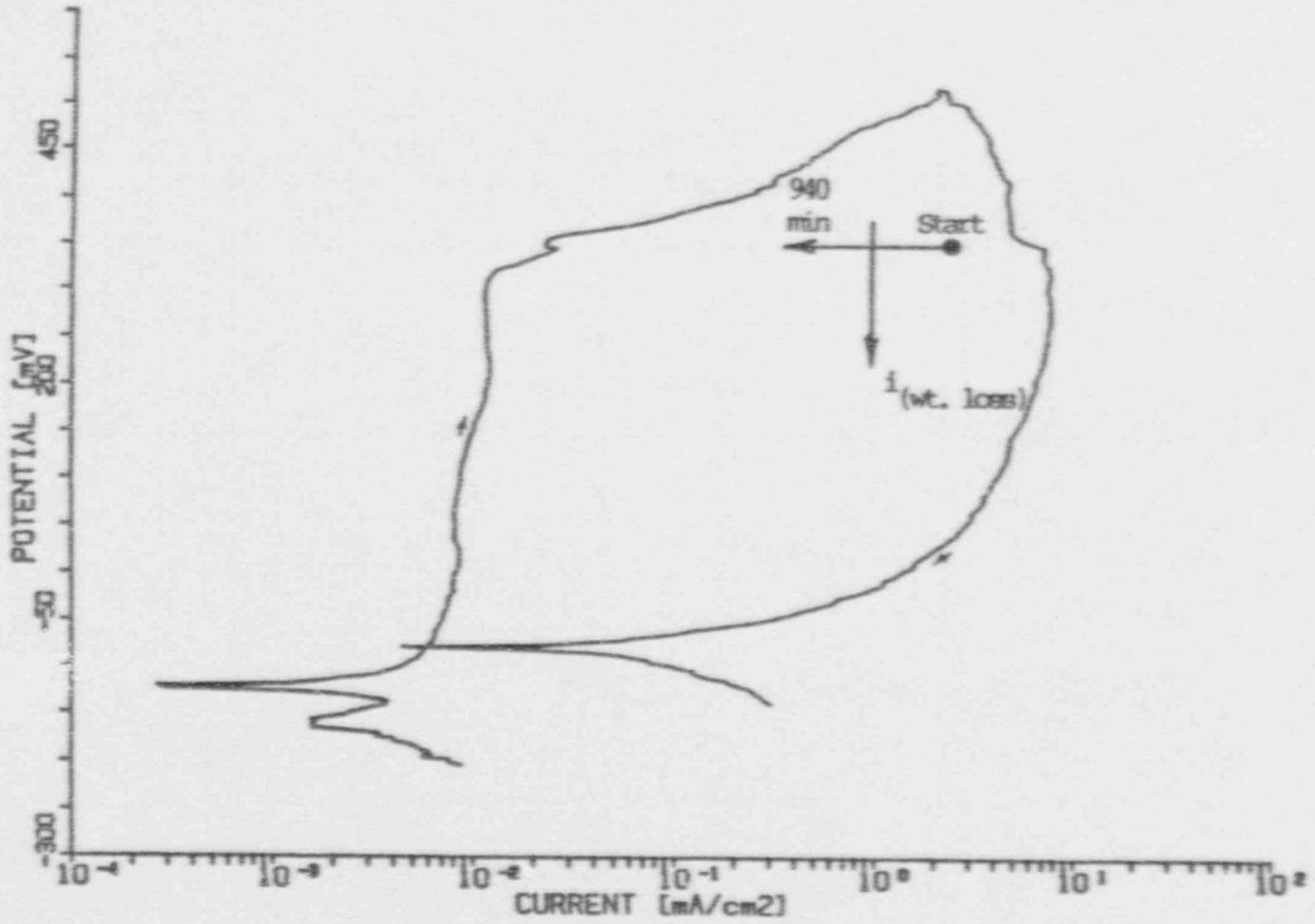

Figure 3.4 Cyclic Potentiodynamic Polarization And Potentiostatic Data For Alloy CDA 102 In Solution No. 10 At 90°C Potentiostated On the Reverse Scan To +350 mV (SCE) (No Pitting, Large Areas Of Locally Active Attack In Potentiostatic Test).

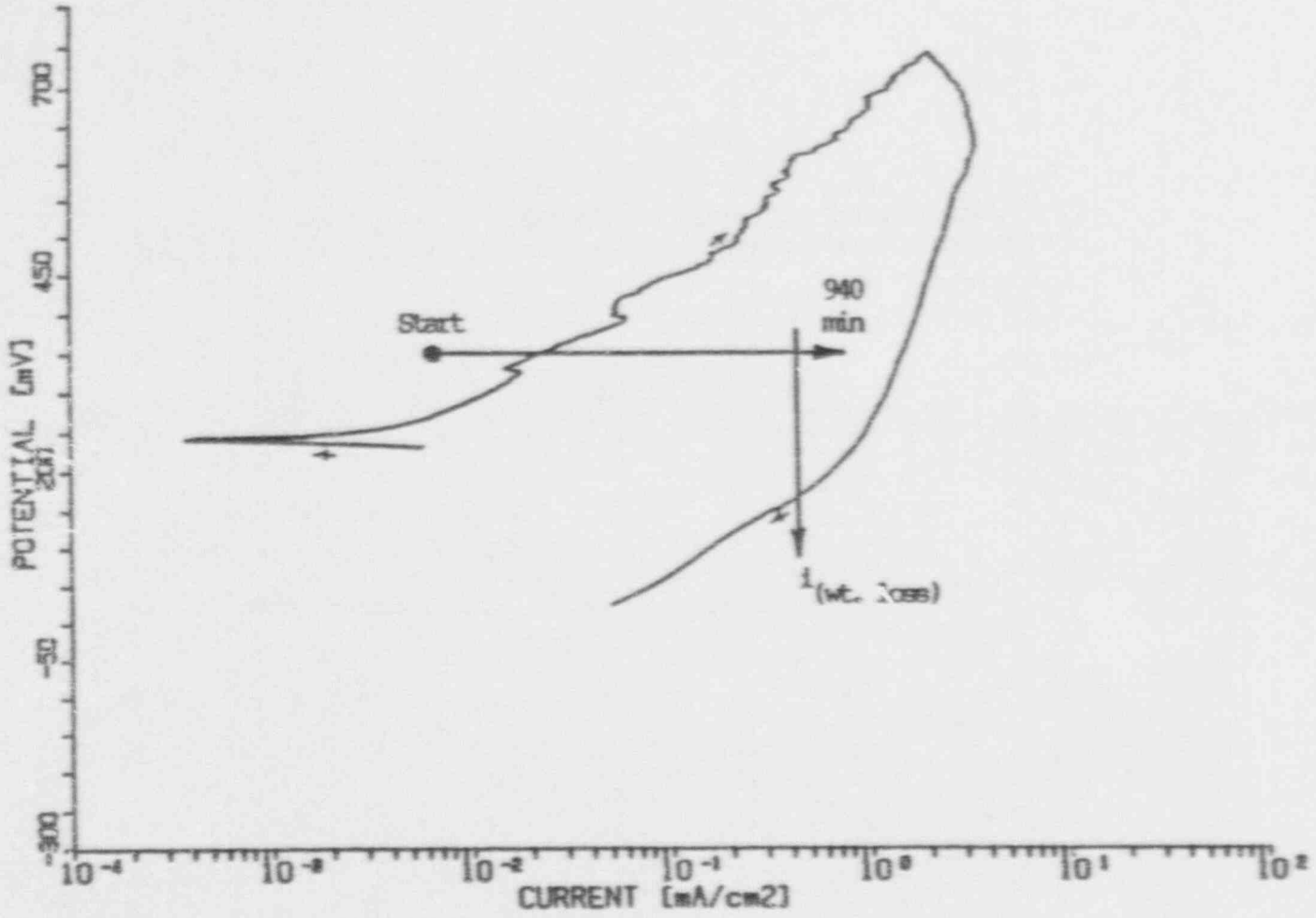

Figure 3.5 Cyclic Potentiodynamic Polarization And Potentiostatic Data For Alloy CDA 715 In Solution No. 14 At 30°C Potentiostated On The Forward Scan To +349 mV (SCE) (No Pitting, Locally Severe Active Attack In Potentiostatic Test).

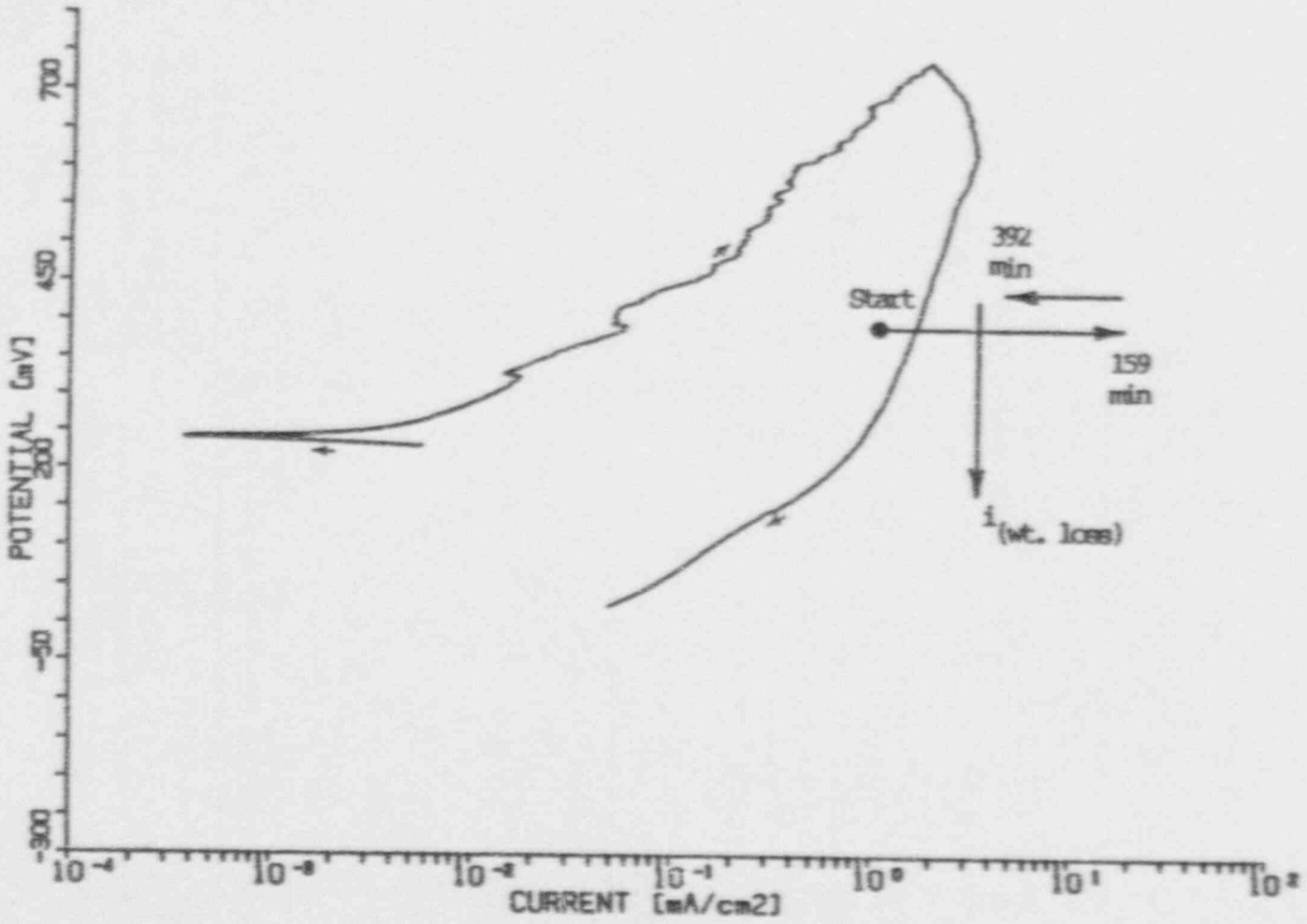

Figure 3.6 Cyclic Potentiodynamic Polarization And Potentiostatic Data For Alloy CDA 715 In Solution No. 14 At 50°C Potentiostated On The Reverse Scan To +399 mV (SCE) (Pitting, Severe Local Corrosion In Potentiostatic Test).

Figures 3.7 and 3.8 show the data for specimens of Alloy CDA 715 potentiostated to -40 mV (SCE) in Solution Number 38 (simulated J-13 well water containing 1000 mg/l Chloride) on the forward and the reverse scans, respectively. In the case of the specimen potentiostated on the forward scan (Figure 3.7), the initial current at the start of the potentiostatic experiment is significantly greater than the current for the CPP experiment at the same potential. This difference in current is most likely due to the difference in scan rates between the CPP curve and the much faster scan rate used to step the potential to the desired value in the potentiostatic experiment. Comparison of Figures 3.7 and 3.8 shows that the final current densities obtained were very similar for the two tests. The somewhat greater current density predicted from weight-loss measurements for the specimen potentiostated on the reverse scan is certainly due to the much higher currents during the initial portions of the potentiostatic tests.

In both cases, the weight-loss measurements appear to be qualitatively in agreement with the currents measured during the tests. Much more severe attack was observed for the specimen whose data are presented in Figure 3.8, but pitting was not observed in either case. Consequently, this illustrates that, even during long-term experiments, as compared with CPP tests, pitting does not necessarily develop although hysteresis is observed in the CPP test. It should be noted, however, that the active attack observed in the post-test examination was somewhat localized and occurred beneath a corrosion product layer.

Specimens of Alloy CDA 715 tested in the other three synthetic environments exhibited some degree of pitting in conjunction with areas of active corrosion. Also, qualitative agreement was observed between weight-loss data and the currents measured during the potentiostatic tests. The different behavior observed for the potentiostatic tests makes long-term predictions difficult from the CPP curves. In Solution Numbers 24 and 28, the significant decrease in current may indicate a decrease in pit-propagation rates with time.

In summary, it has been firmly established that hysteresis in CPP curves for Alloy CDA 102 and CDA 715 does not always correspond with classical pitting, but corresponds with local active corrosion. This active corrosion occurred most often beneath an oxide or corrosion product layer that covered the entire specimen and the rate frequently decreased with time. Thus, standard interpretations of the CPP tests are not appropriate for copper and copper-nickel alloys, especially in the presence of thick oxide layers.

3.1.3 Fe-Cr-Ni Alloys

Potentiostatic testing was performed with Alloy 304L in five different synthetic solutions selected from the experimental matrix in which the CPP curves exhibited slight hysteresis, but optical examination revealed tarnishing and the absence of pitting (Solutions 2, 5, 15, 24, and 27 from Table 2.5). Four other synthetic solutions were evaluated with Alloy 825 in which the specimen exhibited either pitting with crevice attack or tarnishing in the absence of pitting in the CPP tests (Solutions 4, 6, 18, and 34 from Table 2.5). The results of the potentiostatic tests superimposed on the CPP curves of the Fe-Cr-Ni alloys are given in Appendix D. The results of the testing are also presented in tabular form in Tables 3.3 and 3.4 for Alloy 304L and Alloy 825, respectively.

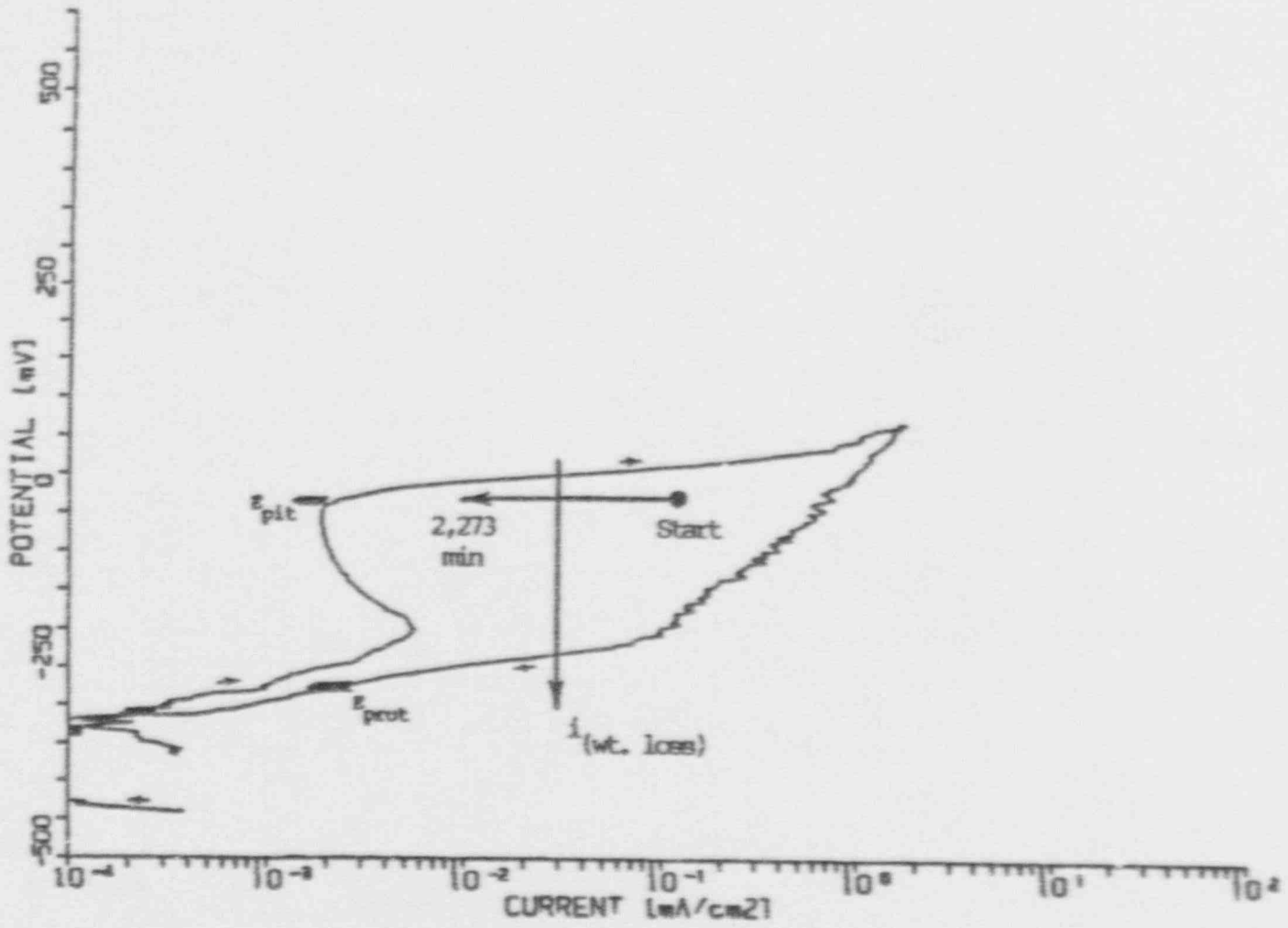

Figure 3.7 Cyclic Potentiodynamic Polarization And Potentiostatic Data For Alloy CDA 715 In Simulated J-13 Well Water Containing 1000 mg/l Chloride as (NaCl) (Solution No. 38) At 90°C Potentiostated On The Forward Scan To -40 mV (SCE) (No Pitting, Local Active Attack In Potentiostatic Test).

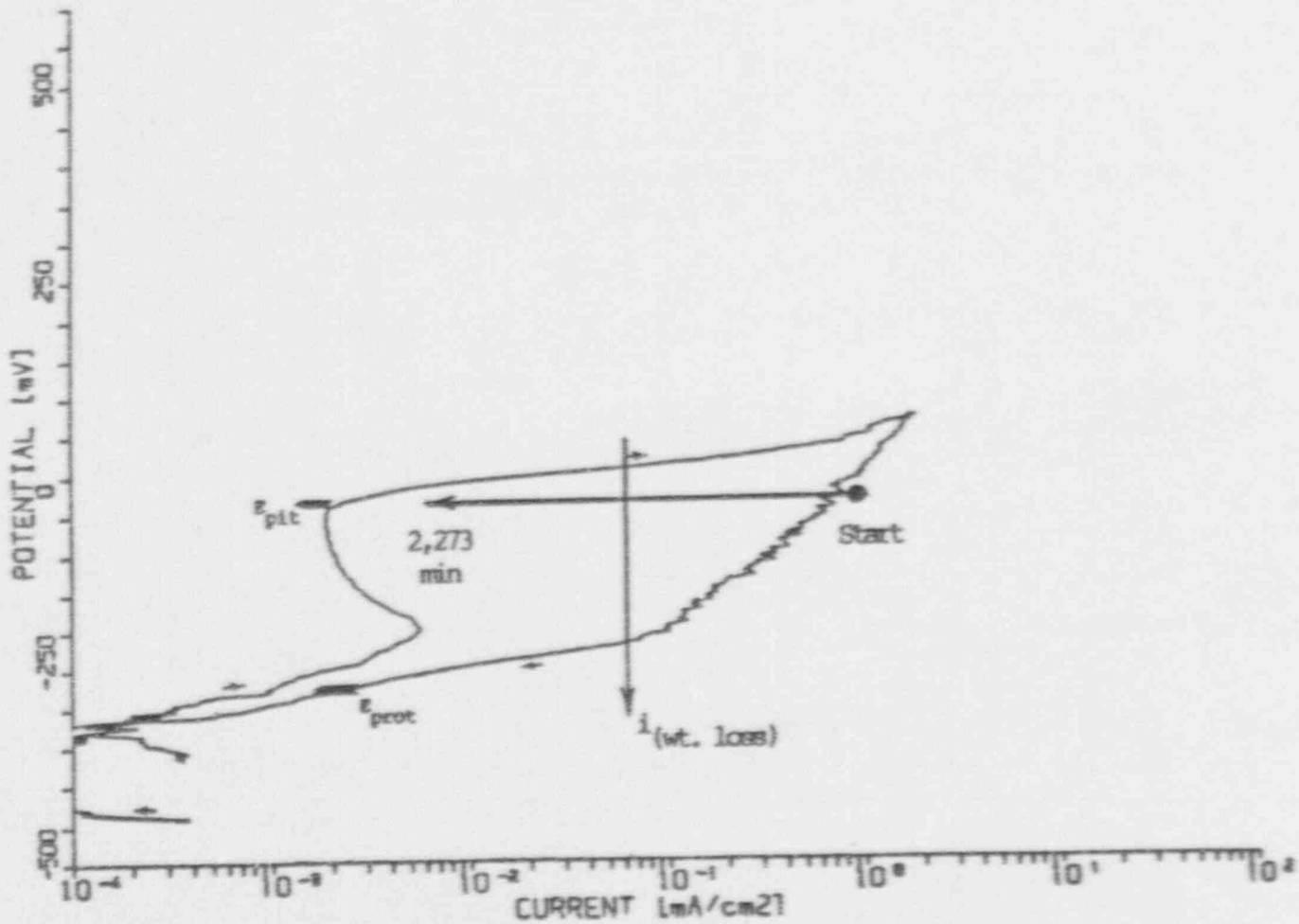

Figure 3.8 Cyclic Potentiodynamic Polarization And Potentiostatic Data For Alloy CDA 715 In Simulated J-13 Well Water Containing 1000 mg/l Chloride (As NaCl) (Solution No. 38) at 90°C Potentiostated On The Reverse Scan To -40 mV (SCE) (No Pitting, Severe Active Attack In Potentiostatic Test).

Table 3.3 Cyclic Potentiodynamic Polarization Data And Data For Potentiostatic Tests Of Alloy 304L In Selected Synthetic Environments.

Solution N°	CPP PARAMETERS			POTENTIOSTATIC TEST PARAMETERS						
	E_{cor} V, SCE	E_{pit} V, SCE	E_{prot} V, SCE	E_{cor} V, SCE	Polorized Potential V, SCE	Initial Current mA/cm²	Final Current mA/cm²	Current* mA/cm²	Total Time hours	Comments
2	-0.030	+0.700	+0.610	—	—	—	—	—	—	CPP: No pitting, local tarnishing, slight hysteresis.
	—	—	—	-0.175	+0.798	2.52×10^{-3}	7.41×10^{-4}	0	68.6	PSP: No pitting, no attack.
5	+0.305	+0.750	+0.750	—	—	—	—	—	—	CPP: No pitting, very slight tarnishing, no hysteresis.
	—	—	—	+0.150	+0.800	4.29×10^{-1}	5.81×10^{-1}	3.02×10^{-1}	69.3	PSP: Severe general attack.
15	-0.195	+0.800	+0.660	—	—	—	—	—	—	CPP: No pitting, local tarnishing, hysteresis.
	—	—	—	-0.323	+0.800®	1.19×10^{0}	7.1×10^{-2}	1.88×10^{-1}	71.4	PSP: Severe pitting and crevice attack.
24	-0.050	+0.730	+0.650	—	—	—	—	—	—	CPP: No pitting, heavy tarnishing, hysteresis.
	—	—	—	-0.233	+0.800	3.96×10^{-2}	1.85×10^{-3}	5.91×10^{-3}	65.9	PSP: No pitting, no attack.
27	+0.185	+0.750	+0.750	—	—	—	—	—	—	CPP: No pitting, local tarnishing, slight hysteresis.
	—	—	—	+0.150	+0.800	7.85×10^{-2}	7.41×10^{-4}	1.30×10^{-3}	67.9	PSP: No pitting, no attack.

* Current calculated from weight-loss. ® Polarized on the reverse scan.
CPP: Description following cyclic-potentiodynamic-polarization. PSP: Description following potentiodynamic polarization.

Table 3.4 Cyclic Potentiodynamic Polarization Data And Data For Potentiostatic Tests Of Alloy 825 In Selected Synthetic Environments.

Solution N°	CPP PARAMETERS			POTENTIOSTATIC TEST PARAMETERS						
	E_{cor} V, SCE	E_{pit} V, SCE	E_{prot} V, SCE	E_{cor} V, SCE	Polarized Potential V, SCE	Initial Current mA/cm^2	Final Current mA/cm^2	Current* mA/cm^2	Total Time hours	Comments
4	+0.030	+0.750	+0.750	—	—	—	—	—	—	CPP: No pitting, slight tarnishing, no hysteresis.
	—	—	—	+0.263	+0.800	3.38×10^{-1}	8.93×10^{-4}	1.90×10^{-5}	24.8	PSP: No pitting, no attack.
6	-0.400	+0.650	+0.530	—	—	—	—	—	—	CPP: No pitting, tarnished, hysteresis.
	—	—		-0.103	+0.800	4.20×10^{-5}	1.38×10^{-2}	7.28×10^{-4}	64.8	PSP: Crevice attack.
18	+0.135	+0.135	+0.090	—	—	—	—	—	—	CPP: Pitting, crevice attack, slight hysteresis.
	—	—	—	+0.135	+0.500	4.69×10^{-5}	3.13×10^{-3}	1.33×10^{-5}	28.3	PSP: No pitting, no attack.
34	+0.100	+0.850	+0.720	—	—	—	—	—	—	CPP: No pitting, heavy tarnishing, hysteresis.
	—	—	—	+0.191	+0.800	8.57×10^{-5}	2.90×10^{-2}	0	1.1	PSP: Slight attack at crevice.

* Current calculated from weight-loss. ③ Polarized on the reverse scan.
CPP: Description following cyclic-potentiodynamic-polarization. PSP: Description following potentiodynamic polarization.

When considering all of the CPP curves performed on the Fe-Cr-Ni alloys on the program, the conventional interpretation of the CPP curves (namely, that hysteresis in the CPP curves is associated with localized corrosion of the specimen) was accurate for the vast majority of the work. However, the tests performed in this subtask demonstrated instances where the interpretation of the curves was not always straightforward. Some of the curves, e.g., Alloy 825 in Solution 4 (Figure 3.9), exhibited high anodic currents in the CPP curves yet there was negligible corrosion on the specimen. The most probable explanation for this behavior is that non-Faradaic (noncorrosion) redox reactions occurred in the solution during the test. This interpretation is consistent with the significant decreases in the anodic currents that occurred with exposure time in the potentiostatic tests. In several instances, e.g., Alloy 304L in Solutions 2 (Figure 3.10), 24, and 27, a small hysteresis loop at noble potential was associated with tarnishing in the CPP tests, as opposed to localized corrosion, of the specimen. In these solutions, localized corrosion also was not observed in the potentiostatic tests and significant decreases in the potentiostatic currents with exposure time occurred.

In other cases, e.g., Alloy 304L in Solution 15 (Figure 3.11), or Alloy 825 in Solution 6 (Figure 3.12), similar CPP behavior was observed (hysteresis with tarnishing and no localized corrosion) but localized corrosion occurred in the potentiostatic test. Thus, the standard interpretation of the hysteresis was accurate. These interpretation problems with the CPP curves may be only of academic interest since the slight hysteresis, which was associated with tarnishing, generally occurred at very noble potentials. In any case, they point to the need to carefully interpret the CPP curves and to factor a post-test examination of the test specimen into the analysis. These analysis problems also are not unique to these alloy-environment combinations, having been observed by the authors for other alloy-environment systems.

3.2 Pit Propagation Studies

Pit propagation studies were conducted with Alloy CDA 102 in Solution Number 22, an environment identified by CPP tests in earlier studies, as likely to promote pitting. The composition of Solution Number 22 is given in Table 2.5 and the CPP curve is shown in Figure 3.13. The pit-propagation experiments involved exposure of simulated pit specimens which permitted electrochemical and gravimetric measurements of the rate of pit propagation as a function of pit depth. The purpose of these experiments was to determine if the rates of pit propagation would be low in comparison to the thickness of the container wall.

3.2.1 Experimental Approach

The pit-propagation experiments were performed in a glass electrochemical cell illustrated in Figure 3.14. A more detailed view of the specimen is illustrated in Figure 3.15. Both the Boldly Exposed Surface (BES) specimen and the pit specimen were wet-abraded to 400 grit SiC, cleaned, measured, degreased, and weighed prior to assembly. Layers of polytetrafluoroethylene (PTFE) tape were wrapped around the pit specimen to isolate it from the inside of the BES specimen. The pit diameter typically measured 3.18 mm (0.125 inch) and the pit depth varied up to a maximum of 15.9 mm (0.625 inch), giving a diameter-to-depth ratio of 1:5 (aspect ratio)

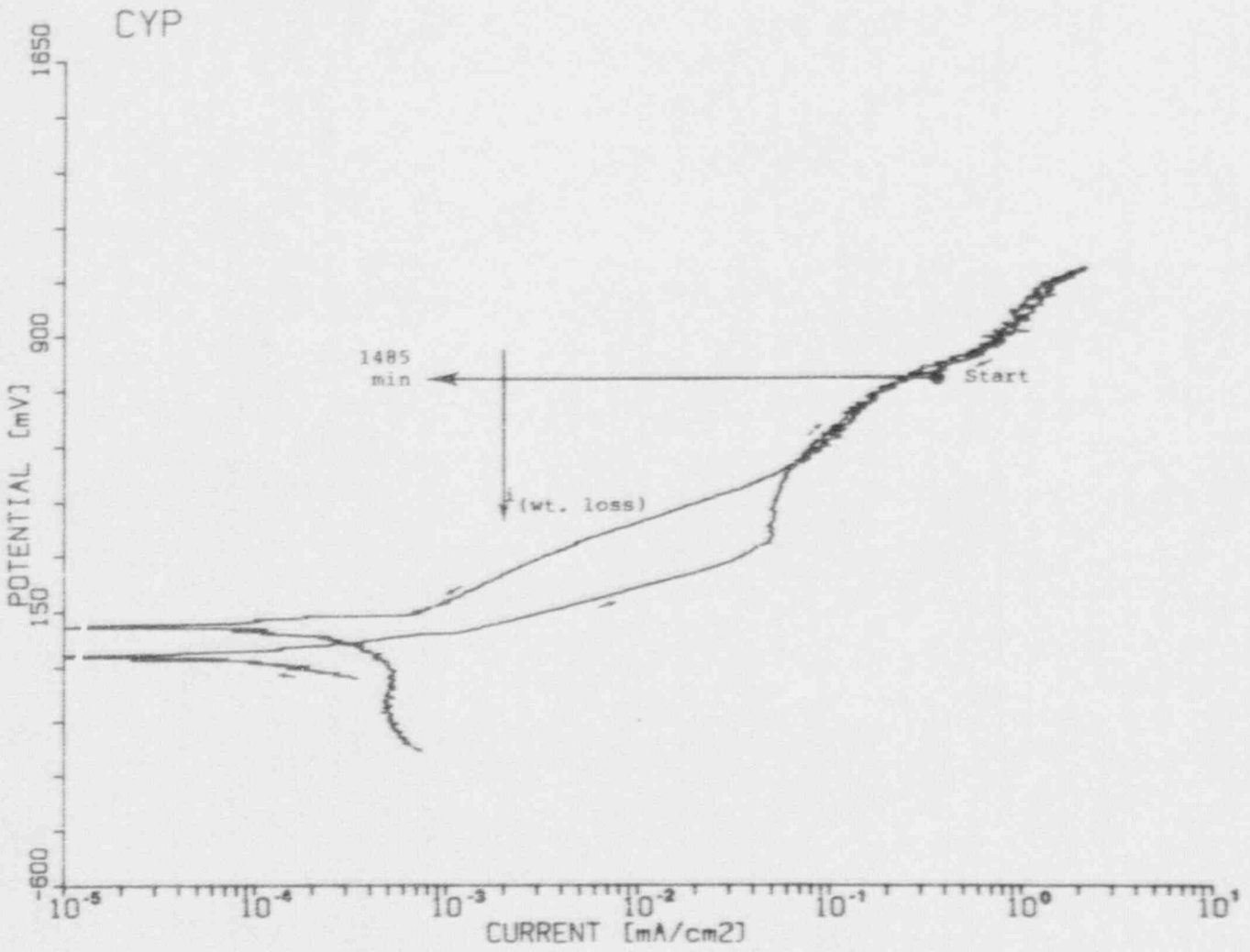

Figure 3.9 Cyclic Potentiodynamic Polarization And Potentiostatic Data For Alloy 825 In Solution No. 4 at 90°C Potentiostated On The Forward Scan To +800 mV (SCE) (No Pitting, No Attack In Potentiostatic Test).

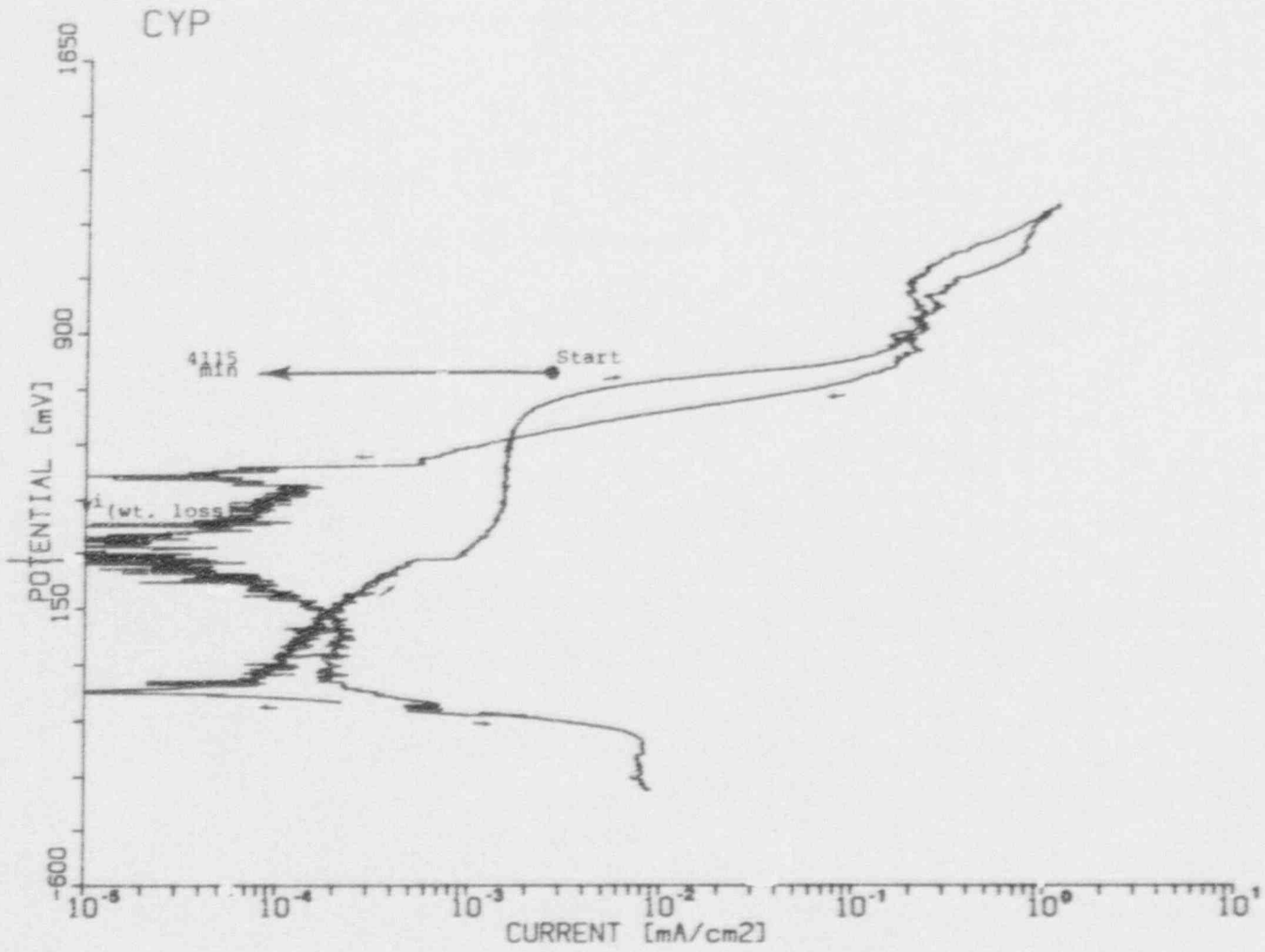

Figure 3.10 Cyclic Potentiodynamic Polarization And Potentiostatic Data For Alloy 304L In Solution No. 2 At 50°C Potentiostated On The Forward Scan To +798 mV (SCE) (No Pitting, Slight Tarnishing In Cyclic Potentiodynamic Polarization Test).

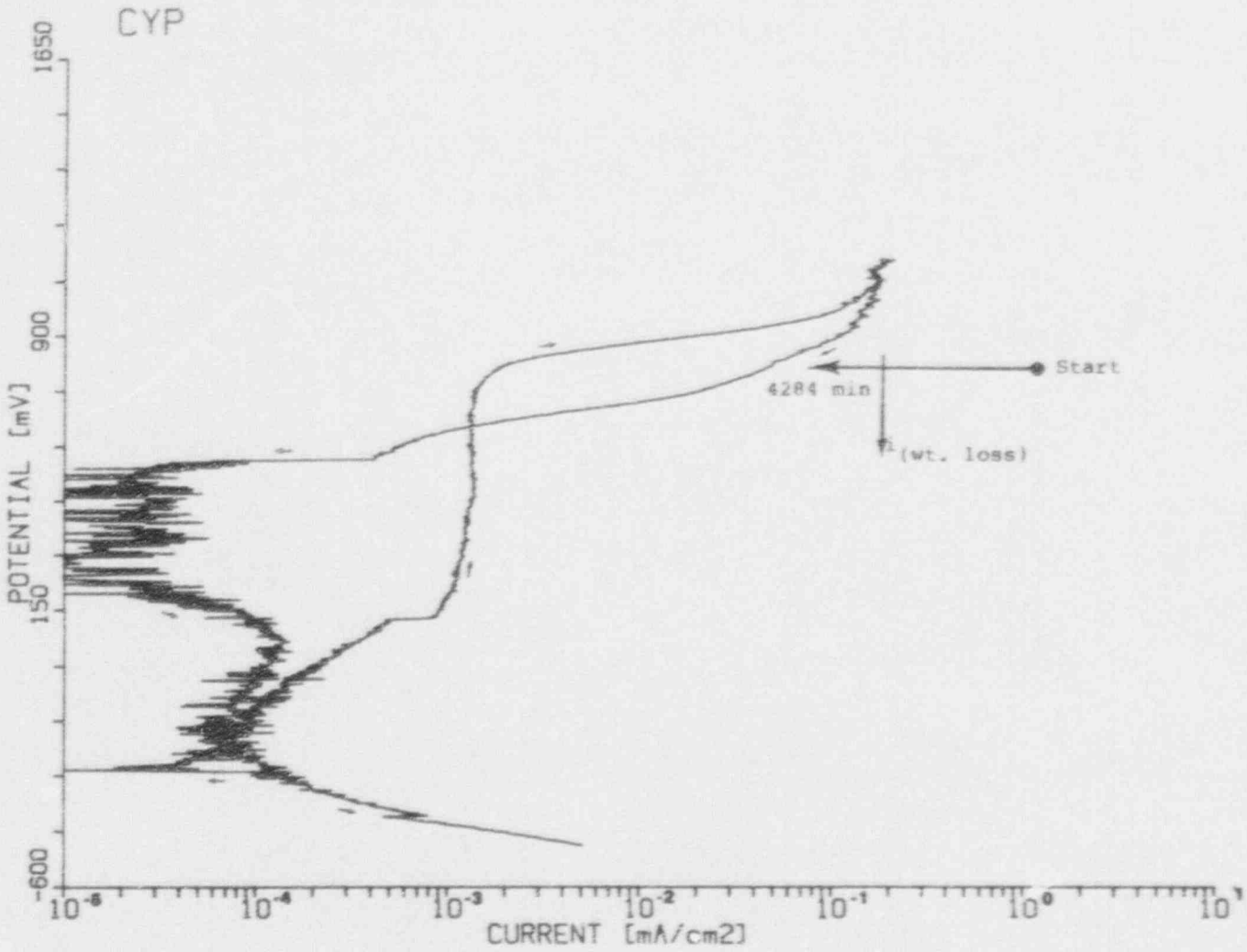

Figure 3.11 Cyclic Potentiodynamic Polarization And Potentiostatic Data For Alloy 304L In Solution No. 15 At 50°C Potentiostated On The Reverse Scan To +800 mV (SCE) (Severe Pitting And Crevice Attack In Potentiostatic Test).

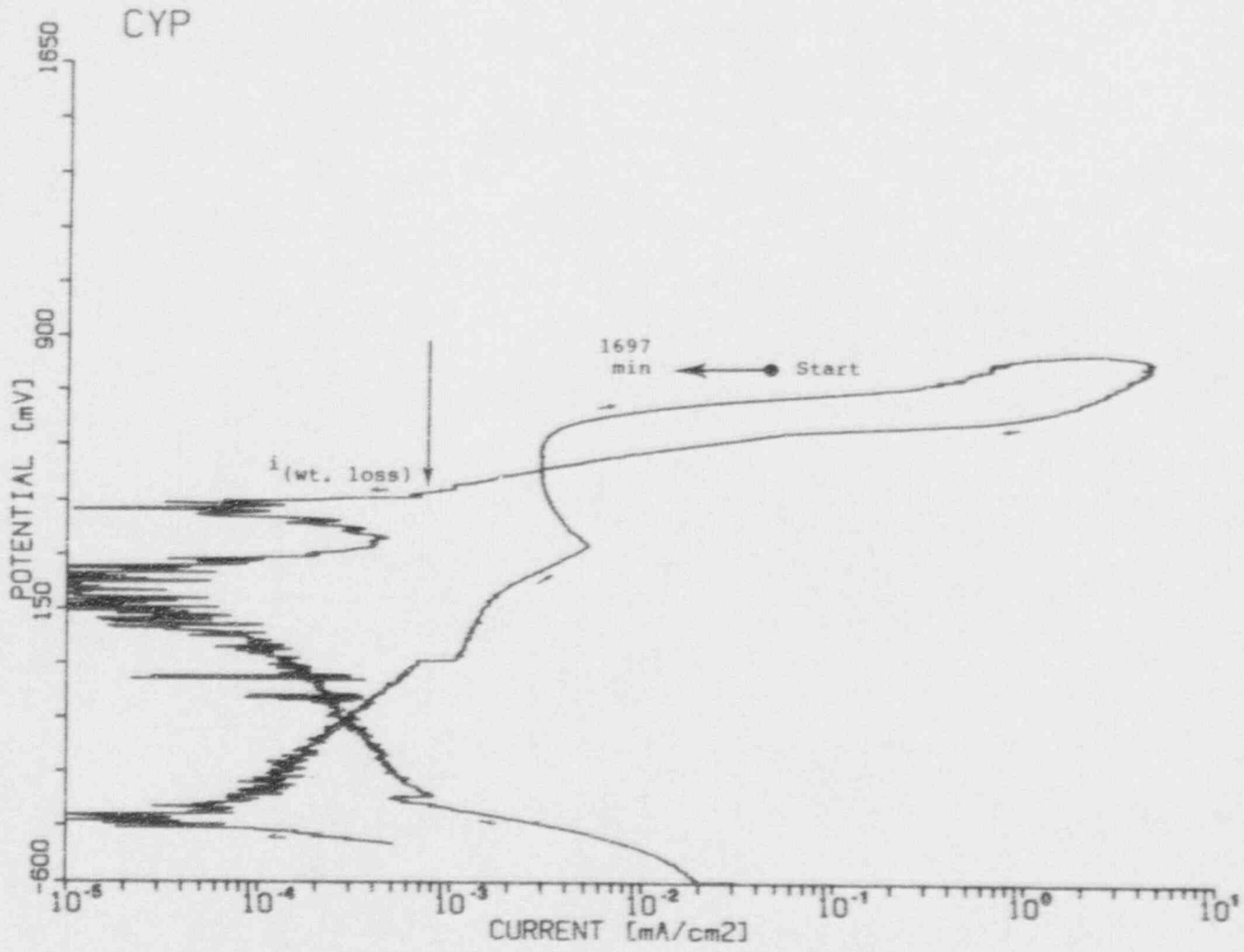

Figure 3.12 Cyclic Potentiodynamic Polarization And Potentiostatic Data For Alloy 825 In Solution No. 6 At 90°C Potentiostated On The Forward Scan To +800 mV (SCE) (Crevice Attack In Potentiostatic Test).

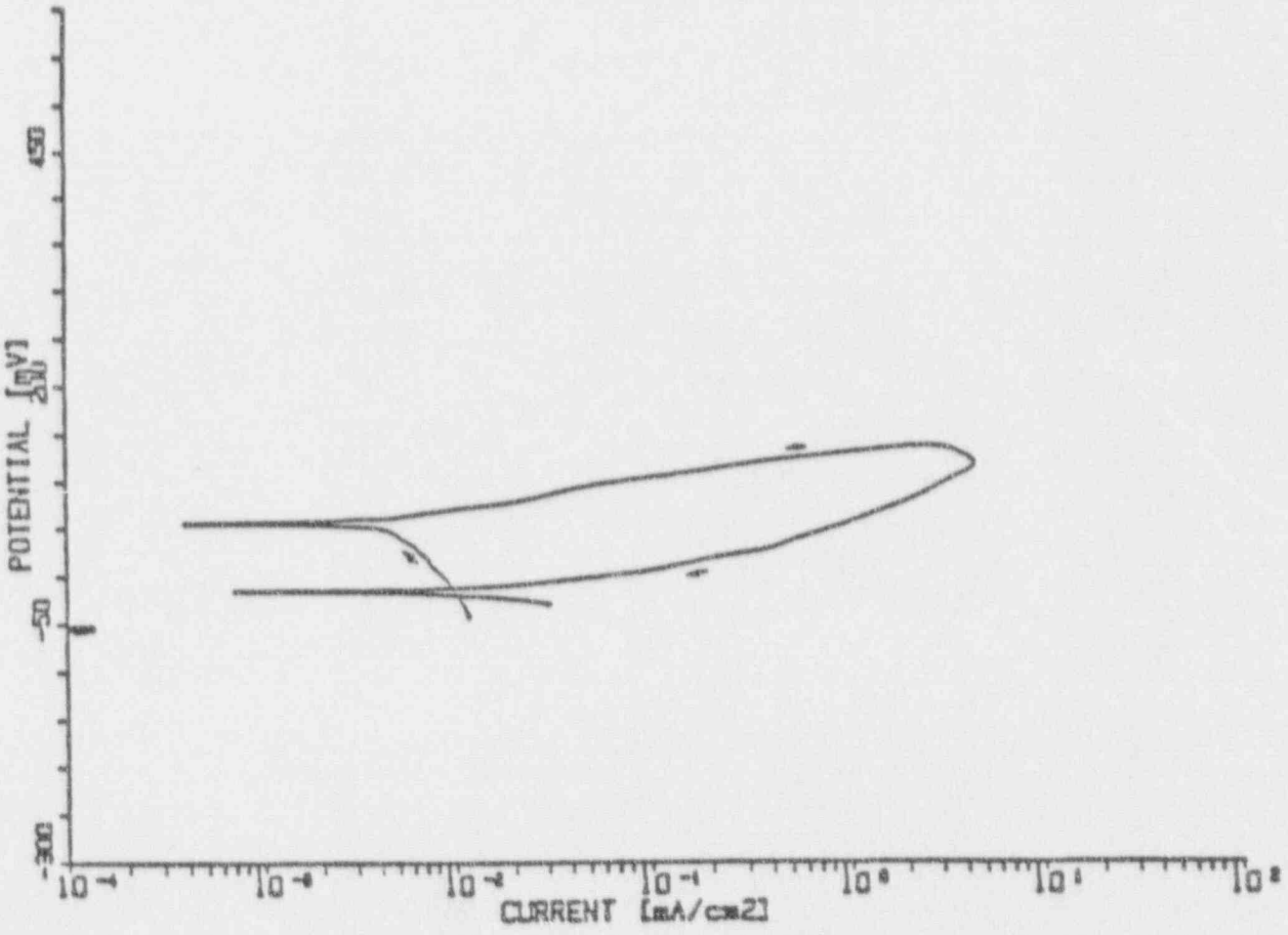

Figure 3.13 Cyclic Potentiodynamic Polarization Curve For Alloy CDA 102 In Test Solution No. 22 At 50°C.

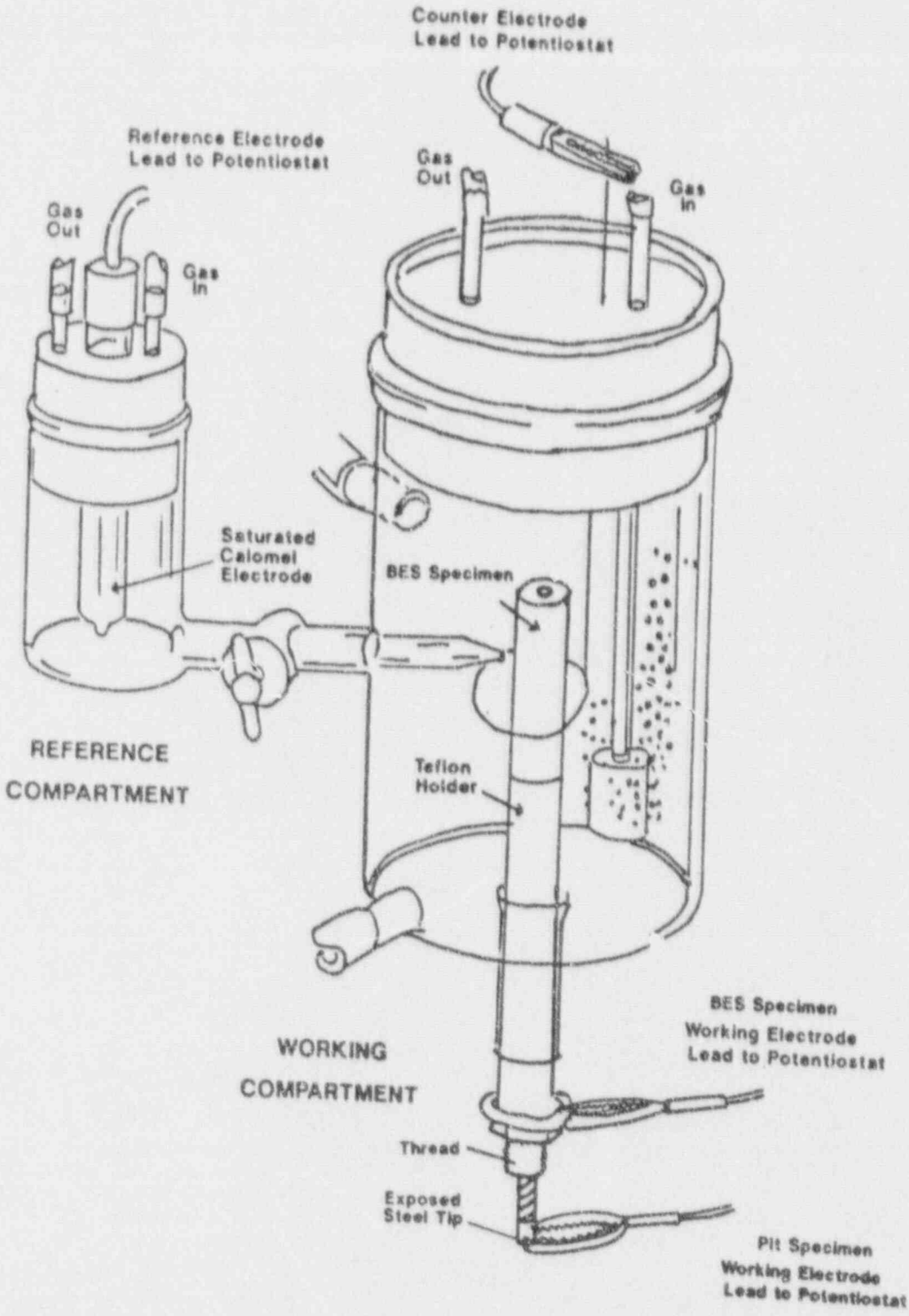

Figure 3.14 Electrochemical Cell Used For Pit-Propagation Testing.

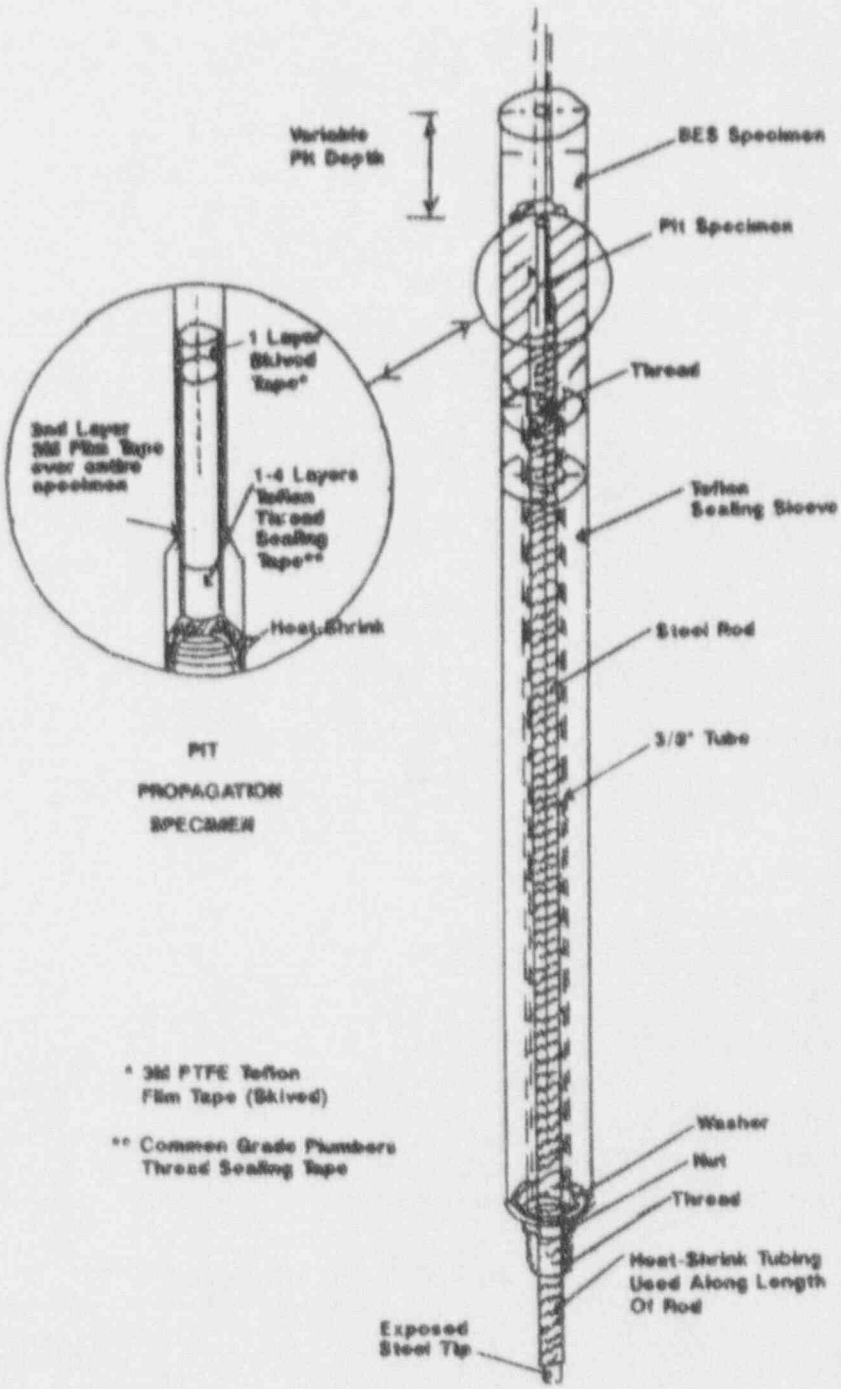

Figure 3.15 Schematic Diagram Of the Pit-Propagation Specimen Assembly Used In Task 4.

for most of the experiments. An aspect ratio of 1:5 is considered to be an extremely deep pit and was used to bound the pit depth parameter.

In all but one experiment, the pit cavity was filled with a corrosion product paste to create an occluded cell and accelerate the pit-initiation process. The corrosion product paste was produced by anodically polarizing an electrochemical specimen of Alloy CDA 102 +200 mV from the free-corrosion potential in Solution Number 22 at 50°C for forty-eight hours. The corrosion products were filtered from the test solution and dried. Just prior to each experiment, the dry corrosion product (or cuprous oxide, as used in one experiment) was mixed with Solution Number 22 to form a paste. This paste was packed into the pit cavity. Excess paste was removed from the top of the BES specimen with distilled water and a cotton swab.

The specimen assembly was inserted through the bottom of a glass electrochemical cell (Figure 3.14) and sealed with heat-shrink tubing. The test cell was filled with the electrolyte and deaerated with nitrogen for twenty-four hours to fully deaerate the pit while heating to 90°C. During this time, the pit and BES specimens were electrically uncoupled. After twenty-four hours, an atmosphere of 95% N_2 + 5% O_2 was introduced into the cell. The potential of each specimen was measured with respect to a saturated calomel electrode coupled (SCE) and both the pit and BES specimens were electrically coupled through a Zero Resistance Ammeter (ZRA). During the experiments, the BES specimen was exposed to the test electrolyte while the galvanic current flow between the pit and BES specimen was monitored continuously through a ZRA and recorded on a strip chart or data acquisition system. Each day, the coupled potential was measured with respect to a calomel reference electrode. Periodically, the pit and BES specimens were uncoupled and the corrosion potential of each specimen was measured with respect to a calomel reference electrode.

In each of the experiments, the potential of the pit was more positive than the potential of the BES specimen initially, and the coupled current reflected this polarity. In an attempt to initiate and propagate pitting, 200 ppm hydrogen peroxide (H_2O_2) was added to the electrolyte. Hydrogen peroxide was chosen as it has been established as a radiolysis product that may occur in the Tuff Repository. In several of the experiments, the pit specimen was cathodically polarized or the BES specimen anodically polarized to maintain the potential difference. With each of the H_2O_2 additions, a rapid decline in potential occurred as the H_2O_2 degraded.

At the conclusion of the first experiment, the potential distribution down the pit cavity was measured with a microcapillary Luggin probe. Gravimetric measurements and optical examinations were performed on both the pit and BES specimens following all of the experiments with the exception of the test using the cuprous oxide paste.

Weight losses on the specimens were measured using the interval weight-loss procedure described in ASTM G-1. This technique involved the alternate descaling of the specimen in an inhibited acid and weighing until the visible corrosion products were removed. Weight loss was plotted as a function of descaling time as shown schematically in Figure 3.16. Generally, the specimen weight changed rapidly as the scales were removed but much more gradually when only metal was removed. This behavior is exhibited graphically as a change in slope to the y-axis, as shown in Figure 3.16. As a verification of the technique, an unexposed control specimen was included in all descaling measurements. The true weight losses were then converted to corrosion rates, in μm/yr, by dividing the weight loss by the density, the specimen surface area

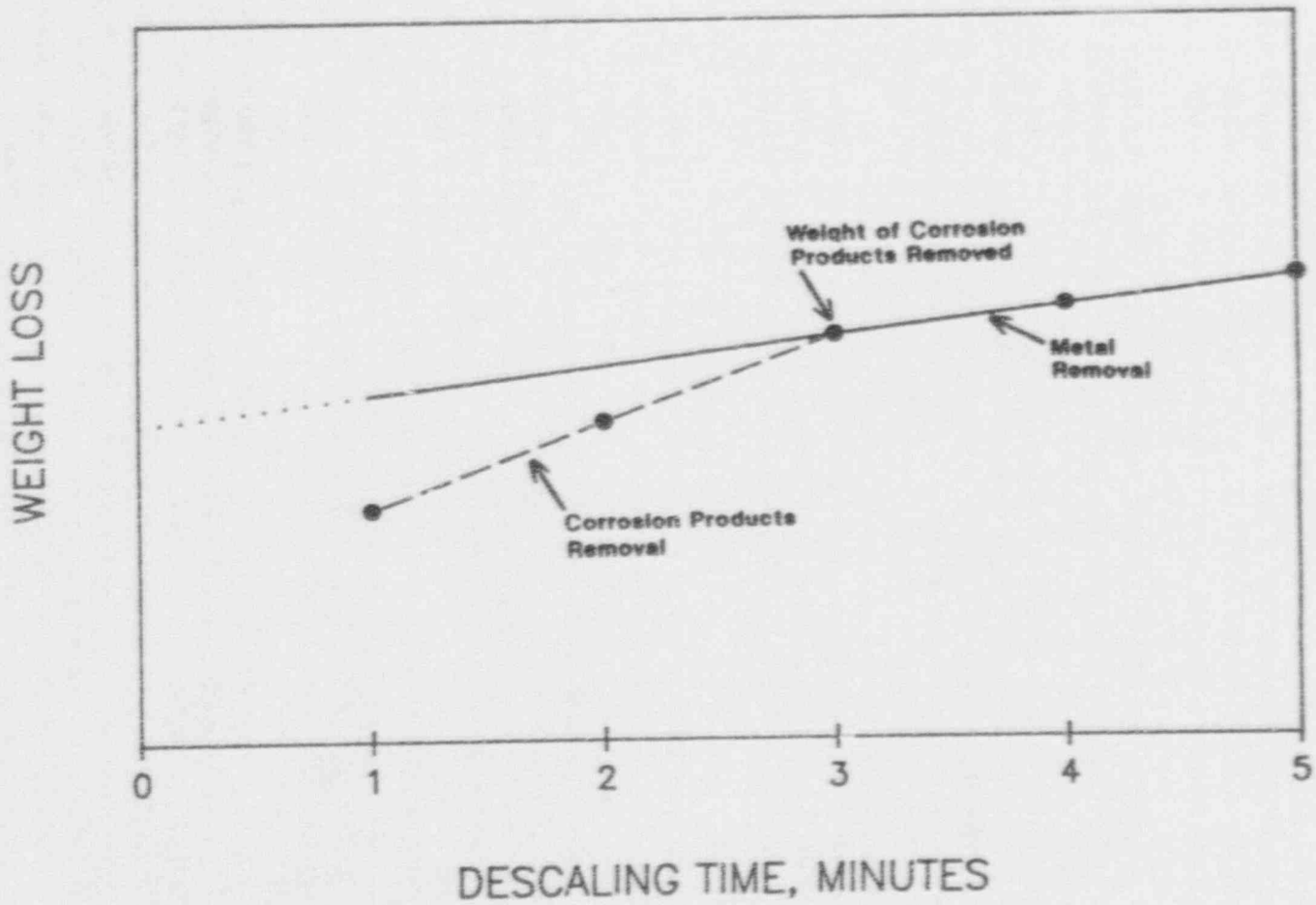

Figure 3.16 Schematic Showing Weight Change As A Function Of Descaling Time For Test Specimen.

and the test time and converting the units. This corrosion rate was then compared to the corrosive rate as a result of galvanic coupling.

3.2.2 Results

A summary of all four of the pit-propagation experiments performed with Alloy CDA 102 exposed to 90°C Solution Number 22 is illustrated in Table 3.5. A discussion of each of these experiments is presented in further detailed below. The initial two tests were performed to verify the experimental set-up and procedures and to help identify an appropriate packing paste.

In Test No. 1, a pit diameter of 3.18 mm set at a depth of 15.9 mm gave a diameter-to-depth ratio (aspect ratio) of 1:5. The resulting pit cavity was filled with the corrosion product paste described above. Prior to coupling the specimens through a ZRA, the potentials of the pit and BES specimens were measured. The potential of the pit (-28 mV (SCE)) was found to be more positive than the potential of the BES specimen (-154 mV (SCE)). The coupled current later reflected this polarity which suggested that the BES specimen was corroding preferentially to, and reducing the corrosion rate of the pit specimen. However, the coupled currents were small, approximately 0.3 μA.

Over the next seventy-two hours, the galvanic current flow was monitored and, periodically, the pit and the BES specimen were uncoupled and the potential of each specimen was measured. During this period, the potential of the BES specimen shifted in the noble direction, while the potential of the pit shifted in the negative direction, reducing the potential difference between the two specimens. However, the relative polarity of the specimens remained the same and the galvanic current remained very low. This behavior suggests that, in the absence of hydrogen peroxide (H_2O_2), the pit did not propagate in this experiment.

After three days of testing, 200 ppm H_2O_2 was added to the electrolyte. The H_2O_2 addition produced an anodic current peak which decreased as the H_2O_2 decayed over the subsequent few hours. Hydrogen peroxide was added daily for the next seven days and similar behavior was observed. A typical current transient is given in Figure 3.17. After each of the H_2O_2 additions, the current became slightly negative by the subsequent day and the uncoupled potentials also indicated that the pit specimen was slightly more noble than the BES specimen.

Prior to the last H_2O_2 addition, and at the conclusion of the test, a microcapillary was placed down the pit and the potential gradient was measured with the pit and BES specimen coupled. Figure 3.18 illustrates the coupled potential gradient as a function of pit depth both before and after the addition of H_2O_2. These data shows that, in the presence of H_2O_2, a 100 mV (SCE) potential gradient existed down the pit; whereas, no gradient existed prior to the addition of H_2O_2. The presence of the gradient indicated that significant current was flowing from the pit following the H_2O_2 addition. The noble shift in the potential value between the two plots at the base of the pit (12 mm depth data) in Figure 3.18, indicates the extent that the pit was anodically polarized by the H_2O_2 addition. The first pit-propagation test was terminated after 404 hours of exposure and gravimetric measurements were performed. The results of the measurements and the optical examination data are given in Table 3.5. These data indicated general corrosion rates of 205 μm/y and 19.9 μm/y for the pit and BES specimens, respectively. The high corrosion rate of the

Table 3.5 Summary Of Results Of Pit-Propagation Tests Performed With Alloy CDA 102 Exposed To Solution No. 22 At 90°C In An Atmosphere Of 95% N_2 + 5% O_2.

Test №	Aspect Ratio	Packing Paste	Test Duration Days	General Procedure	Specimen	Corrosion Rate * µm/y	Post-Test Description
1	1:5	Corrosion Product	17	· Record galvanic current for 3 days · Add 200 ppm H_2O_2 daily after 3 days. · Record potential gradient down pit at 16 days in absence of H_2O_2. · At 17 days add 200 ppm H_2O_2 and record potential gradient down pit.	Pit	205	Tip covered with black oxide, sides tarnished.
					BES	19.9	Outside tarnished. Bright red and orange coloration inside cavity.
2	1:5	Cuprous Oxide	16	· Record galvanic current for 8 days. · Add 200 ppm H_2O_2 on 9th day. · After potential declined and stabilized (H_2O_2 degraded), pit potentiostated to -800 mV over a period of 2 hours. Potential held for 16 hours. · After 16 hours, disconnect potentiostat, monitor potential. · Add 200 ppm H_2O_2 daily for duration of test.	Pit	Not Measured	Tip still shiny. No attack.
					BES	Not Measured	Outside covered with thin oxide film. Inside showed no attack.
3	1:5	Corrosion Product	50	· Record galvanic current for 1 day · Cathodically polarize the pit to -500 mV after 1 day for 24 hours. · Continue to monitor galvanic current for 8 days. · After 11 days of exposure, add 200 ppm H_2O_2 daily for the next 18 days. · After 28 days of exposure, anodically polarize BES specimen +50 mV daily until > E_{pp}. · Hold BES potential at +150 mV for 3 days. · Monitor galvanic current for 9 days.	Pit	42.3	Tip heavily etched with a few shallow pits.
					BES	8.0	Outside lightly etched with localized tarnishing and moderate etching. Top surface was heavily etched. Inside showed shallow pit-like areas.
4	1:2	Corrosion Product	20	· Record galvanic current for 4 days. · After 4 days, anodically polarize BES specimen in 50 mV increments, allowing the current to stabilize between steps. · Hold BES potential at +180 mV for 3 days. · Monitor galvanic current for 2 days before termination of the experiment.	Pit	286	Packing paste deep red rather than blue-green. Tip was heavily etched and deeply pitted.
					BES	41	Outside was lightly etched. Top surface was heavily etched. Inside showed deep pits.

*Based on weight-loss measurements.

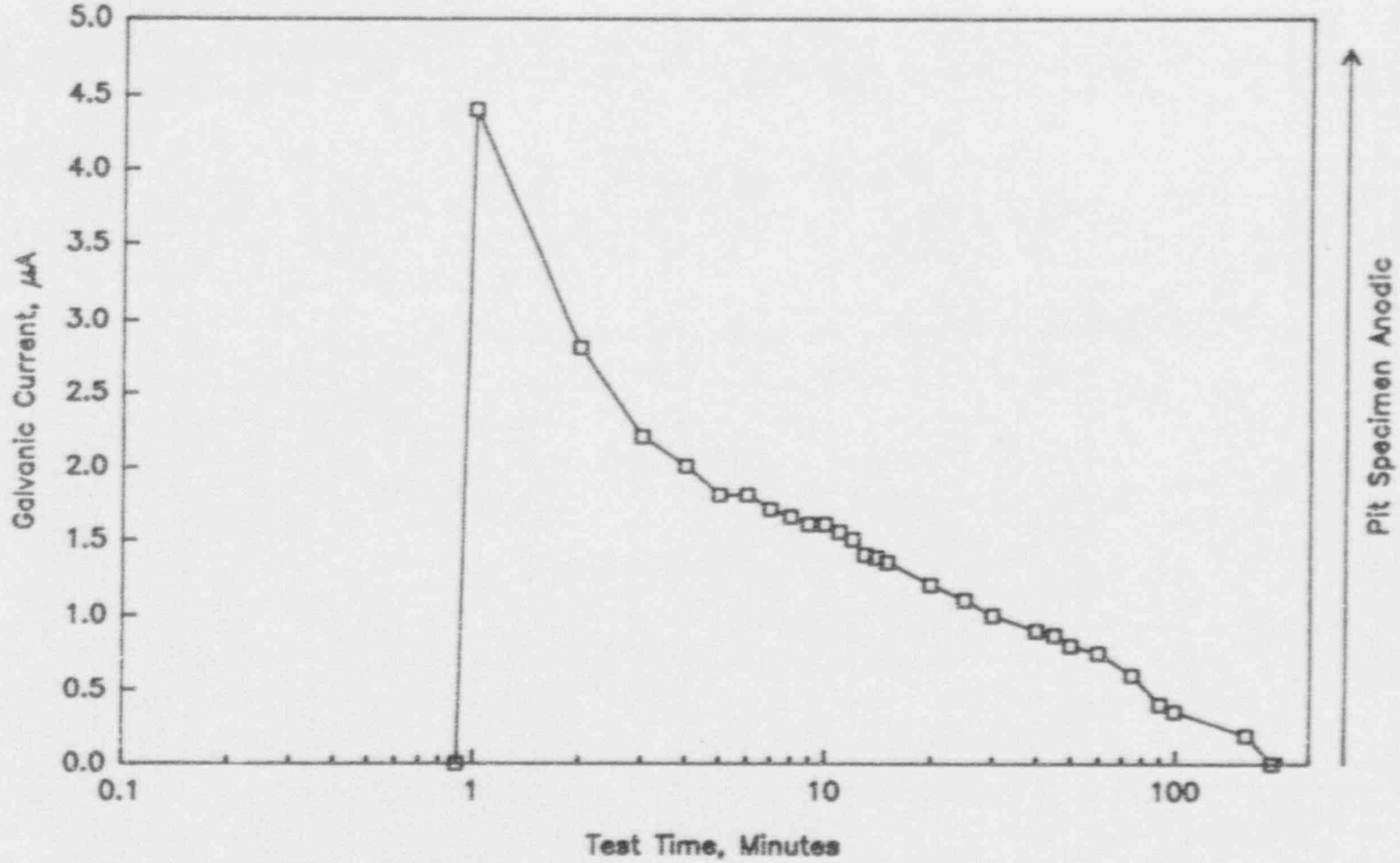

Figure 3.17 Typical Anodic Current - Time Transient Following Addition of H_2O_2 For Alloy CDA 102 In Solution No. 22 At 90°C With An Aspect Ratio of 1:5 (384 Hours Of Exposure) (Test #1).

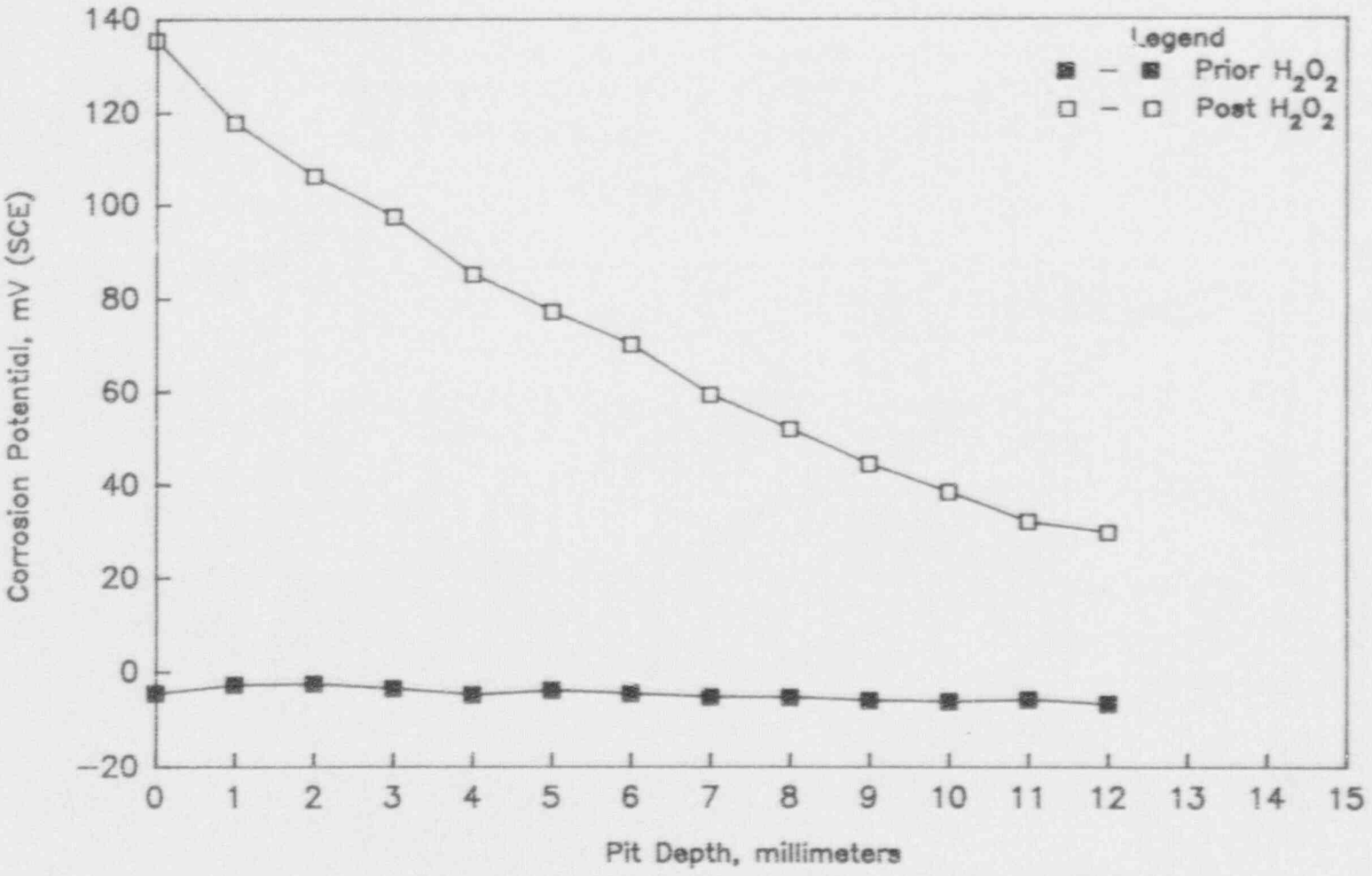

Figure 3.18 Potential Of The Coupled BES And Pit Specimens Measured As A Function Of Depth Down The Pit For Alloy CDA 102 In Solution No. 22 At 90°C.

pit was consistent with the large anodic current transients observed with the ZRA and demonstrates the role of H_2O_2 in promoting and accelerating pit propagation.

The second pit-propagation experiment with Alloy CDA 102 also was performed in Solution Number 22. In this test, the 1:5 aspect ratio was retained, but a packing paste of reduced copper oxide (cuprous oxide, Cu_2O) mixed with the test electrolyte was used. The Cu_2O was chosen to simulate the corrosion product in a reduced state. At the time, the assumption was that the paste used in the first experiment may have been too oxidizing, and prevented the pit from propagating in the absence of H_2O_2.

Initially, the potential of the BES specimen (-147 mV (SCE)) was more negative than that of the pit specimen (-116 mV (SCE)). For the first eight days of the experiment, the potential of the BES specimen remained more negative and the galvanic current was not measurable. In an attempt to promote pit propagation, the pit was cathodically polarized to -800 mV, with respect to the BES specimen, for approximately 16 hours. Upon recoupling the specimens, the galvanic current produced an initial transient which rapidly dropped back to a low current of 0.02 μA. The equivalent of 200 ppm H_2O_2 was added to the electrolyte daily over the next seven days, but had an insignificant effect on the galvanic current. The test was terminated after 16 days.

Optical examination of the specimens following the exposure revealed no evidence of attack of the pit or BES specimens. The Cu_2O packing paste was dry and powdery inside of the pit cavity at the end of the test. The hydrophobic nature of the Cu_2O resulted in a very hard, dry paste which effected a very high resistance and ultimately inhibited galvanic current flow.

The third pit-propagation experiment with Alloy CDA 102 was performed in Solution Number 22 with the 1:5 aspect ratio. The corrosion product paste originally used in the first experiment was used. As before, the initial potential of the BES specimen (-47 mV (SCE)) was more negative compared to that of the pit specimen (+4.0 mV (SCE)). After deaerating the solution for 24 hours, the pit was cathodically polarized -500 mV with respect to the BES specimen for almost 24 hours in an attempt to reverse the polarity. This procedure was effective initially, but, within three days the galvanic current reversed polarity. This behavior indicated that the BES specimen had again become more negative in potential. The galvanic current also decreased rapidly after the pit specimen was removed from the potentiostat and coupled through to the ZRA. Galvanic currents remained very low (0.007 μA) over the next eight days in the absence of H_2O_2, which indicated that, in the absence of H_2O_2, the pit did not propagate.

After 11 days of testing, the equivalent of 200 ppm H_2O_2 was added to the test electrolyte to promote pit propagation. The H_2O_2 produced an anodic peak which decayed over the subsequent few hours. Hydrogen peroxide was added daily for the next 18 days and similar behavior was observed. As in the first experiment, the galvanic current returned to near zero in a relatively short period of time. This behavior suggested that the oxidizing power of the H_2O_2 was insufficient to sustain pit propagation over long periods of time because of its rapid degradation.

The corrosion potentials of the pit and BES specimens were compared with the polarization parameters obtained from the cyclic-potentiodynamic-polarization curve previously illustrated in Figure 3.13. This comparison was made in an attempt to explain the current transient and pit-propagation behavior. Prior to each H_2O_2 addition, the corrosion potentials of both specimens were found to be below the breakdown potential, E_b (+60 mV (SCE)), and the repassivation, E_{rp}

(+20 mV (SCE)) for Alloy CDA 102 in Solution Number 22. Figure 3.19 illustrates the change in the coupled potential over time following an addition of H_2O_2. Daily additions of H_2O_2 only temporarily increased the coupled corrosion potential above E_b, but the potentials declined too rapidly to have any lasting effect.

In a final attempt to propagate the pit, the BES specimen was anodically polarized in 50 mV (SCE) increments daily until the coupled potential was well above E_b. After three days of potentiostatic polarization at +150 mV (SCE), the BES specimen was disconnected from the potentiostat. When the specimens were no longer polarized, the potentials and galvanic current again started to decrease, but with a more gradual decline as compared with the declines observed after H_2O_2 additions. No H_2O_2 was added during this final seven-day period. Figure 3.20 illustrates the effect of the potentiostatic polarization on the corrosion potential. Removal from the potentiostat is clearly visible in this figure by the immediate rapid decline in potential at 1658 hours and the subsequent tapering off over time.

Figure 3.21 illustrates the effect of potentiostatic polarization on the galvanic current. The sharp downward (anodic) spikes occurred as a result of the incremental polarization steps. The current declined rapidly after the first potential step. The second potential step from (0.0 mV (SCE) to 50 mV (SCE)), after 22 hours, caused the pit to propagate as illustrated by the sharply negative current values. The third potential step appeared to have little effect on pit propagation. The final increment in potential from (100 mV (SCE) to 150 mV (SCE)), which is above E_b, propagated the pit for some time before the currents started to decrease slightly. The very slow change in galvanic current following potentiostatic polarization (after 168 hours) suggested that the pit continued to propagate on its own, but eventually stopped after almost 400 hours.

The third pit-propagation experiment was terminated after 1197 hours of exposure. The results of the weight-loss measurements and optical examination data for both specimens was previously given in Table 3.5. The results of the measurements indicated corrosion rates of 42.3 µm/y and 8.0 µm/y for the pit and BES specimens, respectively. Optical examination revealed heavy etching and a few shallow pits on the top of the pit specimen. Very shallow pit-like areas were also visible inside the pit cavity. These data are consistent with the galvanic current measurement and indicate that pit propagation had occurred.

The fourth and final pit-propagation experiment with Alloy CDA 102 performed in Solution Number 22 used an aspect ratio of 1:2 to help evaluate the effects of pit depth on pit propagation. The pit cavity was filled with the corrosion product paste used in the previous experiment. As in the previous tests, the initial potential of the BES specimen (-155 mV (SCE)) was more negative than that of the pit specimen (-67 mV (SCE)). After approximately 90 hours of exposure, the BES specimen was anodically polarized in 50 mV increments from the coupled potential until the coupled potential was above E_b. The galvanic current was allowed to stabilize between each potential step. Figure 3.22 illustrates the effect of potentiostatic polarization on the corrosion potential. Removal from the potentiostat is clearly visible by the immediate drop in potential at 431 hours. Unlike in the previous test, the coupled potential dropped slightly below the voltage prior to potentiostatic polarization.

Figure 3.23 illustrates the effect of potentiostatic polarization on the galvanic current. The sharp downward (anodic) spikes occurred as a result of the incremental polarization steps. Each of these steps is illustrated by solid black symbols on the figure. The first and second potential

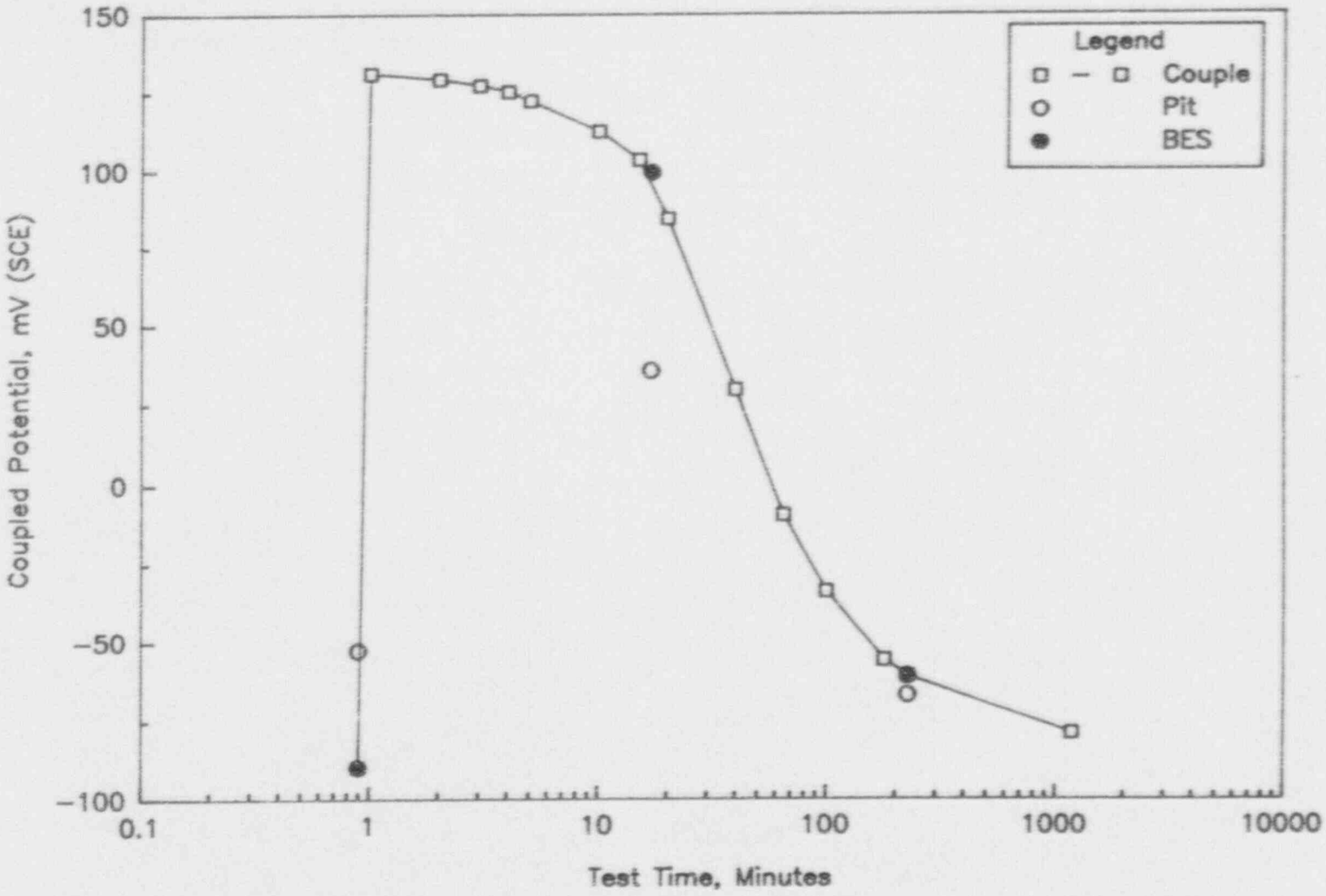

Figure 3.19 Typical Potential - Time Transient Following Addition of H_2O_2 For Alloy CDA 102 in Solution No. 22 At 90°C With An Aspect Ratio Of 1:5 (305 Hours Of Exposure) (Test #3).

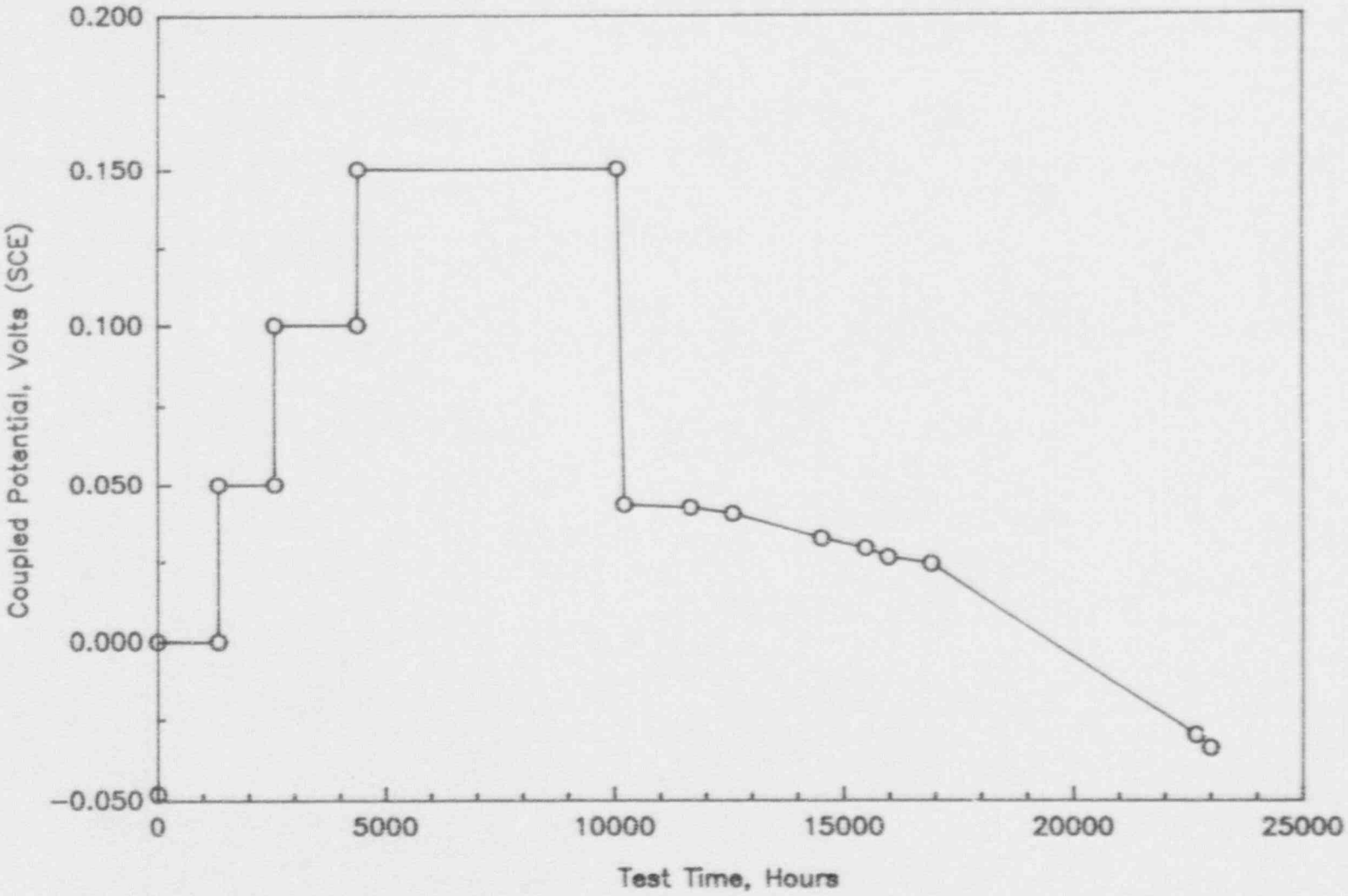

Figure 3.20 Coupled Potential As A Function Of Test Time Showing The Effects Of Anodically Polarizing The BES Specimen; Alloy CDA 102 In Solution No. 22 At 90°C With An Aspect Ratio Of 1:5. Potentiostatic Polarization Was Initiated After 896 Hours Of Exposure (Test #3).

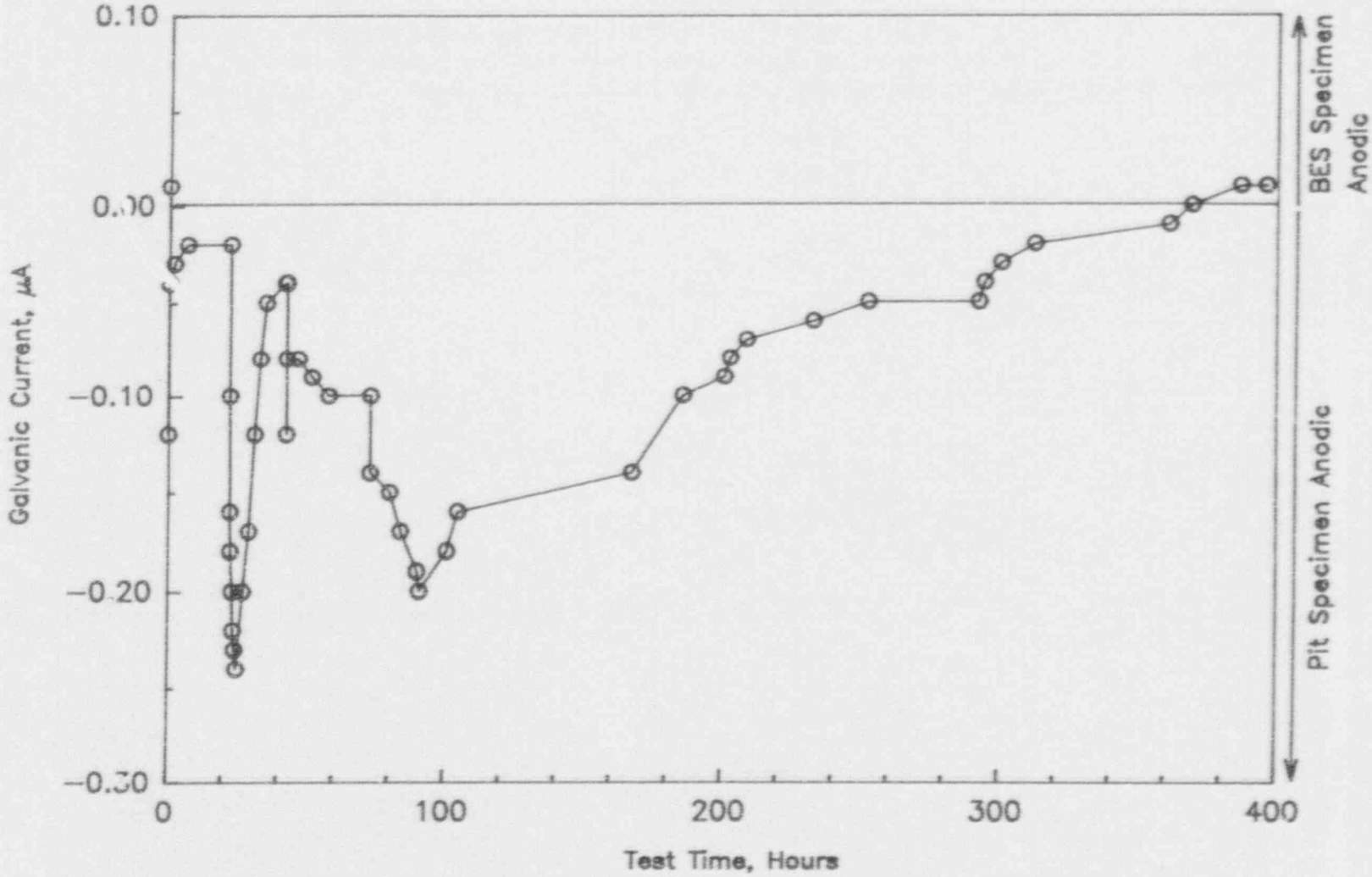

Figure 3.21 Galvanic Current As A Function Of Test Time Showing The Effects Of Anodically Polarizing The BES Specimen; Alloy CDA 102 In Solution No. 22 At 90°C With An Aspect Ration Of 1:5. Potentiostatic Polarization Was Initiated After 896 Hours Of Exposure (Test #3).

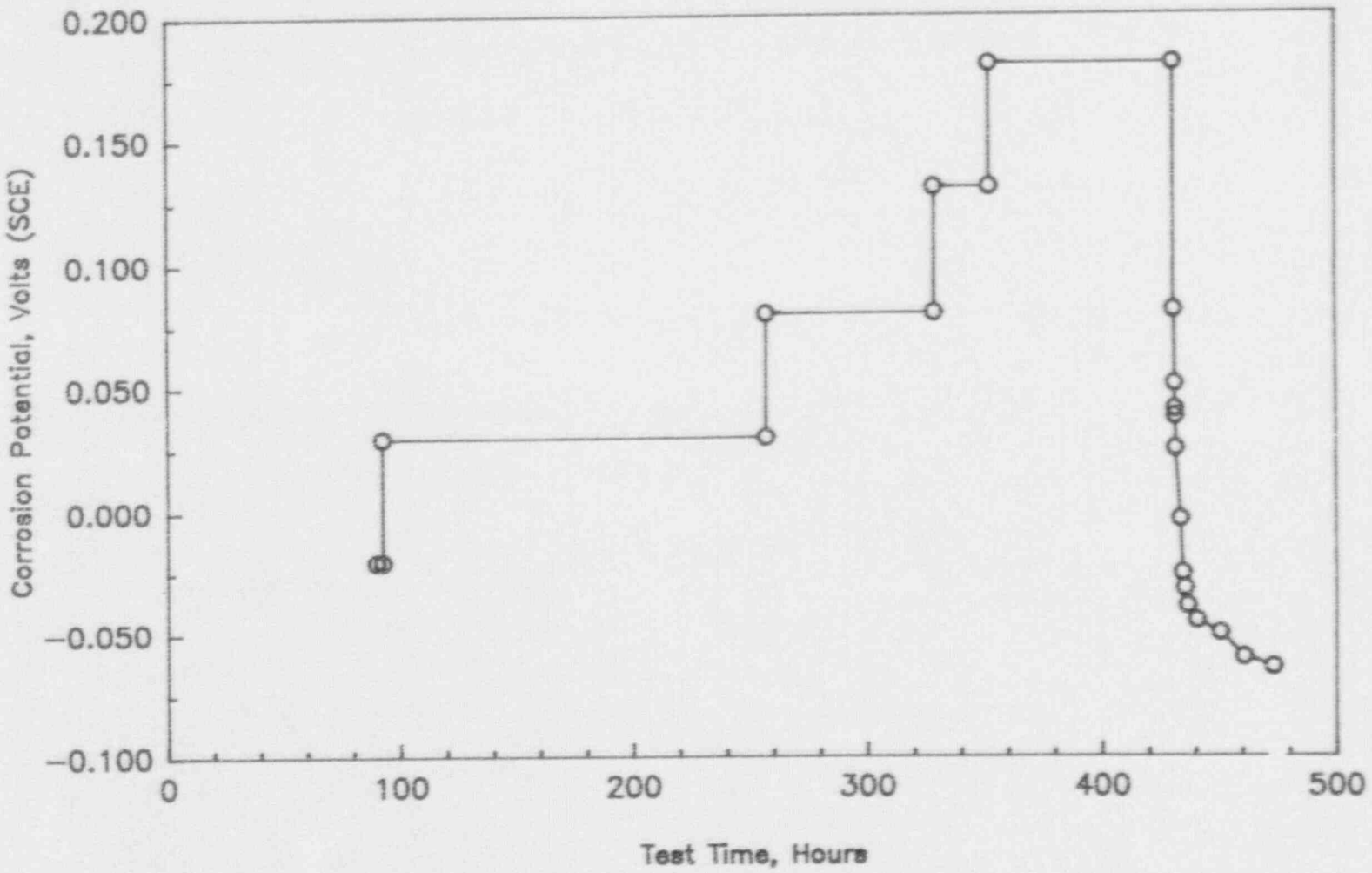

Figure 3.22 Coupled Potential As A Function Of Test Time Showing The Effects Of Anodically Polarizing The BES Specimen; Alloy CDA 102 In Solution No. 22 At 90°C With An Aspect Ratio Of 1:2 (Test #4).

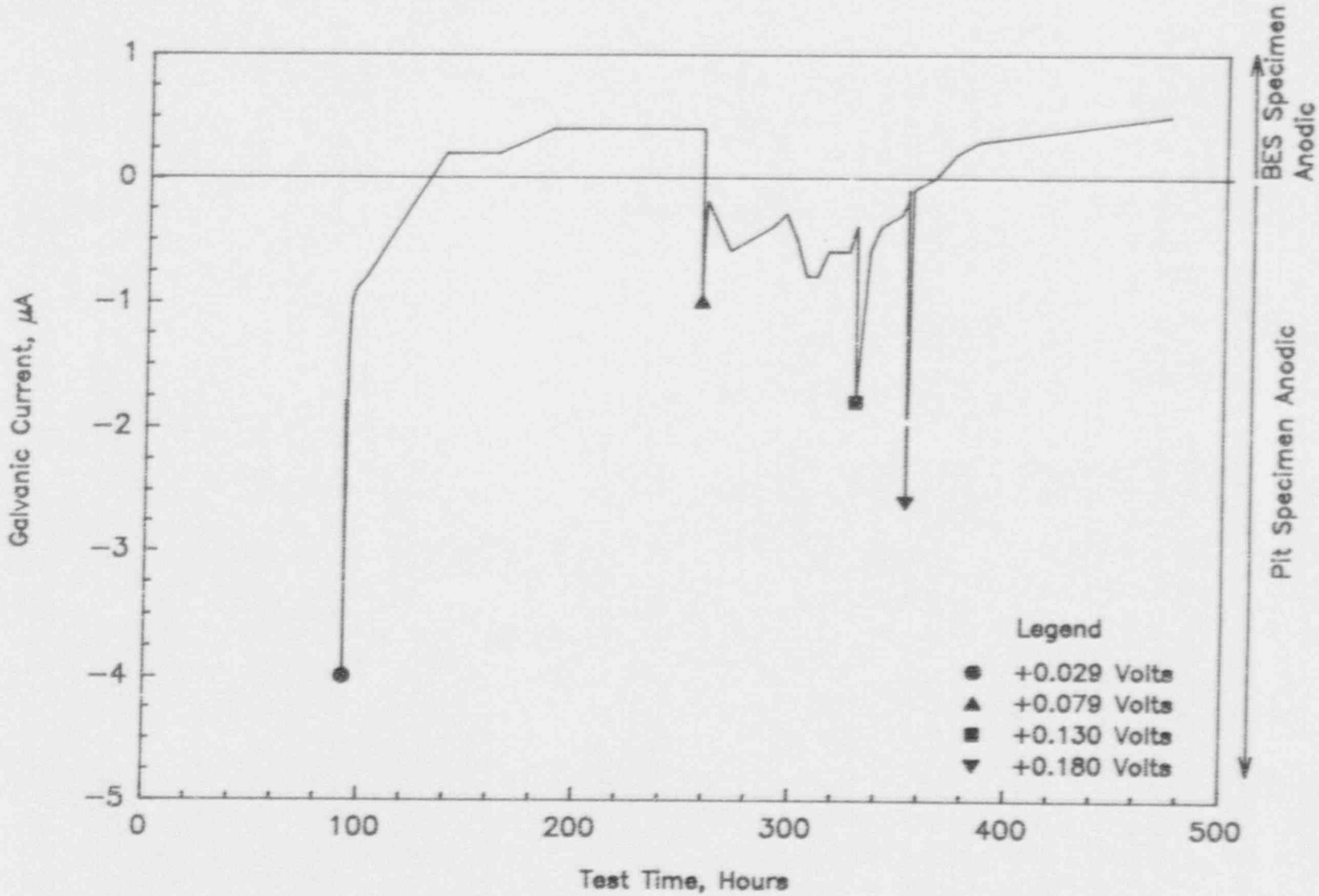

Figure 3.23 Galvanic Current As A Function Of Test Time Showing The Effects Of Anodically Polarizing The BES Specimen: Alloy CDA 102 In Solution No. 22 At 90°C With An Aspect Ratio Of 1:2 (Test #4).

steps caused the pit to propagate as shown by the very slow change and decline in the galvanic current over time. However, the third and fourth potential steps appeared to have little effect on pit propagation. Comparison of Figures 3.21 and 3.23 shows that, in the test having the shallower pit (1:2 aspect ratio), larger galvanic currents resulted from polarization than in the previous test which had the deeper pit. The potentiostatic current was also monitored and is presented in Figure 3.24. These data show that each positive potential step resulted in a transient anodic spike from the BES-pit couple.

The fourth pit-propagation experiment was terminated after 473 hours of exposure. The results of the weight-loss measurements and optical examination data for both specimens are given in Table 3.5. The results of the measurements indicated corrosion rates of 286 μm/y and 41 μm/y for the pit and BES specimens, respectively. The high corrosion rate for the pit is consistent with the large anodic current transients observed and optical examination of the specimens. The top surface of the pit specimen was heavily etched following the test. The BES specimen was heavily etched on the upper surface and showed deep pits inside of the pit cavity in the area exposed to the corrosion product paste.

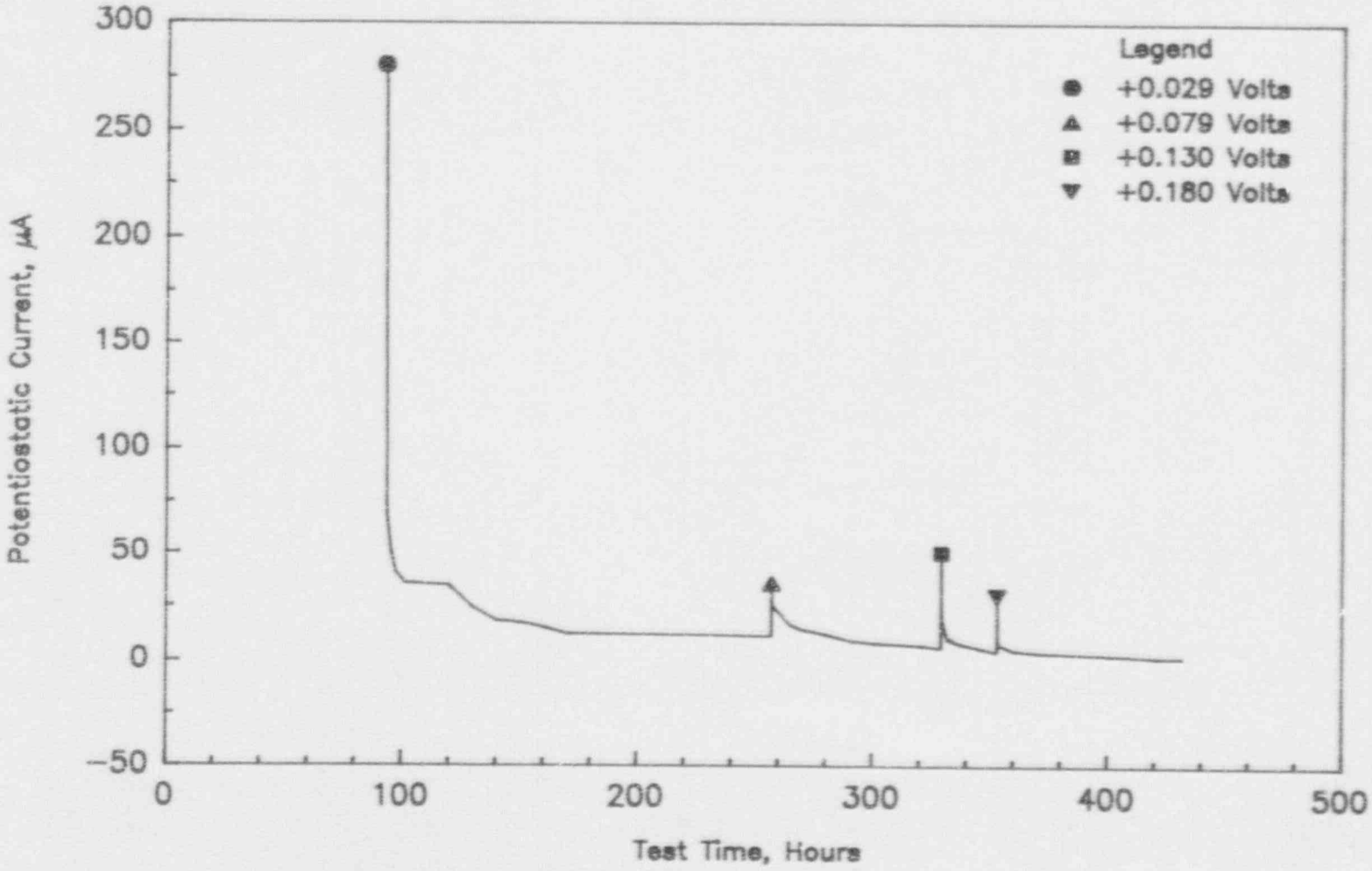

Figure 3.24 Potentiostatic Current As A Function Of Test Time For Alloy CDA 102 In Solution No. 22 At 90°C. Aspect Ratio Of 1:2 (Test #4).

4. GALVANIC-CORROSION STUDIES

Galvanic corrosion studies were conducted in Task 6 of the program. The purpose of these tests was to explore galvanic corrosion failure modes that are likely, according to current knowledge, to produce accelerated attack. This attack may lead to the premature failure of the waste container. Two modes of failure were identified for examination in this task: Thermogalvanic couples, and borehole liner-container interactions.

4.1 Thermogalvanic-Couples Experiments

For a single container, it is likely that a temperature differential will exist from one portion of the surface to another. This temperature differential will produce a potential distribution on the container surface that can result in a differential cell couple similar to a galvanic couple of dissimilar metals. This "thermogalvanic couple" may accelerate the corrosion rate of that portion of the container having the more negative potential. The focus of the subtask was to estimate the accelerating effect of thermogalvanic couples on the corrosion rate of Alloy CDA 102 and Alloy 304L. No thermogalvanic-couples experiments were performed with Alloy CDA 715 or Alloy 825. Cyclic-Potentiodynamic-Polarization curves for the alloy-environment systems examined in this task are given in Appendix E.

4.1.1 Experimental Approach

The thermogalvanic-couples experiments were performed in a glass electrochemical cell illustrated in Figure 4.1. In each of the experiments, an unheated (isothermal) specimen was electrically coupled to an internally heated (heat-transfer) specimen. A more detailed view of the heat-transfer specimen is illustrated in Figure 4.2. Each of the specimens was wet-abraded to 600 grit SiC, cleaned, measured, degreased, and weighed prior to testing. The heat-transfer specimen was inserted through the bottom of the electrochemical cell and sealed with heat-shrink tubing. The isothermal specimen was inserted through a port in the top of the cell. The test cell was filled with the electrolyte so that both specimens were entirely exposed to the solution to prevent vapor-phase attack from altering the results. The desired atmosphere was introduced into the test cell and the electrolyte was slowly heated to 80°C. The heat-transfer specimen was internally heated to 90°C by a cartridge heater.

The potential of each specimen was measured with respect to a saturated calomel electrode (SCE) and both specimens were electrically coupled through a ZRA. After approximately 24 hours of exposure, the temperature of the electrolyte was lowered 10°C. The temperature of the electrolyte continued to be lowered by 10°C every one to two days until a final temperature of 50°C to 55°C was reached. The heat-transfer specimen was maintained at 90°C during this time. The galvanic current density as a function of temperature differential was measured continuously by a strip-chart recorder or a data acquisition system.

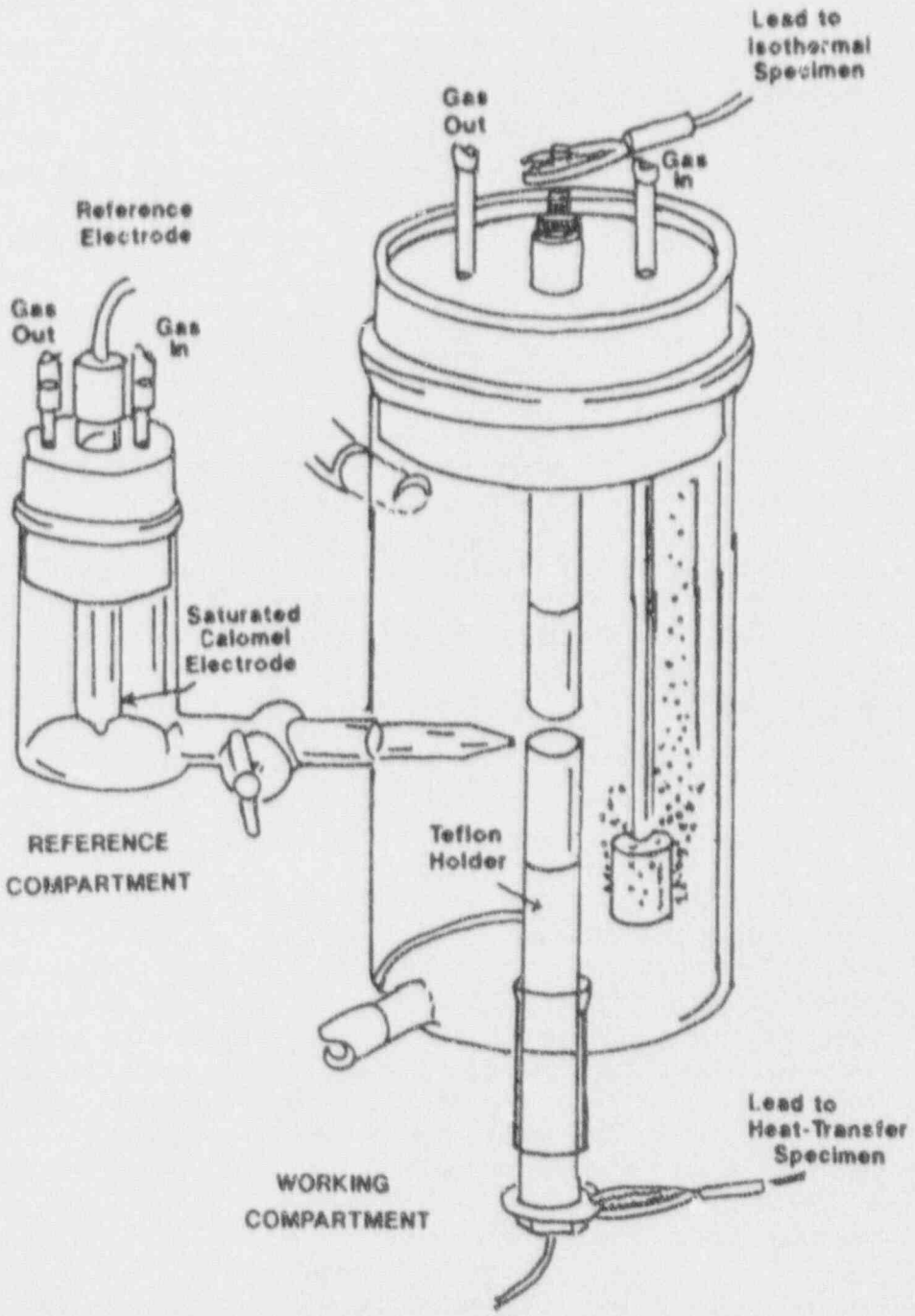

Figure 4.1 Electrochemical Cell Used For Thermogalvanic Couples Experiments.

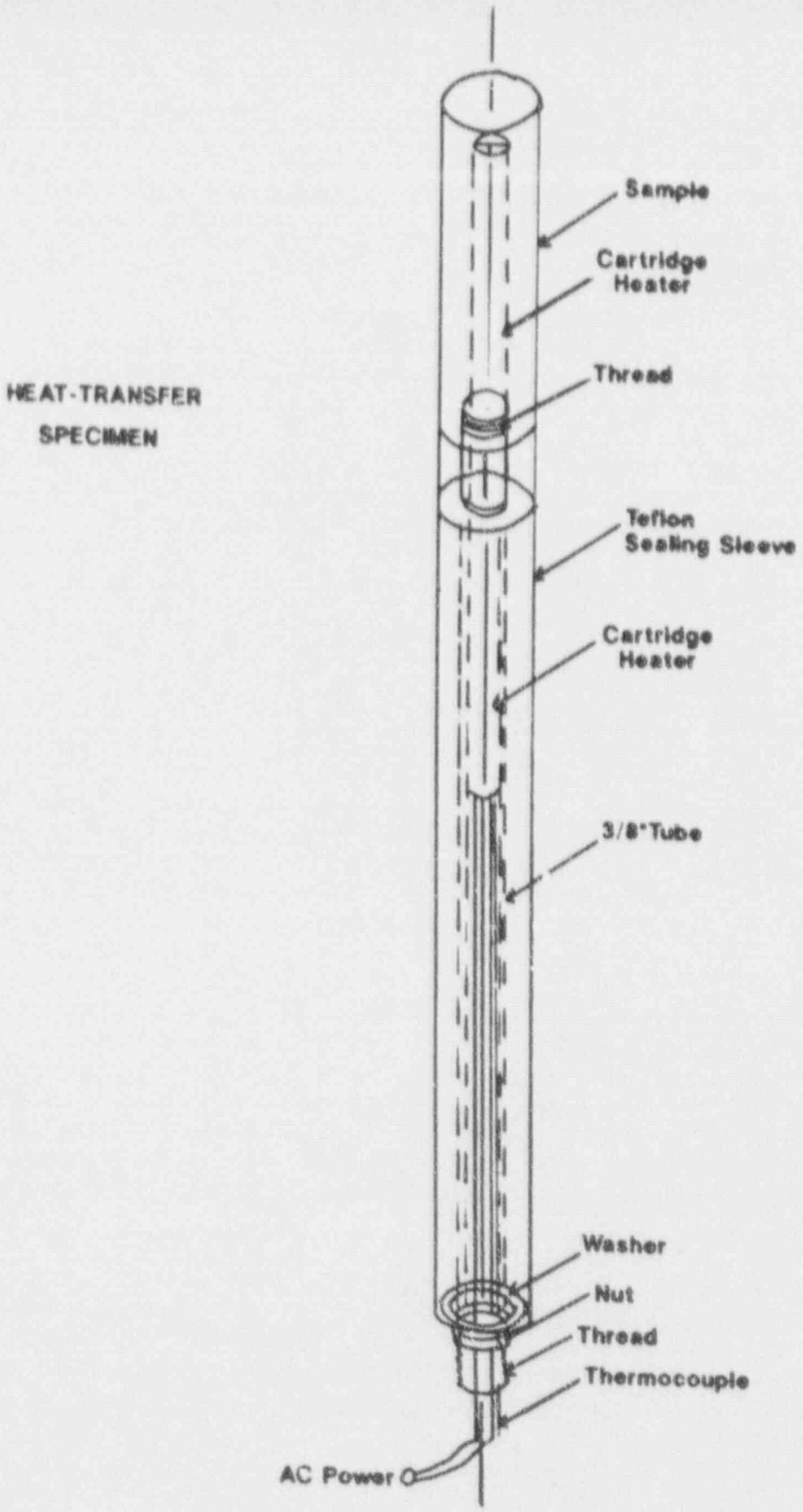

Figure 4.2 Schematic Diagram Of The Heat-Transfer Specimen Assembly Used In Task 6.

During the experiment, the coupled current flow was measured continuously. Each day, the coupled potential was measured with respect to a calomel electrode. Periodically, the two specimens were uncoupled, and the corrosion potential of each specimen was measured with respect to a calomel electrode.

After one week of exposure, daily additions of 200 ppm hydrogen peroxide (H_2O_2) were begun and the changes in potential were monitored. Near the end of the tests, the specimens were uncoupled and the polarization resistance (PR) of each specimen was measured both before and after the addition of H_2O_2. In the actual PR measurements, the specimen potential was scanned between -20 mV (SCE) and +20 mV (SCE) of the free-corrosion potential and the ensuing current was monitored. The tangent to the E-i plot at the free-corrosion potential is the PR value. The PR value was corrected for ohmic potential drop in the solution between the tip of the Luggin probe and the specimen by means of an AC measurement technique.

The polarization resistance values were converted to corrosion rates using the Stern-Geary Equation;

$$i_{cor} = \frac{\beta_a \ \beta_c}{2.3 \ (\beta_a + \beta_c)} \ \frac{1}{PR} \qquad (4\text{-}1)$$

and Faraday's Law. The constants B_a and B_c are the anodic and cathodic Tafel slopes, respectively, which are linear portions of the potentiodynamic polarization curve. Since few polarization curves exhibit good Tafel behavior, our standard procedure is to obtain the Tafel constants by drawing tangents to the polarization curve at over-potentials of +75 and -75 mV from the free-corrosion potential. A typical analysis is shown in Figure 4.3. The polarization curves used were obtained from the Task 2 CPP studies.

At the conclusion of the experiments, gravimetric measurements and optical examinations were performed on both specimens. Weight losses on the specimens were measured using the interval weight-loss procedure described in ASTM G-1. This technique involved the alternate descaling of the specimens in an inhibited acid and weighing until the visible corrosion products were removed. The weight losses were then converted to corrosion rates, in µm/yr, by dividing the weight loss by the density, the specimen surface area and the test time and converting the units. These results were compared with the corrosion rates calculated from PR measurements and those as a result of galvanic coupling.

The coupled current provides a measure of the accelerated corrosion due to coupling and provides a measure of the total corrosion rate, depending on the amount of polarization provided by the couple. Typically, if the more negative specimen is polarized 50 mV or more in the positive direction due to coupling, the coupled current approximately equals the total corrosion rate. The weight-loss measurement provides the average corrosion rate for the entire exposure.

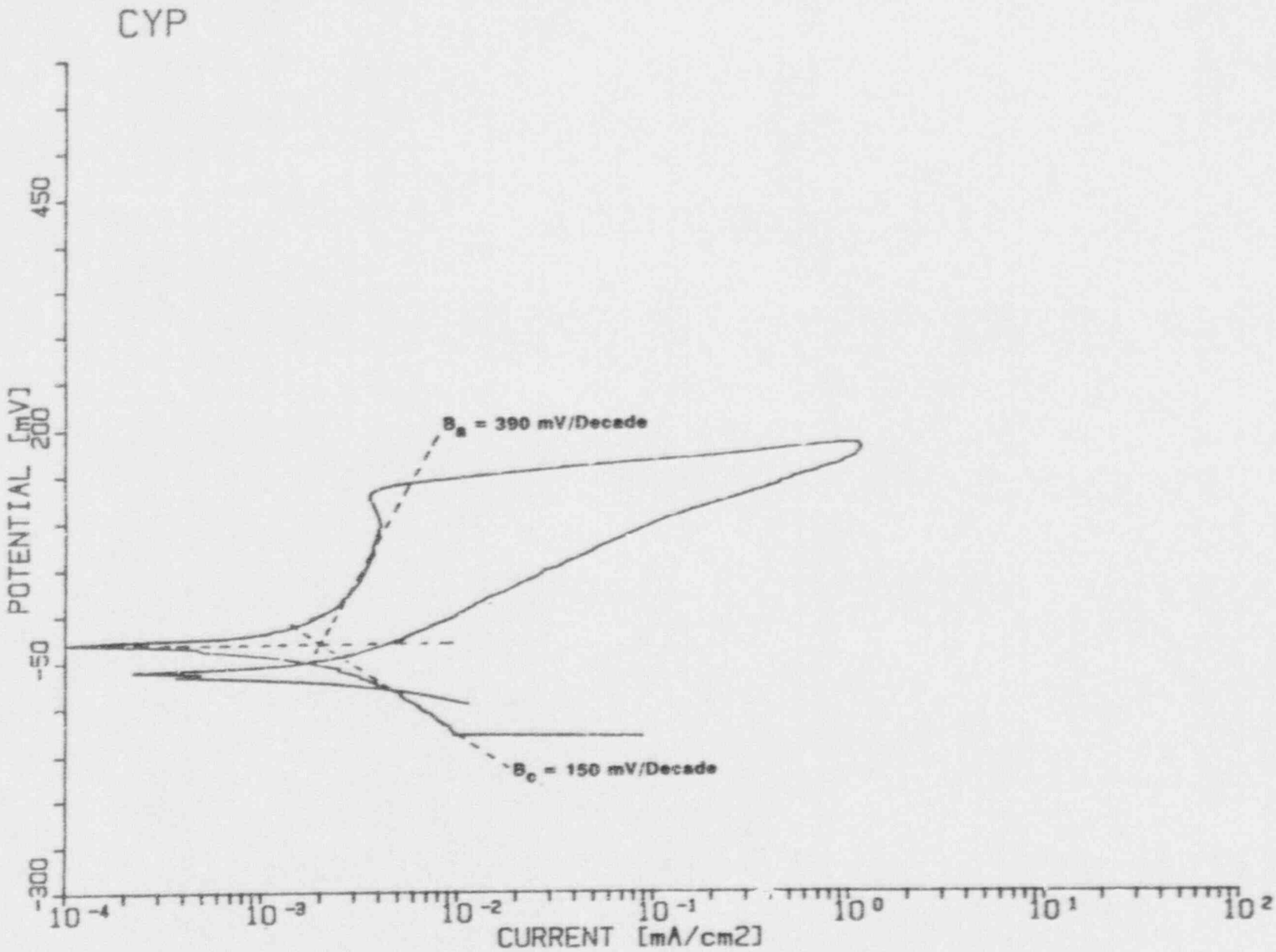

Figure 4.3 Cyclic Potentiodynamic Polarization Curve For Alloy CDA 102 In Simulated J-13 Well Water Showing The Anodic And Cathodic Tafel Slope Determinations (Beavers - 1990).

4.1.2 Copper-Base Alloys

A thermogalvanic-couples experiment was performed with Alloy CDA 102 in simulated J-13 well water for a total of 380 hours. For the first 170 hours, no H_2O_2 was added to the test solution. During this period, the heat-transfer specimen was maintained at about 90°C while the solution temperature was reduced from 80°C to 55°C to increase the temperature differential. For the remaining 210 hours, 200 ppm H_2O_2 was added to the test vessel daily. The temperature differential was maintained at 35°C during this final period of exposure.

A summary of the results of the experiment is given in Figures 4.4 through 4.6 and Table 4.1. As shown in Figure 4.4, there was a systematic trend of increasing thermogalvanic current with increasing temperature differential. In this figure, the direction of the current was such that the corrosion rate of the isothermal specimen was being accelerated by the couple (anodic current from the isothermal specimen). However, the magnitude of the current was very small. The maximum value measures, 0.03 $\mu A/cm^2$ is less than 0.7 µm/yr of general corrosion.

Figure 4.5 graphically shows the coupled and uncoupled potentials as a function of test time. These data shows that the heated specimen was consistently more noble than the isothermal specimen. Prior to the additions of H_2O_2, both the coupled and the uncoupled potentials were near 0.00 V (SCE) and the difference in the potentials of the two specimens was generally small, less than 10 mV.

With each addition of H_2O_2, large potential and current transients were produced, as shown in Figures 4.5 and 4.6, respectively. The first H_2O_2 addition produced a noble shift of about 200 mV and subsequent additions produced somewhat smaller shifts, depending upon the magnitude of the potential decay following the previous addition. Initially, following the H_2O_2 addition, the currents went cathodic for the isothermal specimen, but after a few minutes, the currents became anodic and produced large current transients in excess of 100 (5 $\mu A/cm^2$). These current transients lasted for about 500 minutes, during which time the H_2O_2 in the cell was probably decomposing. Figure 4.6 illustrates a typical current transient, in more detail, as a result of an addition of H_2O_2.

Table 4.1 summarizes the polarization resistance (PR) and corrosion rates measured from PR and weight-loss data for the first thermogalvanic-couples test. As described above, the PR measurements were taken following uncoupling of the specimens and reflect the general corrosion behavior. The PR data show that, prior to the H_2O_2 additions, the corrosion rate of the heat-transfer specimen was higher than that of the isothermal specimen. Following the H_2O_2 additions, the same trend was observed, but the corrosion rate of both specimens increased substantially with a greater increase being experience by the heat-transfer specimen.

Comparison of the electrochemical data with the actual weight-loss data indicated that the electrochemistry overestimated the general corrosion rate. This behavior has been found to be typical for PR measurements of the copper-base alloys. This discrepancy may be a consequence of non-Faradaic (noncorrosion) electrochemical reactions which contribute a current in the measurement, but are not associated with metal loss. However, the discrepancy between the corrosion rates calculated from PR data and the final weight-loss data, after H_2O_2 was added, was not as large as it appears. The weight-loss data were averaged over the entire exposure while

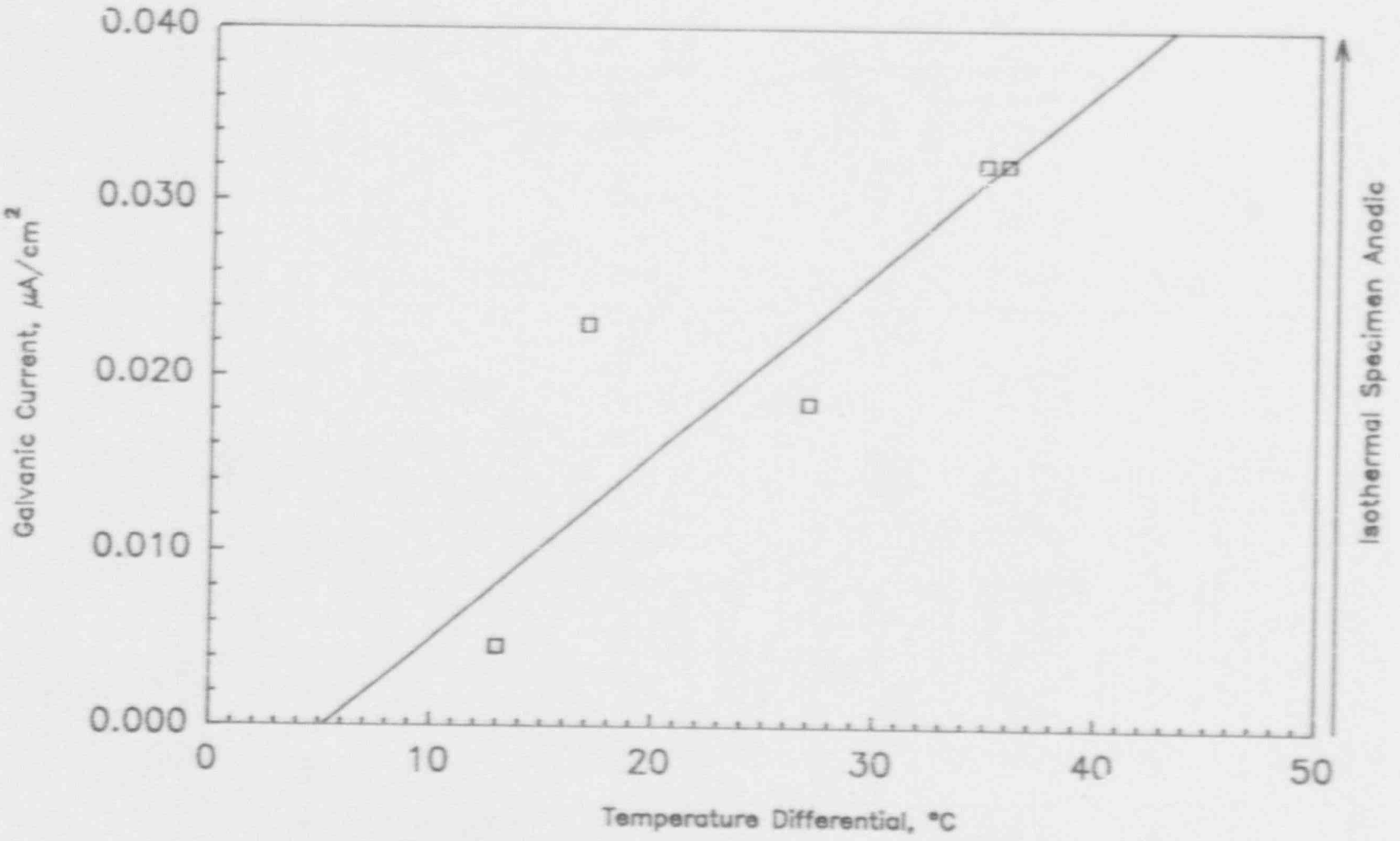

Figure 4.4 Thermogalvanic Current Density As A Function Of Temperature Differential Between Heated and Isothermal Specimens Of Alloy CDA 102 In Simulated J-13 Well Water Prior To Addition of H_2O_2 (Test #1).

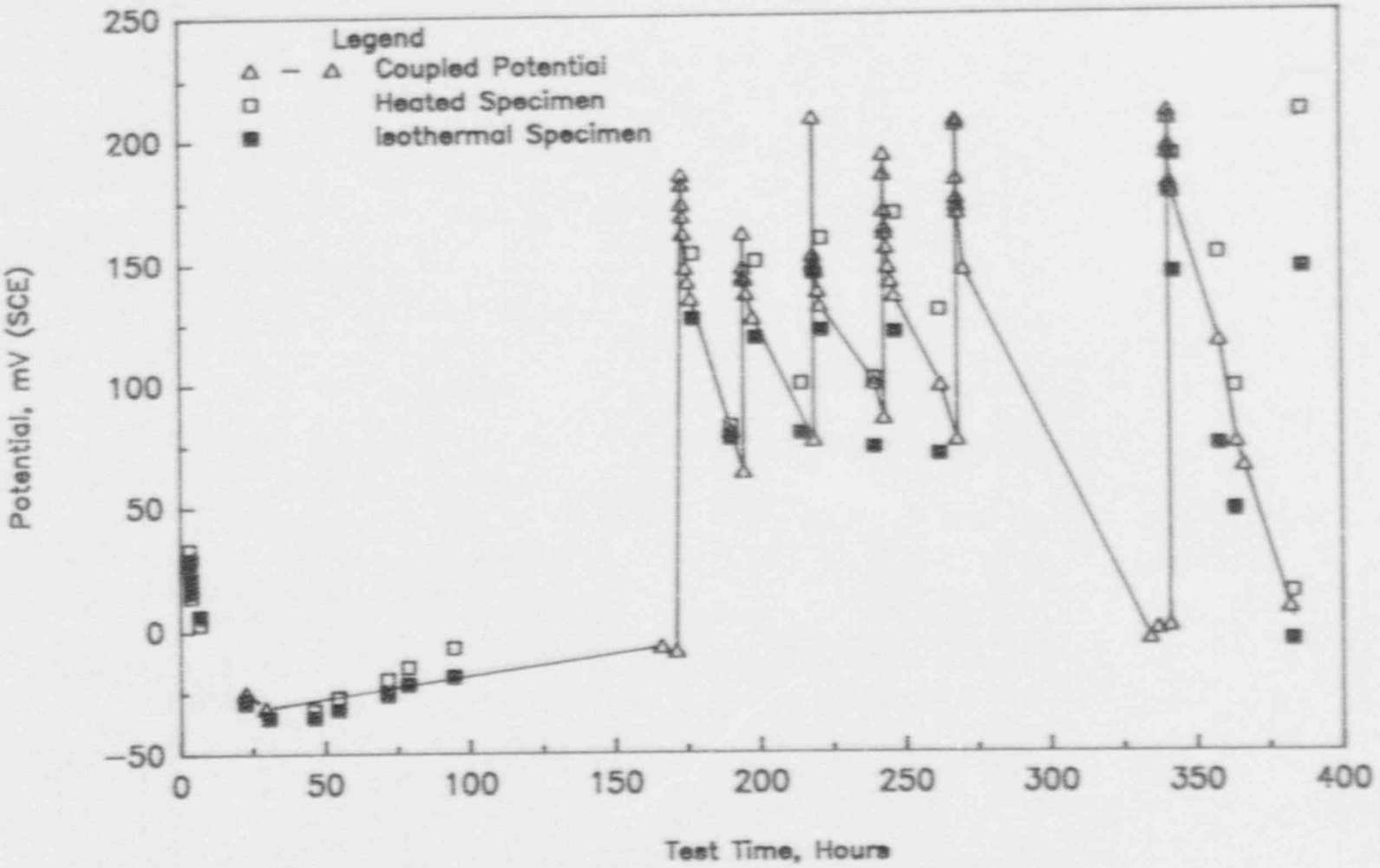

Figure 4. Potential As A Function Of Test Time For Thermogalvanic Specimens Of Alloy CDA 102 In Simulated J-13 Well Water Showing Effects Of 200 ppm H_2O_2 Additions; H_2O_2 Added After 170 Hours (Test #1).

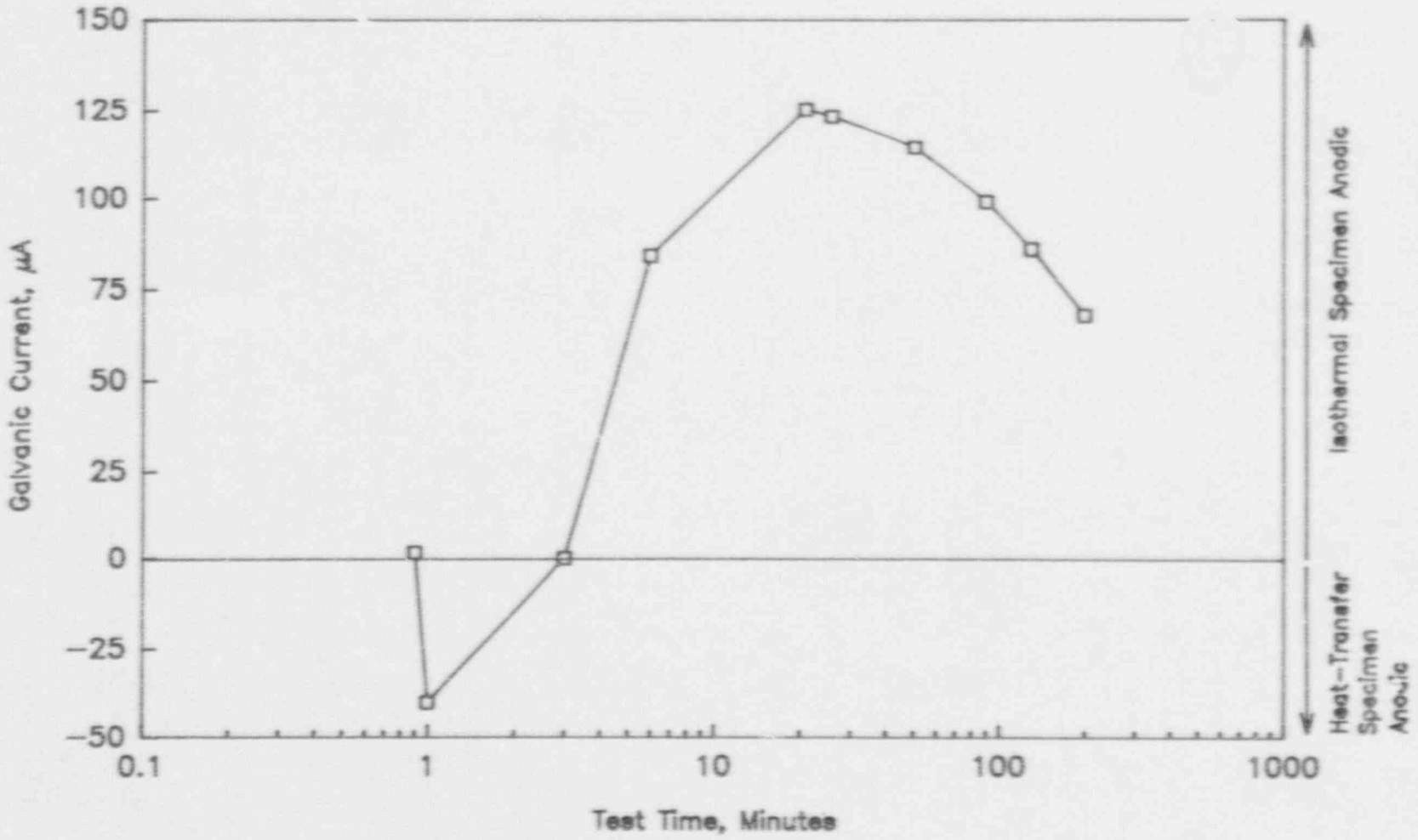

Figure 4.6 Thermogalvanic Current As A Function Of Test Time For Specimens Of Alloy CDA 102 In Simulated J-13 Well Water Showing Effects Of The Fourth Addition of H_2O_2 After 243 Hours Of Exposure (Test#1).

Table 4.1 Summary Of Results Of The Thermogalvanic - Couples Experiment With Specimens Of Alloy CDA 102 In Simulated J-13 Well Water; Test #1.

Condition	Specimen	Polarization Resistance kΩ-cm²	Corrosion (PR) µm/y	Rate (Weight Loss) µm/y	Description
Prior H_2O_2	Isothermal	143	7.68	—	—
Prior H_2O_2	Heat Transfer	93.5	11.7	—	—
Post H_2O_2	Isothermal	1.87	26.9	0.97	Moderate to heavy etching over 90% of surface. Localized dark-colored areas.
Post H_2O_2	Heat Transfer	0.37	143	1.59	Moderate to heavy etching over 67% of surface. Localized dark-colored areas. Heavy etching on top surface.

the PR data with H_2O_2 represent peak, transient corrosion rates directly following the additions of H_2O_2. The PR data did, however, correctly predict the relative corrosion rates of the isothermal and heat-transfer specimens. In conclusion, although thermogalvanic corrosion may accelerate the corrosion rate of that portion of the waste container having the lower temperature, the major effect is the increase in general corrosion rates with increasing temperature. Additional testing in other environments is needed to generalize this conclusion.

4.1.3 Fe-Cr-Ni Alloys

Two thermogalvanic-couples experiments were performed with Alloy 304L; one in simulated J-13 well water and one in Solution Number 7. Solution Number 7 was selected from the experimental matrix as it was shown to promote pitting of Alloy 304L. The composition of Solution Number 7 is given in Table 2.5. In both experiments, the heat-transfer specimen was maintained at 90°C while the solution temperature was lowered to study the effects of temperature differential on galvanic current. The temperature of the solution was decreased 10°C approximately every two days until reaching 50°C. Hydrogen peroxide was then added daily to each of the tests while maintaining the temperature differential at 40°C. For both experiments, a positive current value indicated that the isothermal specimen was anodic (corroding) with respect to the heat-transfer specimen. A negative current value indicated that the heat-transfer specimen was anodic with respect to the isothermal specimen.

The results of the experiment performed with Alloy 304L in simulated J-13 well water are illustrated in Figures 4.7 through 4.9 and in Table 4.2. Figure 4.7 illustrates the trend in thermogalvanic current as a function of temperature differential. At temperature differences less than 25°C, the isothermal specimen was anodic with respect to heat-transfer specimen. At temperature differences greater than 25°C, the heat-transfer specimen became anodic. However, the magnitude of the change in thermogalvanic current was very low in the absence of H_2O_2.

Figure 4.8 illustrates the coupled and uncoupled potentials as a function of test time. For the first 243 hours, no H_2O_2 was added to the simulated J-13 well water. Prior to the addition of H_2O_2, the potentials of both specimens fell between (0.00 mV (SCE) and 50 mV (SCE)), and the difference between the individual potentials were small, less than 3 mV. During this time, the heated specimen was actually slightly more noble than the isothermal specimen, but the currents were insignificantly small in any case.

After 243 hours of exposure, daily additions of 200 ppm H_2O_2 were made to the simulated J-13 well water. The effects of the H_2O_2 additions, made on Mondays, are clearly visible in Figure 4.8 as is shown by the large noble potential shift. A polarity reversal occurred such that the isothermal specimen was more noble. Unlike in the results of the previous experiment with Alloy CDA 102, the H_2O_2 decomposition was very slow and extended over several days. Daily additions of H_2O_2 performed throughout the weekdays had no apparent effect on the potentials. However, when the H_2O_2 additions were not made over the weekends, the decomposition of the H_2O_2 was evidenced by the drop in potential.

The typical effect of H_2O_2 on the thermogalvanic current in simulated J-13 well water is shown in greater detail in Figure 4.9. These data shows that 200 ppm additions of H_2O_2 produced small

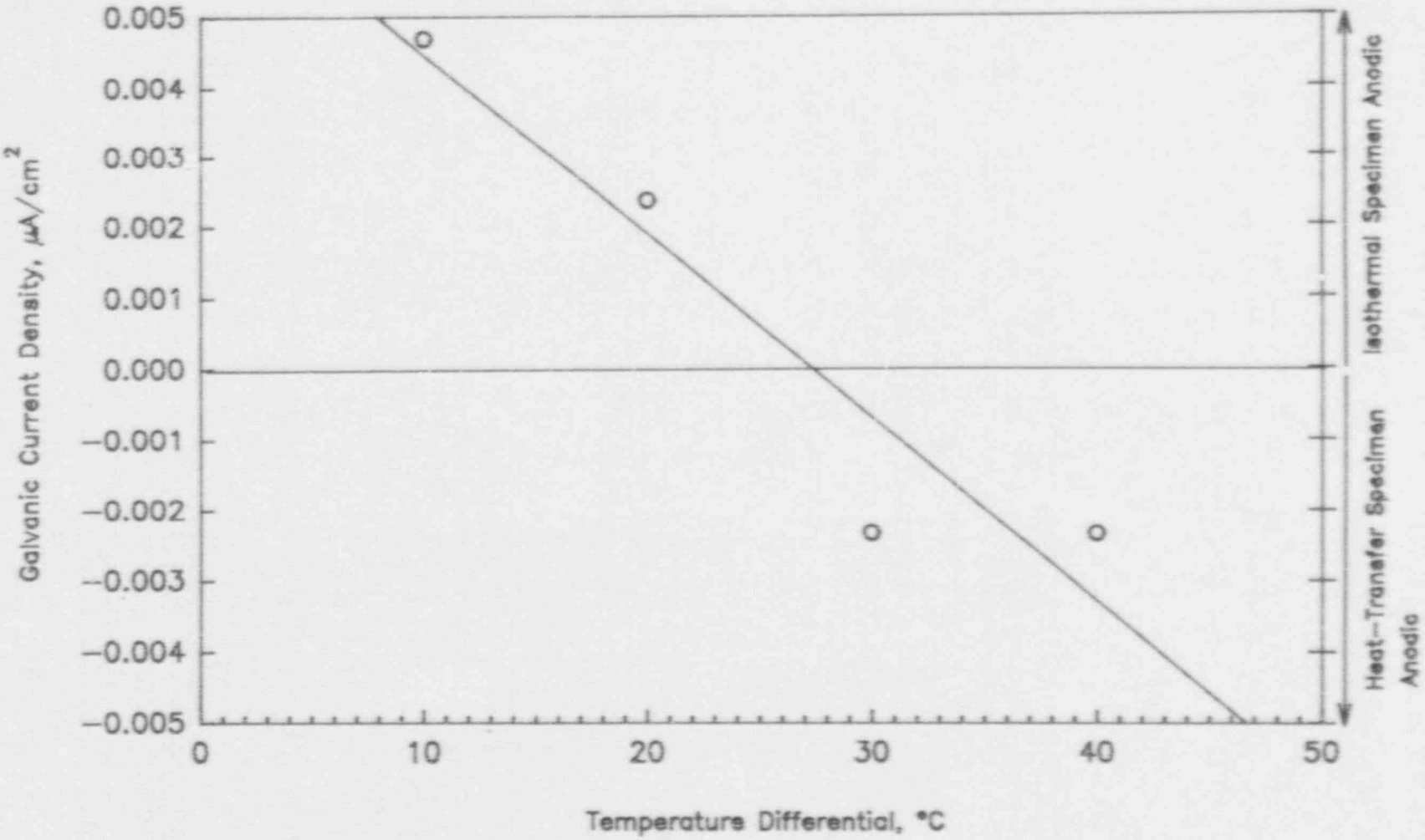

Figure 4.7 Thermogalvanic Current Density As A Function Of Temperature Differential Between Heat Transfer And Isothermal Specimens Of Alloy 304L In Simulated J-13 Well Water Prior To Additions of H_2O_2 (Test #2).

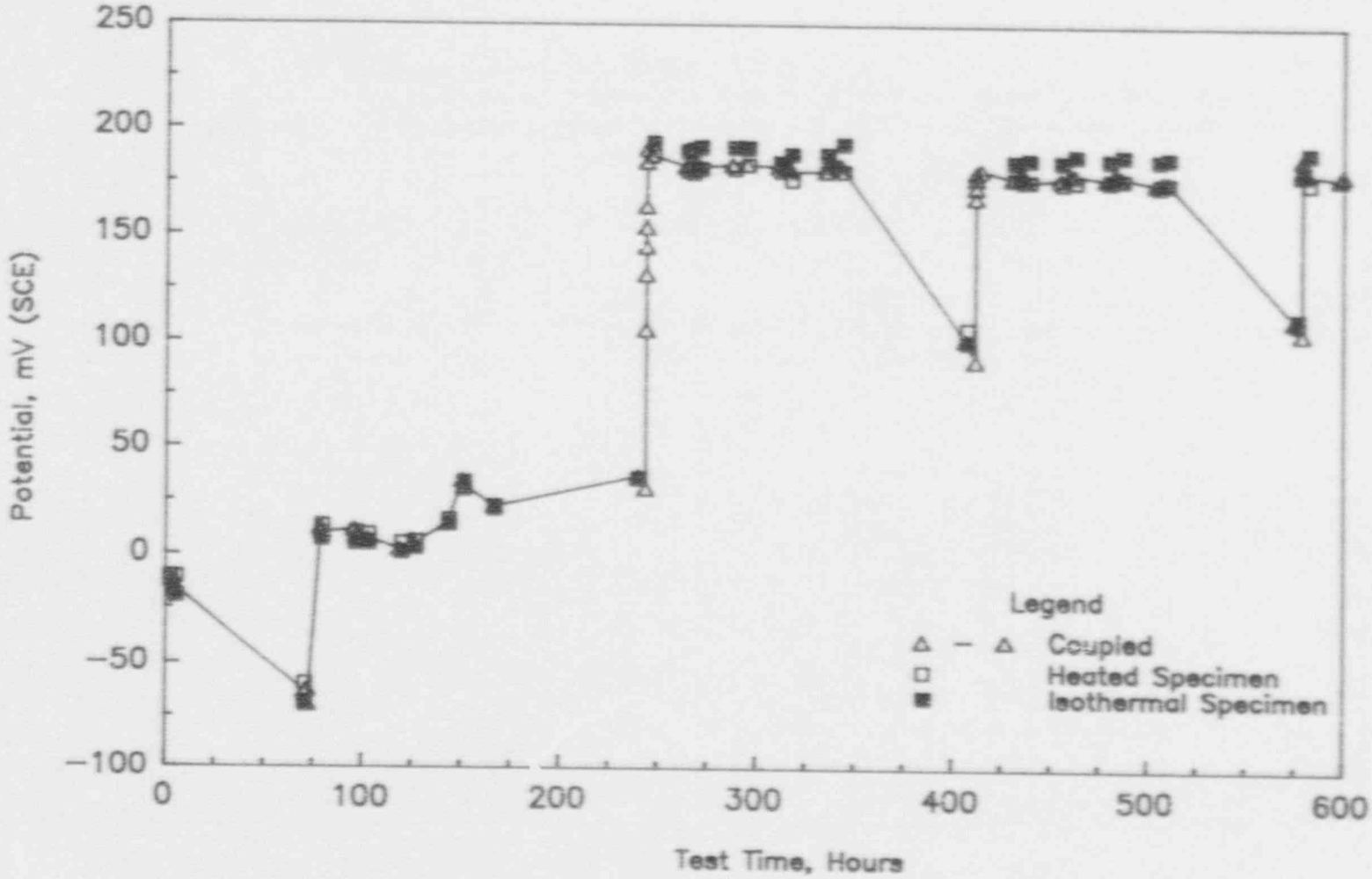

Figure 4.8 Potential As A Function Of Test Time For Thermogalvanic Specimens Of Alloy 304L In Simulated J-13 Well Water Showing The Effects Of 200 ppm H_2O_2 Additions; H_2O_2 Added After 243 Hours (Test #2).

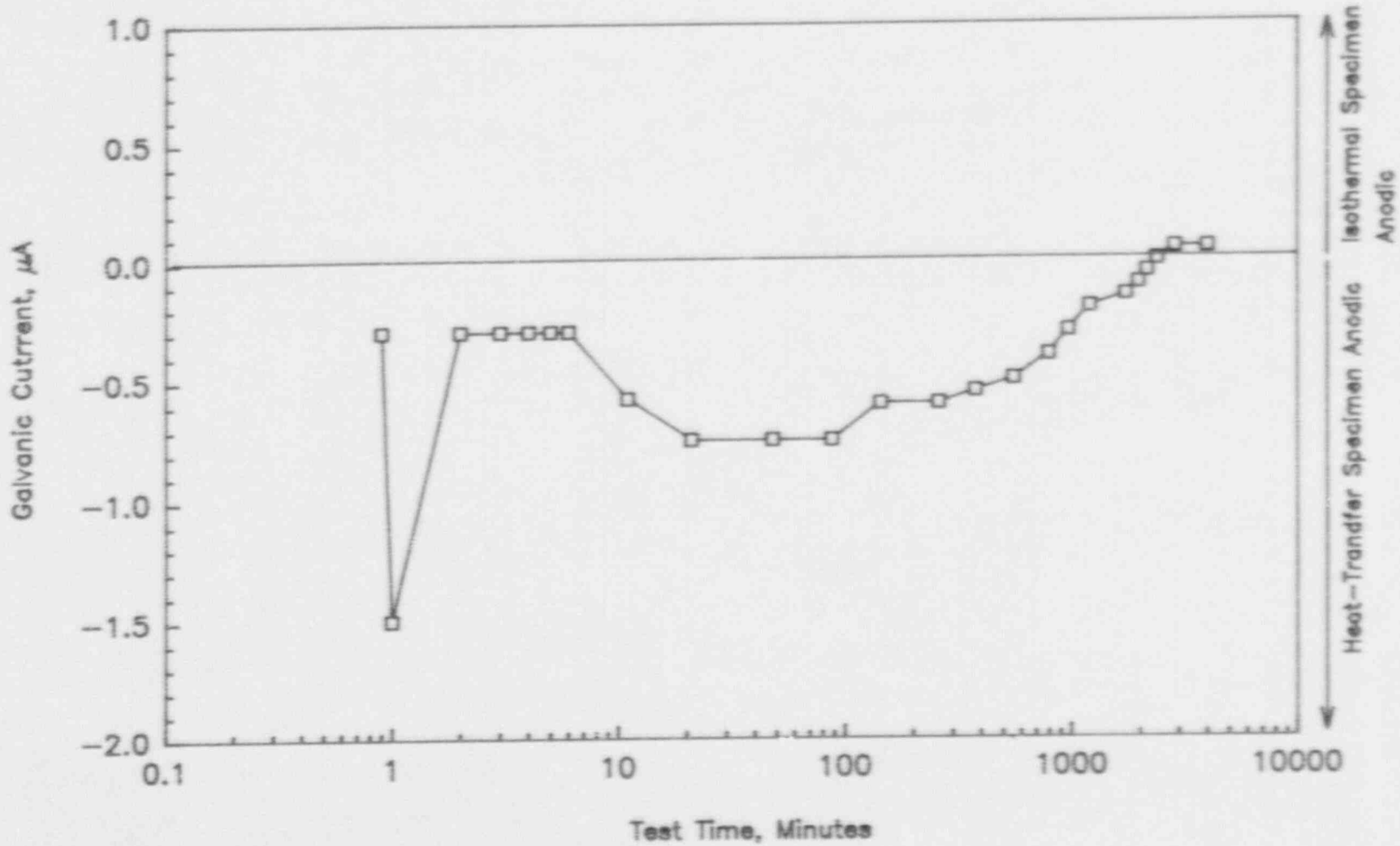

Figure 4.9 Thermogalvanic Current As A Function Of Test Time For Specimens Of Alloy 304L In Simulated J-13 Well Water Showing Effects Of The Fourth Addition Of H_2O_2 After 340 Hours Of Exposure (Test #2).

Table 4.2 Summary Of The Results Of Thermogalvanic - Couples Experiment With Specimens of Alloy 304L In Simulated J-13 Well Water; Test #2.

Specimen	Corrosion Rate (Weight Loss) µm/y	Description
Isothermal	0.17	No visible attack.
Heat Transfer	3.95	No visible attack. Rings of scale encircled the top of the specimen due to minor fluctuations in liquid level.

current transients that lasted over a relatively long period of time; approximately 24 hours. During each transient, the heat-transfer specimen remained anodic.

After 603 hours of exposure, weight losses were measured for each specimen and converted to corrosion rates. Table 4.2 gives a summary of the corrosion rates calculated from these measurements and descriptions of the specimens following testing. These data show that the heat-transfer specimen experienced greater general corrosion than did the isothermal specimen in simulated J-13 well water. Based on the thermogalvanic current measurements, both thermogalvanic effects and accelerated attack, as a result of the higher temperature, contributed to the corrosion.

The second thermogalvanic-couples experiment with Alloy 304L was performed in Solution Number 7, a pitting solution. The results of the experiment in Solution Number 7 are illustrated in Figures 4.10 through 4.12 and in Table 4.3. Galvanic currents were measured as a function of temperature differential over the first 309 hours of exposure, as in the previous experiment. However, in test Solution Number 7, these currents approached the lower detection limit of the test equipment.

The coupled and uncoupled potentials were measured as a function of test time and are illustrated in Figure 4.10. No H_2O_2 was added to Solution Number 7 for the first 426 hours of exposure. During this time, the heated specimen was consistently more noble than the isothermal specimen. The coupled potentials showed a slight noble trend, which approached the pitting potential (E_{pit}) for this alloy-environment system, prior to the addition of H_2O_2; the cyclic-potentiodynamic-polarization curve for Alloy 304L in Solution Number 7 is shown in Figure 4.13.

After 426 hours of exposure, daily additions of 200 ppm H_2O_2 were made to Solution Number 7. The large potential spike, corresponding to the initial H_2O_2 addition, is readily apparent in Figure 4.10. The initiation of pits is believed to have caused the potential of the galvanic couple and the heat-transfer specimen to drop to extremely low levels, which approached the protection potential (E_{prot}) of -120 mV (SCE) for this alloy-environment. Subsequent additions of H_2O_2 appeared to have less of an effect on the potential, as illustrated in Figure 4.10 by the narrow range of potential differences recorded. Pit initiation also may have promoted the very large galvanic current spike illustrated in Figure 4.11, and the numerous smaller current spikes shown in greater detail in Figure 4.12. Subsequent additions of H_2O_2 produced only minor fluctuations in galvanic current (Figure 4.11) which may indicate that the pits either passivated or did not continue to propagate. Rounded areas of rust were visible on the top surface of the heat-transfer specimen within 24 hours of the H_2O_2 addition.

Table 4.3 is a summary of the Polarization Resistance (PR) measurements, corrosion rates calculated from PR, and weight-loss data after 763 hours of exposure. A description of the specimens at the conclusion of the experiment is also included in Table 4.3. All of the PR values given in this table were measured after H_2O_2 was added to the electrolyte. The PR values measured prior to the addition of H_2O_2 were above the limitations of the test equipment. These data show that, in Solution Number 7, the heat-transfer specimen exhibited primarily pitting corrosion. The isothermal specimen exhibited no visible attack in Solution Number 7.

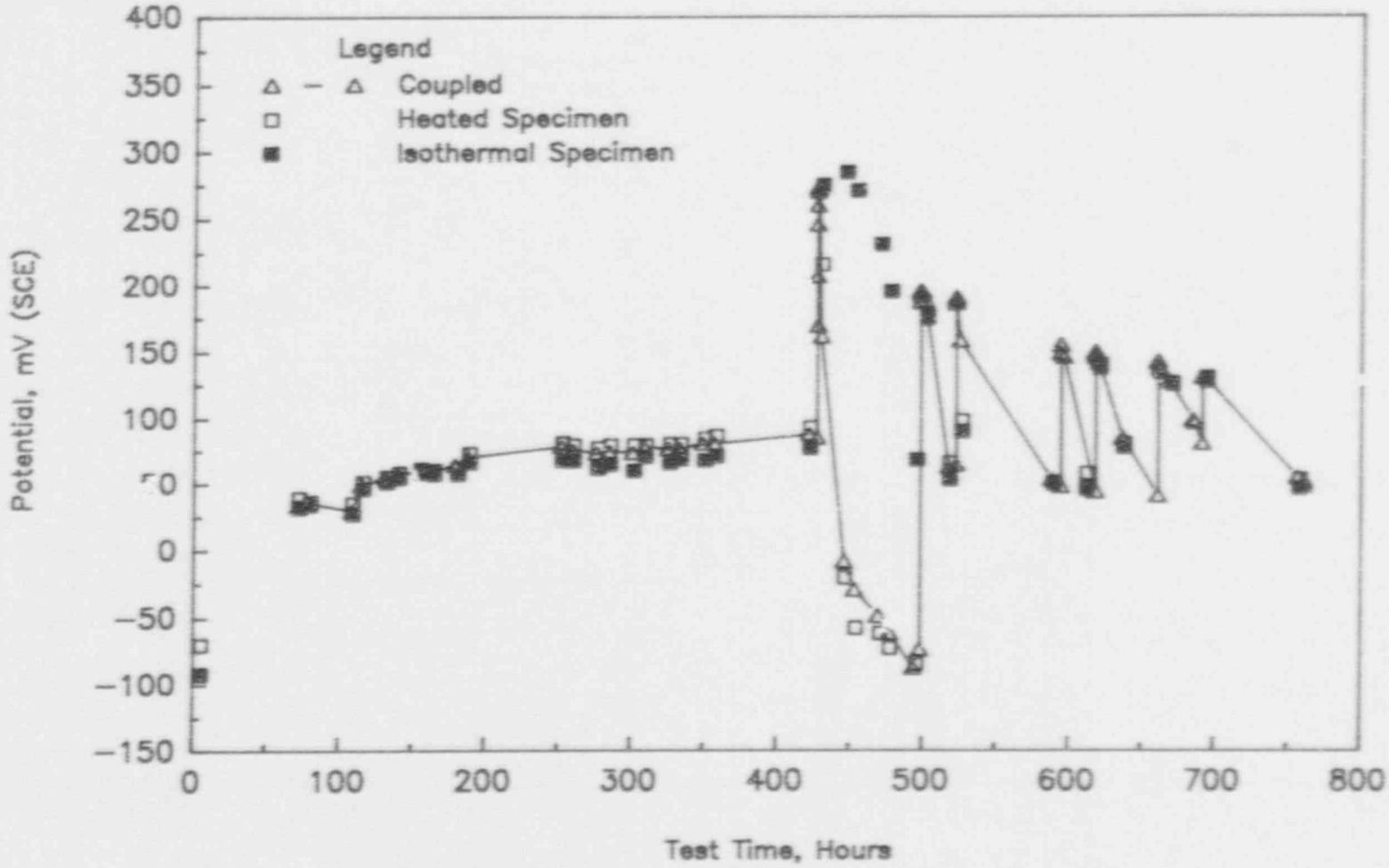

Figure 4.10 Potential As A Function Of Test Time For Thermogalvanic Specimens Of Alloy 304L In Solution No. 7 Showing The Effects Of 200 ppm H_2O_2 Additions; H_2O_2 Added After 427 Hours (Test #3).

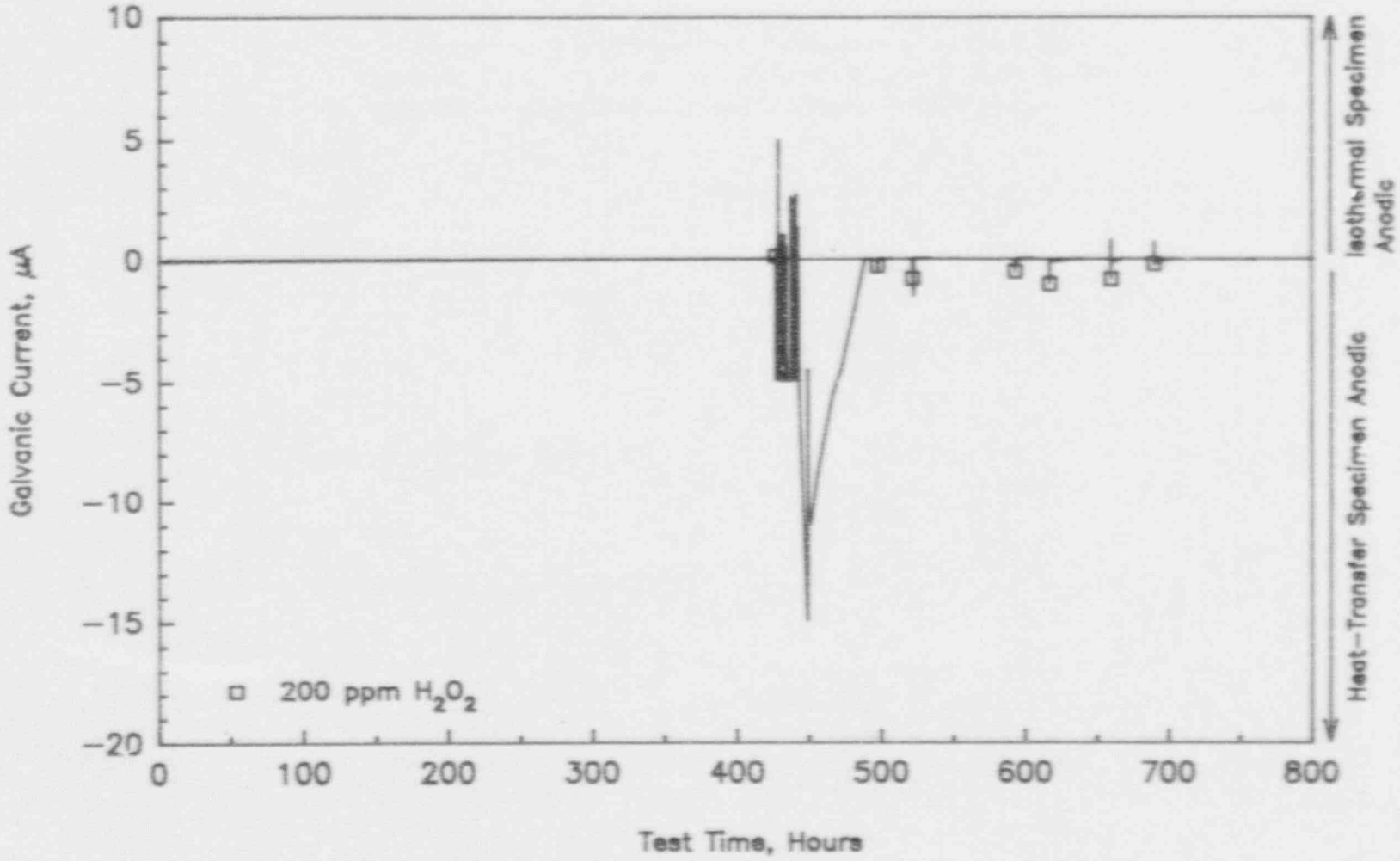

Figure 4.11 Thermogalvanic Current As A Function Of Test Time For Specimen Of Alloy 304L In Solution No. 7 Showing The Effects Of 200 ppm H_2O_2 Additions (Test #3).

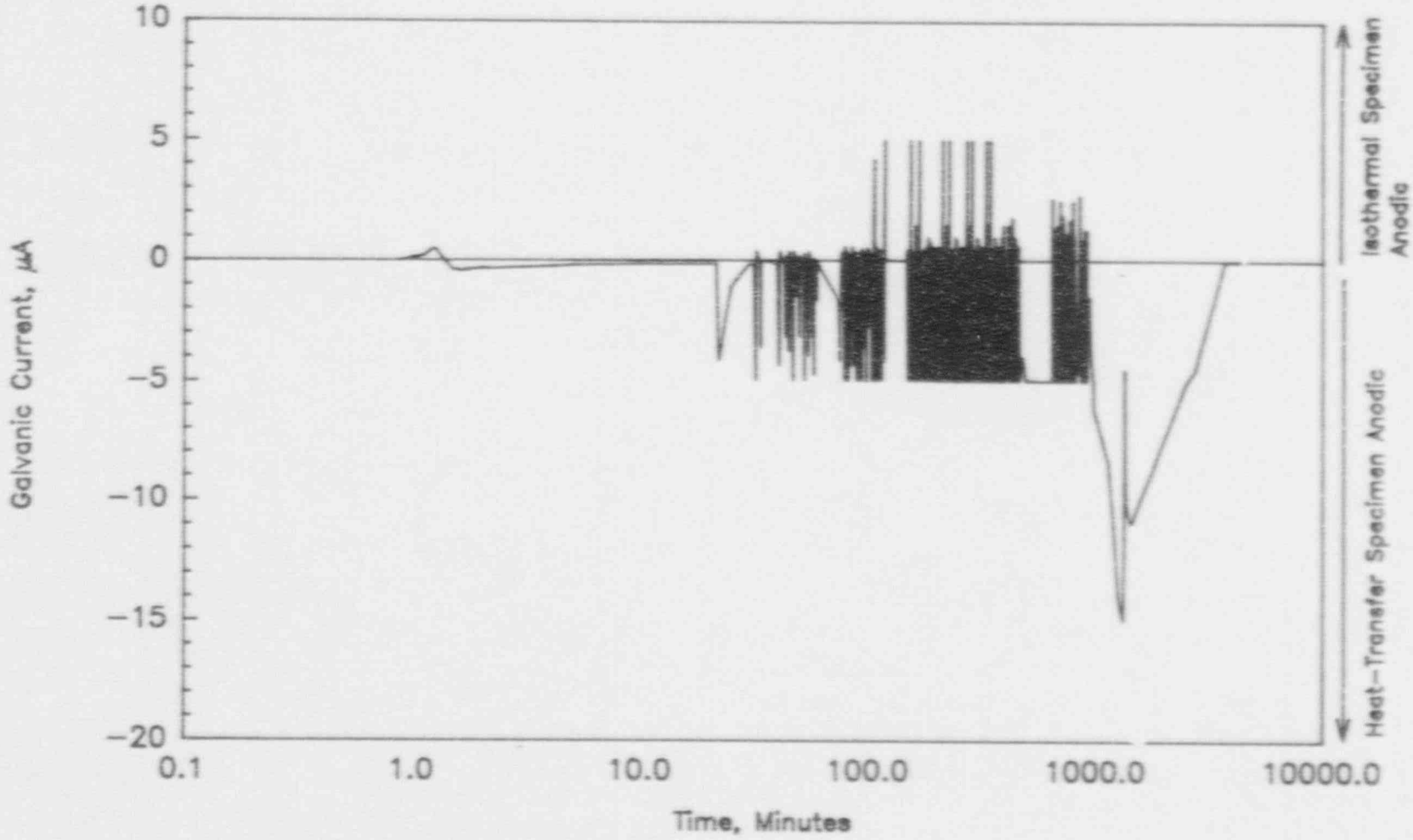

Figure 4.12 Thermogalvanic Current As A Function Of Test Time For Specimen Of Alloy 304L In Solution No. 7 Showing The Effects Of The Initial Addition Of 200 ppm H_2O_2 After 426 Hours Of Exposure (Test #3).

Table 4.3 Summary Of The Results Of Thermogalvanic - Couples Experiment With Specimens Of Alloy 304L In Solution No. 7; Test #3.

Specimen	Polarization Resistance kΩ-cm²	Corrosion Rate		Description
		PR µm/y	Weight Loss µm/y	
Isothermal	415	0.49	<0.07	No visible attack.
Heat Transfer	234	0.87	0.41	Numerous pits on the sides and top associated with halos of rust-colored oxide. Some localized etching.

Note: Polarization resistance (PR) was measured after addition of 200 ppm H_2O_2. The values for PR were above limitations of the test equipment prior to the addition of H_2O_2.

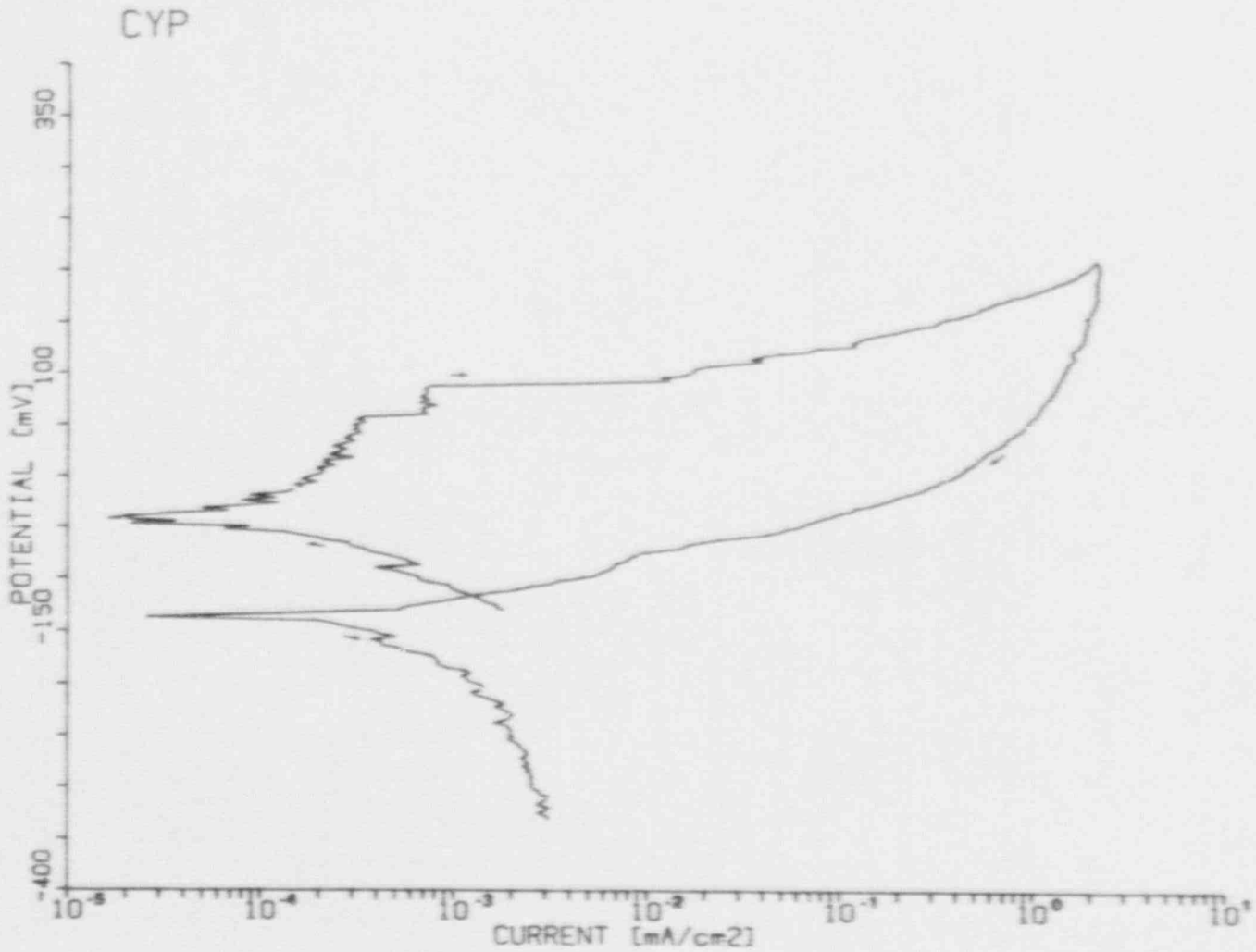

Figure 4.13 Cyclic Potentiodynamic Polarization Curve For Alloy 304L In Test Solution No. 7 At 90°C.

Comparison of the corrosion rates calculated from weight-loss and PR data indicates that, as in previous work, the latter overestimates the corrosion rate. The discrepancy between the two corrosion rate measurement techniques may be attributed to non-Faradaic (noncorrosion) electrochemical reactions and to time related effects. The weight-loss data used to calculated the corrosion rate are averaged over the entire exposure period, while the PR data after the addition of H_2O_2 represent peak, transient corrosion rates.

4.2 Borehole Liner-Container Interaction Studies

Borehole liner-container interaction experiments were conducted in Task 6 of the program. The purpose of these tests was to evaluate the effects of contact of the borehole liner with the container on the corrosion performance of the container material. The initial designs for the Tuff Repository proposed Alloy 304L as the container material and carbon or low alloy steel as the liner material. Later, at the direction of the NRC, the focus of the testing shifted to Alloy 304L and Alloy 825 as the liner and container material, respectively. The purpose of these liners is to facilitate retrieval of the waste containers over a 50-year period following their emplacement. For the current repository design, it is probable that the liners and containers will be in direct contact. Because the stainless steel container is more noble than the low alloy steel liner, it might be expected that galvanic contact would be beneficial to the corrosion performance of the container. However, instances of accelerated attack of the noble member of ferrous alloy couples have been reported (Kearns, 1986). The mechanism of attack involved acidification within the region of contact of the two metals by localized corrosion of the less noble metal, followed by passive film breakdown on the noble metal. This type of behavior could occur at regions of contact between the liner and the stainless steel container.

4.2.1 Experimental Approach

The borehole liner-container interaction experiments were performed in a PTFE electrochemical cell similar to the illustration in Figure 4.14. In each of the experiments, a metal "sandwich" was prepared with one coupon of liner material, a sheet of PTFE, and one coupon of container material. The initial weight and dimension (2.54 cm x 2.54 cm x 0.32 cm) of each coupon were recorded prior to assembly. Each sandwich was mounted onto Alloy C276 threaded rod and electrically isolated by PTFE inserts. Copper wire was threaded into a small hole which was drilled and tapped into the edge of each coupon. Heat-shrink tubing was fitted over each of the electrical lead wires to prevent contact with the electrolyte. A detailed diagram of the specimen configuration is shown in Figure 4.15.

The test cell was filled with the desired electrolyte so that both specimens were fully immersed in the test solution. The desired gas was flowed through the electrolyte for a minimum of 30 minutes at ambient temperature. After 30 minutes of gas flow, the test solution was heated to 90°C by heat tape connected to a temperature controller.

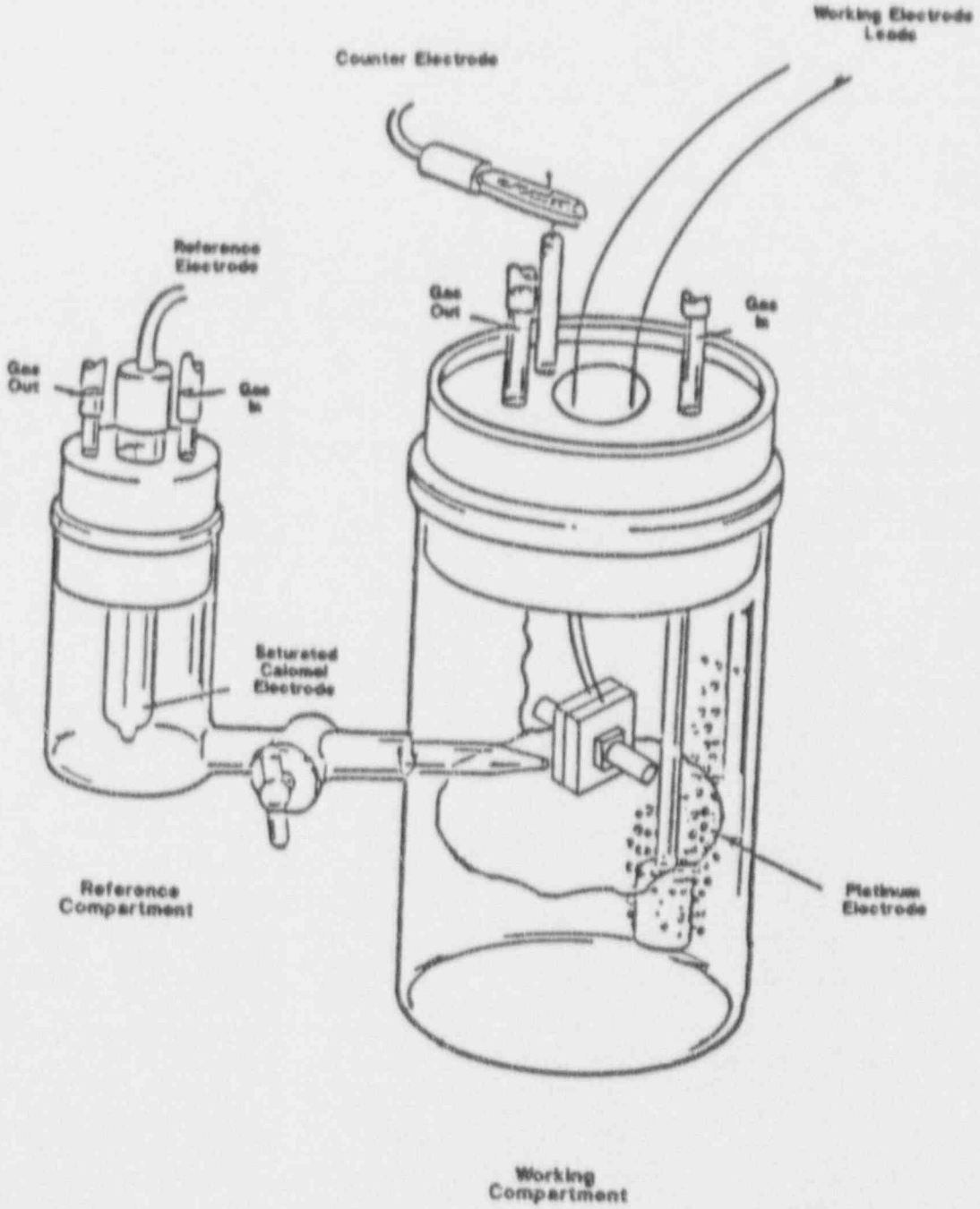

Figure 4.14 Electrochemical Cell Used For Borehole Liner - Container Interaction Testing.

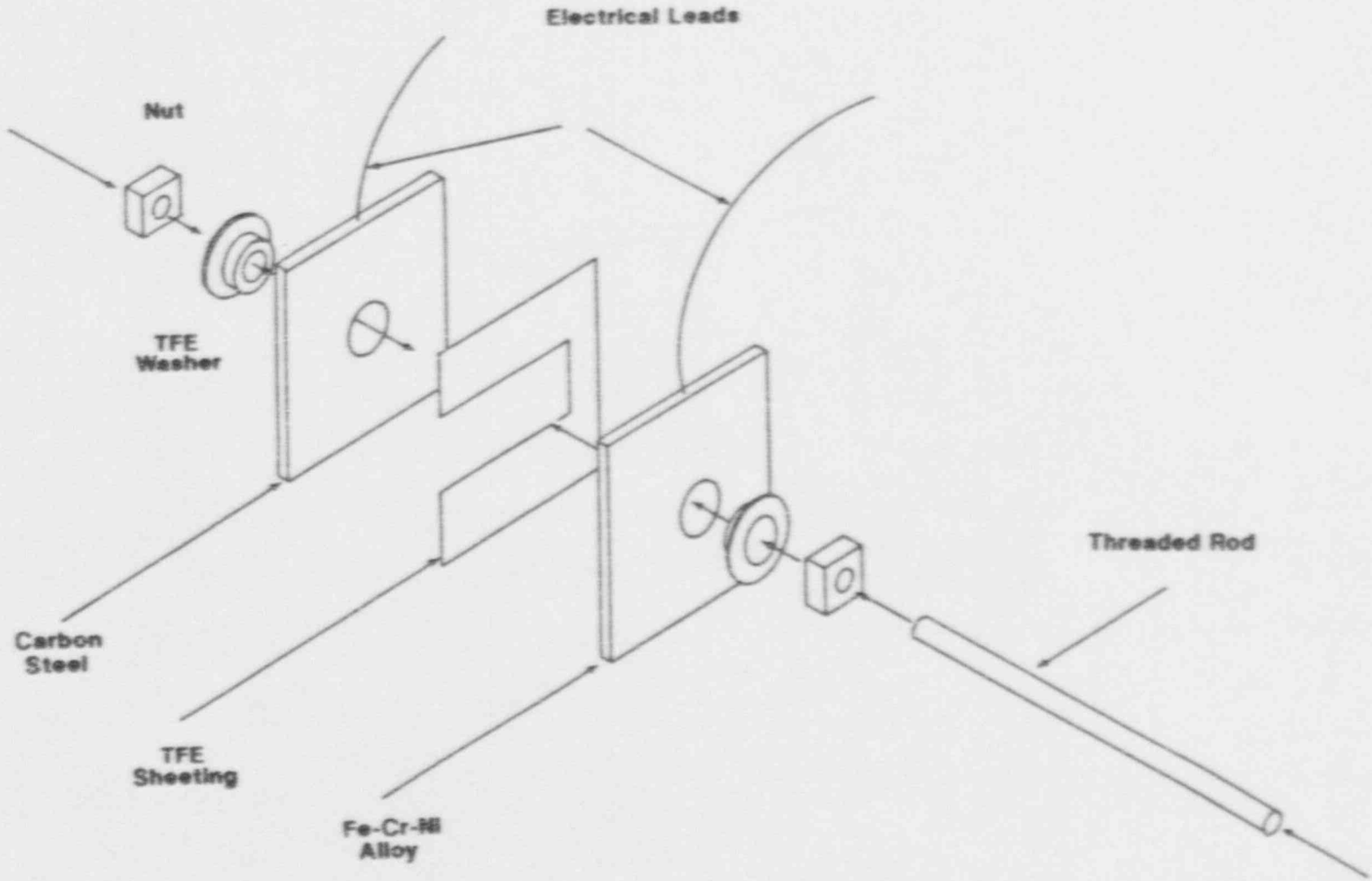

Figure 4.15 Schematic Of Borehole Liner - Container Specimen Assembly.

The potential of each specimen was measured with respect to a standard calomel electrode (SCE) and both specimens were electrically coupled through a ZRA. Each day, the coupled potential and galvanic current were measured. The specimens were then uncoupled for approximately 30 minutes and the potential of each specimen was measured. The coupons were again recoupled. Polarization resistance (PR) measurements were performed weekly after the specimen had been uncoupled for about 30 minutes. As in the previous galvanic-couples experiment, the PR measurements were performed by means of the two-electrode technique. Specimen potentials were scanned between -20 mV (SCE) and +20 mV (SCE) of the free-corrosion potential and the ensuing current was monitored. Current was plotted as a function of potential and the PR value was determined graphically as the tangent to the plot at zero current. The PR values were converted to corrosion rates using the Stern-Geary Equation and Faraday's Law.

At the conclusion of the experiments, gravimetric measurements were performed and the specimens were examined optically. Weight losses on the specimens were measured using the interval weight-loss procedure described in ASTM G-1. This technique involved the alternate descaling of the specimens in inhibited acid and weighing until the visible corrosion products were removed. An unexposed control specimen was included in all descaling measurements. True weight-losses were then converted to corrosion rates, in μm/yr, by dividing the weight loss by the density, the specimen surface area, and the test time and converting the units.

The coupled current provides a measure of the accelerated corrosion due to coupling and provides a measure of the total corrosion rate, depending on the amount of polarization provided by the couple. Typically, if the more negative specimen is polarized 50 mV or more in the positive direction due to coupling, the coupled current approximately equals the total corrosion rate. The weight-loss measurement provides the average corrosion rate for the entire exposure.

4.2.2 Results

Five borehole liner-container interaction tests were performed. The first three experiments were conducted with C1010 Carbon Steel (C1010) and Alloy 304L as the borehole liner and container materials, respectively. In two of these tests, the alloys were exposed to simulated J-13 well water at 90°C. In the third test, the alloys were exposed at 90°C to simulated J-13 well water containing 1000 ppm chloride (Cl) as sodium chloride (NaCl) (Solution Number 38). Later testing focused on Alloy 304L and Alloy 825 as the borehole liner and container materials, respectively. In the fourth experiment, these alloys were evaluated in simulated J-13 well water at 90°C, and in Solution Number 10 at 90°C in the fifth experiment. Solution Number 10 was chosen from the experimental test matrix because of the corrosion behavior observed for these alloys. For Alloy 304L, a large hysteresis loop occurred in the CPP curve and optical examination revealed pitting and crevice attack. However, the CPP curve for Alloy 825 did not exhibit hysteresis and there was no evidence of attack following the CPP tests. Appendix E provides the CPP curves for these alloy-environment systems.

4.2.2.1 C1010 Carbon Steel/Alloy 304L Galvanic Couples

The first borehole liner-container interaction test was performed with C1010 and Alloy 304L for 1303 hours at 90°C in simulated J-13 well water. Corrosion potentials and galvanic current measurements obtained throughout the duration of the exposure are given in Figures 4.16 and 4.17, respectively. The sharp downward spike in galvanic current in Figure 4.17 occurred as a result of electrical problems with the ZRA. Polarization resistance measurements, and corrosion rates determined from these measurements performed over the duration of the exposure are summarized in Table 4.4 and exhibited graphically in Figures 4.18 and 4.19, respectively. These data indicate very high corrosion rates for Alloy 304L which suggested that a deleterious interaction with the carbon steel liner material had occurred. However, optical examination of the specimens and analysis of the weight-loss data after 1303 hours of exposure revealed very low corrosion rates for Alloy 304L. The weight-loss technique showed Alloy 304L to have a corrosion rate of 0.61 µm/yr, whereas the corrosion rate of C1010 was 208 µm/yr. Alloy 304L exhibited a thin blue film on the outside of the specimen which suggests the formation of a passive film. The side of the specimen of Alloy 304L that faced toward the carbon steel specimen exhibited some black deposits and slight etching with one pit having a depth of 18 µm. The outside of the carbon steel specimen showed more severe attack than the side facing the stainless steel. Examination of the outer surface of C1010 revealed severe metal loss and deep pitting. The deepest pit measured 240 µm. Examination of the surface of C1010 facing the stainless steel coupon also showed significant metal loss with the deepest areas measuring 82 µm.

The erroneous PR data for Alloy 304L can be attributed to two factors: (1) the use of the carbon steel specimen as a counter electrode, and (2) a relatively remote reference electrode placed outside of the specimen sandwich. More reliable PR data were obtained for the carbon steel specimen, in which a remote platinum counter electrode was used. This experimental setup was used since it was felt that low PR values for the carbon steel would cause the Alloy 304L specimen (used as a counter electrode) to experience excessive potential perturbations. However, the experimental setup used for the carbon steel primarily provided information from the outer exposed surfaces, as opposed to the region between the two specimens. In an effort to acquire more reliable data, the experimental setup was modified. In the modified procedure, a microcapillary tube was inserted through the face of one of the specimens to connect the reference cell to the area between the specimens. This technique was used to ensure accurate potential measurements. Secondly, all of the PR measurements utilized the other specimen as the counter electrode; a remote platinum wire was not used. This modified procedure was followed for all of the remaining borehole liner-container interaction studies.

The second experiment was performed with C1010 and Alloy 304L at 90°C in simulated J-13 well water using the modified experimental procedure. Corrosion potentials and galvanic current measurements determined daily throughout the exposure period are given in Figures 4.20 and 4.21, respectively. The sharp decline in galvanic current at 1100 hours of exposure followed by a somewhat steady negligible current clearly indicated that the electrical connection was disrupted. Weekly PR measurements, and corrosion rates determined from these measurements, are given in Table 4.5 and are exhibited graphically in Figures 4.22 and 4.23, respectively. The increase in PR and the decrease in corrosion rate of the specimen of C1010 after 1100 hours further indicate that the electrical connection to the carbon steel was disrupted.

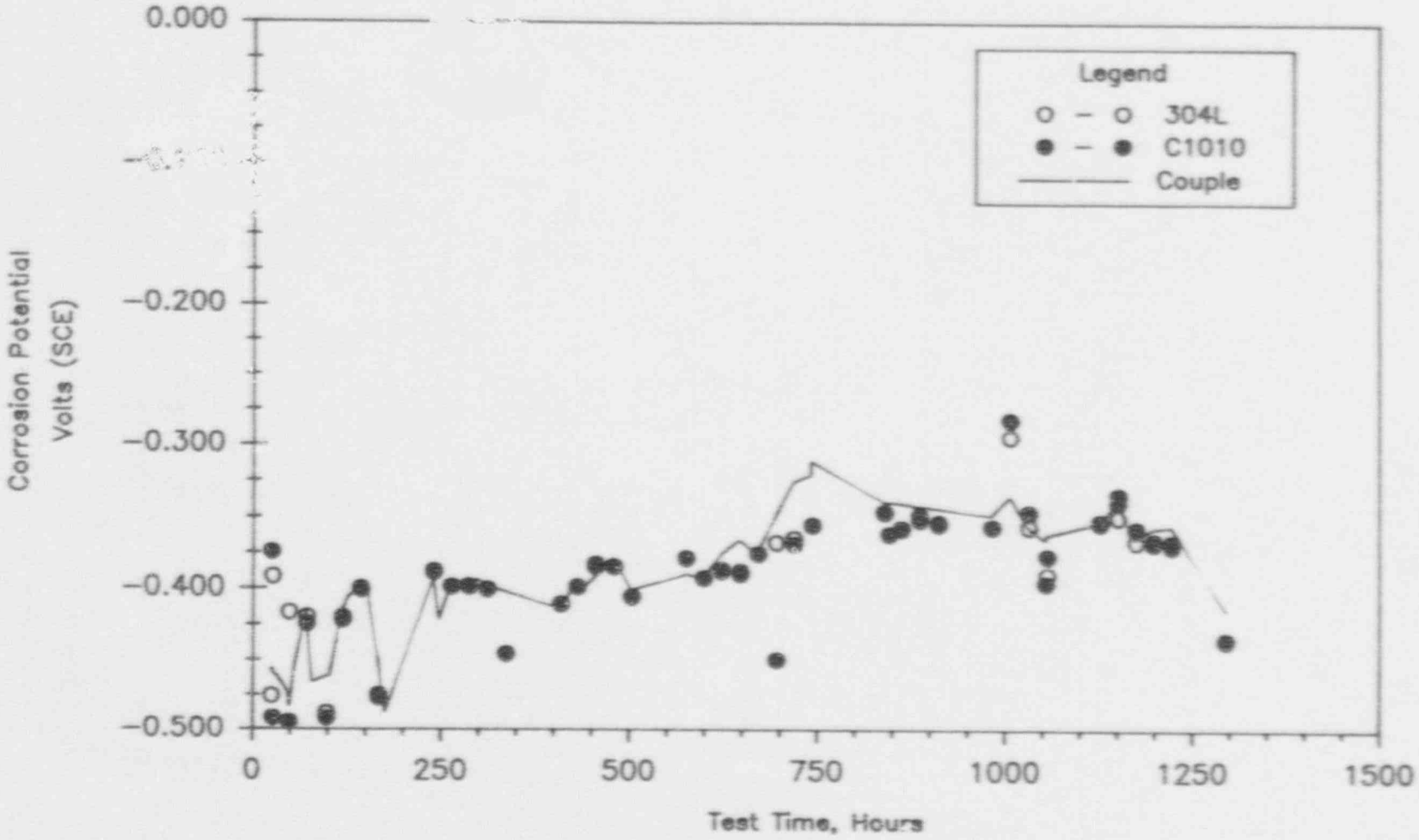

Figure 4.16 Corrosion Potential As A Function Of Test Time For Sandwich Specimens Of Alloy 304L And C1010 Carbon Steel In Simulated J-13 Well Water At 90°C (Test #1).

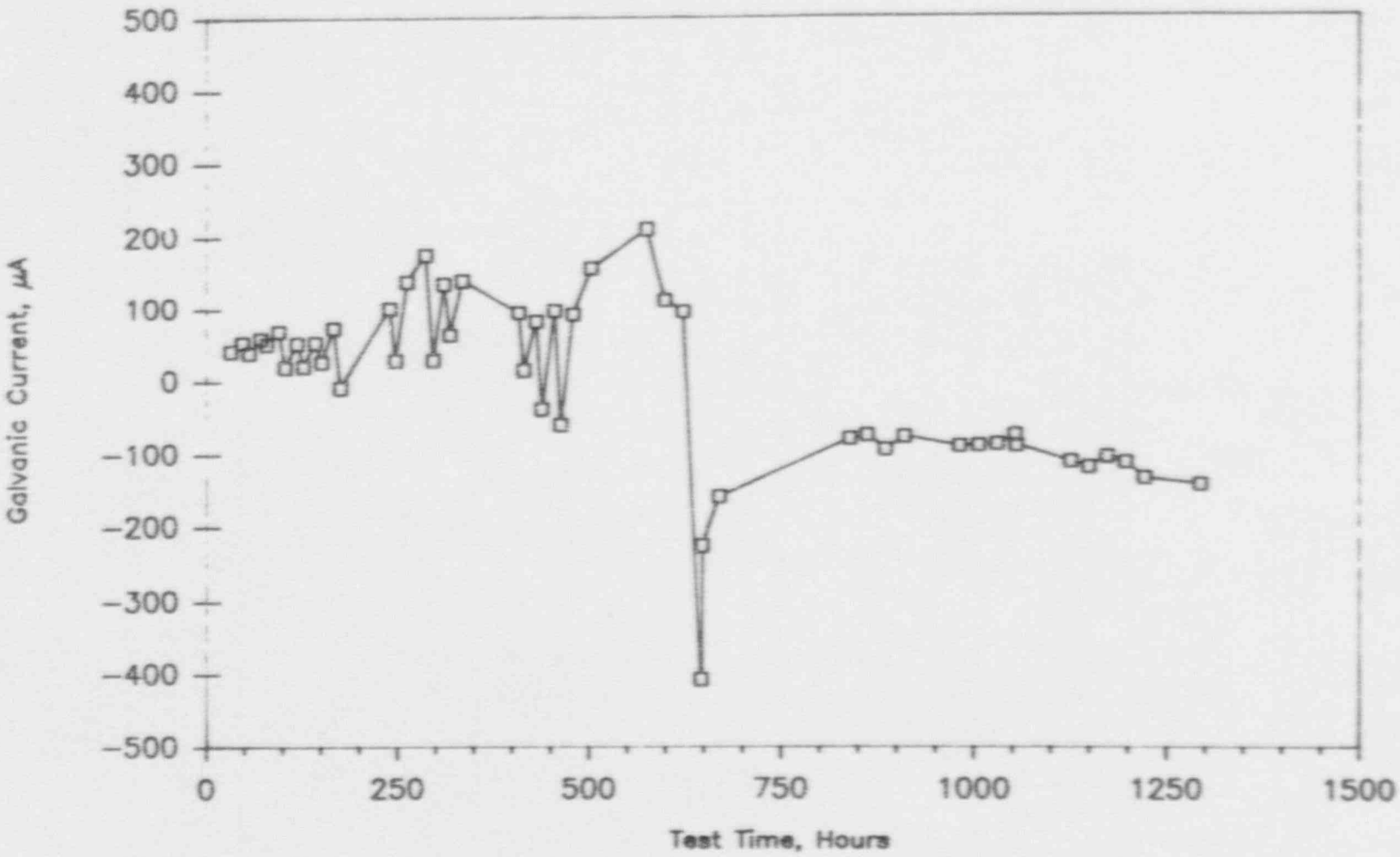

Figure 4.17 Galvanic Current As A Function Of Test Time For Sandwich Specimens Of Alloy 304L And C1010 Carbon Steel In Simulated J-13 Well Water At 90°C (Test #1).

Table 4.4. Summary Of Results Of Electrochemical Measurements Performed On Sandwich Specimens Of Alloy 304L And C1010 Carbon Steel In Simulated J-13 Well Water At 90°C; Test #1.

Alloy	Hours	Polarization Resistance kohm-cm^2	Slope mV/Decade B_a	Slope mV/Decade B_c	Corrosion Rate µm/yr	E_{cor} mV (SCE)
304L	26	22.20	493	131	20.62	-392
304L	287	0.310	493	131	1475	-398
304L	455	0.192	493	131	2383	-383
304L	599	0.163	493	131	2810	-393
304L	696	0.103	493	131	4433	-368
304L	1008	0.095	493	131	4836	-295
304L	1151	0.080	493	131	5695	-350
C1010	26	6.15	159	84	44.89	-492
C1010	287	2.45	159	84	112.68	-399
C1010	455	3.14	159	84	88.02	-385
C1010	599	2.93	159	84	94.10	-393
C1010	696	1.35	159	84	204.50	-450
C1010	1008	0.38	159	84	722.0	-283
C1010	1151	0.32	159	84	875.8	-335

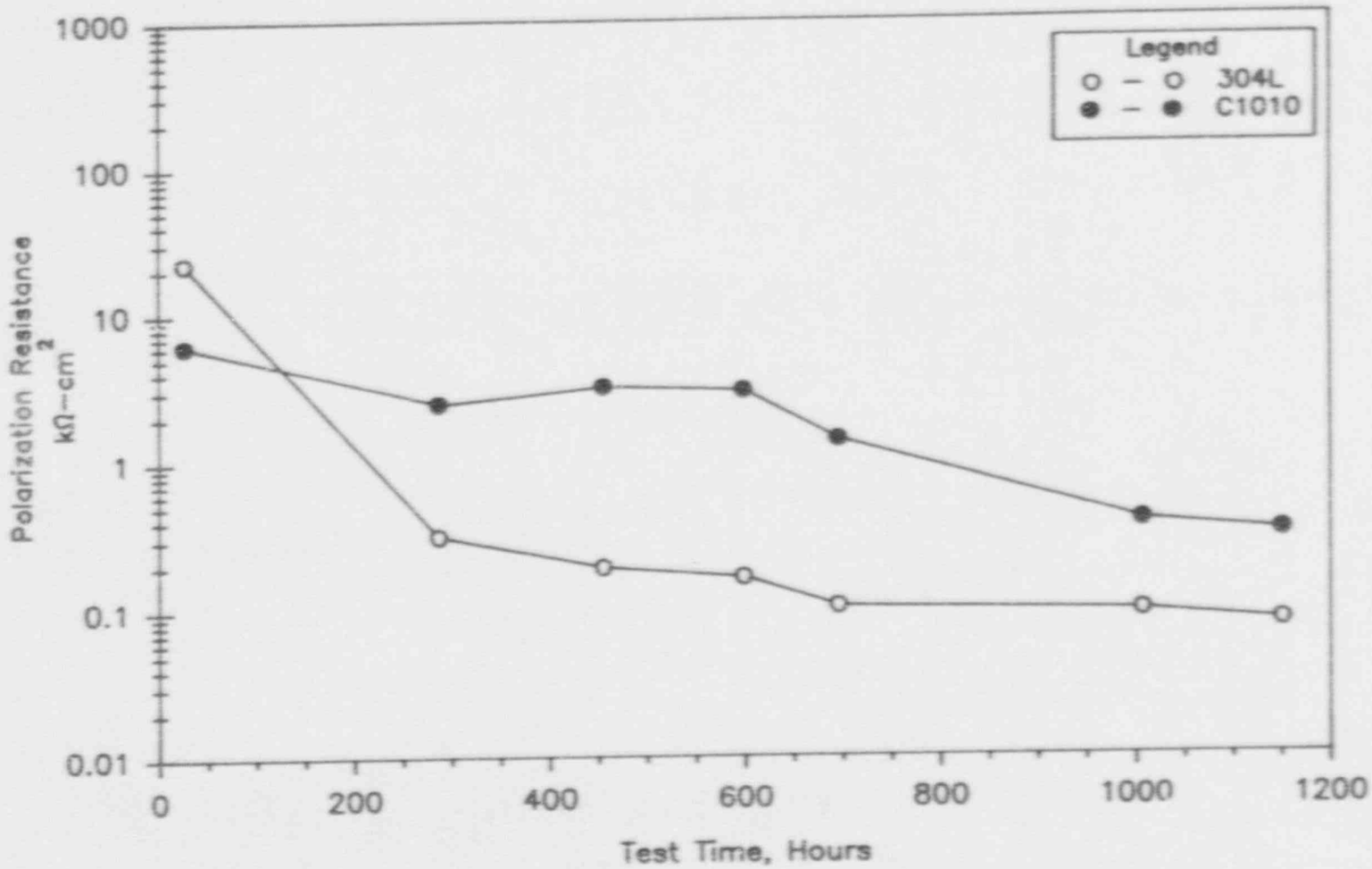

Figure 4.18 Polarization Resistance As A Function Of Test Time For Sandwich Specimens Of Alloy 304L And C1010 Carbon Steel In Simulated J-13 Well Water At 90°C (Test #1).

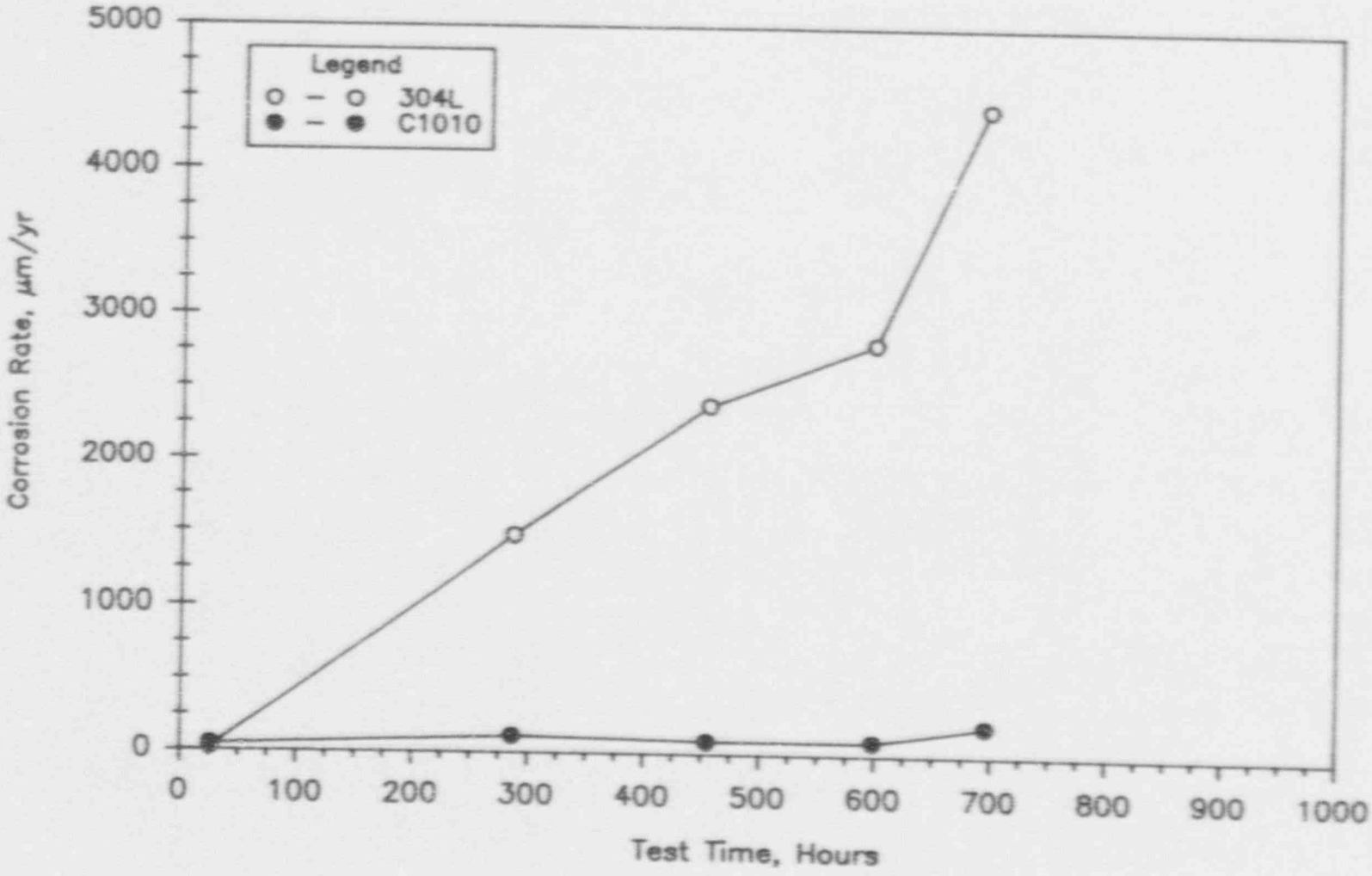

Figure 4.19 Corrosion Rate As A Function Of Test Time For Sandwich Specimens Of Alloy 304L And C1010 Carbon Steel In Simulated J-13 Well Water At 90°C (Test #1).

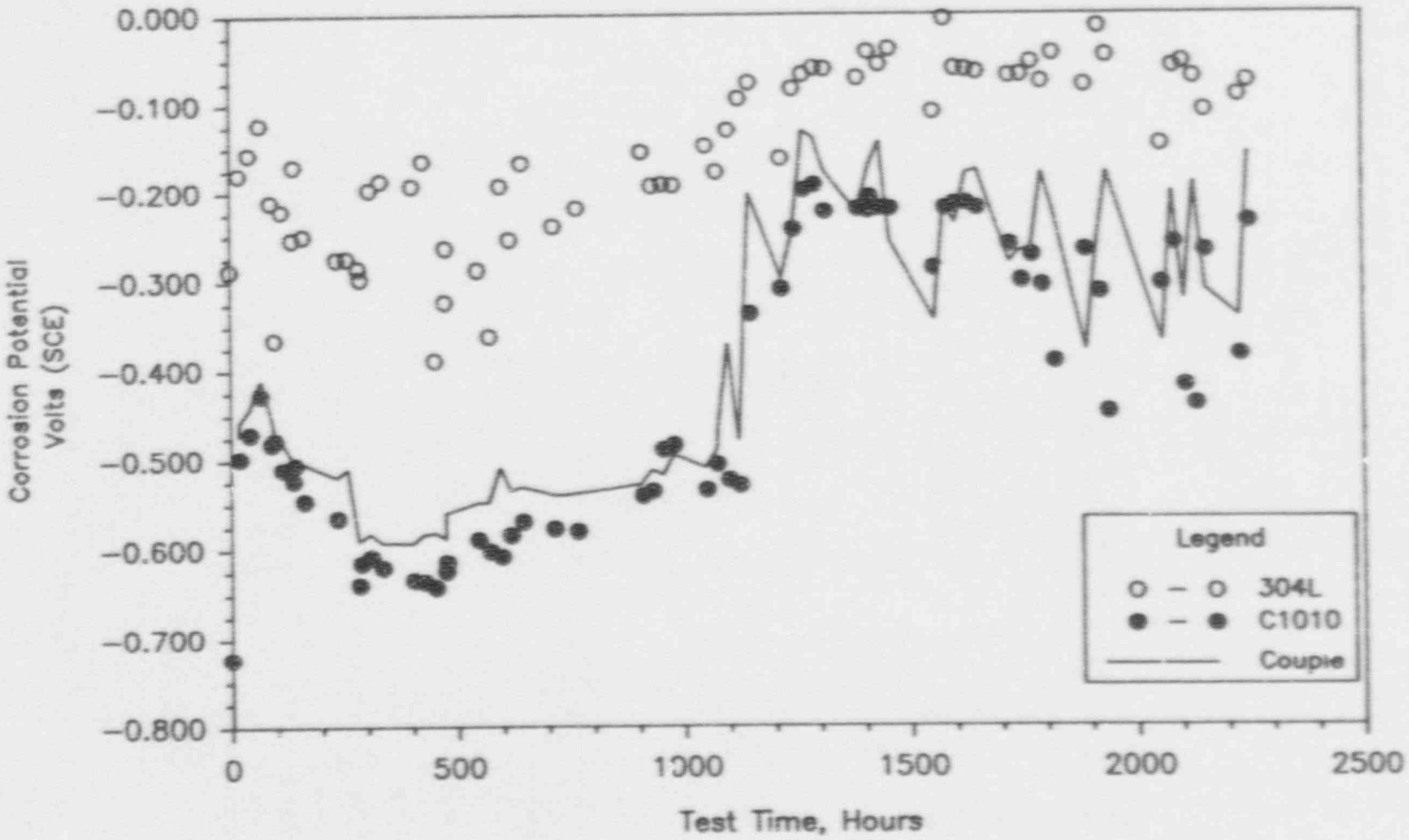

Figure 4.20 Corrosion Potential As A Function Of Test Time For Sandwich Specimens Of Alloy 304L and C1010 Carbon Steel In Simulated J-13 Well Water At 90°C (Test #2).

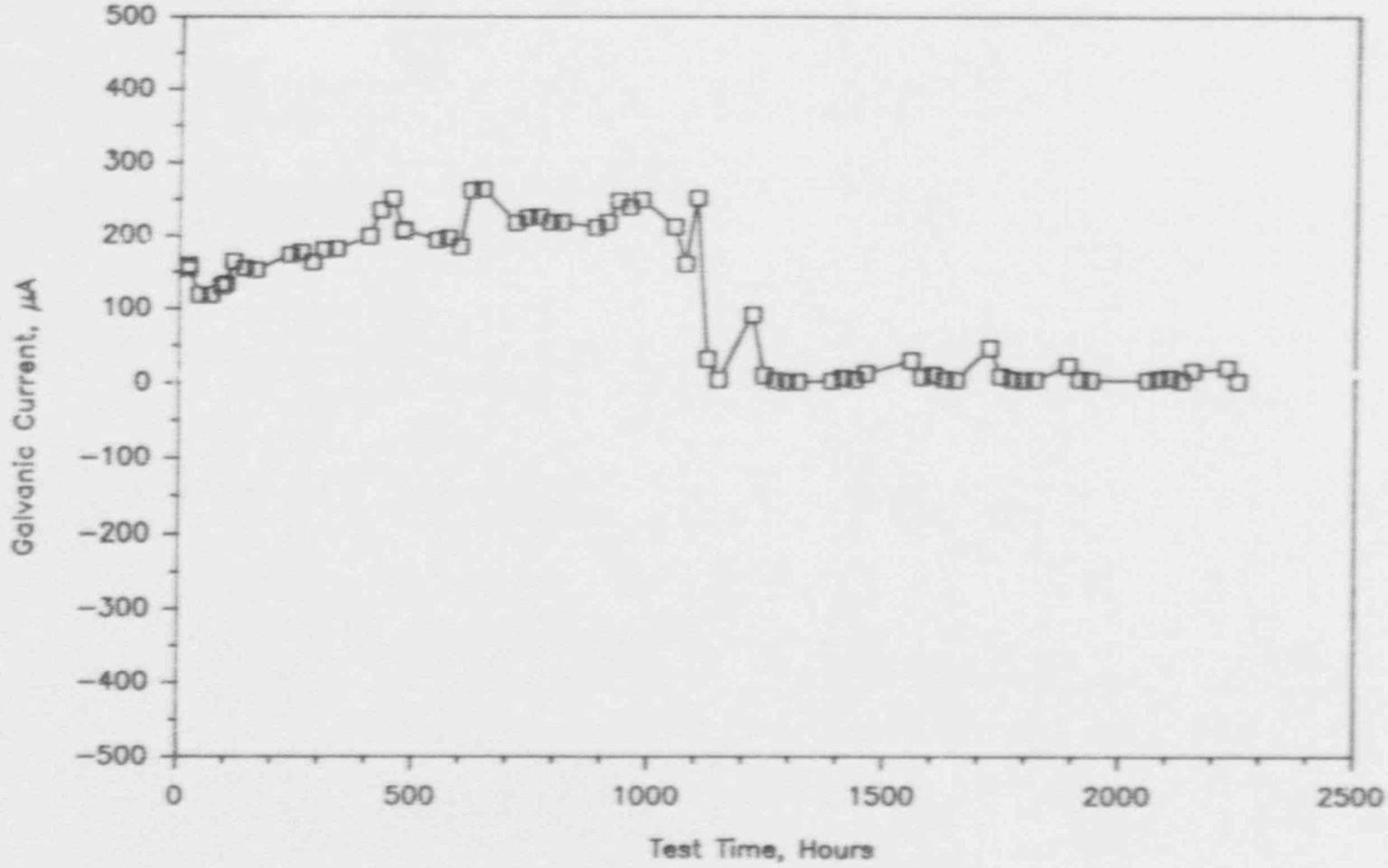

Figure 4.21 Galvanic Current As A Function Of Test Time For Sandwich Specimens Of Alloy 304L And C1010 Carbon Steel In Simulated J-13 Well Water At 90°C (Test #2).

Table 4.5 Summary Of Results Of Electrochemical Measurements Performed On Sandwich Specimens Of Alloy 304L And C1010 Carbon Steel In Simulated J-13 Well Water At 90°C; Test #2.

Alloy	Hours	Polarization Resistance kohm-cm^2	Slope mV/Decade B_a	Slope mV/Decade B_c	Corrosion Rate µm/yr	E_{cor} mV (SCE)
304L	115	44.2	493	131	10.36	-222
304L	287	246.0	493	131	1.86	-265
304L	428	134.0	493	131	3.43	-166
304L	573	34.1	493	131	13.43	-363
304L	742	154.0	493	131	2.98	-170
304L	910	122.0	493	131	3.76	-156
304L	1244	646.0	493	131	0.70	- 84
304L	1413	345.0	493	131	1.33	- 45
304L	1582	725.0	493	131	0.63	- 8
304L	1750	28.50	493	131	0.30	- 53
304L	1924	1520.0	493	131	0.70	- 29
304L	2088	652.0	493	131	1.31	- 60
304L	2252	451.0	493	131	1.01	- 73
C1010	115	4.65	159	84	59.37	-511
C1010	287	16.00	159	84	17.23	-616
C1010	428	6.80	159	84	40.62	-637
C1010	573	[illegible]	159	84	59.17	-603
C1010	742	[illegible]	159	84	17.75	-566
C1010	910	4.32	159	84	63.85	-548
C1010	1244	445.00	159	84	0.62	-245
C1010	1413	156.00	159	84	1.78	-208
C1010	1582	157.00	159	84	1.76	-218
C1010	1750	177.00	159	84	1.56	-285
C1010	1924	87.30	159	84	3.16	-315
C1010	2088	54.30	159	84	5.09	-257
C1010	2252	121.00	159	84	2.28	-237

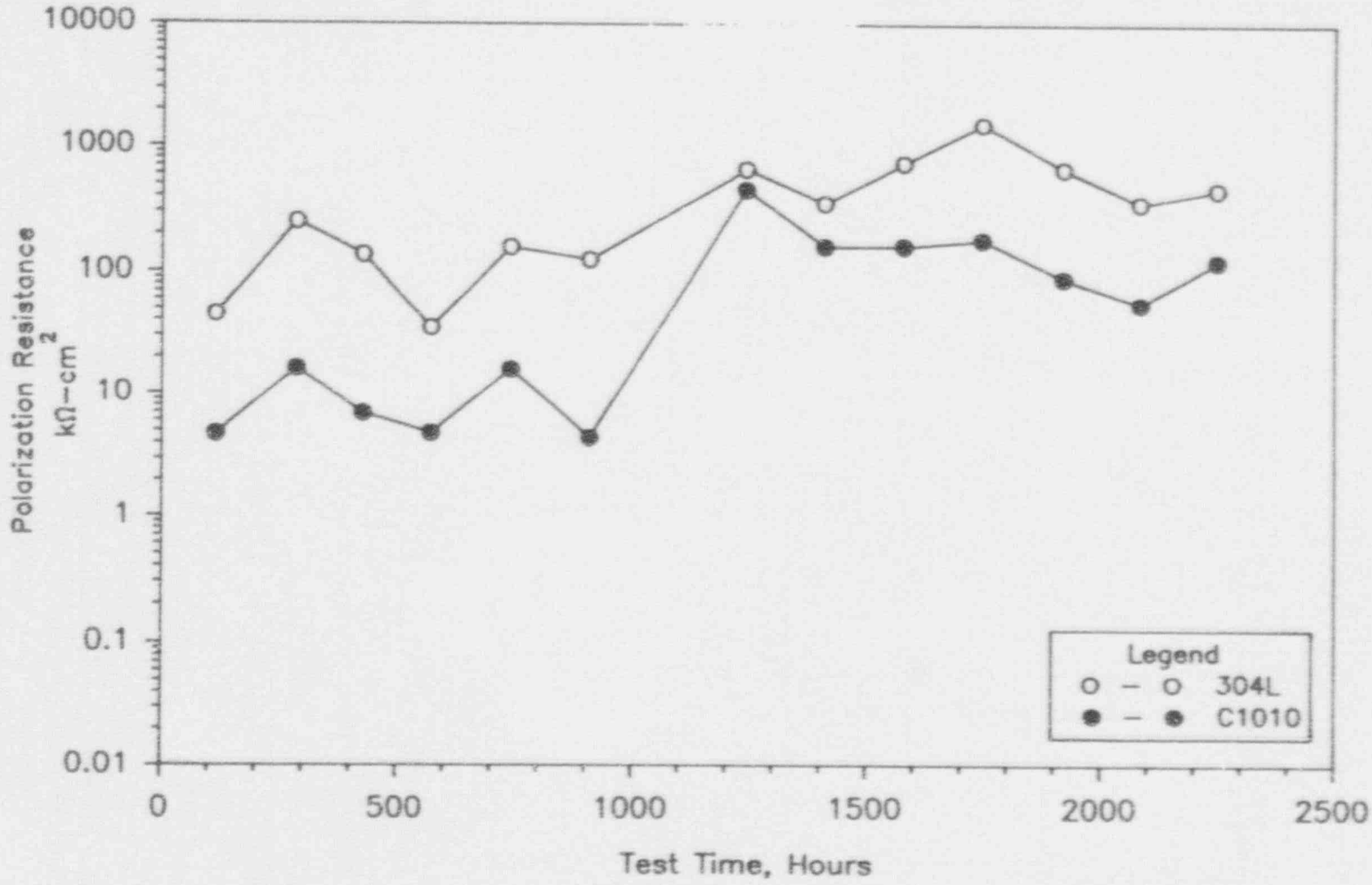

Figure 4.22 Polarization Resistance As A Function Of Test Time For Sandwich Specimens Of Alloy 304L and C1010 Carbon Steel in Simulated J-13 Well Water At 90°C (Test #2).

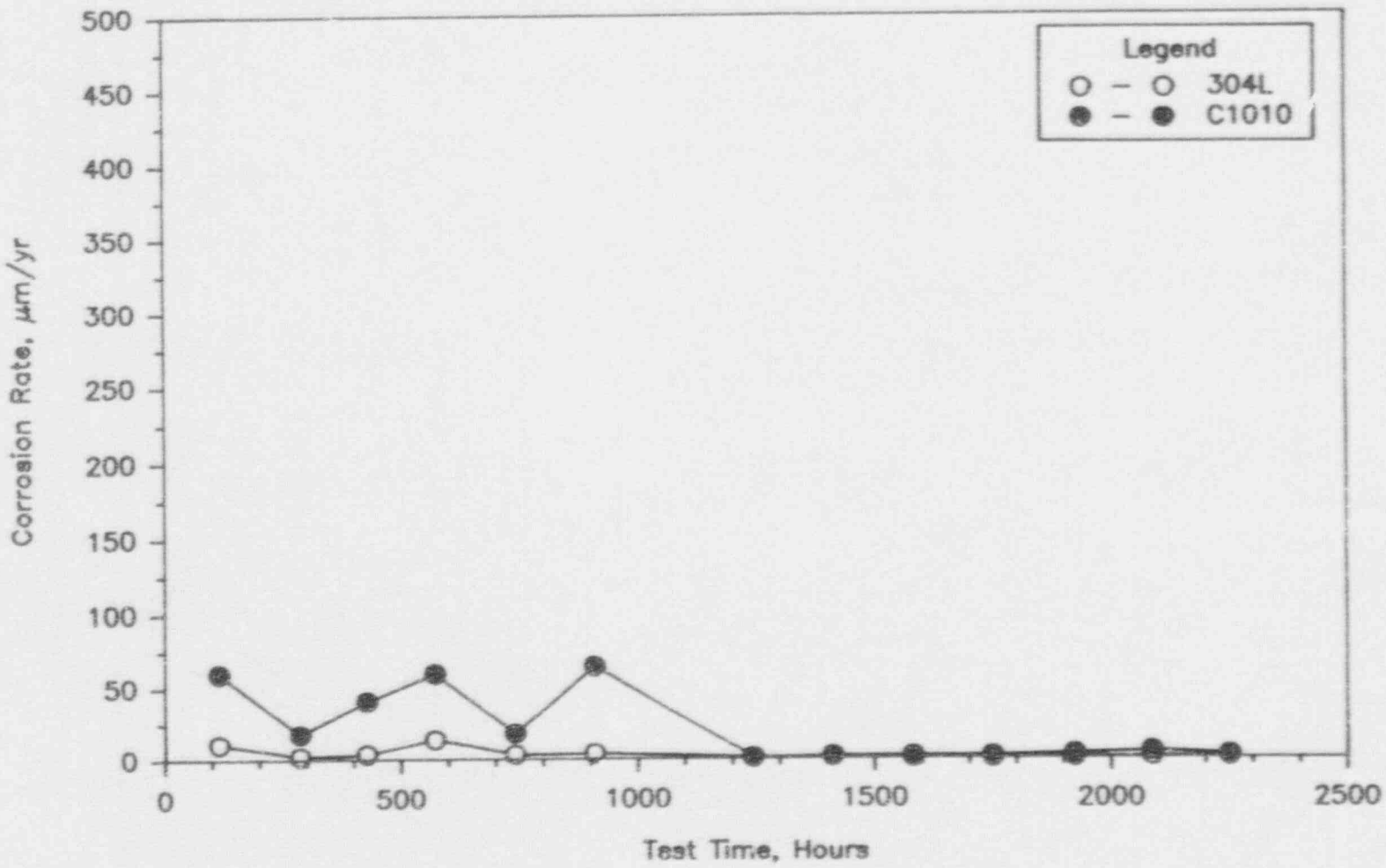

Figure 4.23 Corrosion Rate As A Function Of Test Time For Sandwich Specimens Of Alloy 304L And C1010 Carbon Steel In Simulated J-13 Well Water At 90°C (Test #2).

The second experiment was terminated after 2259 hours of exposure. Optical examination of the specimens and analysis of the weight-loss data revealed very low corrosion rates for Alloy 304L. The weight-loss technique showed Alloy 304L to have a corrosion rate of 0.03 µm/yr, whereas the corrosion rate of C1010 was 398 µm/yr; see Table 4.6. The exterior surface of the Alloy 304L specimen was shiny and showed no visible attack. The interior surface (facing the C1010 coupon) exhibited some localized black deposits, but showed no visible attack. The specimen of C1010 exhibited severe metal loss on both the exterior and the interior surfaces. The edge of the C1010 specimen was severely corroded at the contact for the electrical lead such. Comparison of the corrosion rates calculated from PR measurements to those from weight-loss data show that the PR technique overestimated the corrosion rate of Alloy 304L. On the other hand, the carbon steel had a significantly higher corrosion rate, based on weight loss, than that which was determined by the PR measurements. This discrepancy between the two corrosion rates for carbon steel may have been a reflection of the contribution of galvanic corrosion to the attack.

The third experiment was performed with C1010 and Alloy 304L in 90°C simulated J-13 well water containing 1000 ppm chloride as sodium chloride (NaCl). Corrosion potentials and galvanic current measurements measured throughout the exposure period are given in Figures 4.24 and 4.25, respectively. For comparison, the weekly PR measurements, and corrosion rates determined from these measurements, are given in Table 4.7 and exhibited graphically in Figures 4.26 and 4.27, respectively.

The third experiment was terminated after 2057 hours of exposure. Optical examinations of the specimens and analysis of the weight-loss data revealed very low corrosion rates for Alloy 304L. The weight-loss technique showed Alloy 304L to have a corrosion rate of less than 0.04 µm/yr, whereas the corrosion rate of C1010 was 414 µm/yr. As in the previous experiment without added chloride, the exterior surface of the specimen of Alloy 304L was shiny and showed no visible attack. The interior surface exhibited some localized black deposits, but showed no visible attack. The specimen of C1010 exhibited severe metal loss on both the exterior and interior surfaces. Comparison of the corrosion rates calculated from PR measurements to those from weight-loss data also showed that the PR technique overestimated the corrosion rate of Alloy 304L but underestimated the corrosion rate of Alloy C1010. Again, the higher corrosion rate of Alloy 1010 may be due, in part, to the contribution of galvanic corrosion.

4.2.2.2 Alloy 304L/Alloy 825 Galvanic Couples

The fourth and fifth borehole liner-container interaction experiments were performed with Alloy 304L and Alloy 825 as the liner and container material, respectively. In the fourth experiment, these alloys were evaluated in simulated J-13 well water at 90°C. Corrosion potentials and galvanic current measurements obtained throughout the duration of the exposure are shown in Figures 4.28 and 4.29, respectively. These figures illustrate the similarity in the corrosion potentials of the two alloys, and as a consequence, the very low galvanic current. Polarization resistance measurements, and corrosion rates determined from these measurements, performed over the duration of the exposure are summarized in Table 4.8 and exhibited graphically in Figures 4.30 and 4.31. These data indicate high polarization resistance which correspond to very low corrosion rates.

Table 4.6 Summary Of Corrosion Rates Calculated From Gravimetric Measurements Of Sandwich Specimens Of Alloy 304L And C1010 Carbon Steel In Simulated J-13 Environments At 90°C.

Environment	Exposure Hours	Alloy	Corrosion Rate µm/y	Description
Simulated J-13 (Test #1)	1303	304L	0.61	Exterior side covered with thin blue oxide film. Interior side exhibited some black deposits and slight etching. One pit, 18 µm in depth, was observed on the interior side.
		C1010	208.34	Exterior side exhibited severe metal loss and deep pitting. The deepest pit measured 240 µm. The interior side showed severe metal loss with the deepest areas measuring 82 µm.
Simulated J-13 (Test #2)	2259	304L	0.03	Exterior side was shiny with no visible attack. Interior side showed localized black deposits, but no visible attack.
		C1010	398.46	Exterior and interior sides exhibited severe metal loss.
Simulated J-13 +1000 ppm Cl as NaCl (Test #3)	2057	304L	<0.04	Exterior side was shiny with no visible attack. Interior side showed localized black deposits, but no visible attack.
		C1010	414.44	Exterior and interior sides exhibited severe metal loss.

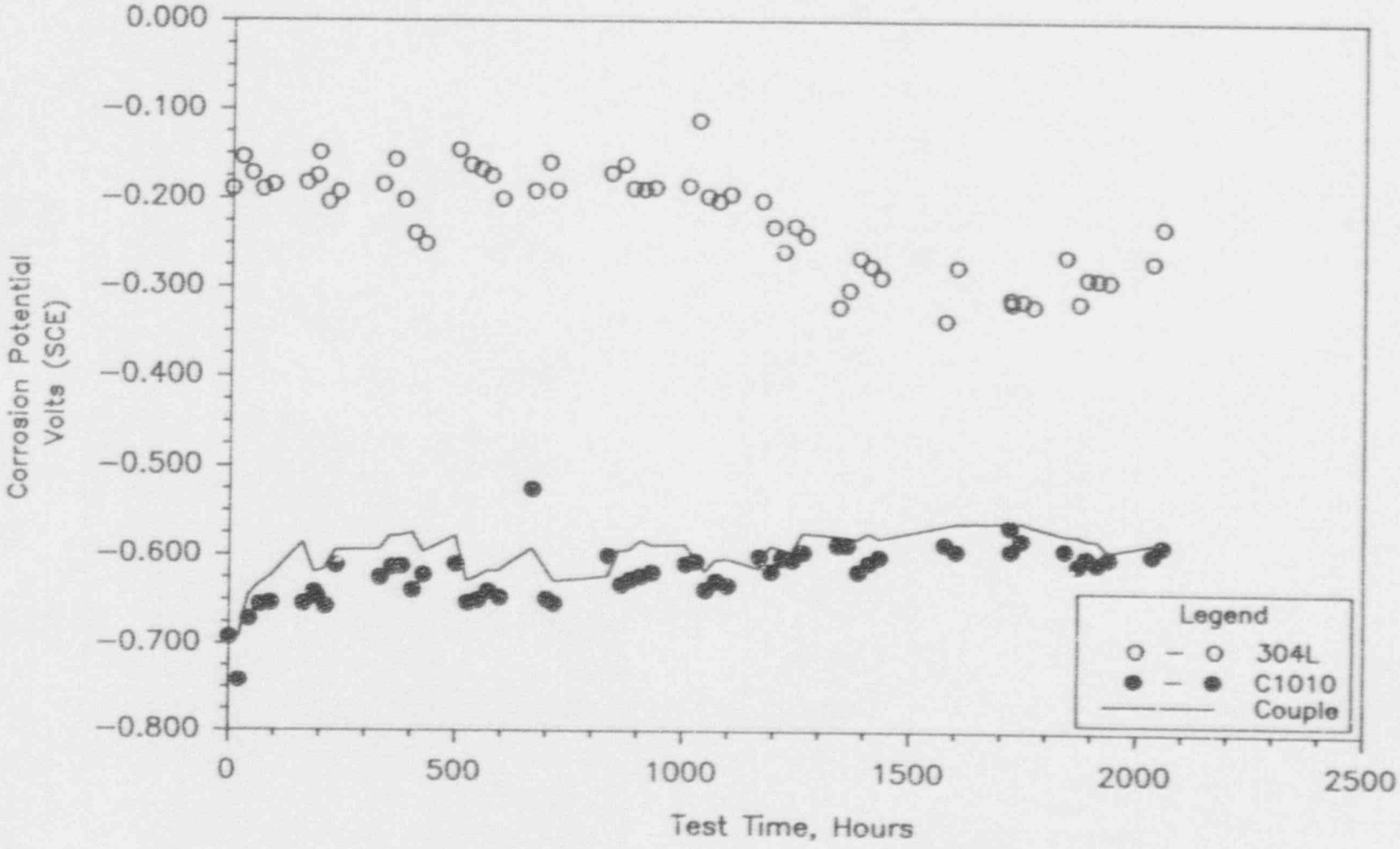

Figure 4.24 Corrosion Potential As A Function of Test Time For Sandwich Specimens Of Alloy 304L And C1010 Carbon Steel Tested At 90°C In Simulated J-13 Well Water Containing 1000 ppm Chloride As Sodium Chloride (Test #3).

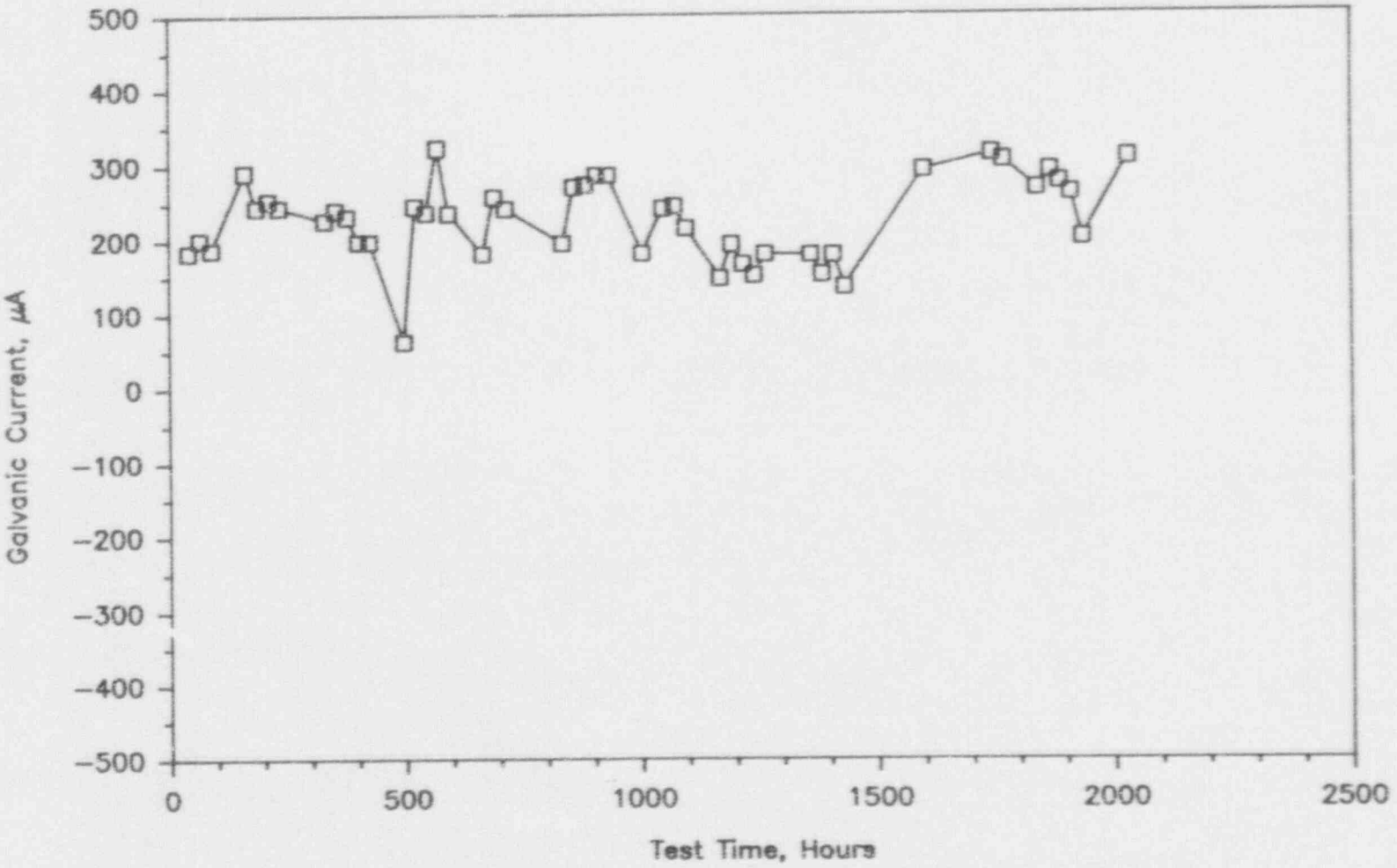

Figure 4.25 Galvanic Current As A Function Of Test Time For Sandwich Specimens Of Alloy 304L And C1010 Carbon Steel Tests At 90°C In Simulated J-13 Well Water Containing 1000 ppm Chloride As Sodium Chloride (Test #3).

Table 4.7 Summary Of Results Of Electrochemical Measurements Performed On Sandwich Specimens Of Alloy 304L And C1010 Carbon Steel In 90°C Simulated J-13 Well Water Containing 1000 ppm Chloride As Sodium Chloride; Test #3.

Alloy	Hours	Polarization Resistance kohm-cm^2	Slope mV/Decade B_a	Slope mV/Decade B_c	Corrosion Rate µm/yr	E_{cor} mV (SCE)
304L	193	383.00	429	123	1.11	-150
304L	359	638.00	429	123	0.66	-157
304L	526	311.00	429	123	1.36	-165
304L	700	369.00	429	123	1.15	-161
304L	864	256.00	429	123	1.65	-163
304L	1028	208.00	429	123	2.03	-117
304L	1195	89.10	429	123	4.75	-232
304L	1363	51.60	429	123	8.20	-303
304L	1722	26.60	429	123	15.90	-317
304L	1872	28.50	429	123	14.84	-317
304L	2034	34.30	429	123	12.33	-270
C1010	193	1.99	97	193	162.60	-647
C1010	359	1.66	97	193	194.80	-614
C1010	526	3.17	97	193	102.20	-657
C1010	700	1.34	97	193	242.90	-650
C1010	864	0.89	97	193	364.10	-634
C1010	1028	0.44	97	193	729.50	-609
C1010	1195	0.68	97	193	480.10	-619
C1010	1363	0.51	97	193	641.10	-588
C1010	1722	0.51	97	193	631.30	-593
C1010	1872	0.51	97	193	633.30	-611
C1010	2034	0.52	97	193	620.20	-598

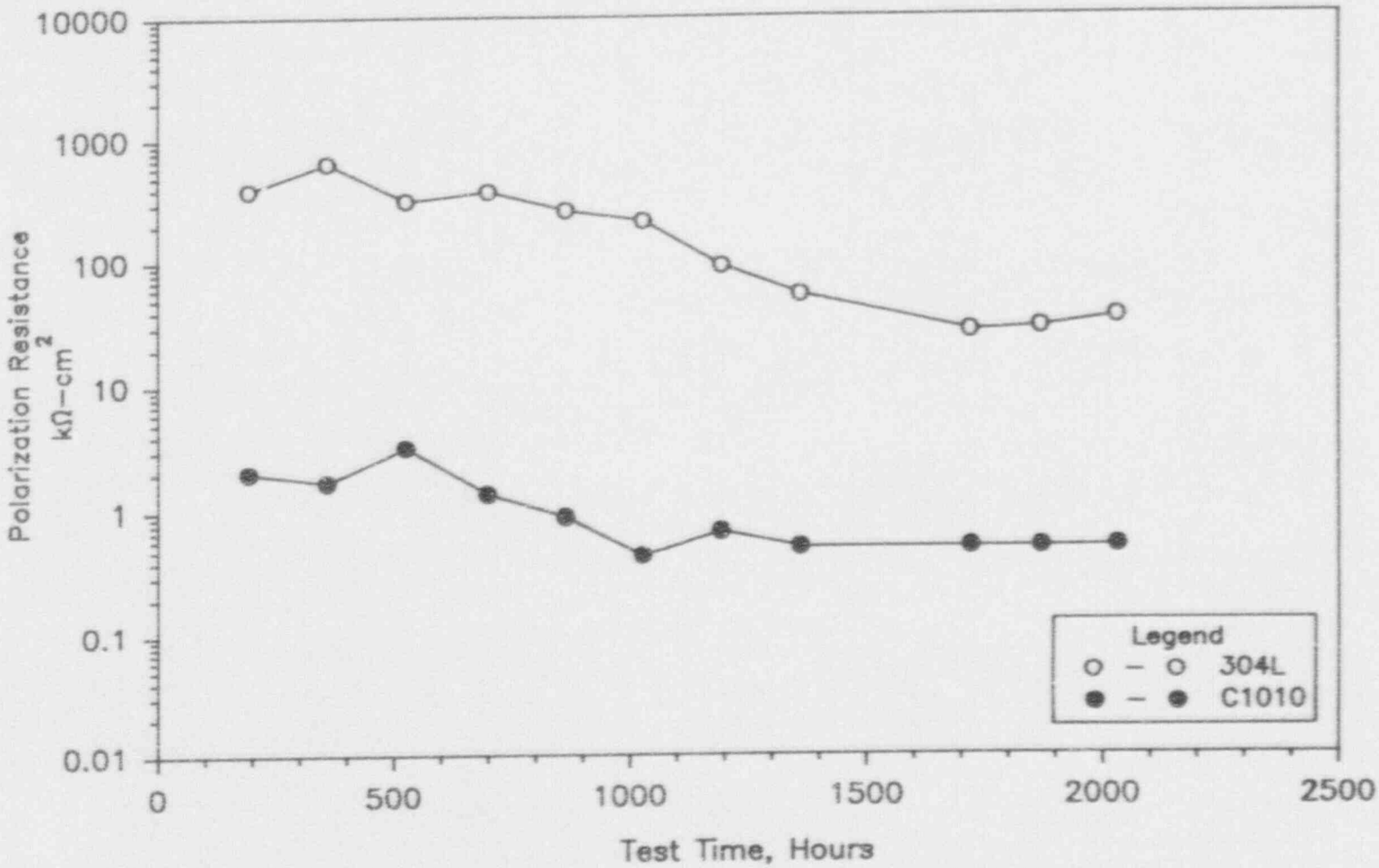

Figure 4.26 Polarization Resistance As A Function Of Test Time For Sandwich Specimens Of Alloy 304L And C1010 Carbon Steel Tested At 90°C In Simulated J-13 Well Water Containing 1000 ppm Chloride As Sodium Chloride (Test #3).

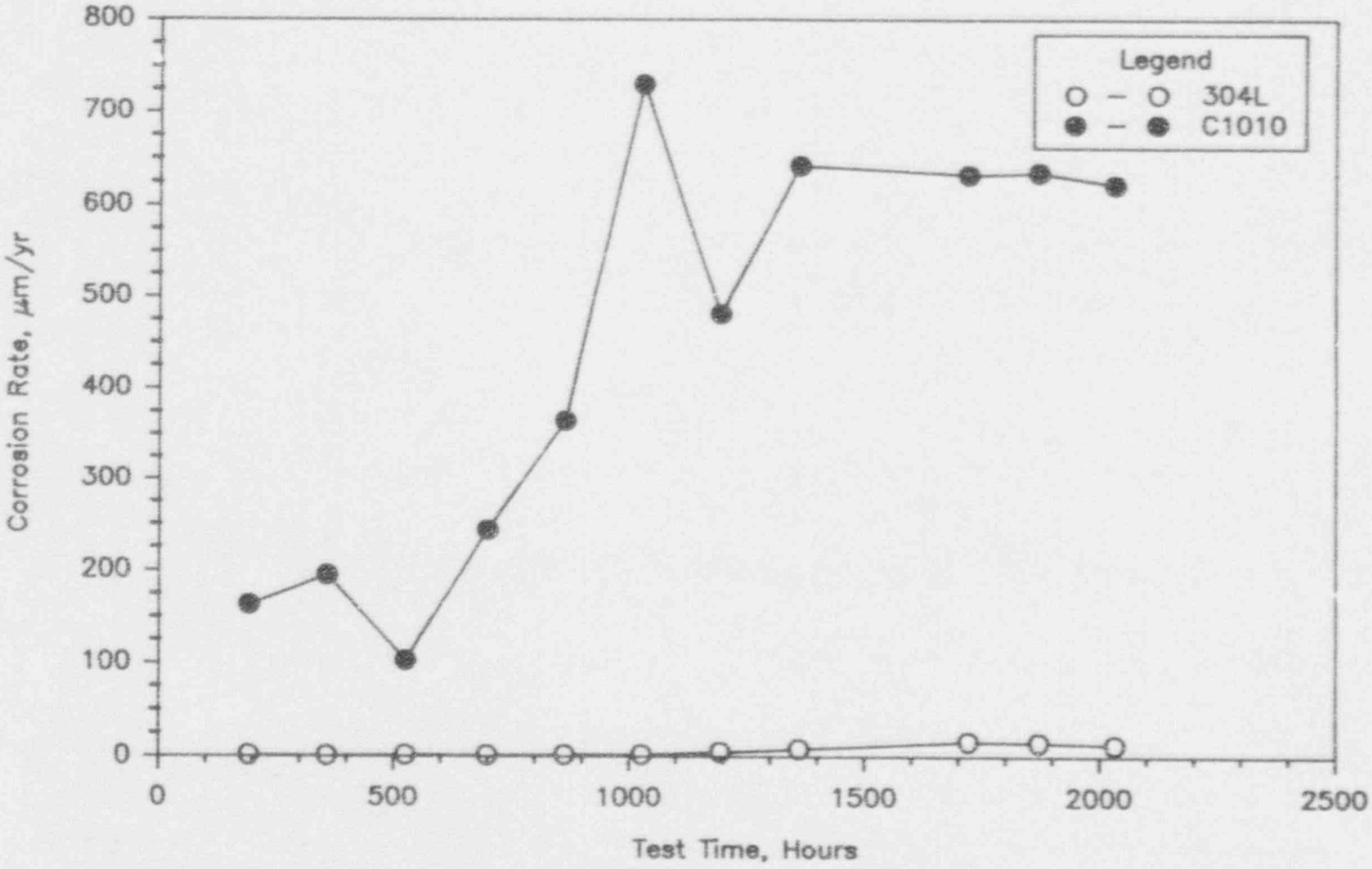

Figure 4.27 Corrosion Rate As A Function Of Test Time For Sandwich Specimens Of Alloy 304L And C1010 Carbon Steel Tested At 90°C In Simulated J-13 Well Water Containing 1000 ppm Chloride As Sodium Chloride (Test #3).

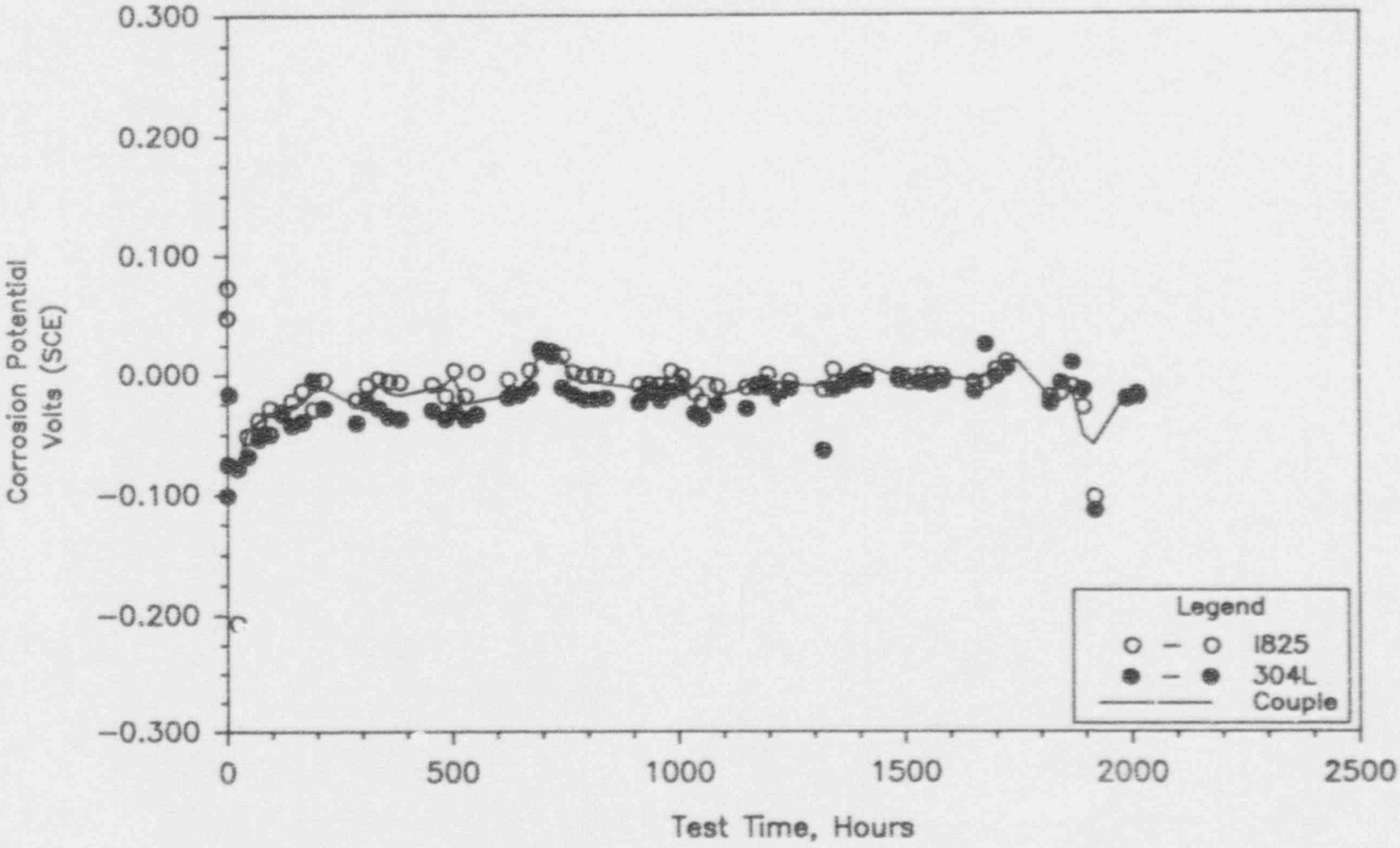

Figure 4.28 Corrosion Potential As A Function Of Test Time For Sandwich Specimens Of Alloy 825 And Alloy 304L In Simulated J-13 Well Water At 90°C (Test #4).

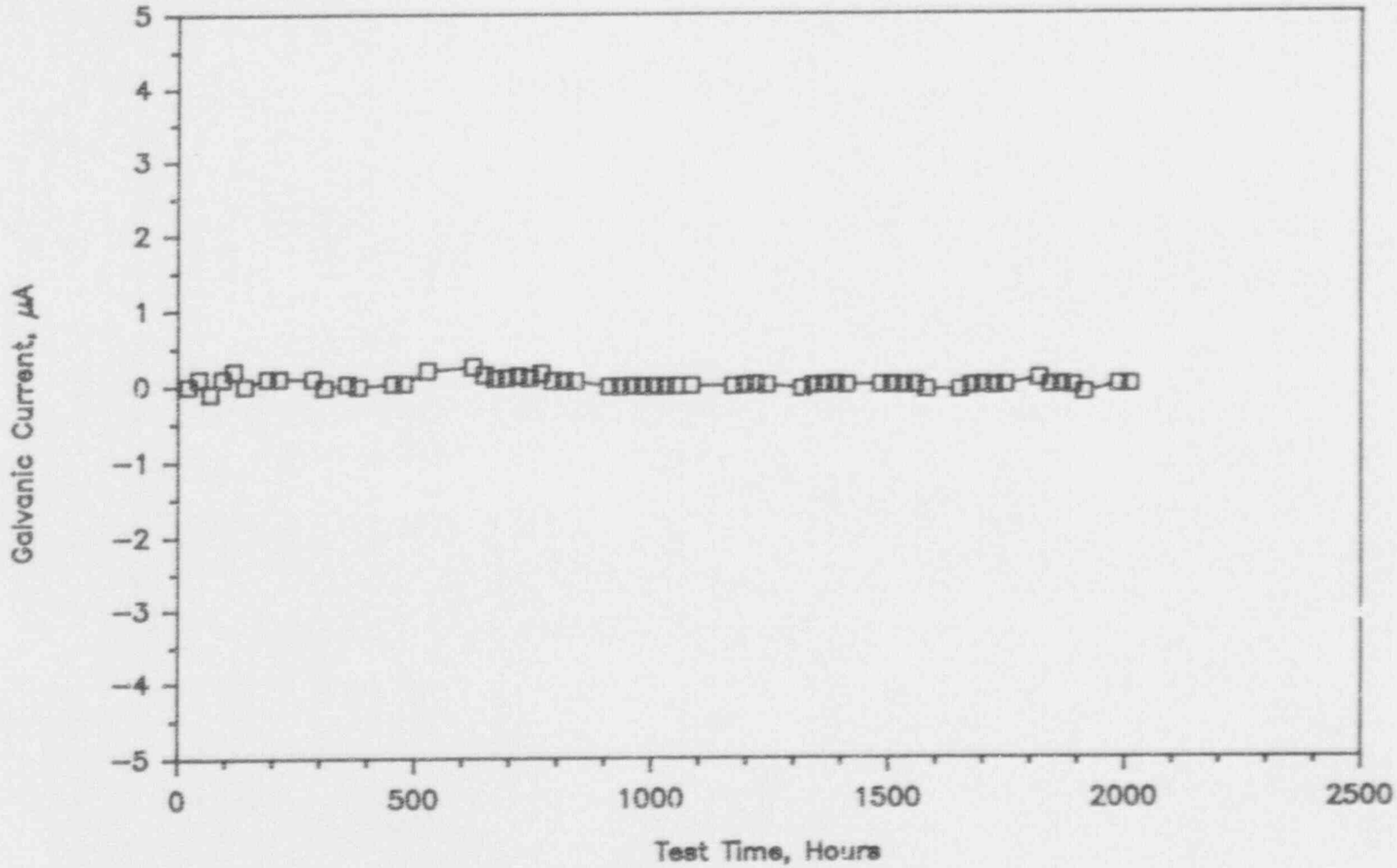

Figure 4.29 Galvanic Current As A Function Of Test Time For Sandwich Specimens Of Alloy 825 And Alloy 304L In Simulated J-13 Well Water At 90°C (Test #4).

Table 4.8. Summary Of Results Of Electrochemical Measurements Performed On Sandwich Specimens Of Alloy 304L And Alloy 825 In Simulated J-13 Well Water At 90°C; Test #4.

Alloy	Hours	Polarization Resistance kohm-cm²	Slope mV/Decade B_a	Slope mV/Decade B_c	Corrosion Rate µm/yr	E_{cor} mV (SCE)
304L	23	1 250	493	131	0.37	-78
304L	144	3 790	493	131	0.12	-40
304L	311	5 220	493	131	0.09	-22
304L	485	4 850	493	131	0.09	-38
304L	649	5 530	493	131	0.08	-16
304L	768	3 100	493	131	0.15	-18
304L	936	—	493	131	—	-15
304L	1 037	6 220	493	131	0.07	-32
304L	1 175	6 950	493	131	0.07	-12
304L	1 367	7 220	493	131	0.06	-9
304L	1 511	9 000	493	131	0.05	1
304L	1 679	11 600	493	131	0.04	24
304L	1 846	8 690	493	131	0.05	-7
304L	2 015	8 700	493	131	0.05	-11
825	23	800	211	221	0.50	-220
825	144	3 000	211	221	0.13	- 22
825	311	4 310	211	221	0.09	-8
825	485	3 780	211	221	0.11	-22
825	649	3 480	211	221	0.11	-19
825	768	2 680	211	221	0.15	+1
825	936	3 920	211	221	0.12	-9
825	1 037	3 170	211	221	0.13	-16
825	1 175	4 350	211	221	0.09	-10
825	1 367	3 010	211	221	0.13	-9
825	1 511	3 780	211	221	0.10	-8
825	1 679	5 120	211	221	0.08	-8
825	1 846	2 220	211	221	0.18	-17
825	2 015	2 350	211	221	0.17	-20

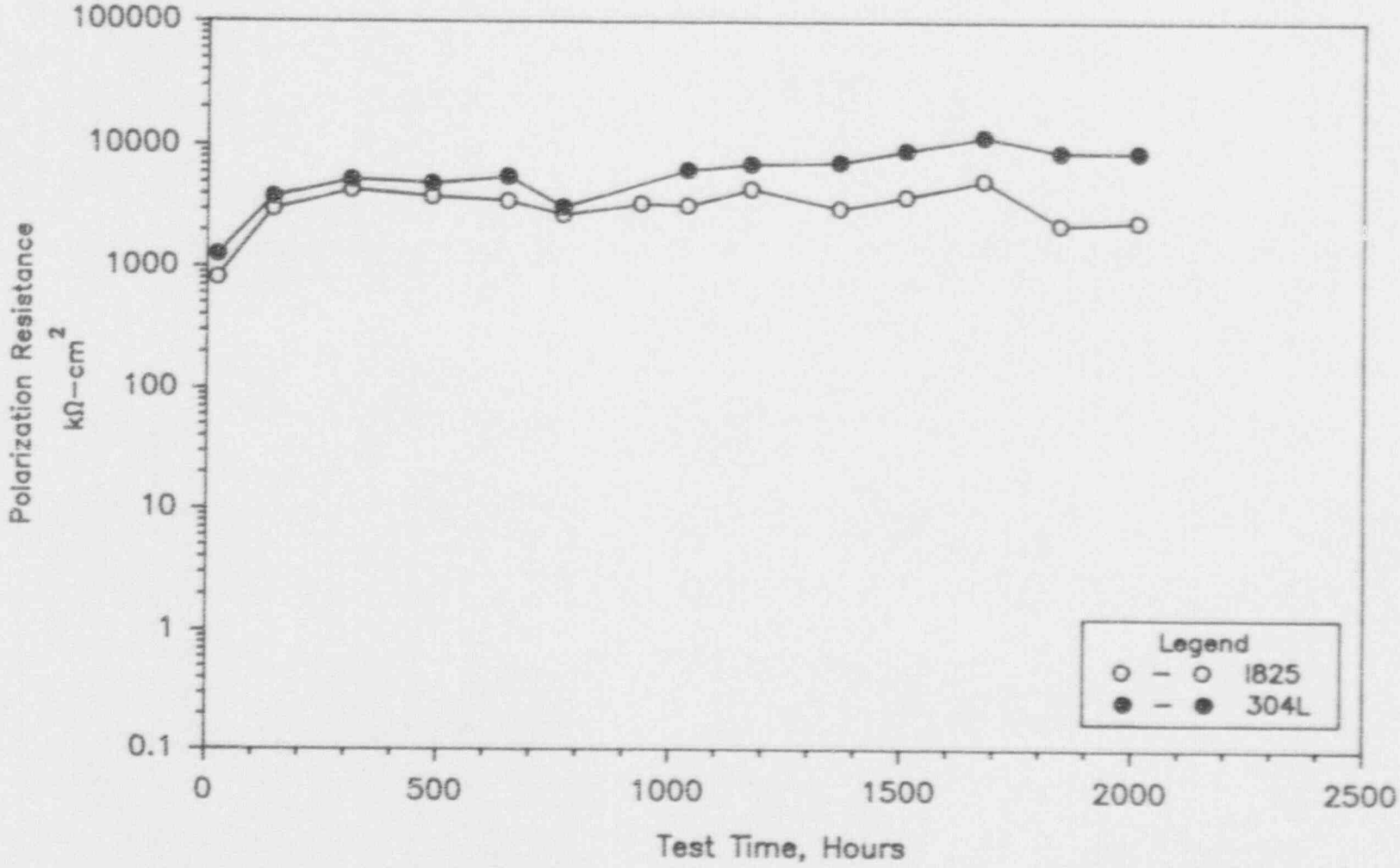

Figure 4.30 Polarization Resistance As A Function Of Test Time For Sandwich Specimens Of Alloy 825 And Alloy 304L In Simulated J-13 Well Water At 90°C (Test #4).

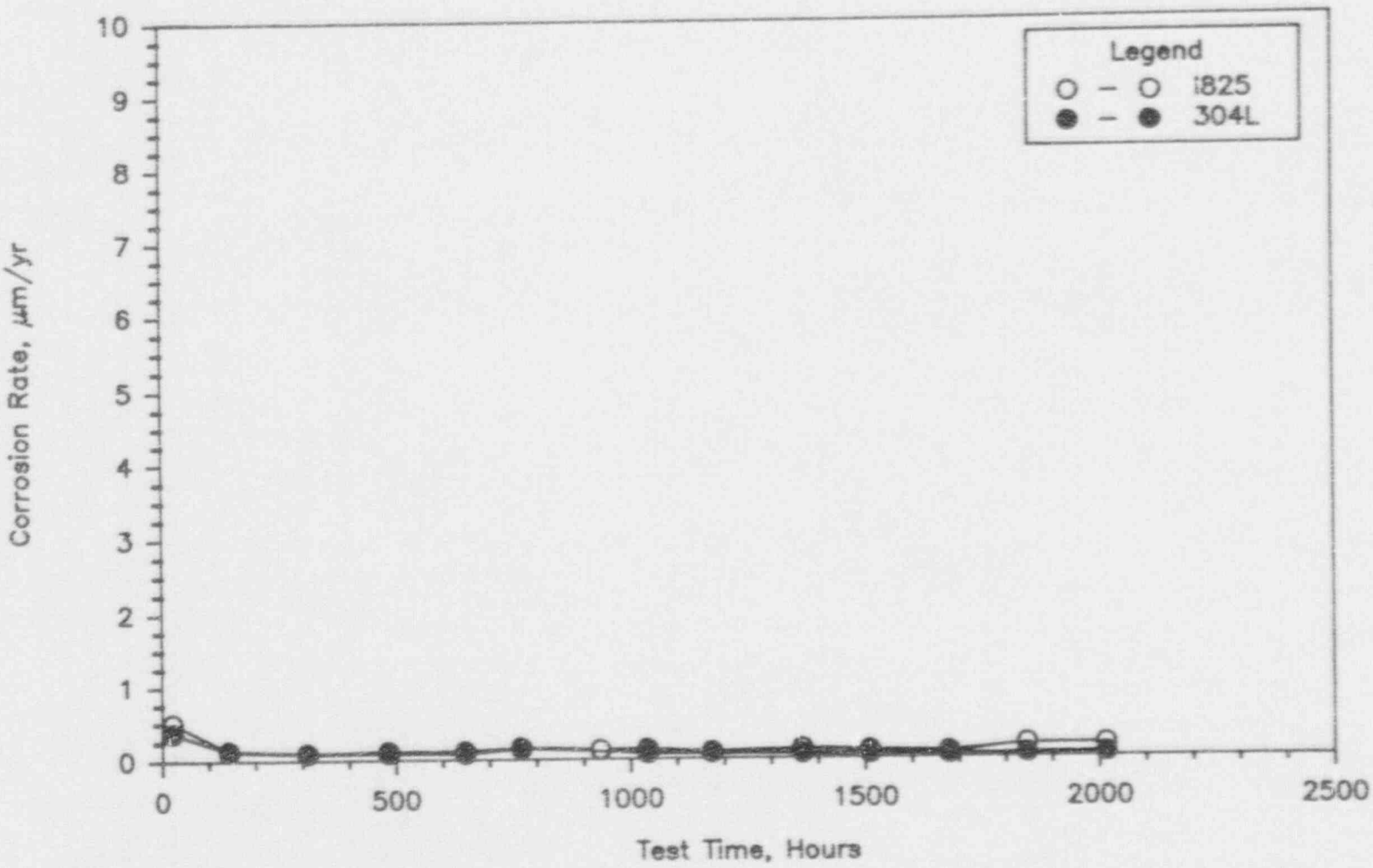

Figure 4.31 Corrosion Rate As A Function Of Test Time For Sandwich Specimens Of Alloy 825 And Alloy 304L In Simulated J-13 Well Water At 90°C (Test #4).

The fourth experiment was terminated after 2019 hours of exposure. Optical examination of the specimens and analysis of the weight-loss data revealed very low corrosion rates for both alloys. These rates were comparable to the corrosion rates calculated from the PR measurements shown in Table 4.8. Neither specimen showed any visible attack and the weight-loss technique indicated corrosion rates of 0.57 µm/yr and 0.24 µm/yr for Alloy 304L and Alloy 825, respectively.

In the fifth experiment, Alloy 304L and Alloy 825 were evaluated in Solution Number 10 at 90°C. The composition of Solution 10 is given in Table 2.5. Solution Number 10 was chosen from the experimental test matrix because of the corrosion behavior observed for these alloys in this environment in previous CPP tests. For Alloy 304L, a large hysteresis loop occurred in the CPP curve and optical examination revealed pitting and crevice attack. The CPP curve for Alloy 825, however, did not exhibit hysteresis and there was no evidence of attack following the CPP test. The CPP curves for these alloys in Solution Number 10 are given in Appendix E.

Corrosion potentials and galvanic current measurements obtained throughout the duration of the exposure are shown in Figures 4.32 and 4.33, respectively. These figures also show similar corrosion potentials for both alloys. As in the previous experiment, the similarity of the corrosion potentials resulted in very low galvanic current. Polarization resistance measurements, and corrosion rates determined from these measurements, performed over the duration of the exposure are summarized in Table 4.9. These same data are exhibited graphically in Figures 4.34 and 4.35. These data also show high polarization resistance values, which correspond to low corrosion rates.

The fifth experiment was terminated after 2021 hours of exposure. Optical examination of the specimens and analysis of the weight-loss data revealed very low corrosion rates for both alloys. As in the previous experiment, corrosion rates calculated from PR measurements (Table 4.9) and gravimetric measurements were similar for both specimens. Neither specimen showed any visible attack. The weight-loss technique showed corrosion rates of 1.57 µm/yr and 0.88 µm/yr for Alloy 304L and Alloy 825, respectively.

Table 4.10 summarizes the corrosion rates calculated from weight-loss measurements and the results of the optical examinations following each of the tests discussed above. These data show corrosion rates of less than 1.6 µm/yr with no visible attack. No pitting was observed in Alloy 304L in Solution Number 10, a solution expected to cause pitting based upon results of previous CPP testing in this environment. The discrepancy between the corrosion behavior observed for Alloy 304L in this test (Test No. 5), and after the CPP test can be explained by comparing the corrosion potentials (Figure 4.32) to the electrochemical parameters, E_{pit} and E_{prot}. Throughout the exposure in Test No. 5, the corrosion potentials of Alloy 304L ranged between -150 mV (SCE) and -100 mV (SCE) which is considerably less than E_{pit} (+700 mV (SCE)) and close to E_{prot} (-120 mV (SCE)).

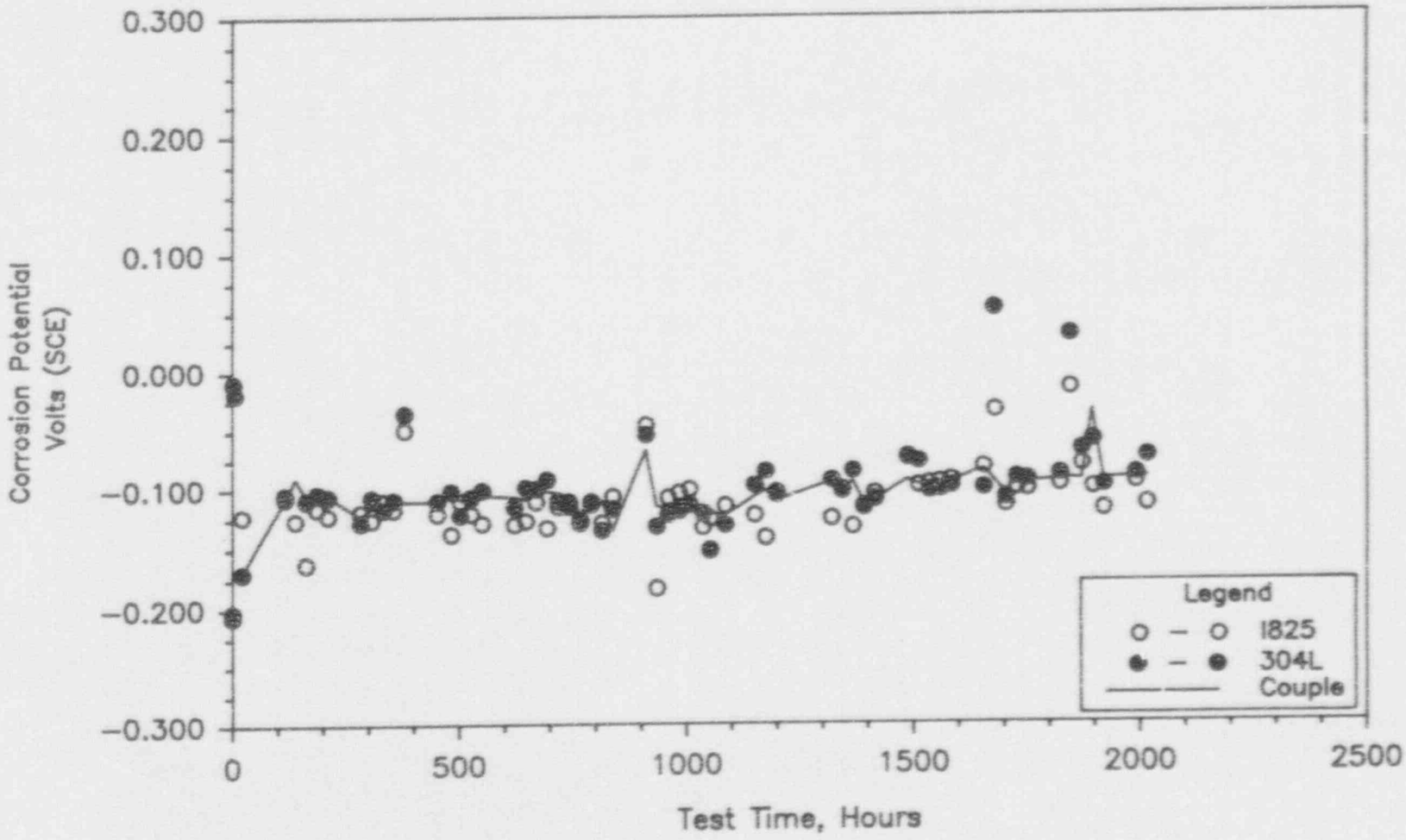

Figure 4.32 Corrosion Potential As A Function Of Test Time For Sandwich Specimens Of Alloy 825 And Alloy 304L In Solution No. 10 At 90°C (Test #5).

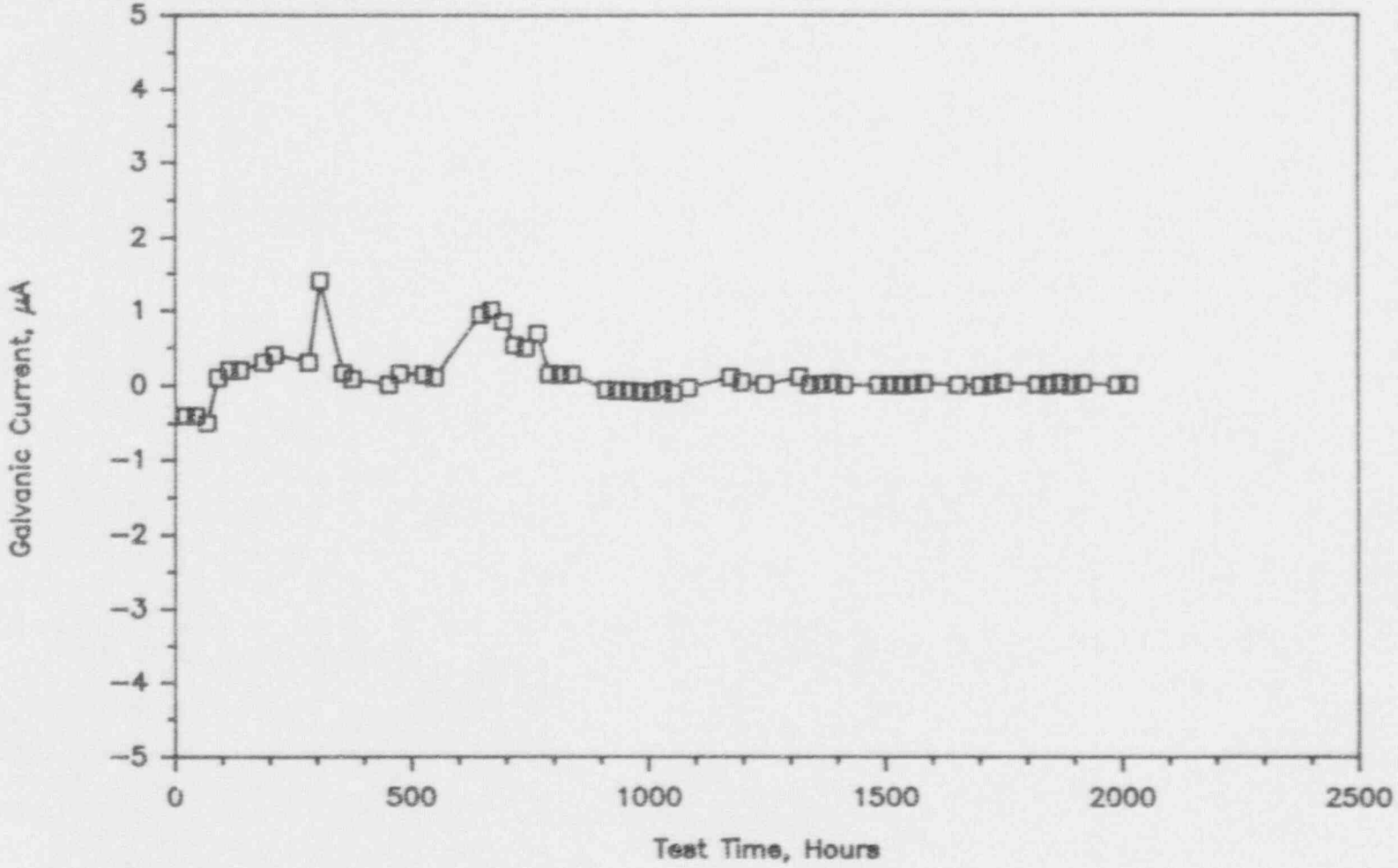

Figure 4.33 Galvanic Current As A Function Of Test Time For Sandwich Specimens Of Alloy 825 And Alloy 304L In Solution No. 10 At 90°C (Test #5).

Table 4.9 Summary Of Results Of Electrochemical Measurements Performed On Sandwich Specimens Of Alloy 304L And Alloy 825 In 90°C Solution Number 10; Test #5.

Alloy	Hours	Polarization Resistance kohm-cm²	Slope mV/Decade B_a	B_c	Corrosion Rate µm/yr	E_{cor} mV (SCE)
304L	23	399	684	111	1.06	-174
304L	140	854	684	111	0.49	-91
304L	308	928	684	111	0.46	-108
304L	483	896	684	111	0.47	-103
304L	648	619	684	111	0.68	-96
304L	766	376	684	111	1.12	-129
304L	936	1 640	684	111	0.26	-133
304L	1 037	328	684	111	1.29	-120
304L	1 175	1 970	684	111	0.21	-87
304L	1 367	2 890	684	111	0.15	-74
304L	1 513	1 700	684	111	0.25	-79
304L	1 681	10 800	684	111	0.04	47
304L	1 848	12 000	684	111	0.04	29
304L	2 017	3 940	684	111	0.11	-75
825	23	1 430	365	100	0.20	-123
825	140	2 430	365	100	0.12	-127
825	308	2 960	365	100	0.10	-127
825	483	1 390	365	100	0.21	-139
825	648	2 180	365	100	0.13	-129
825	766	2 180	365	100	0.13	-127
825	936	3 030	365	100	0.10	-185
825	1 037	2 460	365	100	0.12	-131
825	1 175	5 210	365	100	0.06	-143
825	1 367	3 230	365	100	0.09	-128
825	1 513	13 900	365	100	0.02	-100
825	1 681	9 680	365	100	0.03	-40
825	1 848	13 900	365	100	0.02	-17
825	2 017	10 700	365	100	0.03	-115

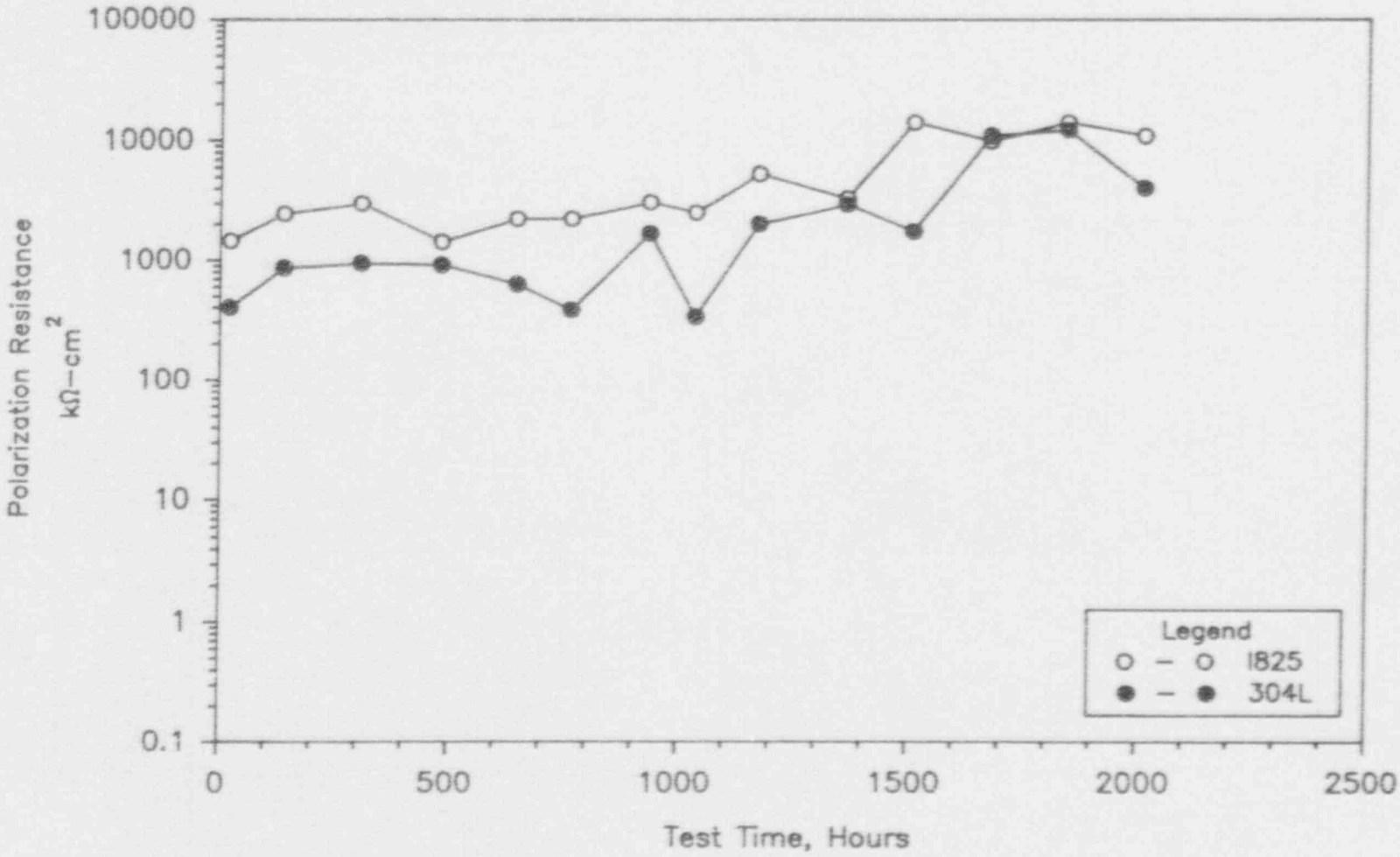

Figure 4.34 Polarization Resistance As A Function Of Test Time For Sandwich Specimens Of Alloy 825 And Alloy 304L In Solution No. 10 At 90°C (Test #5).

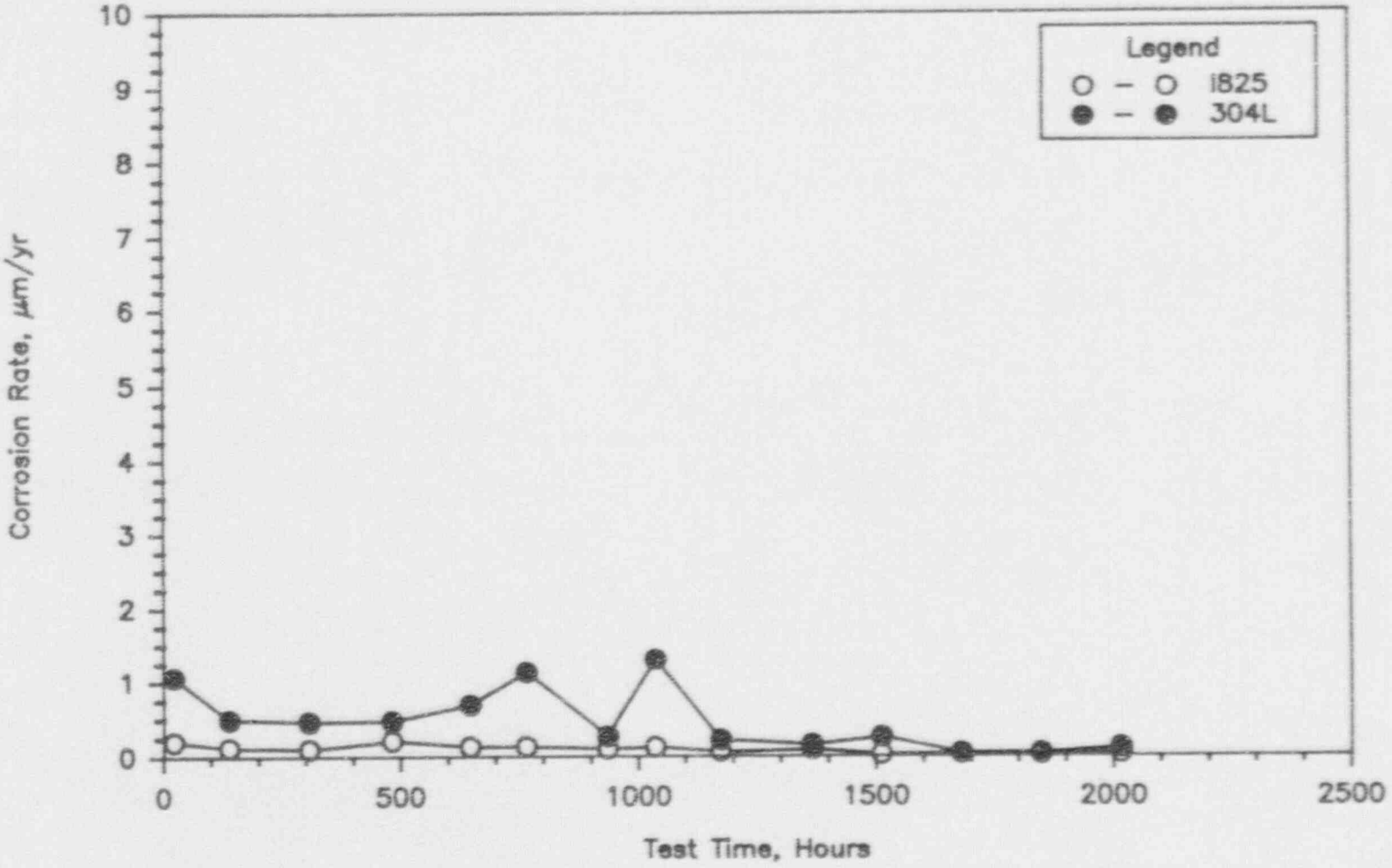

Figure 4.35 Corrosion Rate As A Function Of Test Time For Sandwich Specimens Of Alloy 825 And Alloy 304L In Solution No. 10 At 90°C (Test #5).

Table 4.10 Summary Of Corrosion Rates Calculated From Gravimetric Measurements Performed On Sandwich Specimens Of Alloy 825 And Alloy 304L In Selected Environments At 90°C.

Environment	Exposure Hours	Alloy	Corrosion Rate µn/yr	Description
Simulated J-13	2019	I825	0.24	Shiny, no visible attack
		304L	0.57	Shiny, no visible attack
Solution No. 10	2021	I825	0.88	Shiny, no visible attack
		304L	1.57	Shiny, no visible attack

5. LONG-TERM IMMERSION STUDIES

Long-term immersion tests were conducted in Task 7 of the program. The purpose of these tests was to provide long-term exposure data for evaluating the various modes of corrosion identified in other tasks of the program. The tests were designed to assess the performance of the candidate alloys at times when the temperature of the repository is near the boiling point of water and periodic intrusion of vadose water occurs. These tests differed from those performed in Task 3 of the program in that evaluation of the effects of concentration of salts in the groundwater on corrosion behavior was included. The tests were performed on the four candidate alloys in simulated J-13 well water at 90°C over a period of 80 weeks. During the exposures, the solutions were allowed to evaporate and new solution was added on a weekly basis. The experiments included constant strain (U-bend) specimens to evaluate SCC, weight-loss specimens, and non-destructive electrochemical techniques. The electrochemical techniques included periodic potential and polarization resistance measurements.

5.1 Experimental Approach

The exposure tests were performed in four-liter glass resin kettles in accordance with ASTM G31. These vessels, as shown in Figure 5.1, have a removable lid, four ground glass access ports in the lid, electrical resistance heating mantles, and glass Leibig condensers. One vessel was used for each alloy that was tested. All of the specimens were exposed in triplicate and their placement was designed so that individual "racks" of specimens could be removed and evaluated at three different exposure times. Table 5.1 is a summary of the specimens used in the boil-down studies.

The test specimens (2.54 cm x 2.54 cm x 0.32 cm) were cleaned, measured, and degreased prior to testing. The specimens were then mounted on Alloy C276 threaded rods and electrically isolated from the rods with tetrafluoroethylene (TFE) washers. Serrated TFE washers were clamped to the square coupons to create a TFE-metal crevice. Standard-sized U-bend specimens (ASTM G30) were also included to evaluate susceptibility to SCC. The U-bend specimens did not have serrated crevices.

Every week for 80 weeks, 1800 mL of freshly-prepared simulated J-13 well water was added to each test vessel to completely cover the test specimens. Dry air was passed through the vessels. The rate of air flow and the cooling water flow rate in the condensers were adjusted to obtain nearly complete evaporation in one week.

The instantaneous corrosion rate as a function of time was measured periodically by means of a three-electrode polarization resistance (PR) technique. The submerged working electrode was a cylindrical test specimen attached to a copper wire covered with shrink tubing. One of the Alloy C276 supports was used as the counter or auxiliary electrode. A glass Luggin probe with a saturated calomel electrode (SCE) entered the test vessel vertically and was filled with the test electrolyte during the PR measurements.

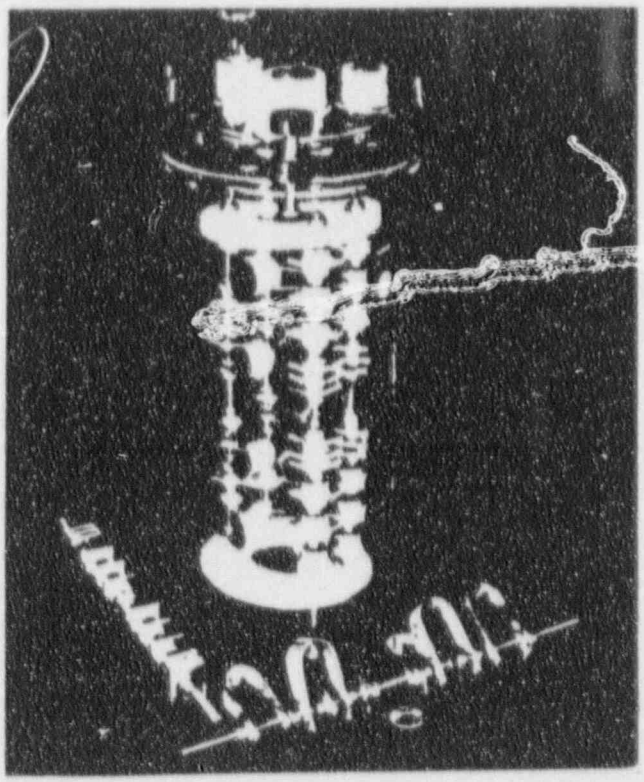

Figure 5.1 Glass Resin Kettles Used In The Task 7 Immersion Studies.

Table 5.1 Summary Of Specimens Used In Task 7 Long-Term Boil-Down Studies.

Vessel	Alloy	Specimen Type	Number Of Specimens	Exposure Time Hours			Total Number Of Specimens
1	I825	Creviced U-Bend	3 3	4000 —	8000 —	13 400 13 400	9 3
2	304L	Creviced U-Bend	3 3	4000 —	8000 —	13 400 13 400	9 3
3	CDA 715	Creviced U-Bend	3 3	4000 —	8000 —	13 400 13 400	9 3
4	CDA 102	Creviced U-Bend	3 3	4000 —	8000 —	13 400 13 400	9 3

The ASTM G-59 procedure was used for the actual PR measurements and the specimen potential was scanned between -20 mV (SCE) and +20 mV (SCE) of the free-corrosion potential. The ensuing current was monitored as a function of potential. The tangent to the potential-current plot at the free-corrosion potential is the PR value. The PR value was corrected for ohmic potential drop in the solution between the tip of the Luggin probe and the specimen by means of an AC measurement technique.

The polarization resistance values were converted to corrosion rates using the Stern-Geary Equation and Faraday's Law. The Tafel constants, B_a and B_c, were obtained from the potentiodynamic polarization curves by drawing tangents to the curves at over-potentials of +75 and -75 mV from the free-corrosion potential. The polarization curves for the alloys in J-13 well water were used for the Tafel slope analysis.

Weight losses on the specimens were measured using the interval weight-loss procedure described in ASTM G-1. This technique involves the alternate descaling of the specimen in an inhibited acid and weighing until the visible corrosion products are removed. Weight losses were then converted to corrosion rates, in µm/yr, by dividing the weight loss by the density, the specimen surface area and the test time and converting the units.

The pit depths on the specimens were measured optically, following descaling. A focusing technique was used with a microscope having a calibrated stage. The pits were first located at a low power magnification. At a high power, the microscope was focused on the specimen adjacent to the pit and the stage position recorded. The microscope was then refocused at the pit bottom and the final stage position was recorded; the difference between the two recordings was then calculated. The deepest of up to five pits were reported after each exposure period.

5.2 Copper-Base Alloys

Long-term boil-down testing was performed with Alloy CDA 715 and Alloy CDA 102 in simulated J-13 well water at 90°C for a period of 80 weeks (13,400 hours). Table 5.2 is a summary of the results of electrochemical measurements performed over the exposure period. Figure 5.2 illustrates the trends in PR with time for each of the copper-base alloys and Figure 5.3 illustrates the corrosion potential trends. These data show a slight decrease in PR, corresponding to an increase in corrosion rate, over the exposure period for Alloy CDA 715. The calculated corrosion rates for Alloy CDA 715, however, were low. The data for Alloy CDA 102 show a significant decrease in PR over the first 12,000 hours of exposure, followed by an increase over the remaining 1,400 hours. The lowest PR values measured corresponded to quite high corrosion rates; >500 µm/y. The potential behavior, shown in Figure 5.3, mirrored this PR behavior. The root cause of the peculiar behavior was not established.

Optical examinations of the specimens and analyses of the weight-loss data are summarized in Table 5.3. These data indicate low corrosion rates for both of the copper-base alloys. The weight-loss data also indicate that the corrosion rates decreased over the exposure period. Corrosion rates for Alloy 715 and Alloy CDA 102, calculated from weight-loss measurements, were <0.2 µm/yr and 1.16 µm/yr, respectively, after 4034 hours of exposure. After 13,400 hours, these rates were <0.005 µm/yr and 0.45 µm/yr for Alloy CDA 715 and Alloy CDA 102,

Table 5.2 Summary Of Results Of Electrochemical Measurements For Copper-Base Alloys in Aerated Simulated J-13 Well Water At 90°C; Long-Term Boil-Down Tests.

Alloy	Hours	Polarization Resistance kohm/cm²	Slope mV/Decade B_a	Slope mV/Decade B_c	Corrosion Rate µm/yr	E_{cor} mV (SCE)
715	502	2250.0	203	123	0.26	-119
715	669	1850.0	203	123	0.31	-121
715	1 345	3870.0	203	123	0.15	-134
715	2 012	4330.0	203	123	0.13	- 76
715	2 686	2030.0	203	123	0.28	-132
715	3 381	827.0	203	123	0.70	-167
715	4 032	2190.0	203	123	0.26	-155
715	4 703	43.0	203	123	13.40	-151
715	5 374	618.0	203	123	0.93	-116
715	6 044	377.0	203	123	1.53	-109
715	6 716	361.0	203	123	1.60	-130
715	7 654	313.0	203	123	1.84	-175
715	8 062	412.0	203	123	1.40	-125
715	8 737	328.0	203	123	1.76	-156
715	9 404	366.0	203	123	1.58	- 92
715	10 078	220.0	203	123	2.62	-175
715	10 754	611.0	203	123	0.94	-100
715	11 421	229.0	203	123	2.52	-124
715	12 093	214.0	203	123	2.69	-160
715	12 765	288.0	203	123	2.00	- 55
715	13 436	282.0	203	123	2.04	-192
102	523	63.0	390	150	17.37	-159
102	668	59.6	390	150	18.36	-270
102	1 345	69.3	390	150	15.80	-157
102	2 012	43.9	390	150	24.93	-151
102	2 685	89.2	390	150	12.27	-139
102	3 381	48.7	390	150	22.47	-167
102	4 031	102.0	390	150	10.75	-208
102	4 701	14.5	390	150	75.30	-273
102	5 372	15.2	390	150	71.90	-236
102	6 044	7.6	390	150	144.00	-292
102	6 715	13.5	390	150	80.80	-235
102	7 654	9.3	390	150	118.00	-208
102	8 062	5.1	390	150	215.00	-314
102	8 736	9.3	390	150	118.00	-288
102	9 404	5.2	390	150	210.60	-259
102	10 077	6.0	390	150	181.20	-321
102	11 421	4.3	390	150	256.30	-362
102	12 093	2.1	390	150	534.70	-390
102	12 764	71.2	390	150	15.36	-262
102	13 435	174.0	390	150	6.28	-189

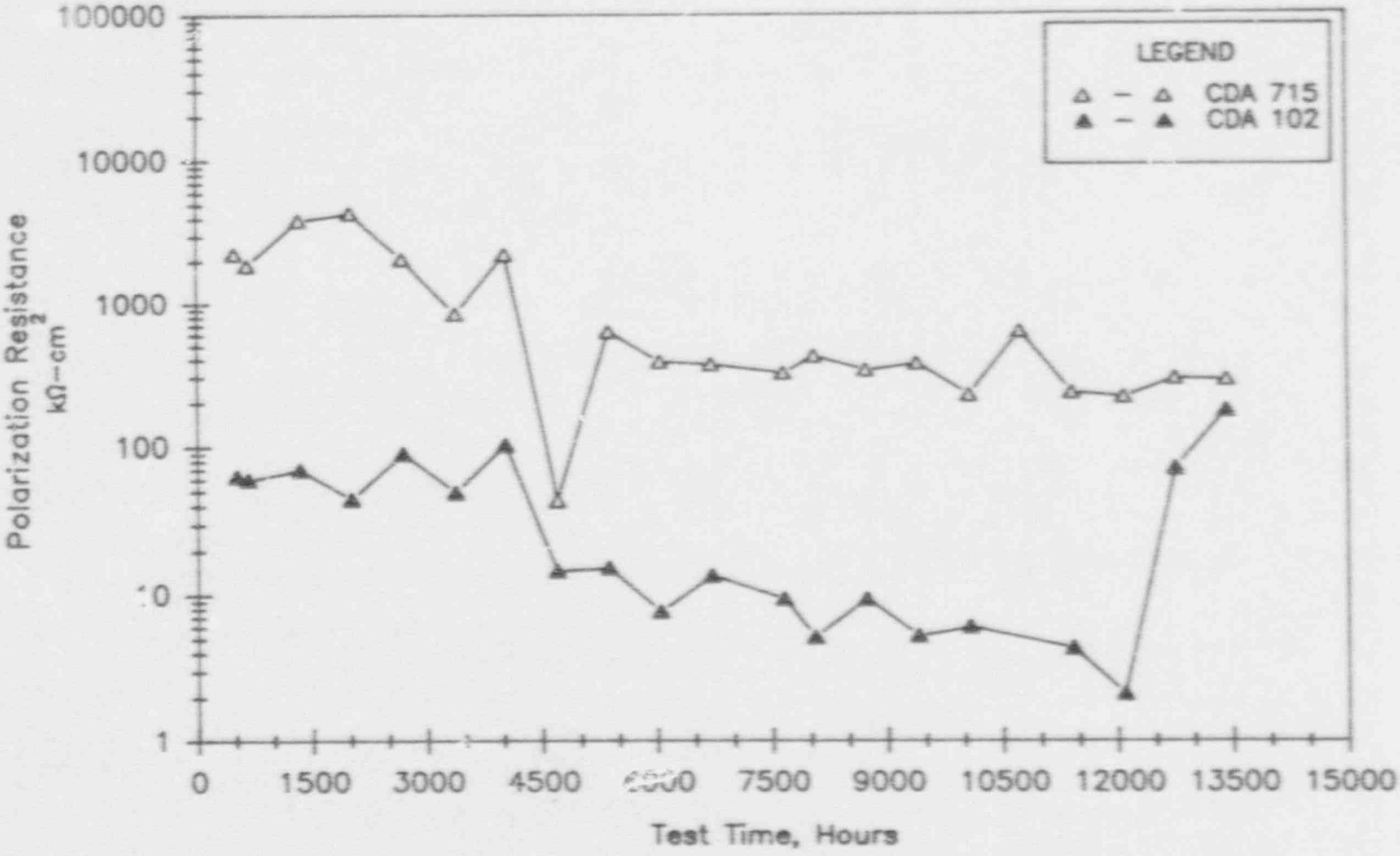

Figure 5.2 Polarization Resistance As A Function Of Test Time For Liquid - Phase Specimens Of Alloy CDA 102 And Alloy CDA 715 In Aerated Simulated J-13 Well Water At 90°C; Long-Term Boil-Down Tests.

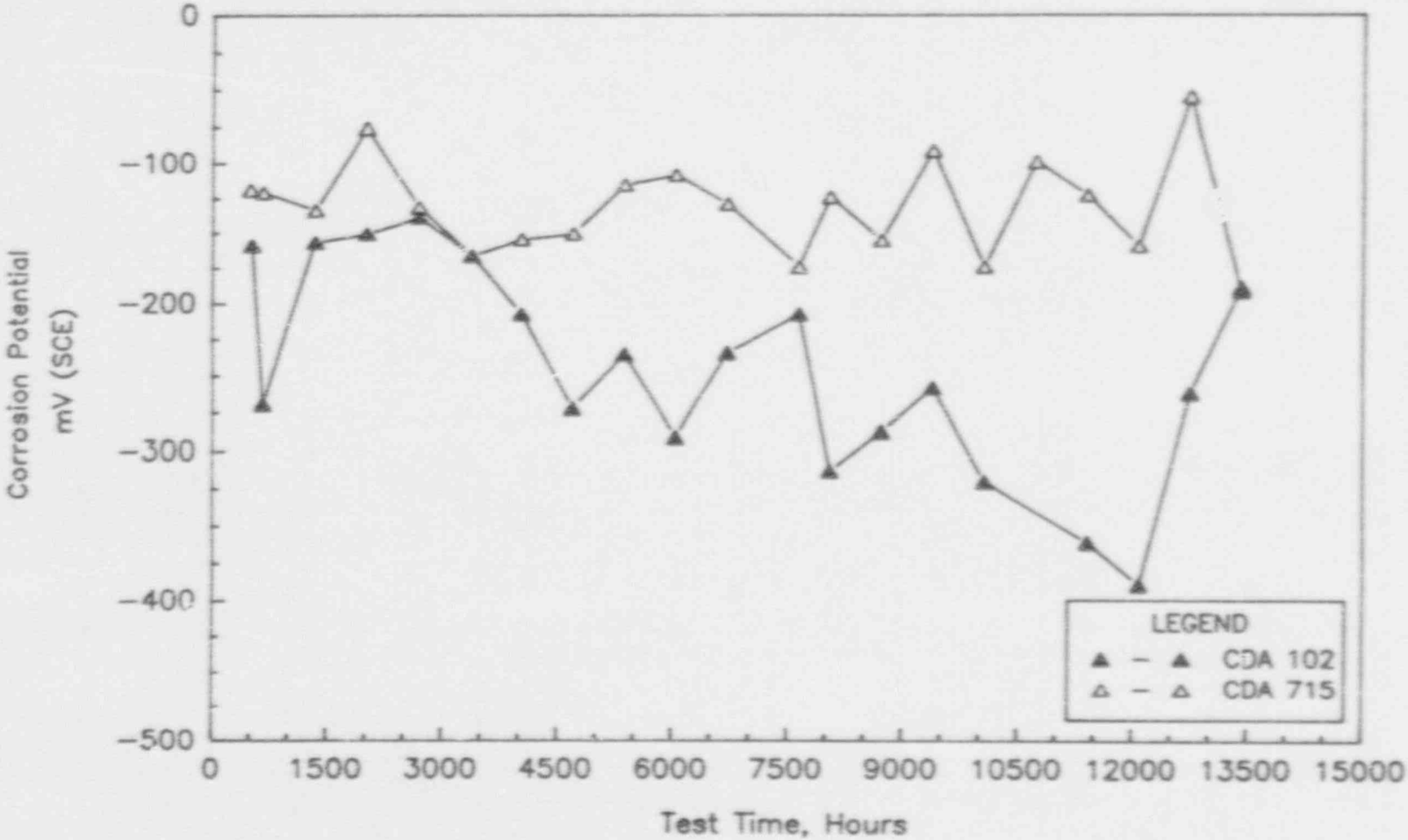

Figure 5.3 Corrosion Potential As A Function Of Test Time For Liquid - Phase Specimens Of Alloy CDA 102 And Alloy CDA 715 In Aerated Simulated J-13 Well Water At 90°C; Long-Term Boil-Down Tests .

Table 5.3 Summary Of Results Of Exposure Of Creviced Copper-Base Specimens In Aerated Simulated J-13 Well Water At 90°C; Long-Term Boil-Down Tests.

Alloy	Test Time Hours	Specimen Type	Corrosion Rate µm/yr	Maximum Pit Depth µm	Comments	Specimen
CDA715	4 034	Coupon	<0.2	—	Localized etching at crevice; very slight scaling.	32A 33A 33A
CDA715	8 064	Coupon	0.02	—	Localized etching at crevice; very slight scaling.	35A 36A 37A
CDA715	13 440	Coupon	<0.005	—	Slight etching at crevice; very slight scaling.	38A 39A 40A
CDA715	13 440	U-Bend **	—	—	No SCC or attack.	A22 A23 A24
CDA102	4 033	Coupon	1.16	10	Heavy etching; slight pitting on one specimen.	801 811 821
CDA102	8 064	Coupon	0.65	—	Heavy etching.	831 841 851
CDA102	13 349	Coupon	0.45	32 *	Moderate to heavy etching.	861 871 881
CDA102	13 349	U-Bend **	—	—	No SCC or attack.	U10 U11 U12

* Depth of etched areas, measurable on only one specimen.
** Not creviced.

respectively. The latter correspond to thickness losses of <0.005 mm and 0.45 mm in 1000 years for Alloy CDA 715 and Alloy CDA 102, respectively.

Comparison of Tables 5.2 and 5.3 indicates that the PR technique overestimated the actual corrosion rates by over two orders of magnitude. The higher corrosion rates calculated from the PR technique may be a result of non-Faradaic (noncorrosion) reactions in the solution. The PR technique also incorrectly predicted the trends in the corrosion rates with time. The PR technique predicted an increase in corrosion rate with time for the two alloys while actual corrosion rates decreased with time. This discrepancy may be a reflection of an increase in the non-Faradaic electrochemical reactions with time. The use of Tafel slopes for the non-concentrated simulated J-13 well water, as opposed to actual Tafel slopes for the concentrated solutions, may have contributed to the discrepancy.

Optical examination of specimens of Alloy CDA 715 following the exposure periods revealed some localized etching at the creviced areas. No pitting was observed in any of the specimens of Alloy CDA 715. U-bend specimens of Alloy CDA 715 showed no evidence of SCC, pitting, or etching. Examination of specimens of Alloy CDA 102 following the exposure period revealed moderate to heavy etching. Shallow pitting, 10 µm in depth, was observed on one specimen following 4033 hours of exposure. After 13,345 hours, heavy etching, up to 32 µm, was observed. U-bend specimens of Alloy CDA 102, however, showed no evidence of SCC, pitting, or etching.

5.3 Fe-Cr-Ni Alloys

Long-term boil-down testing was performed with Alloy 825 and Alloy 304L in simulated J-13 well water at 90°C for a period of 80 weeks (13,400 hours). Table 5.4 is a summary of the electrochemical measurements performed over the exposure period. Figure 5.4 illustrates the trends in PR for each of the Fe-Cr-Ni alloys with time and Figure 5.5 illustrates the corrosion potential trends. These data indicate low corrosion rates and relatively stable PR values.

Optical examinations of the specimens and analyses of the weight-loss data are summarized in Table 5.5. These data also show very low corrosion rates for both of the Fe-Cr-Ni alloys. Comparison of Tables 5.4 and 5.5 shows that the PR technique tended to overestimate actual corrosion rates. Corrosion rates of both Alloy 825 and Alloy 304L, calculated from weight-loss measurements were less than 0.2 µm/yr after about 4000 hours and less than 0.005 µm/yr after about 13,440 hours of exposure. These corrosion rates correspond to a thickness loss of less than 0.2 mm to less than 0.005 mm in 1000 years. Optical examination of specimens of both alloys indicated negligible attack after any of the exposure periods.

5.4 Solution and Deposit Analyses

Following the termination of the long-term boil-down tests, duplicate samples of solution were obtained from each of the resin kettles and analyzed. Duplicate samples of simulated J-13 well water were also submitted as a control and to act as a check on our quality assurance procedure

Table 5.4 Summary Of Results Of Electrochemical Measurements For Fe-Cr-Ni Alloys In Aerated Simulated J-13 Well Water At 90°C; Long-Term, Boil-Down Tests.

Alloy	Hours	Polarization Resistance kohm-cm²	Slope mV/Decade B_a	Slope mV/Decade B_c	Corrosion Rate µm/yr	E_{cor} mV (SCE)
I825	356	1230	211	221	0.39	-149
I825	697	1530	211	221	0.31	-209
I825	1 341	1740	211	221	0.27	-284
I825	2 013	99	211	221	4.85	-146
I825	2 713	9450	211	221	0.05	-101
I825	3 359	>108 (a)	211	221	<4.42	-238
I825	4 055	264	211	221	1.81	-208
I825	4 702	280	211	221	1.71	-201
I825	5 377	266	211	221	1.20	-214
I825	6 382	242	211	221	1.97	-227
I825	6 719	230	211	221	2.03	-185
I825	7 389	244	211	221	1.96	-248
I825	8 061	117	211	221	4.08	-168
I825	8 741	154	211	221	3.11	-118
I825	9 410	214	211	221	2.24	-205
I825	10 076	260	211	221	1.84	-215
I825	10 756	470	211	221	1.02	-209
I825	11 589	361	211	221	1.33	-169
I825	12 094	355	211	221	1.35	-132
I825	13 102	337	211	221	1.42	-169
I825	13 485	134	211	221	3.58	-164
304L	339	4960	493	131	0.10	- 67
304L	672	5290	493	131	0.09	-166
304L	1 515	1800	493	131	0.26	- 91
304L	2 038	3610	493	131	0.13	- 73
304L	2 688	438	493	131	1.08	-103
304L	3 366	369	493	131	1.28	-146
304L	4 034	784	493	131	0.60	- 96
304L	4 704	40	493	131	11.8	-230
304L	5 374	601	493	131	0.78	-168
304L	6 215	61	493	131	7.71	-205
304L	6 719	105	493	131	4.49	-176
304L	7 393	54	493	131	8.76	-232
304L	8 065	142	493	131	3.34	-190
304L	8 735	210	493	131	2.25	-174
304L	9 407	222	493	131	2.13	-115
304L	10 081	140	493	131	3.36	-125
304L	10 754	126	493	131	3.14	-124
304L	11 593	134	493	131	3.54	-131
304L	12 097	244	493	131	1.93	-115
304L	12 935	205	493	131	2.31	-128
304L	13 440	203	493	131	2.32	-153

(a) By Electrochemical Impedance Spectroscopy.

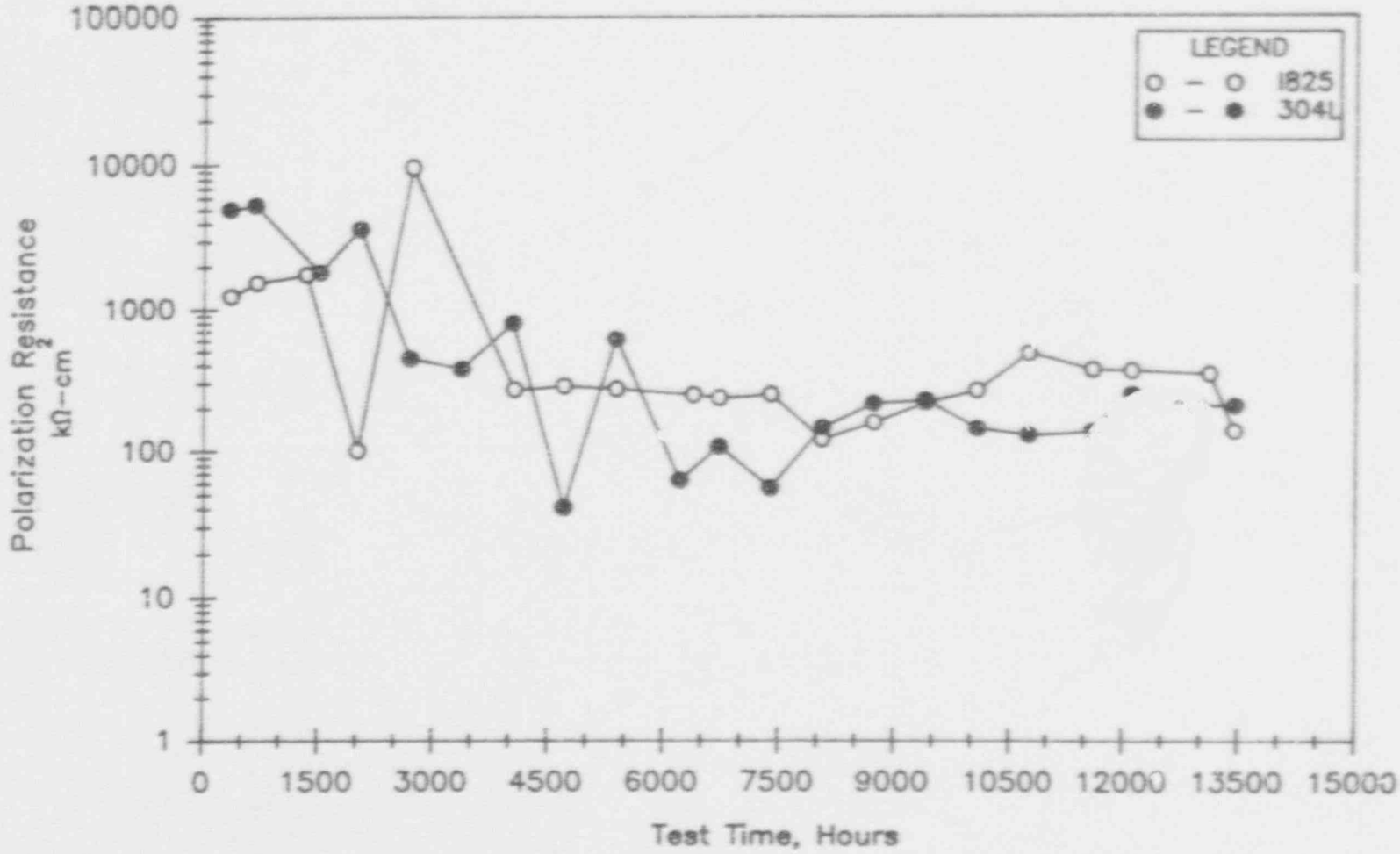

Figure 5.4 Polarization Resistance As A Function Of Test Time For Liquid-Phase Specimens Of Alloy 825 And Alloy 304L In Aerated Simulated J-13 Well Water At 90°C; Long-Term Boil-Down Tests.

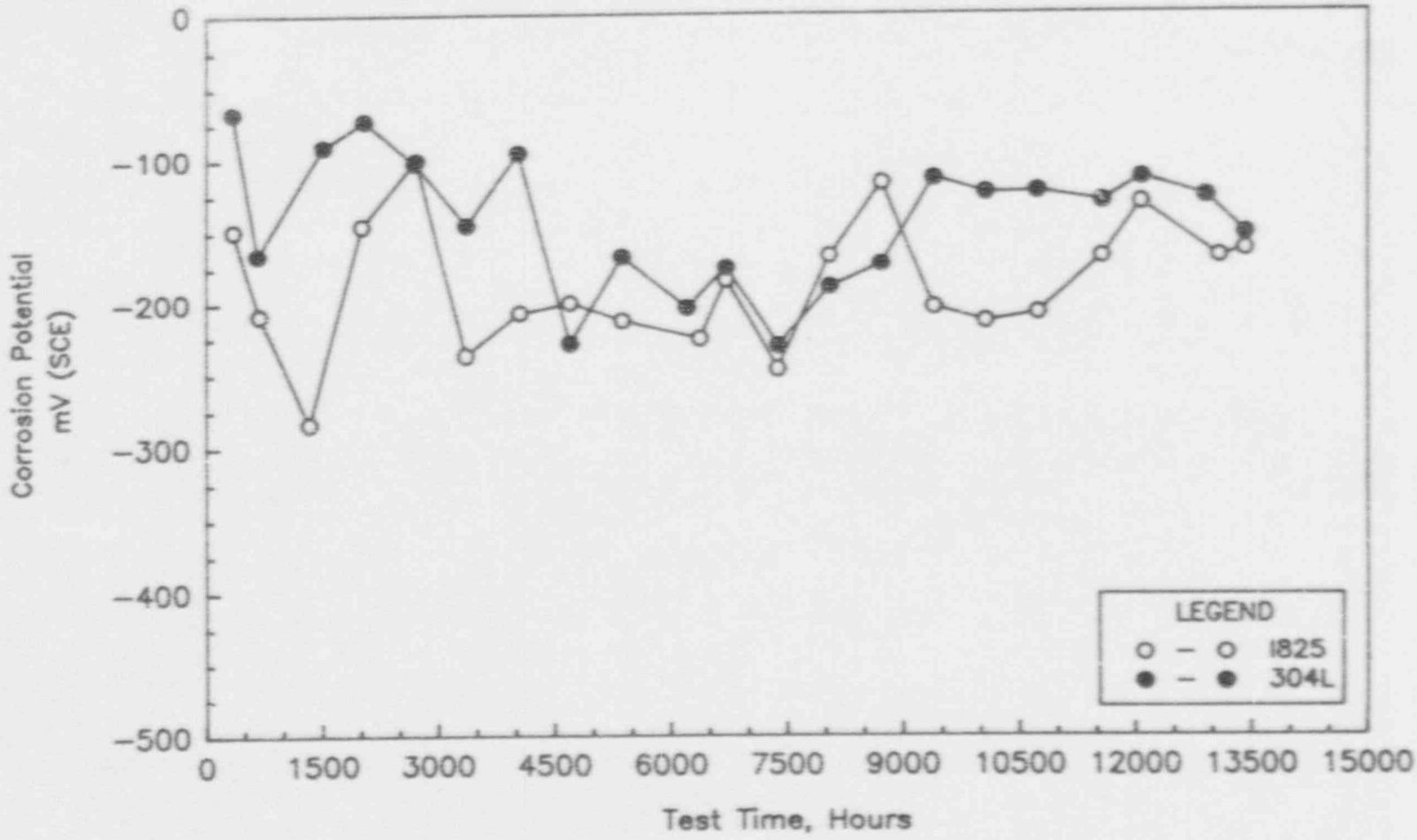

Figure 5.5 Corrosion Potential As A Function Of Test Time For Liquid - Phase Specimens Of Alloy 825 And Alloy 304L In Aerated Simulated J-13 Well Water At 90°C; Long-Term Boil-Down Tests.

Table 5.5. Summary Of Results Of Exposure Of Creviced Fe-Cr-Ni Specimens In Aerated Simulated J-13 Well Water At 90°C.

Alloy	Test Time Hours	Specimen Type	Corrosion Rate µm/yr	Maximum Pit Depth µm	Comments	Specimen
825	4 056	Coupon	<0.2	—	No attack; very slight scaling.	I1 I2 I3
825	8 062	Coupon	<0.009	—	No attack; slight scaling.	I4 I5 I6
825	13 435	Coupon	<0.005	—	No attack; slight scaling.	I7 I8 I9
825	13 435	U-Bend **	—	—	No SCC or attack.	U1 U2 U3
304L	4 034	Coupon	<0.2	—	No attack; slight scaling.	L1 L2 L3
304L	8 065	Coupon	<0.009	—	No attack; slight scaling.	L4 L5 L6
304L	13 441	Coupon	<0.005	—	No attack; slight scaling.	L7 L8 L9
304L	13 441	U-Bend **	—	—	No SCC or attack.	U1 U2 U3

** Not creviced.

for solution preparation. Table 5.6 summarizes the results of these solution analyses and compares these results with the predicted concentration. The predicted concentration was calculated assuming that the test solutions boiled to dryness weekly during the 80 week exposures. These data show that the actual compositions of the test solutions was very similar and slightly less than the calculated composition, with a few exceptions. These exceptions in composition included calcium, magnesium, silicon, and bicarbonate, which were thought to have precipitated from solution.

Duplicate samples of the precipitated salts were obtained from the test vessels after the exposure periods. Several techniques were used to analyzed these precipitates. Carbonates were determined by acid digestion and titration. The percentage of carbonates was calculated as the calcium carbonate equivalent. The total cation analyses were determined by the Inductively Coupled Plasma (ICP) method. For this analysis, the samples were fused with LiB_2O_4 and dissolved in 4% nitric acid. Elemental analyses also were performed by semiquantitative Energy Dispersive Spectroscopy (EDS). For this analysis, the precipitates were mixed with epoxy and metallographically prepared. Results of the analyses are given in Table 5.7. These data confirm the presence of the constituents that were nearly absent from the solutions following 80 weeks of boiling and concentration. The deposits show relatively high concentrations of calcium, silicon, and alkalinity constituents such as $CaC0_3$.

The precipitates also were analyzed by X-Ray Diffraction (XRD). Both the total samples and the residues from the acid treatment were analyzed. A typical diffraction pattern is given in Figure 5.6. The nature of the diffraction patterns, with little definition in the peaks, indicates a large amount of amorphous (non-crystalline) material is present in the precipitates.

Table 5.6 Comparison Of Compositions Of Simulated J-13 Well Water To The Compositions Of Solutions Following 80 Weeks Of Boil Down and Concentration.

Environmental Species	Calculated J-13 mg/l	Actual J-13 mg/l	Predicted J-13 After 80 weeks mg/l	CDA 715 In J-13 mg/l*	CDA 102 In J-13 mg/l*	I825 In J-13 mg/l*	304L In J-13 mg/l*
Nitrate, as N	2.8	2.8	224	154	179	264	224
Total Phosphorous, P	0.0	<0.1	0	0.5	0.6	1.1	0.7
Sulfate, SO_4	19.2	23.5	1536	17.5	2125	1975	2050
Chloride, Cl	6.4	5.5	512	42.0	495	750	675
Fluoride, F	1.7	1.8	136	81.5	85	144	125
Calcium, Ca	12.0	10.0	960	2	2	2	3
Magnesium, Mg	1.7	1.5	136	<1	<1	<1	<1
Sodium, Na	46.0	42.0	3680	2450	2950	4450	3500
Potassium, K	5.5	6.3	440	240	200	380	230
Aluminum, Al	0.0	<0.2	0	<0.2	<0.2	<0.2	<0.2
Soluble Silicon, Si	30.0	27.5	2400	605	990	1170	1105
Alkalinity, HCO_3	121.0	102.0	—	0	0	0	0
Alkalinity, Phenolphthalein	0.0	0.0	—	2630	2990	4925	3820
Alkalinity, Total	121.0	102.0	—	3750	4330	7150	5700
pH	7.0 ± 0.2	7.0 ± 0.2	>7.0	10.41	10.41	10.68	10.44

* Average Concentration From Duplicate Samples.
NOTE: In all cases, J-13 well water was simulated.

Table 5.7 Composition Of Precipitated "Salts" Following 80 Weeks Of Boil-Down Testing With Simulated J-13 Water At 90°C; Average Of Duplicate Tests.

Composition	ALLOY CDA 715		ALLOY CDA 102		ALLOY 304L		ALLOY 825	
	ICP	EDS[a]	ICP	EDS	ICP	EDS	ICP	EDS
Al	0.34%	—	0.39%	—	0.31%	—	0.40%	—
Si	24.41%	64.5%	25.46%	62.9%	25.47%	63.4%	25.61%	65.2%
Na	3.61%	—	3.74%	—	4.24%	—	4.09%	—
Mg	0.90%	—	1.01%	—	1.09%	—	0.93%	—
K	0.73%	3.3%	1.05%	4.7%	1.03%	3.8%	0.93%	3.0%
Ca	8.47%	32.2%	8.78%	32.4%	10.42%	32.8%	8.50%	29.4%
$CaCO_3$ (eq)	39.60%	—	36.20%	—	38.40%	—	35.60%	—
Sr	425 ppm	—	390 ppm	—	425 ppm	—	395 ppm	—
Ni	70 ppm	—	55 ppm	—	160 ppm	—	215 ppm	—
Cu	350 ppm	—	1610 ppm	—	65 ppm	—	<50 ppm	—
Fe	—	—	—	—	750 ppm	—	1870 ppm	—
Cr	—	—	—	—	<20 ppm	—	75 ppm	—
Mo	—	—	—	—	<2 ppm	—	<2 ppm	—
Cl	—	—	—	—	—	—	—	2.4%

a EDS data normalized to 100%.

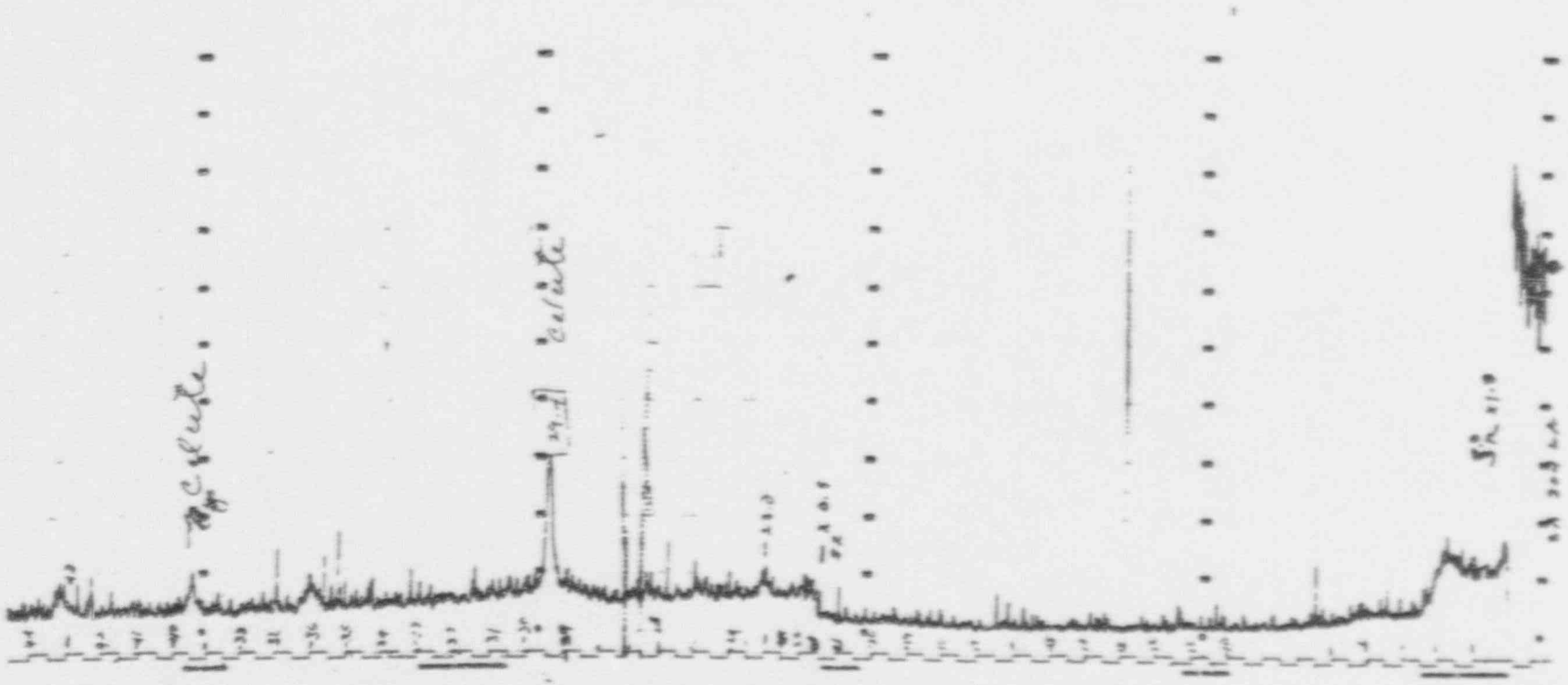

Figure 5.6 X-Ray Diffraction Data Of Precipitated "Salts" Following 80 Weeks Of Boil-Down Testing Of Alloy 304L With Simulated J-13 Water At 90°C

6. DISCUSSION

The scope of the overall NRC program at CC Technologies Inc. consisted of employing short-term techniques, such as electrochemical and mechanical techniques to examine a wide range of possible failure modes for the high level waste canister. Long-term tests were used to verify and further examine specific failure modes identified as important by the short-term studies.

Two classes of alloys were evaluated for use as container materials for the Tuff Repository; Fe-Cr-Ni alloys and copper-base alloys. The candidate Fe-Cr-Ni alloys were Type 304L Stainless Steel (Alloy 304L) and Incoloy Alloy 825 (Alloy 825). The candidate copper-base alloys were CDA 102 Copper (Alloy CDA 102) and Copper-30 Nickel (Alloy CDA 715).

This report summarizes the results of pitting, galvanic, and long-term corrosion studies performed in Tasks 4, 6, and 7 of the program respectively.

6.1 Pitting-Corrosion Studies

The overall objectives of Task 4 were (1) to study the relationships between the pitting parameters E_{pit} and E_{prot} and long-term pit initiation behavior and (2) to evaluate pit propagation behavior. The majority of the research in this task was performed on the copper-base alloys but limited pit initiation studies also were performed with the Fe-Cr-Ni alloys.

6.1.1 Pit-Initiation Studies

In the pit initiation studies, the relationship between the long-term pitting behavior and the electrochemical parameters was assessed by potentiostatic-polarization tests. The specimens were polarized over a range of potentials between the free-corrosion potential (E_{cor}) and pitting potential (E_{pit}) and the relationship between the corrosion morphology and potential was determined. The research was focused primarily on the copper-base alloys. The earlier CPP studies, performed in Task 2 of the program, suggested that the conventional interpretation of CPP curves is not appropriate for either Alloy CDA 102 or Alloy CDA 715. Hysteresis in the CPP curves was not always associated with classical pitting. In many instances, hysteresis in the CPP curves was associated with thick tarnish growth on the specimen and active attack beneath the tarnish.

For the pit-initiation studies on the copper-base alloys, environments were selected from the Task 2 matrix that exhibited either hysteresis and pitting in the CPP tests or hysteresis and thick tarnish growth with active attack in the CPP tests. Results of the potentiostatic tests were consistent with the behavior observed in the Task 2 CPP tests. When specimens were potentiostated for long periods of time at potentials within the hysteresis loop, the morphology of attack of the specimens was similar to that observed in the CPP tests. It also was generally observed that, in environments that promoted tarnish growth, the potentiostatic current decreased with time. On

the other hand, in environments that promoted pitting, the potentiostatic currents generally remained at high values during the testing. This behavior is consistent with the morphologies observed. The high stable potentiostatic currents are indicative of high rates of pitting or general attack while the decrease in currents with time are consistent with the growth of thick tarnish layers. These layers may grow very slowly over longer periods of time as compared with passive films which develop on stainless steels.

A limited number of pit-initiation studies was also conducted with Alloy 304L and Alloy 825. Current waste package designs for the Tuff Repository specify relatively thin-walled containers. Thus, if pits initiate, container failure by pitting corrosion may occur within a relatively short time span. Accordingly, the resistance to pit initiation is critical for the adequate performance of an Fe-Cr-Ni container.

Potentiostatic testing was performed with each of the Fe-Cr-Ni alloys in several synthetic solutions selected from the matrix of CPP tests in Task 2 of the program. In general, the results of the Task 2 testing of the Fe-Cr-Ni alloys conformed with a conventional interpretation of the CPP curves; namely the occurrence of hysteresis in the CPP curves corresponded with localized corrosion (either pitting or crevice corrosion) on the specimens. Several instances were noted in the Task 2 studies where hysteresis in the CPP curves at noble potentials was associated with tarnish film growth as opposed to pitting. This behavior has been observed by the authors with the Fe-Cr-Ni alloys on other programs as well. It has been speculated that the hysteresis is the result of a catalytic effect of the tarnish film on non-Faradaic electrochemical reactions in the solution. In Task 4, the potentiostatic tests were performed on solutions that exhibited both types of behavior; namely hysteresis and pitting and hysteresis at noble potentials and tarnish growth. The specimens were potentiostated at potentials within the hysteresis region. In some cases, pitting and crevice corrosion occurred in the potentiostatic tests where only tarnishing was evident in the CPP tests. Thus, the conventional interpretation of the CPP tests was accurate. However, there were a few instances where no localized corrosion occurred in the potentiostatic tests even though slight hysteresis was present in the CPP tests.

These interpretation problems with the CPP curves for the Fe-Cr-Ni alloys may be only of academic interest since the slight hysteresis, which was associated with tarnishing, generally occurred at very noble potentials. In any case, they point to the need to carefully interpret the CPP curves and to factor a post test examination of the test specimen into the analysis.

6.1.2 Pit-Propagation Studies

The results of previous studies (Beavers-1991a, McCright-1985) have confirmed that pits readily initiate in the copper-base alloys in the Tuff Repository environment. Accordingly, for a copper container to provide adequate containment, it must be demonstrated that the rates of pit propagation are low in comparison to the thickness of the container wall. In the pit-propagation studies, exposures of simulated pits were used to assess the rate of pit propagation as a function of pit depth.

Four pit-propagation experiments were performed with Alloy CDA 102 at 90°C in Solution Number 22 using a simulated pit. The simulated pit was created by inserting a small-diameter

rod of Alloy CDA 102 into a hole inside a larger rod of the same alloy at a variable depth. Two diameter-to-depth aspect ratios were evaluated 1:5 and 1:2. The artificial pit was packed with corrosion products generated from anodic polarization of Alloy CDA 102 in Solution Number 22 in three of the experiments. Solution Number 22 was chosen as it was shown to promote pitting of specimens of Alloy CDA 102 in previous CPP tests. During the tests, pit propagation was stimulated either by adding 200 ppm H_2O_2 daily to the test solution or by potentiostating the BES-pit specimen couple.

In each of the experiments, the potential of the pit was more positive than the potential of the boldly exposed surface (BES) specimen, prior to addition of H_2O_2, and the pits did not propagate, based on the direction of current flow. Current transients indicative of pit propagation occurred following each H_2O_2 addition but these were not sustained. As the H_2O_2 degraded, the rate of propagation rapidly decreased. Gravimetric measurements of the specimens following testing confirmed that pit propagation had occurred in the presence of H_2O_2. The corrosion rate of the pit specimen in the first experiment was 205 µm/yr while that of the BES specimen was 19.9 µm/yr.

In two subsequent pit propagation tests, the BES-pit couple were potentiostatically polarized at potentials above E_b in order to sustain pit propagation. The value of E_b was determined from previous CPP tests performed in Task 2 of the program. The potentiostatic approach was found to sustain pit propagation, based on current and weight-loss measurements. Comparison of pit propagation experiments, performed under potentiostatic control, at the two pit diameter to depth ratios (1:5 and 1:2), indicated that rates of propagation were higher for the shallower pit. This behavior was expected and provides further confirmation of the experimental technique.

One experiment was performed to evaluate cuprous oxide (Cu_2O) as a packing paste. The Cu_2O was chosen to simulate the corrosion products in a reduced state, as the original corrosion product paste was thought to be too oxidizing based on the results of the first experiment. However, galvanic current was not measurable and the experiment was terminated after 16 days. Optical examination of the specimens following the exposure revealed no evidence of attack of either the pit or BES specimens. The packing paste was a hard, dry powder inside the pit cavity following the exposure. The hydrophobic nature of the Cu_2O resulted in the hard, dry paste which effected a very high resistance that ultimately inhibited galvanic current flow.

Results of CPP testing performed in Task 2 of the program showed that pits initiate in Alloy CDA 102 within the experimental range of possible groundwater compositions. The results of the four pit-propagation experiments show that their propagation may be limited in the absence of oxidizing species such as H_2O_2. However, H_2O_2 is a chemical species that has been shown to occur as a result of irradiation of the J-13 groundwater. Other oxidizing species also will be present. These oxidizing species, if present in sufficient concentrations, will promote pit propagation in Alloy CDA 102. Sufficient testing was not performed to well characterize the kinetics of propagation but the limited testing performed suggests that rates will decrease with depth. However, one aspect of the testing that could not be addressed, without the use of actual radiation, is the generation of oxidizing species within the pit. In situations where the container wall is shielding the radiation, the rate of pit propagation may be significantly affected by the generation of radiolysis products at the bottom of the pits.

6.2 Galvanic-Corrosion Studies

Galvanic corrosion studies were conducted in Task 6 of the overall program. The purpose of Task 6 was to explore failure modes that are likely to produce accelerated attack and lead to premature failure of the waste container. Two modes of failure were identified for examination in this task: Thermogalvanic couples and borehole liner-container interactions.

6.2.1 Thermogalvanic-Couples Experiments

For a single container, it is likely that a temperature differential will exist from one portion of the surface to another. This temperature differential will produce a potential distribution on the container surface that can result in a differential cell couple similar to a galvanic couple of dissimilar metals. This "thermogalvanic couple" may accelerate the corrosion rate of that portion of the container having the more negative potential. The focus of this subtask was to estimate the accelerating effect of thermogalvanic couples on the corrosion rate of Alloy CDA 102 and Alloy 304L. No thermogalvanic-couples experiments were performed with Alloy CDA 715 or Alloy 825.

In each of the three experiments, an unheated (isothermal) specimen was electrically coupled to an internally heated (heat-transfer) specimen. The galvanic current flow between the two was monitored as a function of time. Periodically, the specimens were uncoupled and the free-corrosion potential and polarization resistance of each specimen were measured. For specimens of Alloy CDA 102 exposed to simulated J-13 well water, there was an increase in galvanic current as the temperature differential increased, although the magnitude of the current was very small, less than 0.7 µm/yr of general corrosion. The direction of the current was such that the corrosion rate of the isothermal specimen was being accelerated by the couple. The addition of 200 ppm H_2O_2 increased the magnitude of the thermogalvanic current but the effect was transient; the H_2O_2 rapidly decreased.

Two thermogalvanic-couples experiments were performed with Alloy 304L. These two tests evaluated the corrosion behavior in simulated J-13 well water and in Solution Number 7, a solution previously shown to promote pitting of Alloy 304L. For specimens of Alloy 304L exposed to the simulated J-13 well water, there was a change in polarity as the temperature differential increased. At low temperature differentials, the isothermal specimen was anodic (corroding). At greater temperature differences, the heat transfer specimen became anodic. Again, these currents were very low, less than 0.005 µA/cm^2 in the absence of hydrogen peroxide. Daily additions of 200 ppm hydrogen peroxide (H_2O_2) produced small current transients. The direction of these current transients showed the heat-transfer specimen to be anodic. Gravimetric measurements showed general corrosion rates of 0.17 µm/yr and 3.95 µm/yr for the isothermal and heat-transfer specimens, respectively. Optical examination revealed the absence of visible attack at 30X magnification. Both thermogalvanic effects and accelerated attack as a result of the higher temperature may have contributed to the corrosion.

The second thermogalvanic-couples experiments with Alloy 304L was performed in Solution Number 7. In this experiment, the galvanic current was negligible and approached the detection

limits of the test equipment in the absence of H_2O_2. The first H_2O_2 addition promoted pitting of the heat-transfer specimen, as was evidenced by galvanic current spikes and the development of rounded ares of rust on the specimen within 24 hours of the H_2O_2 addition. The initiation of pits also caused the potential of the galvanic couple to drop to levels that approached the protection potential for this alloy-environment system. Subsequent additions of H_2O_2 showed only minor fluctuations in galvanic current which may indicate that the initial pits passivated. Corrosion rates determined from polarization resistance measurements, performed after the final addition of H_2O_2, were consistent with corrosion rates determined from weight-loss measurements. General corrosion rates were found to be less than 0.078 µm/yr and 0.41 µm/yr for the isothermal and heat-transfer specimens, respectively. Optical examination of the specimens at 30X magnification showed no visible attack of the isothermal specimen, but numerous pits and localized etching on the heat-transfer specimen.

In summary the results of these tests indicate that thermogalvanic corrosion may affect corrosion performance of the waste containers in the presence of oxidizing radiolysis products. The direction of the galvanic effect may be different, depending on the alloy-environment system examined. Considering the two alloys evaluated; the corrosion attack of the cooler isothermal specimen of Alloy CDA 102 was consistently accelerated by the thermogalvanic effect. On the other hand, for Alloy 304L, the heat-transfer specimen generally experienced accelerated attack as a result of thermogalvanic corrosion. However, the major effect still appears to be an increase in rates of attack (general or pitting corrosion) with increasing temperature.

6.2.2 Borehole Liner-Container Interaction Studies

Borehole liner-container interaction studies were conducted to evaluate the effects of metal-to-metal contact of the liner and container materials. The initial designs for the Tuff Repository proposed Alloy 304L and carbon or low alloy steel as the container and liner materials, respectively. The focus was later shifted to Alloy 825 and Alloy 304L as the container and liner materials. The purpose of these liners is to facilitate retrieval of the waste containers over a 50-year period following their emplacement. For the current repository design, it is probable that the liners and containers will be in direct contact, resulting in possible galvanic attack.

Galvanic attack is normally considered to be the accelerated attack of the less noble member of a dissimilar-metal couple. However, evidence in the literature indicates that the less noble member of the couple can promote accelerated corrosion of the more noble member by creating an aggressive environment in the crevice between the two alloys.

Sandwich-like specimens of Alloy 304L/C1010 carbon steel and Alloy 304L/Alloy 825 were evaluated in this subtask. The first experiment was performed with Alloy 304L/C1010 at 90°C in simulated J-13 well water and was primarily an evaluation of the experimental design and was found to yield erroneous data. As a consequence, the experiment was modified for subsequent tests.

In the revised experiments, a microcapillary tube was inserted through the face of one of the specimens to act as a Luggin probe. The actual experimental procedure was similar to that used in the thermogalvanic experiments. The coupled potential and galvanic current flow between the

two specimens was monitored as a function of time. Periodically the specimens were uncoupled and the free-corrosion potentials and polarization resistance of each specimen were measured. In the PR measurements, the opposing specimen was used as a counter electrode in order to polarize the region of the specimen with the crevice.

Galvanic experiments were performed with the Alloy 304L/C1010 carbon steel couple in simulated J-13 well water with and without the addition of 1000 ppm Cl. In both tests, the carbon steel specimen experienced high corrosion rates, around 400 µm/yr based on weight loss, while negligible attack of the Alloy 304L (less than 0.5 µm/yr) occurred. These results were consistent with the electrochemical measurements performed during the tests. There was no evidence of accelerated corrosion of the Alloy 304L during the course of the tests.

The fourth and fifth experiments were performed with Alloy 304L and Alloy 825 as the liner and container materials, respectively. In the fourth experiment, these alloys were evaluated in simulated J-13 well water at 90°C. Gravimetric measurements and optical examination of the specimens were performed after 2019 hours of exposure. Corrosion rates calculated from the weight-loss technique were 0.24 µm/yr and 0.57 µm/yr for the container and liner materials, respectively. Neither specimen showed any visible attack at 30X magnification. These results were consistent with the galvanic current and PR measurements made throughout the exposure period.

Specimens of Alloy 304L and Alloy 825 were evaluated in Solution Number 10 at 90°C in the fifth experiment. Solution Number 10 was chosen from the experimental test matrix based on CPP behavior. These CPP curves showed a large hysteresis loop for Alloy 304L in Solution Number 10 which was consistent with pitting and crevice attack of the specimen. No hysteresis or evidence of attack occurred as a result of CPP testing of Alloy 825 in Solution Number 10.

This final experiment was terminated after 2021 hours of exposure. General corrosion rates, calculated from weight-loss measurements, were found to be 0.88 µm/yr and 1.57 µm/yr for Alloy 825 and Alloy 304L, respectively. Neither specimen showed any visible attack at 30X magnification. The discrepancy between pitting observed on a specimen of 304L following CPP tests and the absence of attack following galvanic coupling may be explained by their potential measurements. Throughout the exposure in this fifth experiment, the corrosion potentials of Alloy 304L ranged between -150 mV (SCE) and -100 mV (SCE) which is considerably less than E_{pit} (+700 mV (SCE)) and close to E_{prot} (-120 mV (SCE)).

In summary, in these borehole liner-container interaction tests, there was no evidence of accelerated corrosion of the more noble member of the galvanic couple: the less noble member of the couple consistently experienced galvanic corrosion. However, in the case of the Alloy 304L - Alloy 825 couple, the environment was not sufficiently aggressive to promote significant attack of Alloy 304L, which is necessary for the crevice corrosion mechanism to operate.

6.3 Long-Term Immersion Studies

Long-term immersion tests were conducted in Task 7 of the program. The purpose of these tests was to provide long-term exposure data for evaluating the various modes of corrosion identified

in other tasks of the program. The tests were designed to assess the performance of the candidate alloys at times when the temperature of the repository is near the boiling point of water and periodic intrusion of vadose water occurs. These tests differed from those performed in Task 3 of the program in that evaluation of the effects of concentration of salts in the groundwater on corrosion behavior was included. The tests were performed on the four candidate alloys in simulated J-13 well water at 90°C over a period of 80 weeks. During the exposures, the solutions were allowed to evaporate and new solution was added on a weekly basis. The experiments included constant strain (U-bend) specimens to evaluate SCC, weight-loss specimens, and non-destructive electrochemical techniques. The electrochemical techniques included periodic potential and polarization resistance measurements.

Corrosion rates, calculated from weight-loss measurements, after 23.8 weeks (4000 hours) of exposure were less than 0.2 µm/yr for each of the alloys except Alloy CDA 102 which had a corrosion rate of 1.11 µm/yr. After 80 weeks, Alloys CDA 715, 304L and 825 all showed corrosion rates of less than 0.005 µm/yr, whereas Alloy CDA 102 showed a corrosion rate of 0.45 µm/yr. No SCC was evident on any of the U-bend specimens of the four alloys. Alloy 304L and Alloy 825 also exhibited no evidence of localized corrosion (pitting or crevice corrosion) in the exposure tests. However, some localized corrosion was evident on specimens of Alloy CDA 102 and Alloy CDA 715. The latter alloy experienced shallow etching while Alloy CDA 102 experienced deep etching, up to 32 um, and shallow pitting, 10 um in depth.

Following the termination of the long-term boil-down tests, solution and deposit samples were obtained from the test vessels and analyzed. It was found that the compositions of the test solutions were very similar and slightly less than the calculated composition (based on fully evaporating the solution weekly), with a few exceptions. These exceptions in composition included calcium, magnesium, silicon, and bicarbonate, which were found in the precipitates present in the test vessels.

Table 6.1 is a comparison of the corrosion data for each of the four alloys exposed to simulated J-13 well water in Tasks 3 and 7. The exposure tests performed in Task 3 were similar to those performed in Task 7 with the exception that the Task 3 tests were shorter in duration and did not consider solution concentration. These data suggest that uniform concentration of ionic species in simulated J-13 well water does not appear to be detrimental to the corrosion behavior of the candidate alloys and, in fact, the more concentrated groundwater appeared to be less aggressive, from the standpoint of general corrosion, than the dilute simulated J-13 well water.

Although very low corrosion rates were obtained, these tests do not fully simulate actual repository conditions because of (1) rock-water interactions, (2) the absence of radiolysis, and (3) interaction of the groundwater with species from failed containers.

Table 6.1 Comparison Of Corrosion Rates, Calculated From Gravimetric Measurements, For Creviced Coupons Of Each Of The Four Alloys Exposed To Simulated J-13 Water In Tasks 3 And 7.

Alloy	Experiment	Exposure Hours	Corrosion Rate µm/yr	Description
CDA 102	Immersion	2024	2.48	Light etch ; a few shallow pits.
	Boil Down	4033	1.16	Heavy etching; slight pitting on one specimen.
CDA 715	Immersion	2024	0.17	Considerable etching; marbled appearance.
	Boil Down	4034	<0.2	Localized etching at crevice. Very slight scaling.
825	Immersion	2039	<0.2	Blue interference films; light etching near crevices; several small pits.
	Boil Down	4056	<0.2	No attack, very slight scaling.
304L	Immersion	2039	<0.2	Blue interference films; light etching and scaling near crevices.
	Boil Down	4034	<0.2	No attack, slight scaling.

7. CONCLUSIONS

- Pit-initiation studies of the copper-base alloys confirmed that standard interpretations of CPP tests are not always appropriate in the presence of thick oxide layers. Hysteresis in CPP tests may not always be indicative of pitting.

- Pit-initiation studies of the Fe-Cr-Ni alloys confirmed that, in general, the standard interpretation of the CPP curves appears to be accurate. However, slight hysteresis at noble potential may, in some instances, be associated with tarnish film growth, as opposed to pitting.

- Pit-propagation studies with specimens Alloy CDA 102 showed that, if pits initiate, their propagation may be limited in the absence of an oxidizing species such as hydrogen peroxide (H_2O_2).

- One possible radiolysis product, H_2O_2, was found to significantly promote pit propagation of Alloy CDA 102 in a simulated groundwater solution.

- Galvanic corrosion caused by temperature differences on the surface of the waste canister may accelerate corrosion in the presence of radiolysis products. The direction of the thermogalvanic effect (whether the corrosion rate of the higher or lower temperature portion of the canister is accelerated) appears to be a function of the alloy-environment system considered.

- Thermogalvanic effects on corrosion were, in general, minor in comparison to the deleterious effect of increasing temperature on corrosion rate.

- In borehole liner-container interaction studies, performed with Alloy 304L - C1010 and Alloy 825 - Alloy 304L galvanic couples, there was no evidence of accelerated corrosion of the noble member of the couple. The active member of the couple consistently experienced accelerated corrosion, which is the expected behavior for classical galvanic corrosion.

- Long-term, boil-down studies showed negligible general corrosion rates (<0.005 µm/yr) for Alloys 825, 304L, and CDA 715 following eighty weeks of exposure in concentrated simulated J-13 well water at 90°C. Alloy CDA 102 experienced a general corrosion rate of 0.45 µm/yr in this environment.

- No SCC of U-bend specimens of any of the four alloys occurred following eighty weeks of exposure in concentrated simulated J-13 well water at 90°C in the long-term, boil-down tests.

- Alloy 304L and Alloy 825 exhibited no evidence of localized corrosion (pitting or crevice corrosion) in the long-term boil down tests. However, some localized corrosion was evident on specimens of Alloy CDA 102 and Alloy CDA 715.

8. RECOMMENDATIONS FOR FURTHER RESEARCH

- Pit-propagation testing needs to be pursued with other candidate alloys. Emphasis needs to be placed on the propagation of pits in the Fe-Cr-Ni alloys. If pits initiate in these alloys, container failure by pitting corrosion may occur in a relatively short period of time.

- The influence of major parameters such as pit geometry and radiolysis on pit-propagation needs to be well characterized.

- The electrochemical techniques for studying pit propagation need to be confirmed by means of long-term exposure tests.

- Thermogalvanic testing needs to be expanded to help verify if thermogalvanic coupling will indeed accelerate the corrosion rate of the cooler part of the canister. This type of testing needs to be expanded to include Alloy CDA 715 and Alloy 825 and testing with each of the four alloys in various simulated environments. Long-term testing also needs to be considered.

- Borehole liner-container interaction testing needs to be expanded to evaluate more aggressive simulated repository environments.

- Long-term exposures need to be performed with candidate alloys in environments that consider all of the factors that are established to affect the repository environment. These include concentration of the groundwater at the heated container surface, radiation, rock-groundwater interaction, corrosion product-groundwater interaction, and interaction of the groundwater with actual high-level waste from breached containers.

9. REFERENCES

Abraham-1986 - Abraham, T., Jain, H., and Soo, P., "Stress-Corrosion Cracking Tests on High-Level-Waste Container Materials in Simulated Tuff Repository Environments," Brookhaven National Laboratory, NUREG/CR-4619, BNL-NUREG-51996, June, 1986.

Beavers-1987 - Beavers, J. A., Thompson, N. G., et al, "Long-Term Performance of Container Materials for High-Level Waste," NUREG/CR-4955, BMI-2155, September, 1987.

Beavers-1989 - Beavers, J. A., Thompson, N. G., and Harper, W. V., "Potentiodynamic Polarization Studies of Candidate Container Materials in Simulated Tuff Repository Environments," Cortest Columbus Technologies, Inc., Columbus, Ohio, November, 1989.

Beavers-1990 - Beavers, J. A., and Thompson, N. G., "Environmental Effects on Corrosion in the Tuff Repository," Cortest Columbus Technologies, Inc., Columbus, Ohio, NUREG/CR-5435, February, 1990.

Beavers-1991 - Beavers, J. A., and Durr, C. L., "Immersion Studies on Candidate Container Alloys for the Tuff Repository," Cortest Columbus Technologies, Inc., Columbus, Ohio, NUREG/CR-5598, May, 1991.

Beavers-1991a - Beavers, J. A., Thompson, N. G., and Durr, C. L., "Potentiodynamic Polarization Studies on Candidate Container Alloys for The Tuff Repository," Cortest Columbus Technologies, Inc., Columbus, Ohio, NUREG/CR-5708, November, 1991.

Cragnolino-1991 - Cragnolino, G. A., and Sridhar, N., "Localized Corrosion of a Candidate Container Material for High-Level Nuclear Waste Disposal," Southwest Research Institute, San Antonio, Texas, Corrosion '91, Paper No. 35, March, 1991.

Glass-1985 - Glass, R. S., Overturf, G. E., Van Konynenburg, R. A., and McCright, R. D., "Gamma Radiation Effects on Corrosion: I Electrochemical Mechanisms for The Aqueous Corrosion Processes of Austenitic Stainless Steels," Lawrence Livermore National Laboratory, Livermore, CA, UCRL-92311, February, 1985.

Glass-1986 - Glass, R. S., Van Konynenburg, R. A., and Overturf, G. E., "Corrosion Processes of Austenitic Stainless Steels and Copper-Based Materials in Gamma-Irradiated Aqueous Environments," Corrosion '86, Paper No. 258 and Lawrence Livermore National Laboratory, Livermore, CA, UCRL-92941, September, 1985.

Glassley-1986 - Glassley, W. E., "Reference Waste Package Environment Report," Lawrence Livermore National Laboratory, Livermore, CA, UCRL-53726, October 1, 1986.

Johnstone-1981 - Johnstone, J. K. and Wolfsberg, K., editors, "Evaluation of Tuff As a Medium for a Nuclear Waste Repository: Interim Status Report on the Properties of Tuff," Sandia National Laboratories, SAND80-1464, July, 1981.

Knauss-1985a - Knauss, K. G., Beiriger, W. J, and Peifer, D. W., "Hydrothermal Interaction of Crushed Topopah Spring Tuff and J-13 Water at 90, 150, and 250°C Using Dickson-Type, Gold-Bag Rocking Autoclaves," Lawrence Livermore National Laboratory, Livermore, CA, UCRL-53630, DE86-014752, May, 1985.

Knauss-1985b - Knauss, K. G., Beiriger, W. B., Peifer, D. W., and Piwinskii, A., "Reaction of Solid Wafers of Topopah Spring Tuff With J-13 Water at 90, 150, and 250°C in Dickson-Type, Gold-Bag Rocking Autoclaves: 1. Short-Term Experiments," Lawrence Livermore National Laboratory, Livermore, CA, UCRL-53645.

Koch-1988 - Koch, G. A., Spangler, J. M., and Thompson, N. G., "Corrosion Studies in Complex Environments," The Use of Synthetic Environments for Corrosion Testing, ASTM STP 970, P. E. Francis and T. S. Lee, Eds., American Society for Testing and Materials, Philadelphia, PA, 1988, pp. 3-17.

McCright-1984 - McCright, R. D., Weiss, H., Juhas, M. C., and Logan, R. W., "Selection of Candidate Canister Materials for High-Level Nuclear Waste Containment in a Tuff Repository," Lawrence Livermore National Laboratory, Livermore, CA, UCRL 89988 and Corrosion '84, Paper No. 198, April, 1984.

McCright-1985 - McCrights, R. D., "FY 1985 Status Report on Feasibility Assessment of Copper-Base Waste Package Container Materials in a Tuff Repository," Lawrence Livermore National Laboratory, Livermore, CA, UCID-20509, September, 1985.

Montazer-1984 - Montazer, P. and Wilson, W. E., "Conceptual Hydrologic Model of Flow in the Unsaturated Zone, Yucca Mountain, Nevada," U.S. Geological Survey - Water Resources Investigation Report,. USGS-WRI-84-4345, 1984.

Oversby-1983 ersby, V. M., Knauss, K. G., "Reaction of Bullfrog Tuff With J-13 Well Water at 90°C and 150 C," Lawrence Livermore National Laboratory, Livermore, CA, UCRL-53442, DE84-000659, September, 1983.

Pitman-1986 - Pitman, S. G., Westerman, R. E., Haberman, J. H., "Corrosion and Slow Strain Rate Testing of Type 304L Stainless Steel in Tuff Groundwater Environments," Pacific Northwest Laboratory, Richland, WA, PNL-SA-14396, DE87-006404, October, 1986.

Schuraytz-1985 - Schuraytz, B., "Geochemical Gradients in the Topopah Spring Member of the Paintbrush Tuff: Evidence for Eruption Across a Magmatic Interface," Lawrence Livermore National Laboratory, Livermore, CA, UCRL-53698.

Van Konynenburg-1986 - Van Konynenburg, R. A., "Radiation Chemical Effects in Experiments to Study the Reaction of Glass in a Gamma Irradiated Air, Groundwater, and Tuff Environment," Lawrence Livermore National Laboratory, Livermore, CA, UCRL-53719.

Yunker-1986a - Yunker, W. H., "Corrosion of Copper-Based Materials in Gamma Radiation," Westinghouse Hanford Company, HEDL-7612, DE87-005494, June 1986.

Yunker-1986b - Yunker, W. H., Westinghouse Hanford Company, and Glass, R. S., Lawrence Livermore National Laboratory, "Long-Term Corrosion Behavior of Copper-Base Materials in a Gamma-Irradiated Environment," UCRL-94500, DE87-007098, December, 1986.

Site Characterization f ›∧, Yucca Mountain Site, Nevada Research and Development Area, Nevada, DOE/RW-0199, Volume 3, Part A, Chapter 7 - Waste Package, December 1988, U. S. Department of Energy, Office of Civilian Radioactive Waste Management.

(Kearns (1986)) Kearns, J. R. Johnson, M. J., and Grubb, J. F., "Accelerated Corrosion In Dissimilar Metal Crevices," Corrosion 86, Paper No. 228, Houston, TX, March 1986.

APPENDIX A

THE POTENTIODYNAMIC POLARIZATION TECHNIQUE FOR CORROSION EVALUATION

APPENDIX A

THE POTENTIODYNAMIC POLARIZATION TECHNIQUE FOR CORROSION EVALUATION

The cyclic-potentiodynamic-polarization (CPP) technique was used in this project to provide an understanding of how the specific variables such as environmental composition, temperature, and alloy composition affect the general- and pitting- corrosion behavior of the alloys in simulated repository environments.

In the CPP procedure, the polarity and magnitude of the current flow between a specimen of the material of interest and an inert counter electrode are measured as a function of electrochemical potential. For the anodic portions of the curve, the current measured is equal to the corrosion rate of the specimen if two conditions are met: (1) The electrochemical potential is far enough away from the open-circuit potential that the rate of the cathodic reaction is negligible; and (2) The rates of spurious oxidation reactions are negligible.

Schematics of anodic polarization curves showing several types of behavior are given in Figure A.1. For the active-corrosion case, the anodic curve is linear on an E-log i plot, and the forward and reverse scans are coincident. The presence of a peak in the anodic portion of the curve, followed by decreasing current, is generally indicative of the onset of passivation. The occurrence of hysteresis between the forward and reverse scans is indicative of pitting. Where the hysteresis loop is very large, the protection potential may be very close to the open-circuit potential, indicating a high probability of pitting in that particular environment.

The polarization behavior of the alloys was determined using conventional polarization techniques. The specific polarization equipment used for these experiments included a Princeton Applied Research Model 273 potentiostat coupled to a computer data-acquisition system or a Santron Electrochemical Measuring System. A two-compartment electrochemical cell was employed that utilized a saturated-calomel reference electrode (SCE) and a platinum counter electrode (Figure A.2). Originally, it was planned to use a three-compartment cell (working, counter, and reference compartments), but the relatively high resistance of several of the solutions prevented its use, and the two-compartment cell was used for all tests. The working electrode specimens were cylindrical rods that were drilled, tapped at one end, and sealed off using PTFE gaskets. The specimens were typically 1.3 cm in length with the diameter depending on the metal being tested. The electrodes were polished with successively finer grades of silicon carbide paper, finishing with a 600-grit grade.

A typical experiment consisted of setting up the electrochemical cell containing the test solution. The test solution was slowly brought up to the desired temperature while being sparged with the desired gas. The specimen was immersed in the heat solution after sparging for 1 to 2 hours. The specimen was exposed to the test solution under freely corroding conditions for 16-24 hours to permit steady-state conditions to be achieved.

The working electrode lead was connected to the test specimen while the auxiliary (counter) electrode lead was connected to an inert electrode (platinum wire) placing in the test cell. The

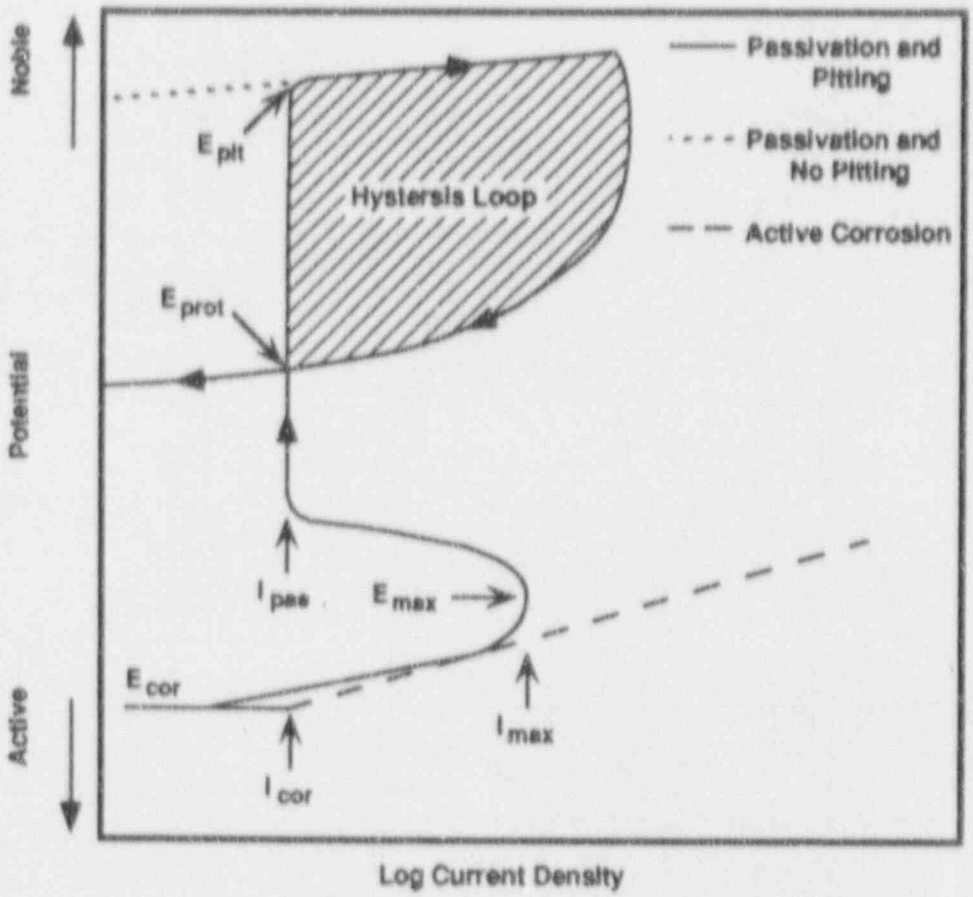

Figure A.1 Schematic Of Typical Cyclic Potentiodynamic Polarization Curve.

E_{cor} = corrosion potential; E_{pit} = potential at which pits initiate on forward scan; E_{prot} = potential at which pits repassivate on reverse scan; i_{cor} = current density at the free-corrosion potential; i_{max} = current density at active peak; i_{pas} = current density in passive range.

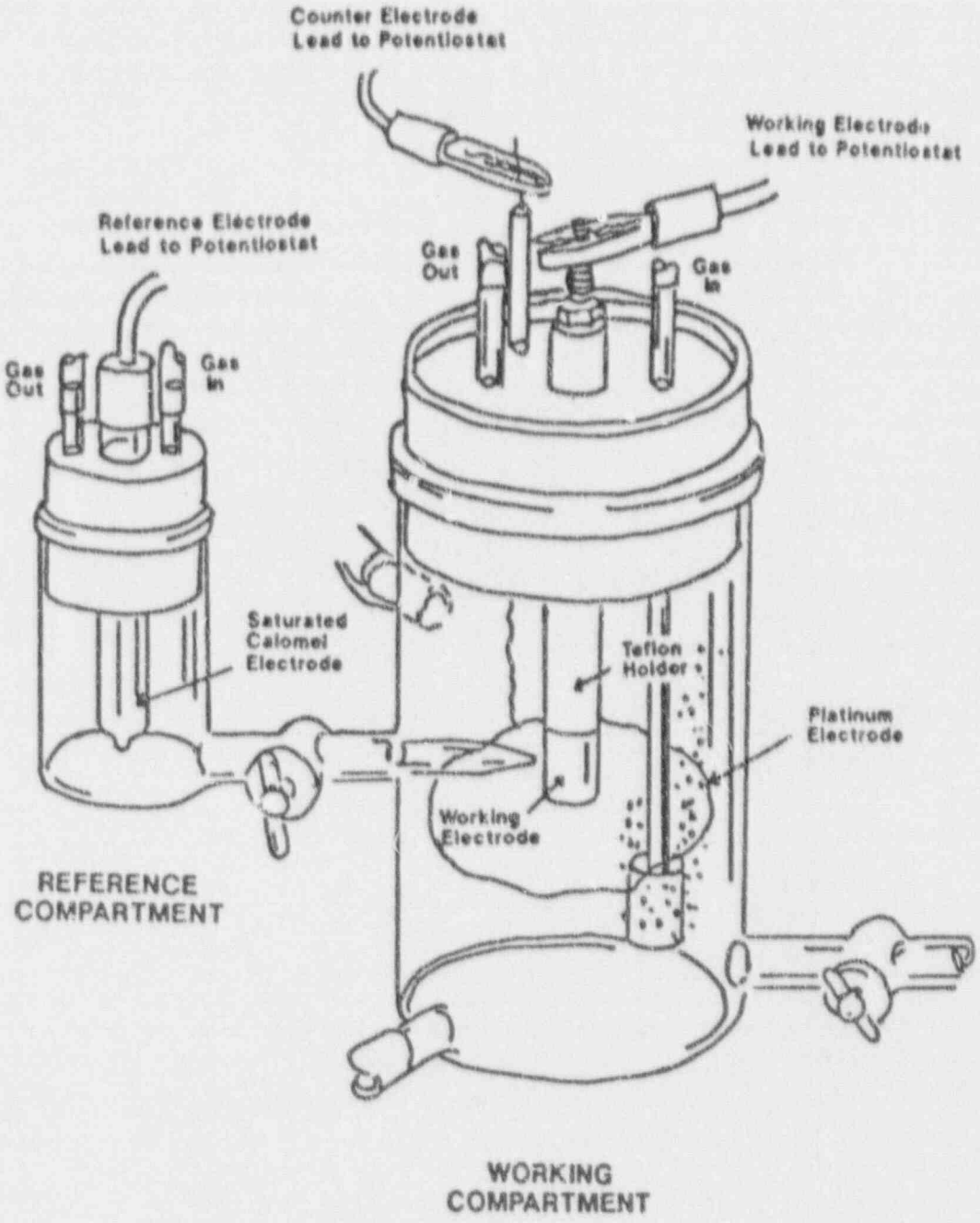

Figure A.2 Electrochemical Cell Used For Ambient Pressure Potentiodynamic Polarization Experiments.

reference electrode lead was connected to the reference electrode which communicates with the test cell electrolyte through a small diameter tube filled with electrolyte, referred to as a Luggin probe or salt bridge. The tip of the probe is placed near the test specimen to minimize measurement errors due to ohmic potential drops.

Partial cathodic and full anodic polarization curves were obtained by scanning at a rate of 0.6 V/h and beginning the scan approximately 100 mV (SCE) more negative than the free-corrosion potential. The current for the anodic curve was scanned until a current density of approximately 2×10^{-3} A/cm^2 was attained; the potential scan was then reversed until repassivation occurred and the current changed polarity, becoming cathodic. In those cases in which the current density did not attain 2×10^{-3} A/cm^2, the potential scan was reversed at a critical potential of 1.2 volts relative to E_{cor}.

After completion of the polarization scans, the following polarization parameters were obtained from the polarization curves of potential (E) versus logarithm of current density (log i) when applicable: i_{cor}, E_{cor}, i_{pas}, E_{ph} or E_b, E_{prot} or E_{rp}, i_{max} and E_{max}. Tafel slopes could be obtained from the polarization curves if desired. The specimens were also optically examined at 30X magnification following the scan as a comparison for the corrosion behavior observed from the polarization curves.

APPENDIX B

ENVIRONMENTAL TEST MATRIX:
A STATISTICAL APPROACH

APPENDIX B

ENVIRONMENTAL TEST MATRIX: A STATISTICAL APPROACH

Synthetic environments which, historically, have been used to simulate field conditions in laboratory corrosion studies are usually relatively simple. More often than not, the effects of variables are studied by varying a single variable at a time. Such an approach does not account for the dependency of effects among multiple variables. In this project, a statistical approach is used that was specifically designed to examine corrosion behavior in complex environments (Koch, et al.). By using a statistically based experimental design, a mathematical expression is developed that relates a dependent variable or response, such as corrosion rate, to a number of independent solution variables or factors, such as species concentration, temperature, and pH. In such an analysis, the mathematical expressions can include main-effect terms (linear), two factor interactions (cross products), and quadratic terms. High-order terms, such as three-way interactions, can also be evaluated but their physical significance is often difficult to explain and the magnitude of the terms are expected to be much smaller than the main-effect terms or two-factor interaction terms. Because of the large number of solution variables (15), and the large number of alloys (4) being examined in this study, it was decided that the most effective approach was to determine the main-effect terms for each of the variables free and clear of two-factor interactions but not to perform the much larger matrix of experiments required to begin to determine the two-factor interactions and quadratic terms. To estimate the main-effect terms of the variables, a Resolution IV experimental design was selected. In this design, each environmental variable has a high and low level. Thirty-six high-low combinations are required to determine the main-effect terms for 15 variables.

The initial step was to define the solution variables of interest for inclusion into the test matrix. Table B.1 presents the compositional ranges of important environmental species for (1) Tuff well water, (2) Tuff groundwater heated to temperatures from 90-250°C in the presence of Tuff rock, and (3) Tuff groundwater heated to 90-150°C in the presence of radiation. The references from which the data were obtained are indicated in Table B.1.

The 15 environmental variables that were included in the experimental matrix and their high and low concentrations are given in Table B.2. The 15 variables selected for examination in the Task 2 tests included 12 variables associated with the J-13 groundwater and three variables produced by radiolysis. Nitrogen, sulfate, and sodium were chosen as the gas, anion and cation, respectively, used for balancing the solution chemistry. One variable that is missing from the 15 environmental variables listed in Table B.2 is the radiolysis product hydrogen. Because of the experimental difficulties in mixing hydrogen and oxygen, it was decided to remove hydrogen from the matrix of experiments and to perform a few experiments separately to establish its effect. A complete summary of the solution matrix investigated during the entire 3.5 year program is outlined in Table B.3.

In the following paragraphs, each variable is briefly discussed and justification for inclusion of the variable into the matrix and the concentrations selected are presented based on a review of the literature (Knauss-1985, Glass-1986, Oversby-1983, Yunker-1986, et al.).

Table B.1 Concentration Ranges For Environmental Species In Tuff Groundwater.

Environmental Variable	Nominal Concentration Of Well Water,[a] mg/l	Concentration Range Of Groundwater Heated To 90-250°C With Tuff Rock,[a, b] mg/l	Concentration Range Of Groundwater Heated To 90-150°C In Presence Of Radiation[c], mg/l
pH	7.6	5.8 - 8.3	7.6 - 9.0
SiO_2	58	29 - 394	1.05 - 3.10
HCO_3^-	125	45 - 195	8.1 - 21
F^-	2.2	2.2 - 4.4	0.38 - 1.4
Cl^-	6.9	6.5 - 8.9	2.5 - 5.8
NO_3^-	9.6	8.5 - 16.8	2.5 - 18.8
SO_4^{2-}	18.7	13.3 - 22	1.8 - 6.2
NO_2^-	-	0.7 - 1.5	1.2 - 3.8
H_2O_2	-	-	0 - 4.8[d]
Al^{3+}	.012	0.016 - 4.8	<0.15 - 0.18
Fe^{2+}	0.006	-	<0.02 - 0.04
Ca^{2+}	12.5	0.21 - 13.2	2.7 - 9.8
Mg^{2+}	1.9	0.009 - 2.0	0.6 - 1.1
K^+	5.1	3.2 - 19.4	2.4 - 4.8
Na^+	44	35 - 74	2.8 - 36

(a) Knauss, 1985.
(b) Oversby, 1983.
(c) Yunker, 1986.
(d) Glass, 1985.

Table B.2 List Of Variables Included In The Matrix Of Potentiodynamic Polarization Tests In Task 2.

Variable Number	Variable Name	Origin	Test Matrix High Concentration mg/l	Test Matrix Low Concentration mg/l	Nominal Concentration Of J-13, mg/l
1	SiO_2	J-13	215	2.2	58
2	HCO_3^-	J-13	2000	0.4	125
3	F^-	J-13	200	0.04	2.2
4	Cl^-	J-13	1000	0.2	6.9
5	NO_3^-	J-13	1000	0.2	9.6
6	NO_2^-	Radiolysis	200	0	—
7	H_2O_2	Radiolysis	200	0	—
8	Ca^{2+}	J-13	20	0.004	12
9	Mg^{2+}	J-13	20	0.004	1.9
10	Al^{3+}	J-13	0.8	0.0004	0.01
11	PO_4^{3-}	J-13	2.0	0.01	0.12*
12	Oxalic Acid	Radiolysis	172	0	—
13	O_2	Open Repository and Radiolysis	30**	5**	—
14	Temp	J-13	90°C	50°C	—
15	pH	J-13	10	5	7.6

* McCright, R. D. FY 1985 Status Report, UCID-20509, September 30, 1985.
** Volume %.

Table B.3 Series Of Tests Included In The Matrix Of Potentiodynamic Polarization Tests In Task 2.

Test No.	SiO_2	HCO_3^-	F^-	Cl^-	NO_3^-	NO_2^-	H_2O_2	Ca^{2+}	Mg^{2+}	Al^{3+}	PO_4^{3-}	Oxalic Acid	O_2	Temp °C	pH
1	2.2	0.4	200	1000	1000	200	200	0.8	0.004	0.0004	0.01	0	5	90	5
2	2.2	2000	200	1000	1000	0	0	0.004	0.004	0.8	2.0	172	5	50	5
3	215	0.4	0.04	0.2	1000	200	0	0.8	0.004	0.8	2.0	0	30	50	5
4	215	2000	0.04	0.2	1000	0	200	0.004	0.004	0.0004	0.01	172	30	90	5
5	2.2	0.4	200	0.2	0.2	0	200	0.8	0.8	0.8	0.01	172	30	50	5
6	2.2	2000	200	0.2	0.2	200	0	0.004	0.8	0.0004	2.0	0	30	90	5
7	215	0.4	0.04	1000	0.2	0	0	0.8	0.8	0.0004	2.0	172	5	90	5
8	215	2000	0.04	1000	0.2	200	200	0.004	0.8	0.8	0.01	0	5	50	5
9	2.2	0.4	0.04	1000	0.2	200	200	0.004	0.004	0.0004	2.0	172	30	50	10
10	2.2	2000	0.04	1000	0.2	0	0	0.8	0.004	0.8	0.01	0	30	90	10
11	215	0.4	200	0.2	0.2	200	0	0.004	0.004	0.8	0.01	172	5	90	10
12	215	2000	200	0.2	0.2	0	200	0.8	0.004	0.0004	2.0	0	5	50	10
13	2.2	0.4	0.04	0.2	1000	0	200	0.004	0.8	0.8	2.0	0	5	90	10
14	2.2	2000	0.04	0.2	1000	200	0	0.8	0.8	0.0004	0.01	172	5	50	10
15	215	0.4	200	1000	1000	0	0	0.004	0.8	0.0004	0.01	0	30	50	10
16	215	2000	200	1000	1000	200	200	0.8	0.8	0.8	2.0	172	30	90	10
17	215	2000	0.04	0.2	0.2	0	0	0.004	0.8	0.8	2.0	172	30	50	10
18	215	0.4	0.04	0.2	0.2	200	200	0.8	0.8	0.0004	0.01	0	30	90	10
19	2.2	2000	200	1000	0.2	0	200	0.004	0.8	0.0004	0.01	172	5	90	10
20	2.2	0.4	200	1000	0.2	200	0	0.8	0.8	0.8	2.0	0	5	50	10
21	215	2000	0.04	1000	1000	200	0	0.004	0.004	0.0004	2.0	0	5	90	10
22	215	0.4	0.04	1000	1000	0	200	0.8	0.004	0.8	0.01	172	5	50	10
23	2.2	2000	200	0.2	1000	200	200	0.004	0.004	0.8	0.01	0	30	50	10
24	2.2	0.4	200	0.2	1000	0	0	0.8	0.004	0.0004	2.0	172	30	90	10
25	215	2000	200	0.2	1000	0	0	0.8	0.8	0.8	0.01	0	5	90	5
26	2.2	0.4	200	0.2	1000	200	200	0.004	0.8	0.0004	2.0	172	5	50	5
27	2.2	2000	0.04	1000	1000	0	200	0.8	0.8	0.0004	2.0	0	30	50	5
28	2.2	0.4	0.04	1000	1000	200	0	0.004	0.8	0.8	0.01	172	30	90	5
29	215	2000	200	1000	0.2	200	0	0.8	0.004	0.0004	0.01	172	30	50	5
30	215	0.4	200	1000	0.2	0	200	0.004	0.004	0.8	2.0	0	30	90	5
31	2.2	2000	0.04	0.2	0.2	200	200	0.8	0.004	0.8	2.0	172	5	90	5
32	2.2	0.4	0.04	0.2	0.2	0	0	0.004	0.8	0.0004	0.01	0	5	50	5
33*	108	500	50	250	250	50	50	0.2	0.2	0.2	1.3	43	15	70	7.5
34*	108	500	50	250	250	50	50	0.2	0.2	0.2	1.3	43	15	70	7.5
35*	108	500	50	250	250	50	50	0.2	0.2	0.2	1.3	43	15	70	7.5
36*	108	500	50	250	250	50	50	0.2	0.2	0.2	1.3	43	15	70	7.5
37±	64.2	121	1.7	6.4	12.4	0	0	12	1.7	0	0	0	0	90	7.0
38+	64.2	121	1.7	1000	12.4	0	0		1.7	0	0	0	0	90	7.0
39	108	500	50	250	250	50	50	0.1	0.1	0.5	1.3	50	15	70	5
40	108	500	50	250	250	50	50	20	20	0.5	1.3	50	15	70	5
	108	500	50	250	250	50	50	20	0.1	0.5	1.3	50	15	70	10
42	108	500	50	250	250	50	50	0.1	20	0.5	1.3	50	15	70	10

* Tests 33 through 36 are quadruplicate midpoint tests which help to establish the degree of reproducibility of the CPP Tests.

± Simulated J-13 well water.

\+ Simulated J-13 well water containing 1000 ppm Cl^-.

Silicon dioxide, SiO_2, is present in the J-13 well water at a concentration of 58 mg/l. Data by Knauss-1985 and Oversby-1983 indicate that, at 90°C, this is the approximate steady-state concentration which likely represents the solubility limit of SiO_2 at 90°C. During radiation, Yunker-1986 found that the concentration of SiO_2 decreased to a value of 1.1 to 3.2 mg/l. Because of this, a low concentration of 2.2 mg/l was selected. A high concentration of 215 mg/l provides a factor of 100X between the low and high concentration examined. Also, the 100 mg/l concentration is likely to exceed the solubility limit such that the high concentration primarily insures that saturation is attained during the high concentration tests. Silicon dioxide was added to the test solutions as silicic acid.

Bicarbonate, HCO_3^-, is present in the J-13 well water at a concentration of 125 mg/l. Heating the J-13 well water in the presence of Tuff rock at 90°C produced an increase in the concentration to 190 mg/l while radiation tended to decrease the concentration to 8-20 mg/l. Therefore, a low concentration of 0.4 mg/l was selected and a factor of 5000X was used to provide a high concentration of 2000 mg/l. Bicarbonate was added to the test solutions as sodium bicarbonate.

Fluoride, F^-, is present in the J-13 well water at a concentration of 2.2 mg/l. Heating in the presence of Tuff rock resulted in a very slight increase in fluoride concentration. Radiation produced a slight decrease in fluoride concentration to 0.4-1.4 mg/l. Based on these results, a 0.04 mg/l low concentration was selected and a factor of 500X provides a high concentration of 200 mg/l. Fluoride was added to the test solutions as potassium fluoride.

Chloride, Cl^-, is present in the J-13 well water at a concentration of 7 mg/l. Heating of the J-13 well water in the presence of Tuff rock produced little or no change in the chloride concentration. The effect of radiation was to produce a slight decrease in the chloride concentration to 2.5-5.8 mg/l. The low concentration was selected at 0.2 mg/l and a factor of 5000X increase provides a high concentration of 1000 mg/l. Chloride was added to the test solution as sodium chloride.

Nitrate, NO_3^-, is present in the J-13 well water at a concentration of 10 mg/l. Very little change was observed in the nitrate concentration upon heating in the presence of Tuff rock. In the presence of radiation, the nitrate concentration varied from 2.5 to 19 mg/l. Thereby, no systematic increase or decrease in the nitrate concentration was observed. The low concentration for nitrate was selected at 0.2 mg/l and a factor of 200X provides a high concentration of 1000 mg/l. Nitrate was added to the test solutions as sodium nitrate.

Nitrite, NO_2^-, is a radiolysis product which has been shown to achieve concentrations from 0.7 to 3.8 mg/l. The low concentration for nitrite is zero. A high concentration of 200 mg/l was selected and is approximately 50X the concentration indicated by Yunker (1986). Nitrite was added to the test solutions as sodium nitrite.

Peroxide, H_2O_2, is a radiolysis product and was shown to achieve a concentration of 5 mg/l in the presence of radiation. The low concentration was selected as zero and a high concentration was selected at 200 mg/l which provides a factor of approximately 40X over the concentration indicated by Glass (1986).

Calcium, Ca^{2+}, is present in the J-13 well water at a concentration of 12 mg/l. The concentration of calcium changed little when the J-13 well water was heated in the presence of Tuff rock at 90°C. At higher temperatures, the calcium concentration decreased to 0.2 mg/l. In the presence

of radiation, the concentration of calcium decreased to 2-9.8 mg/l. The low concentration for calcium was selected at 0.004 mg/l and a factor of 5000X provides a high concentration of 20 mg/l. Calcium was added to the test solutions as calcium sulfate, one-half hydrate.

Magnesium, Mg^{2+}, is present in the J-13 well water at a concentration of 1.9 mg/l. The concentration of magnesium changed little when the J-13 well water was heated in the presence of Tuff rock and showed only a slight decrease in concentration in the presence of radiation. The low concentration for magnesium was selected at 0.004 mg/l and a factor of 5000X provides a high concentration of 20 mg/l. Magnesium was added to the test solutions as magnesium sulfate, seven hydrate.

Aluminum, Al^{3+}, is present in the J-13 well water at a concentration of 0.01 mg/l. Upon heating the J-13 well water in the presence of Tuff rock, the aluminum concentration increased to 2-3 mg/l. In the presence of radiation, the aluminum increased to 0.18 mg/l. Therefore, a much larger range of concentration was observed for aluminum than was observed for other species. Thereby, a low concentration of 0.0004 was selected and a factor of 2000X provides a high concentration of 0.8 mg/l. Aluminum was added to the test solutions as aluminum sulfate, 16 hydrate.

Phosphate, PO_4^{3-}, has been reported at a concentration of 0.12 mg/l in J-13 well water (McCright-1985) and has not been reported, at all, in other referenced J-13 well waters. The low concentration for phosphate was selected to be 0.01 mg/l and a factor of 200X provides a high concentration of 2.0 mg/l. Phosphate was added to the test solutions as phosphoric acid.

Organic acids have been reported as naturally occurring in groundwaters and have been indicated as possible radiolysis products. For this study, oxalic acid was selected as the organic acid to examine. The low concentration of oxalic acid will be zero and the high concentration for oxalic acid will be 172 mg/l which approximates to the concentration range of other radiolysis products.

Oxygen, O_2, is present in the repository because of its location above the water table and because no airtight sealing arrangement is proposed for the repository. It is likely that the concentration of O_2 could be somewhat less than that normally occurring in air and, on the high side, could be greater than that occurring in air due to radiolysis. The low concentration of O_2 was selected at 5 volume percent and the high concentration at 30 volume percent.

Because the repository design will not permit any significant pressure buildup, the aqueous phase corrosion, which is being examined in this task, has a limiting temperature at the boiling point of the J-13 well water. The low temperature to be examined was selected at 50°C and the high temperature was selected at 90°C. The high temperature of 90°C was selected to provide a temperature near boiling but that can be controlled relatively easily and accurately in the laboratory.

The pH of the J-13 well water is slightly alkaline, having been reported at pH 7.6. Upon heating of the J-13 well water in the presence of Tuff rock, the pH varied only slightly when heated at 90°C and decreased down to 6.0 when heated at 250°C. In the presence of radiation, the pH has been observed to increase to 9.0. To provide a somewhat larger range of pH for the test matrix, the low pH was selected at 5 and the high pH was selected at 10.

For balancing the solution chemistry, sodium and sulfate, as well as the nitrogen concentration of the purging gas, was be permitted to vary.

APPENDIX C

POTENTIOSTATIC POLARIZATION TESTING OF THE COPPER-BASE ALLOYS

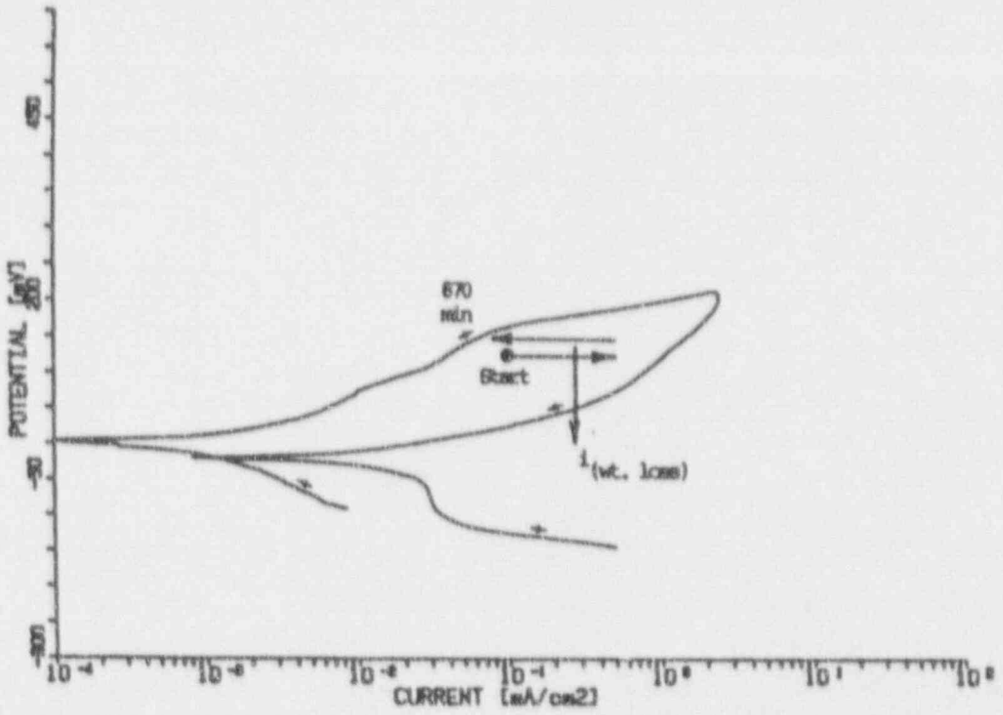

Figure C.1 Cyclic Potentiodynamic Polarization And Potentiostatic Data For Alloy CDA 102 In Test Solution No. 1 Potentiostated To +125 mV (No Pitting, Active Corrosion Beneath Oxide).

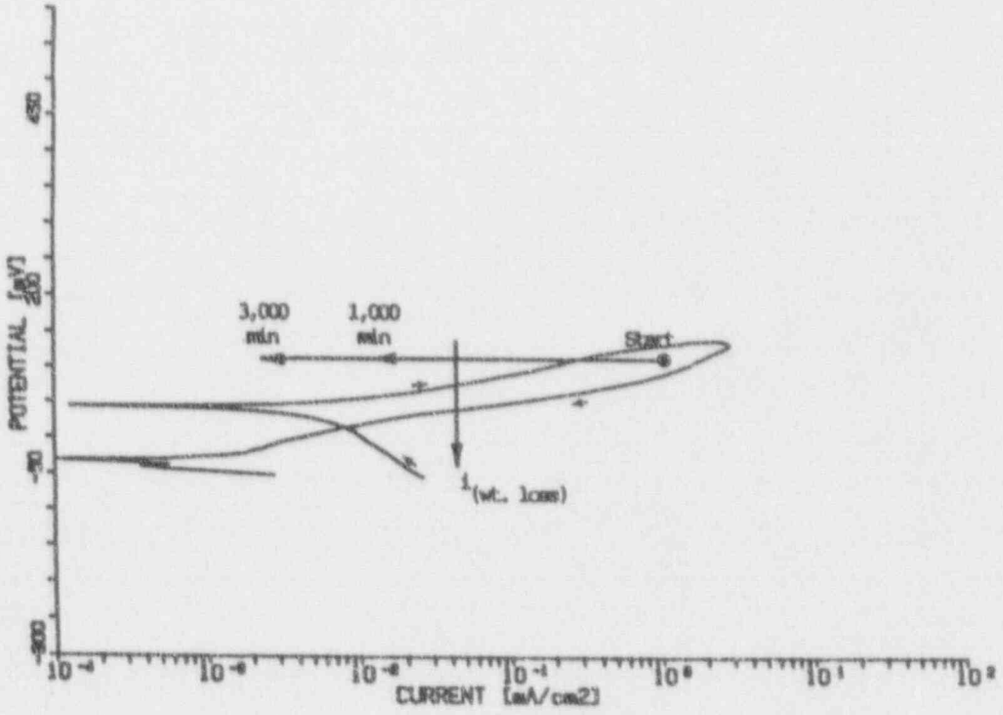

Figure C.2 Cyclic Potentiodynamic Polarization And Potentiostatic Data For Alloy CDA 102 In Test Solution No. 9 Potentiostated To +120 mV (SCE) (No Pitting, Active Corrosion Beneath Oxide).

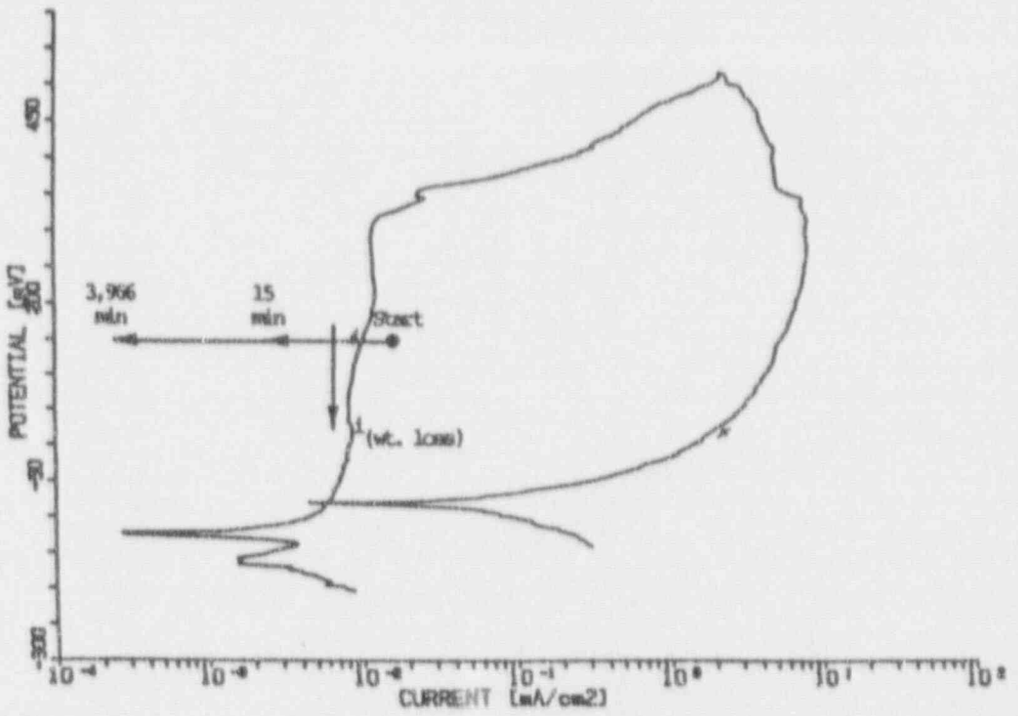

Figure C.3 Cyclic Potentiodynamic Polarization And Potentiostatic Data For Alloy CDA 102 In Test Solution No. 10 Potentiostated To +151 mV (No Pitting, Slightly Tarnished).

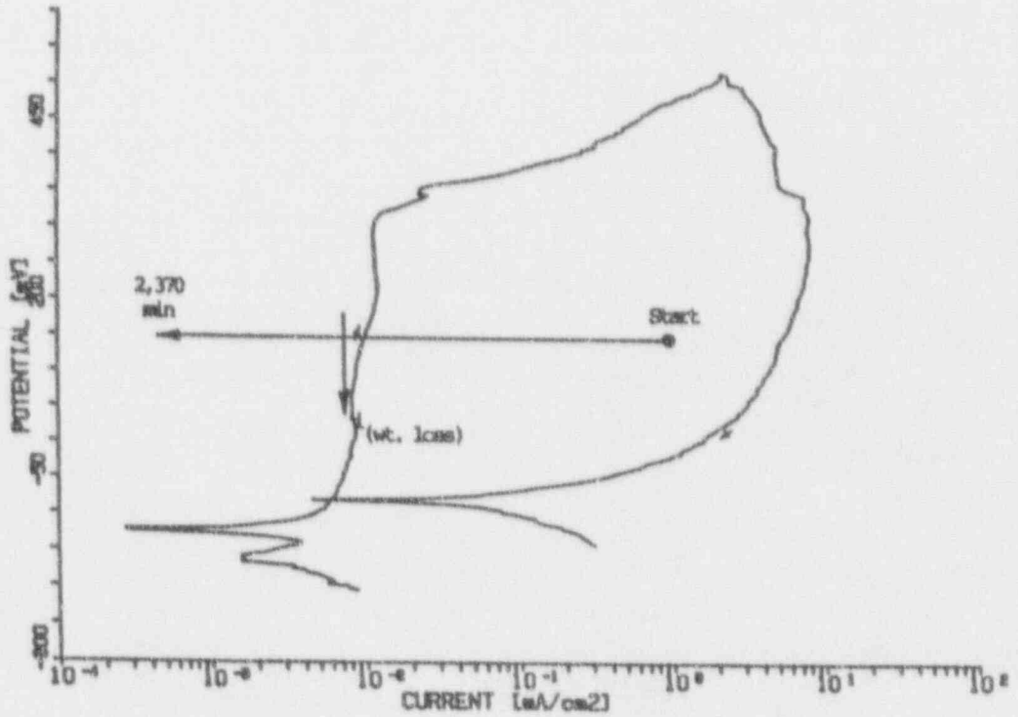

Figure C.4 Cyclic Potentiodynamic Polarization And Potentiostatic Data For Alloy CDA 102 In Test Solution No. 10 Potentiostated On The Reverse Scan To +150 mV (SCE) (No Pitting, Locally Active Attack Beneath Oxide).

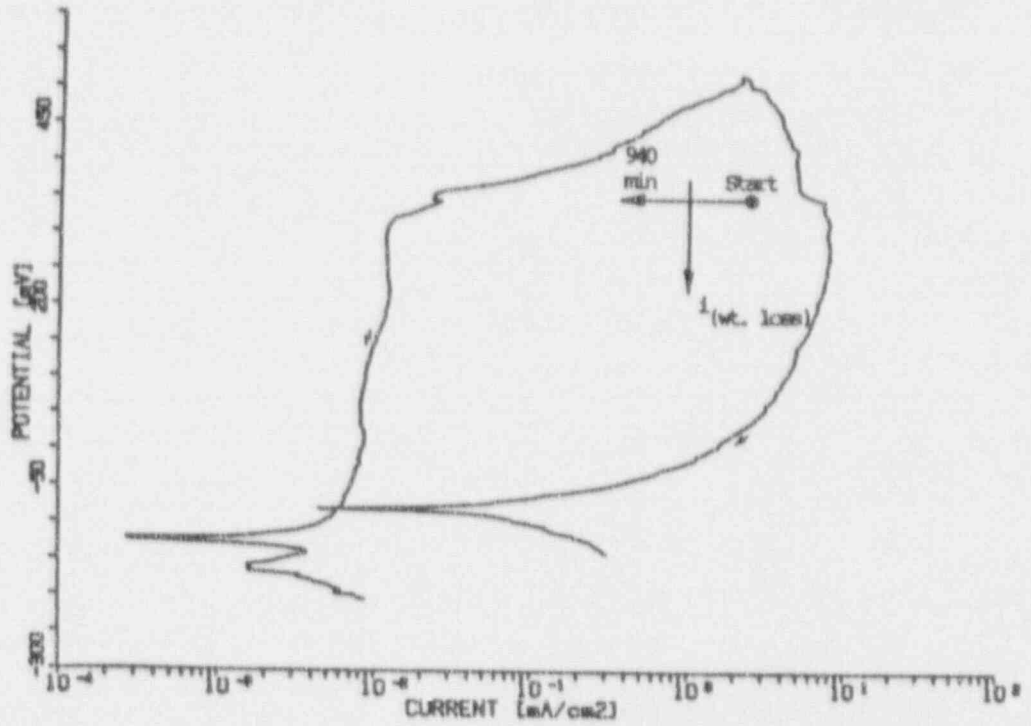

Figure C.5 Cyclic Potentiodynamic Polarization And Potentiostatic Data For Alloy CDA 102 In Test Solution No. 10 Potentiostated On The Reverse Scan To +350 mV (No Pitting, Large Areas Of Locally Active Attack).

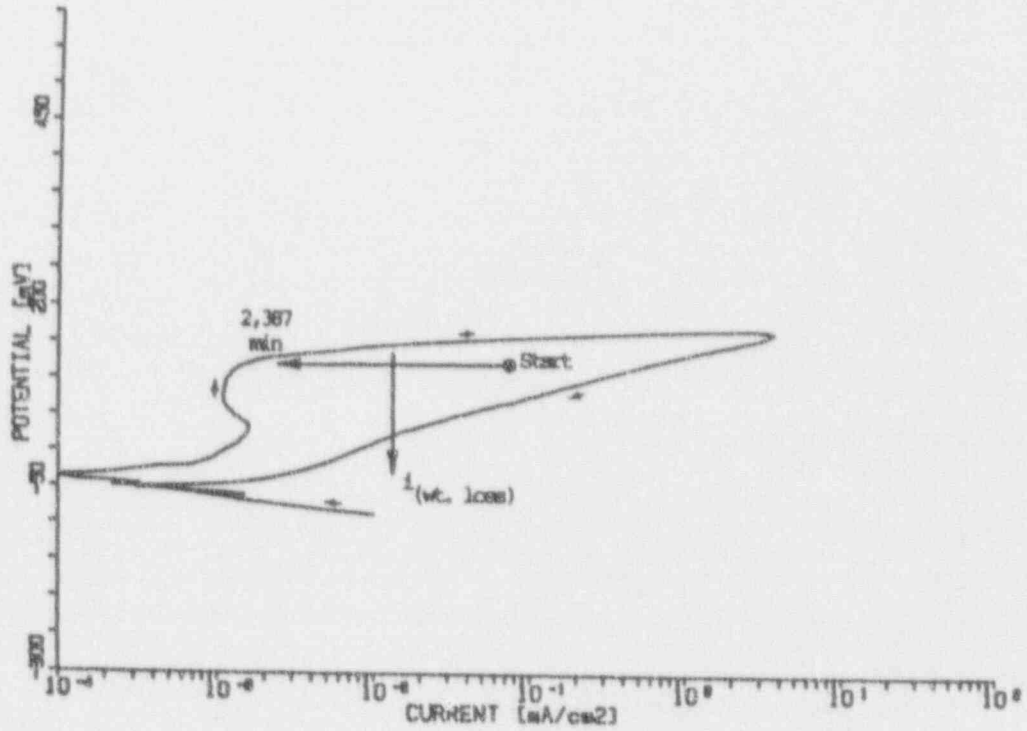

Figure C.6 Cyclic Potentiodynamic Polarization And Potentiostatic Data For Alloy CDA 102 In Test Solution No. 13 Potentiostated To +110 mV (SCE) (No Pitting, Shallow Locally Active Attack).

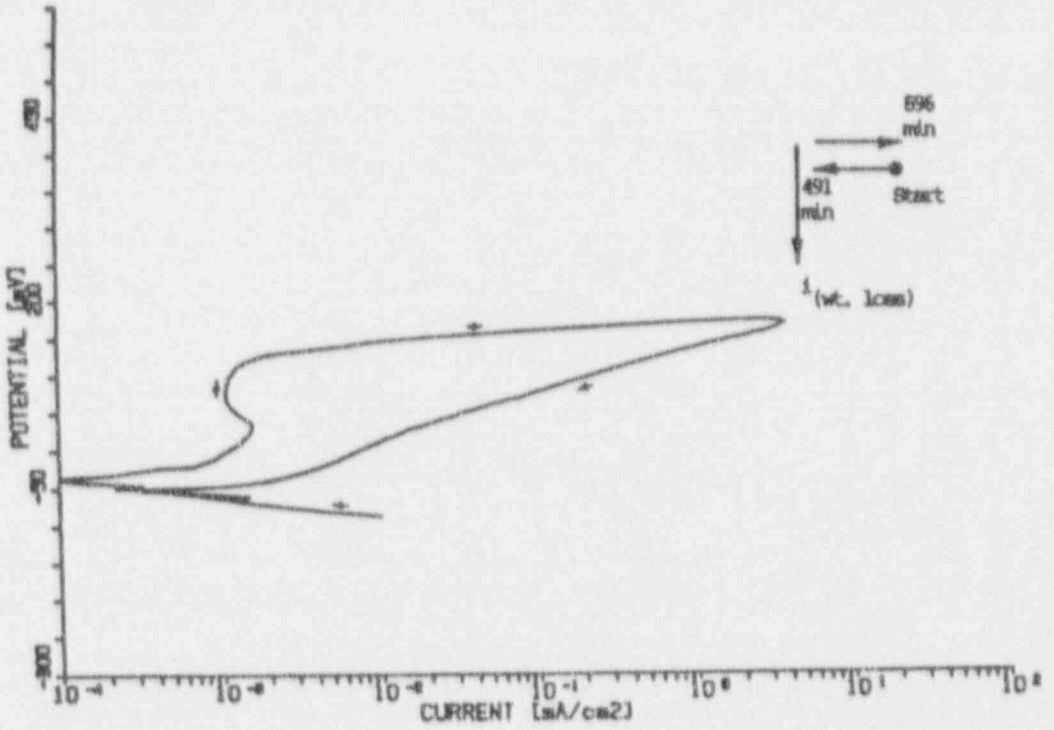

Figure C.7 Cyclic Potentiodynamic Polarization And Potentiostatic Data For Alloy CDA 102 In Test Solution No. 13 Potentiostated To +376 mV (No Pitting, Severe Attack Beneath Oxide).

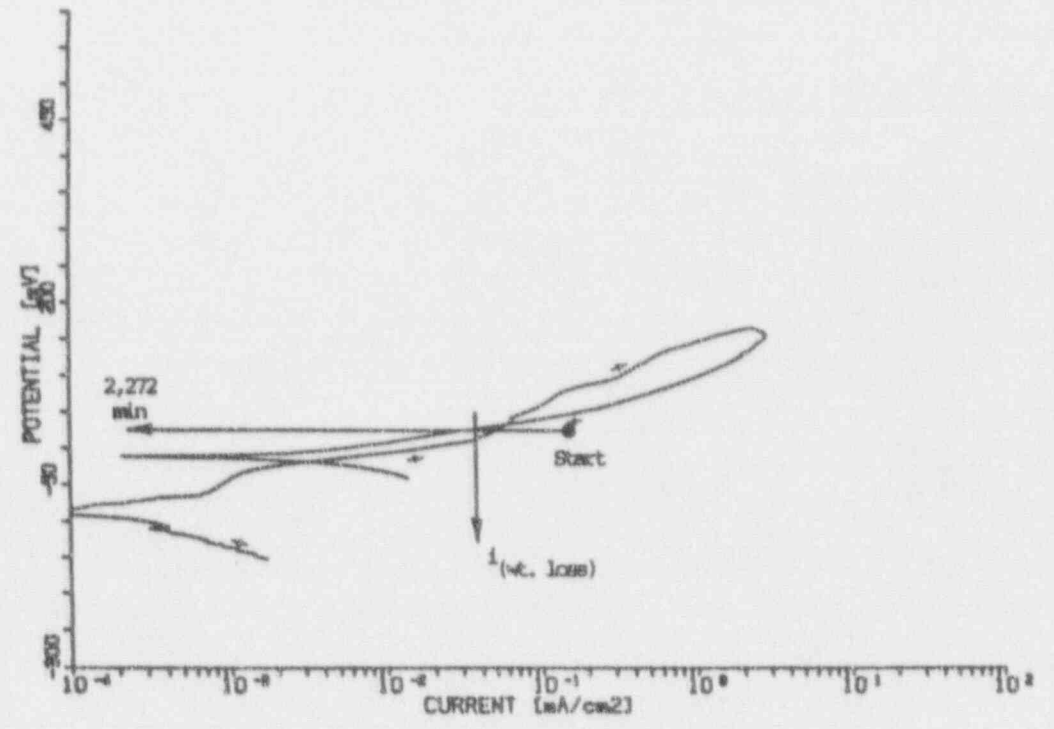

Figure C.8 Cyclic Potentiodynamic Polarization And Potentiostatic Data For Alloy CDA 102 In Test Solution No. 20 Potentiostated To -20 mV (SCE) (No Pitting, Very Few Active Sites).

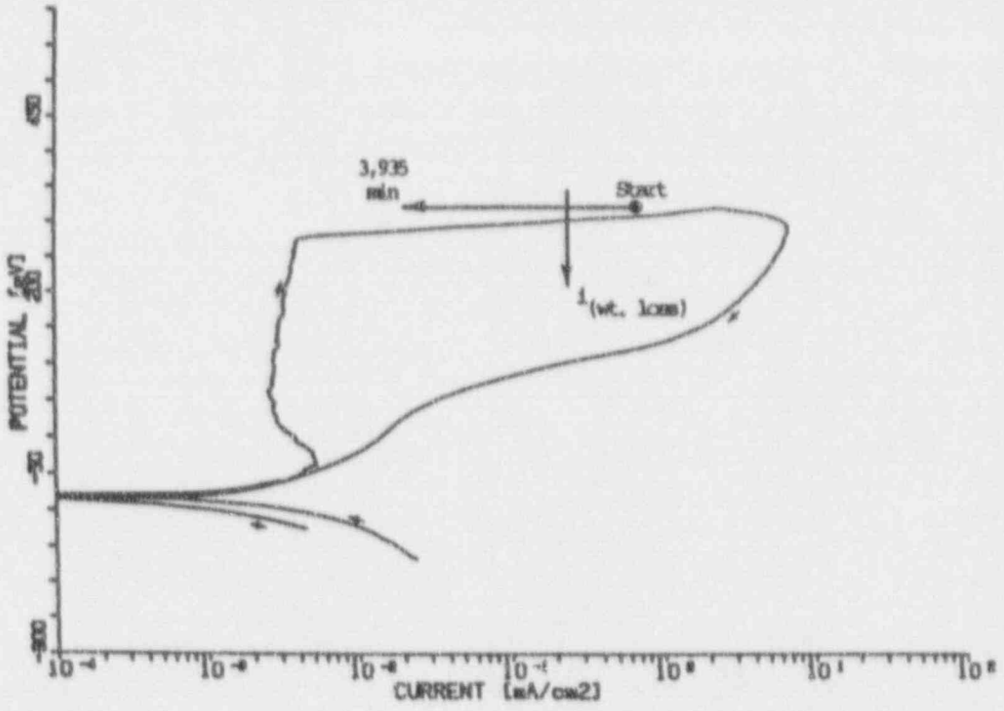

Figure C.9 Cyclic Potentiodynamic Polarization And Potentiostatic Data For Alloy CDA 102 In Test Solution No. 23 Potentiostated To +325 mV (Pitting, Severe Active Attack).

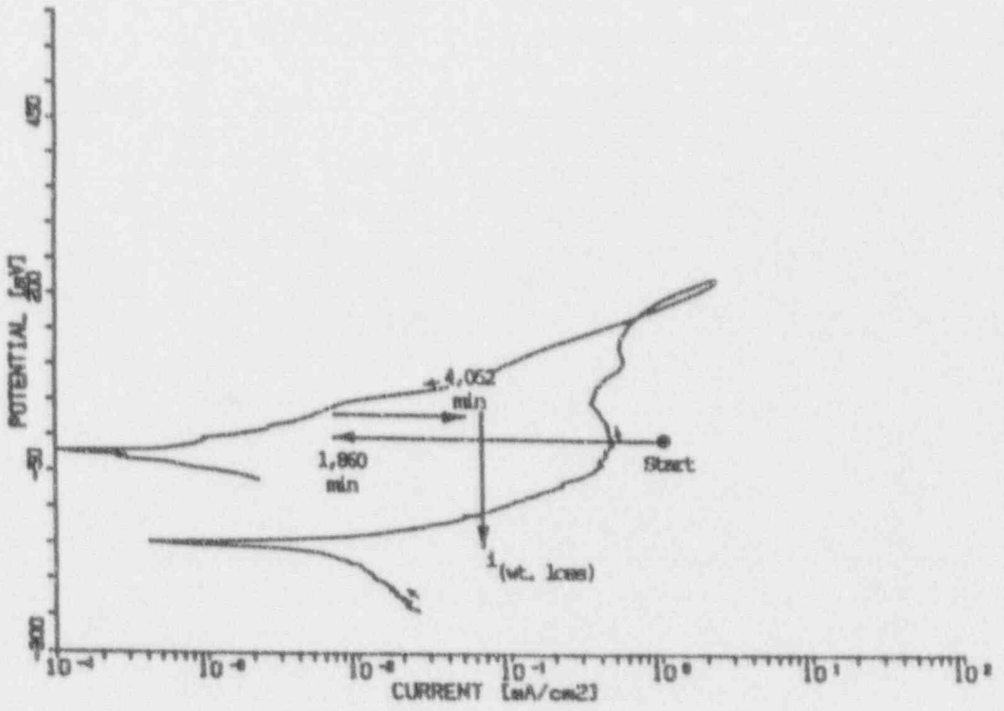

Figure C.10 Cyclic Potentiodynamic Polarization And Potentiostatic Data For Alloy CDA 102 In Test Solution No. 30 Potentiostated To 0 mV (SCE) (No Pitting, Severe Active Corrosion).

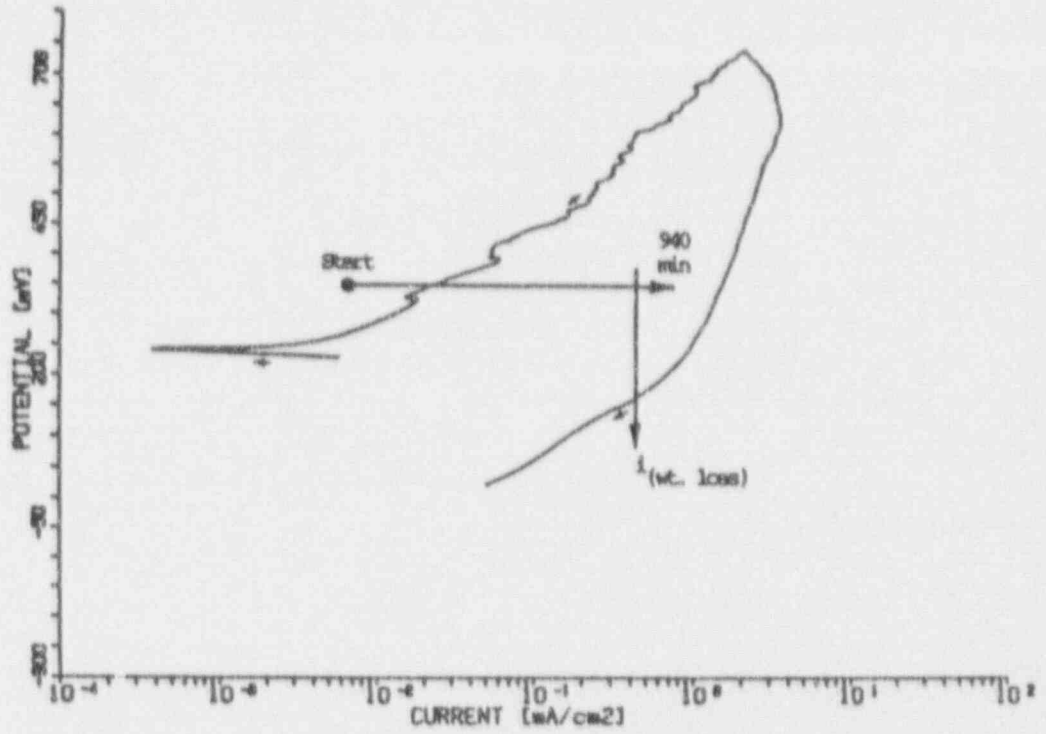

Figure C.11 Cyclic Potentiodynamic Polarization And Potentiostatic Data For Alloy CDA 715 In Test Solution No. 14 Potentiostated To +349 mV (No Pitting, Locally Severe Active Attack).

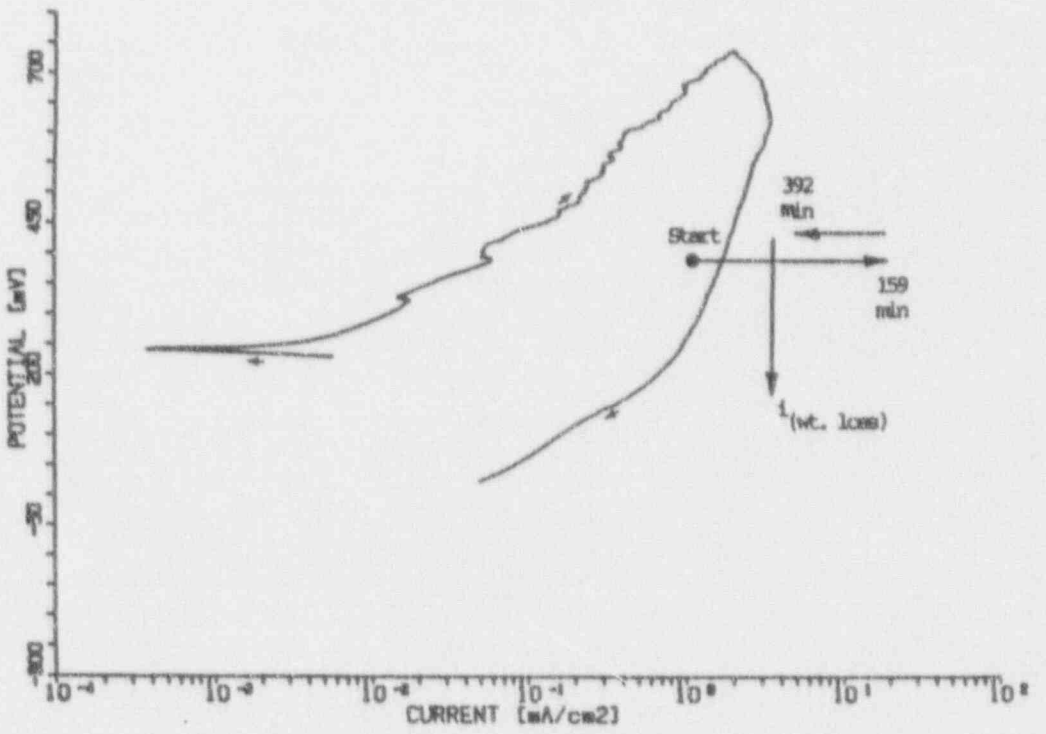

Figure C.12 Cyclic Potentiodynamic Polarization And Potentiostatic Data For Alloy CDA 715 In Test Solution No. 14 Potentiostated On The Reverse Scan To +399 mV (SCE) (Pitting, Severe Local Corrosion).

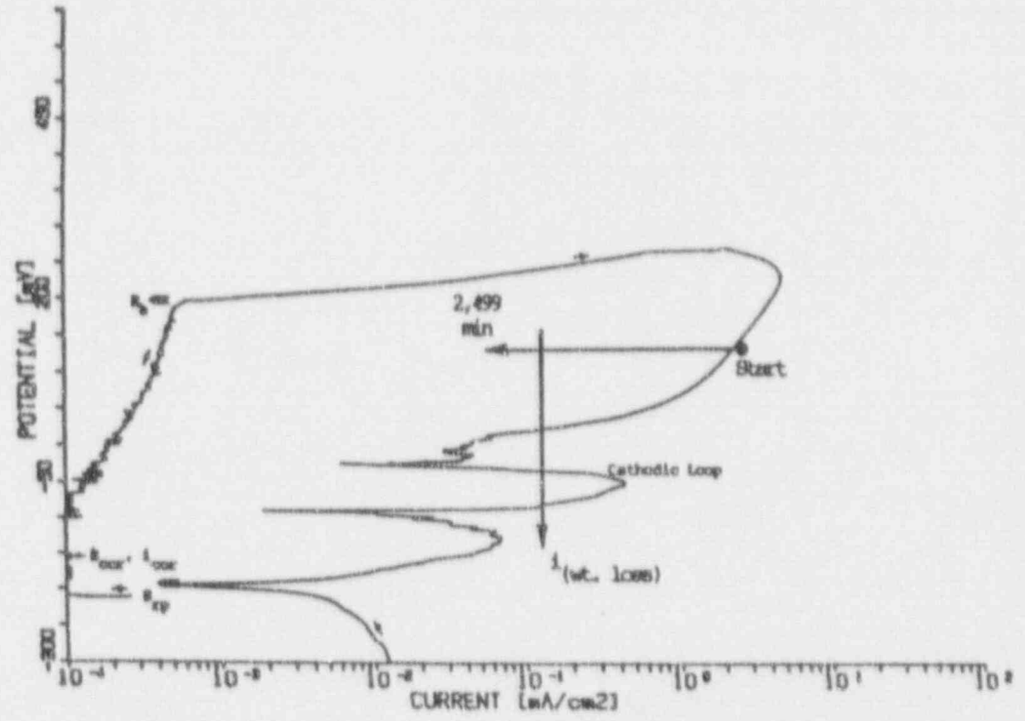

Figure C.13 Cyclic Potentiodynamic Polarization And Potentiostatic Data For Alloy CDA 715 In Test Solution No. 13 Potentiostated On The Reverse Scan To +125 mV (Pitting, Severe Active Corrosion).

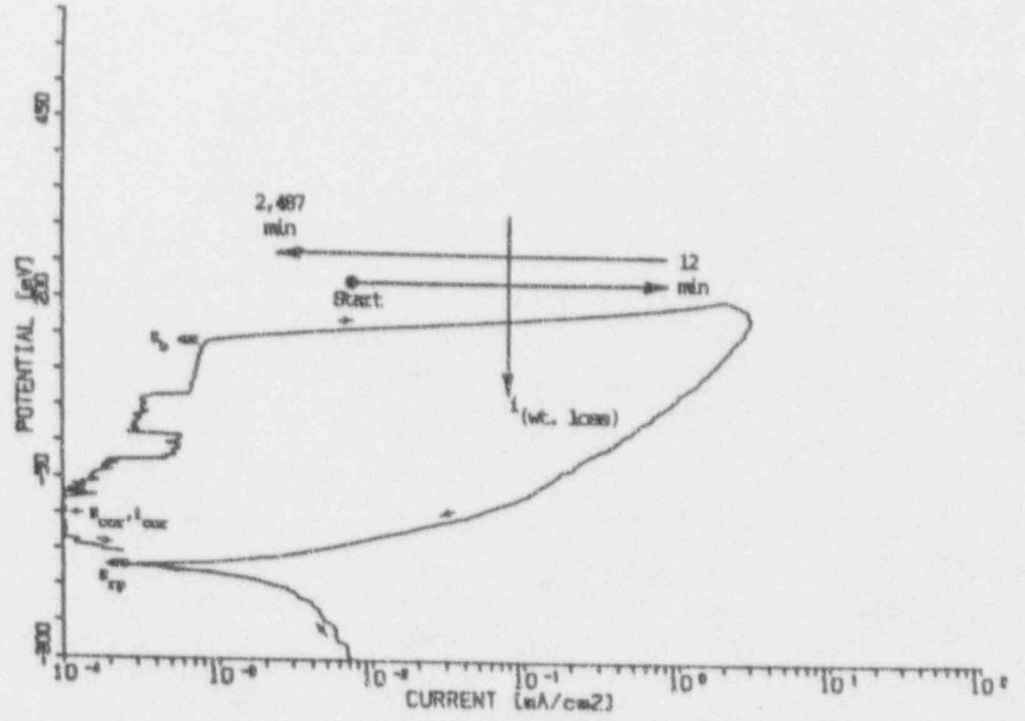

Figure C.14 Cyclic Potentiodynamic Polarization And Potentiostatic Data For Alloy CDA 715 In Test Solution No. 24 Potentiostated To +226 mV (SCE) (Few Pits, Active Attack).

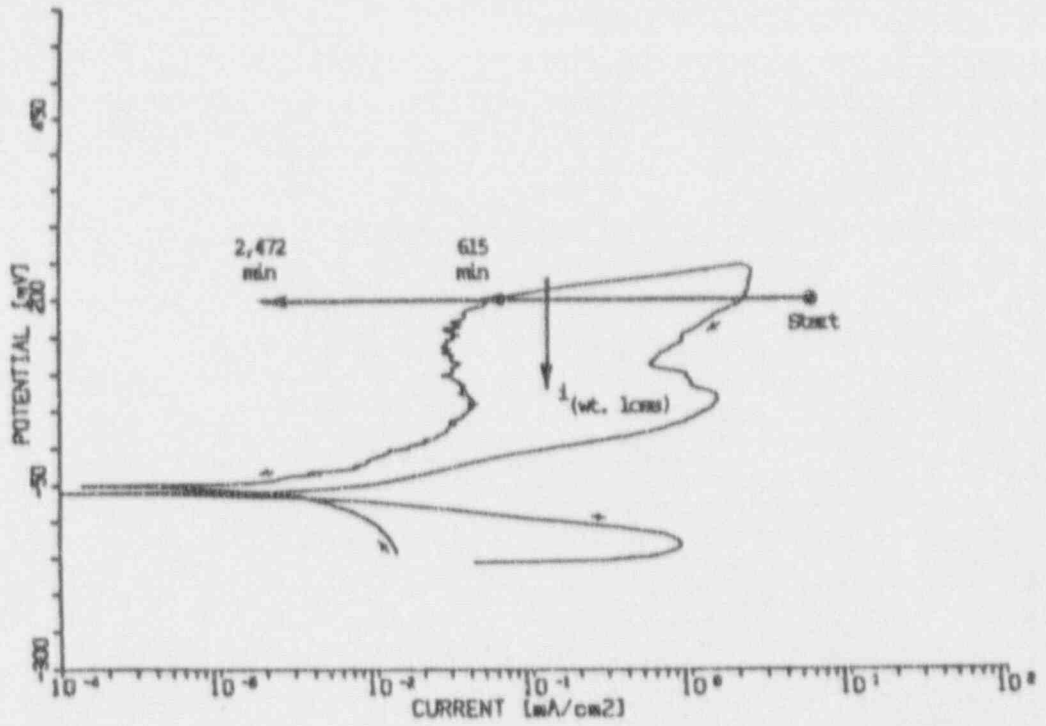

Figure C.15 Cyclic Potentiodynamic Polarization And Potentiostatic Data For Alloy CDA 715 In Test Solution No. 28 Potentiostated To +200 mV (Pitting, Active Attack).

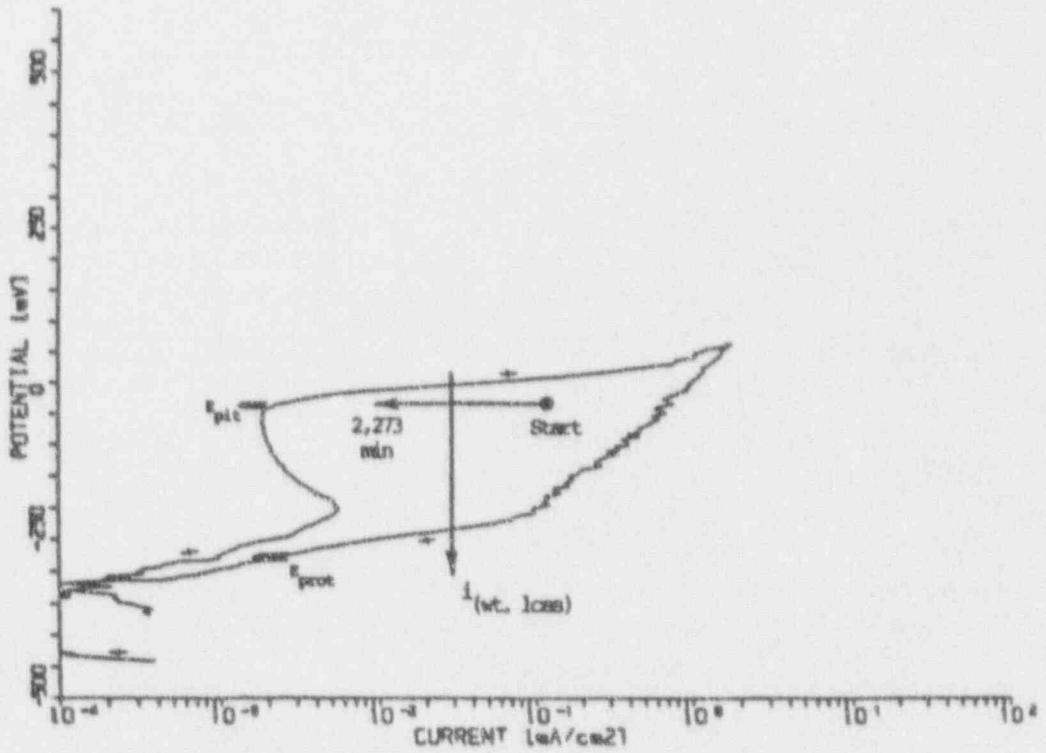

Figure C.16 Cyclic Potentiodynamic Polarization And Potentiostatic Data For Alloy CDA 715 In J-13 Well Water Containing 1000 ppm Chloride Potentiostated To -40 mV (SCE) (No Pitting, Local Active Attack).

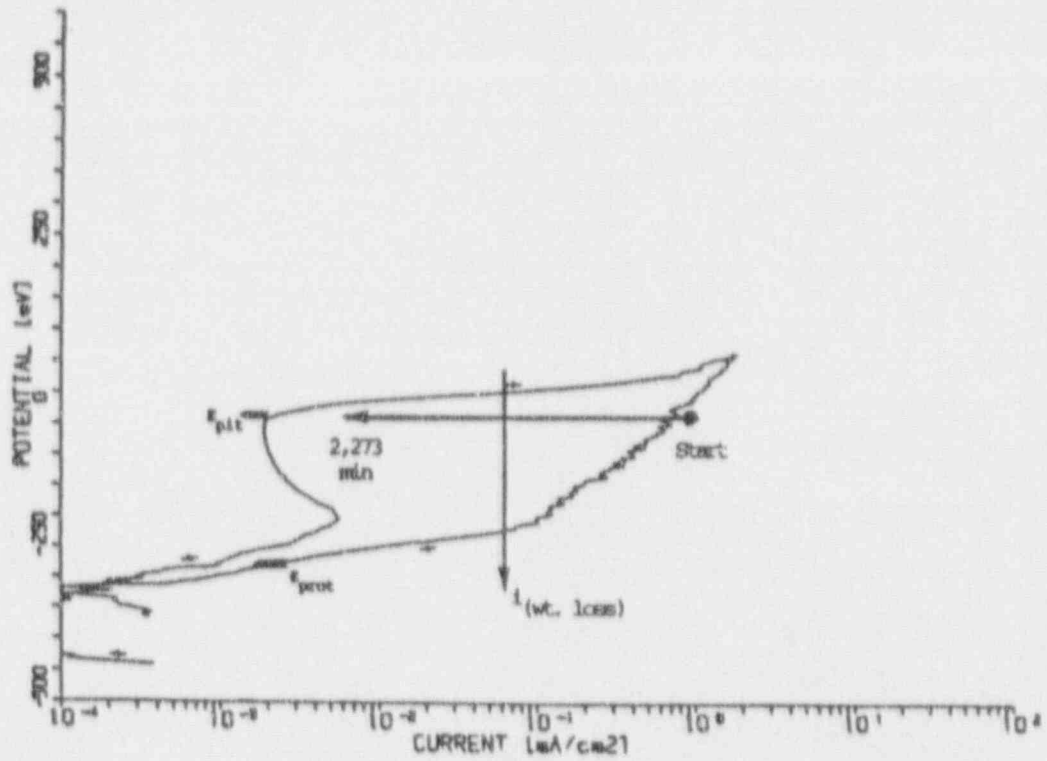

Figure C.17 Cyclic Potentiodynamic Polarization And Potentiostatic Data For Alloy CDA 715 In J-13 Well Water Containing 1000 ppm Chloride Potentiostated On the Reverse Scan To -40 mV (No Pitting, Severe Active Attack).

APPENDIX D

POTENTIOSTATIC POLARIZATION TESTING OF THE Fe-Cr-Ni ALLOYS

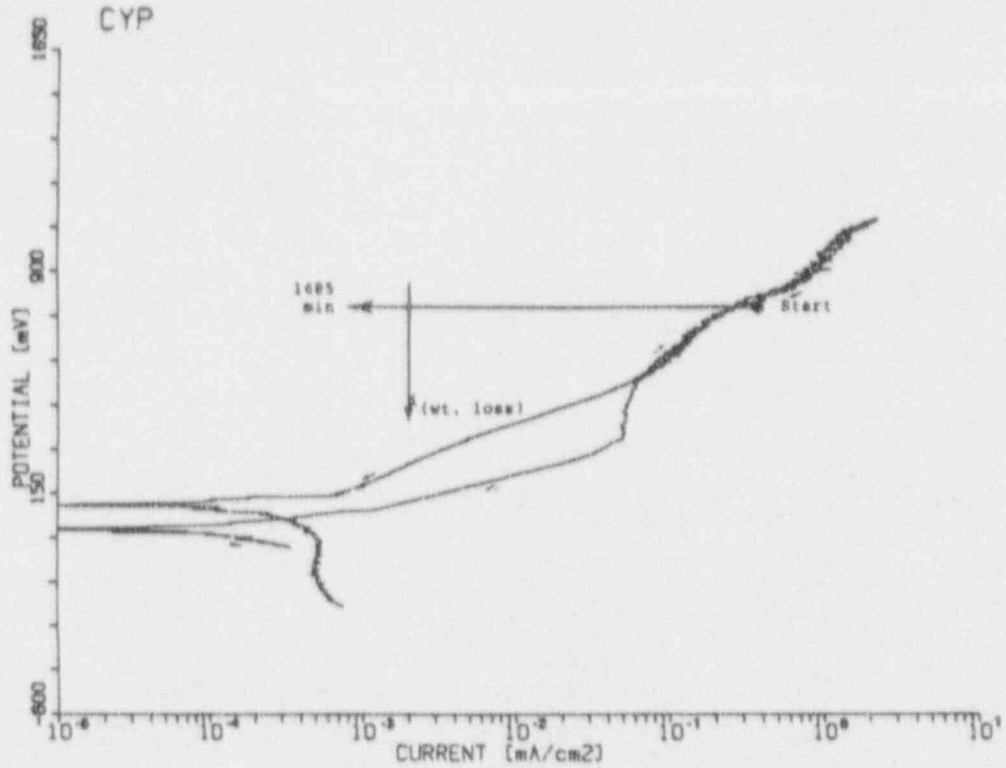

Figure D.1 Cyclic Potentiodynamic Polarization And Potentiostatic Data For Alloy 825 In Solution No. 4 At 90°C Potentiostated On The Forward Scan To +800 mV (SCE) (No Pitting, No Attack In Potentiostatic Test)

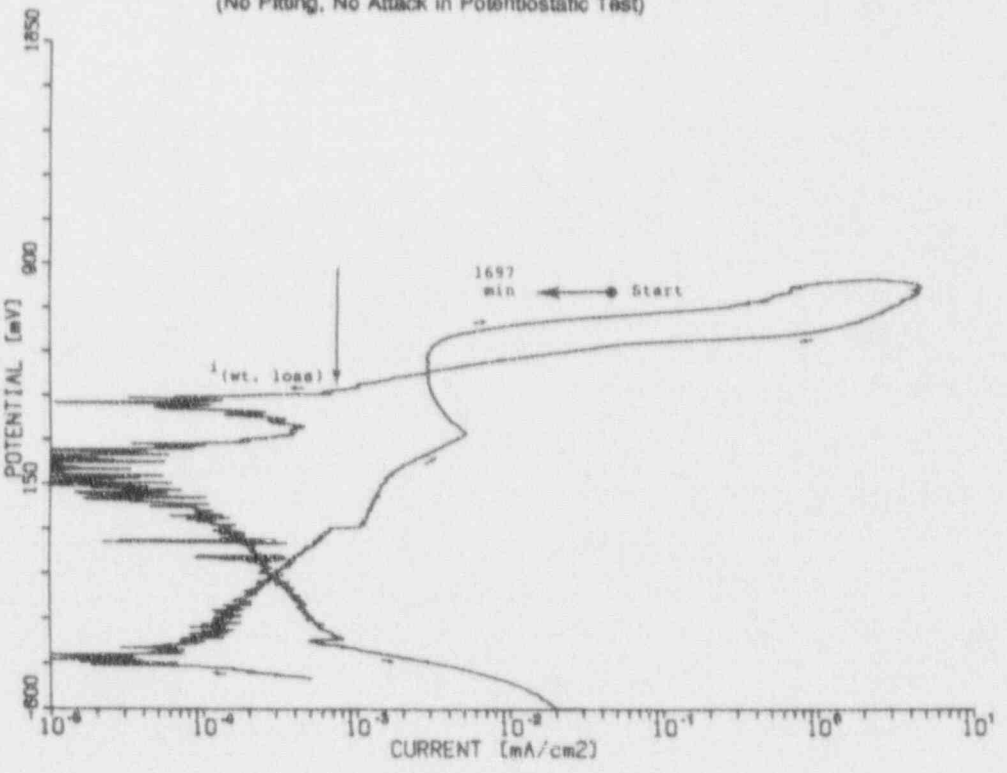

Figure D.2 Cyclic Potentiodynamic Polarization And Potentiostatic Data For Alloy 825 In Solution No. 6 At 90°C Potentiostated On The Forward Scan To +800 mV (SCE) (Crevice Attack In Potentiostatic Test)

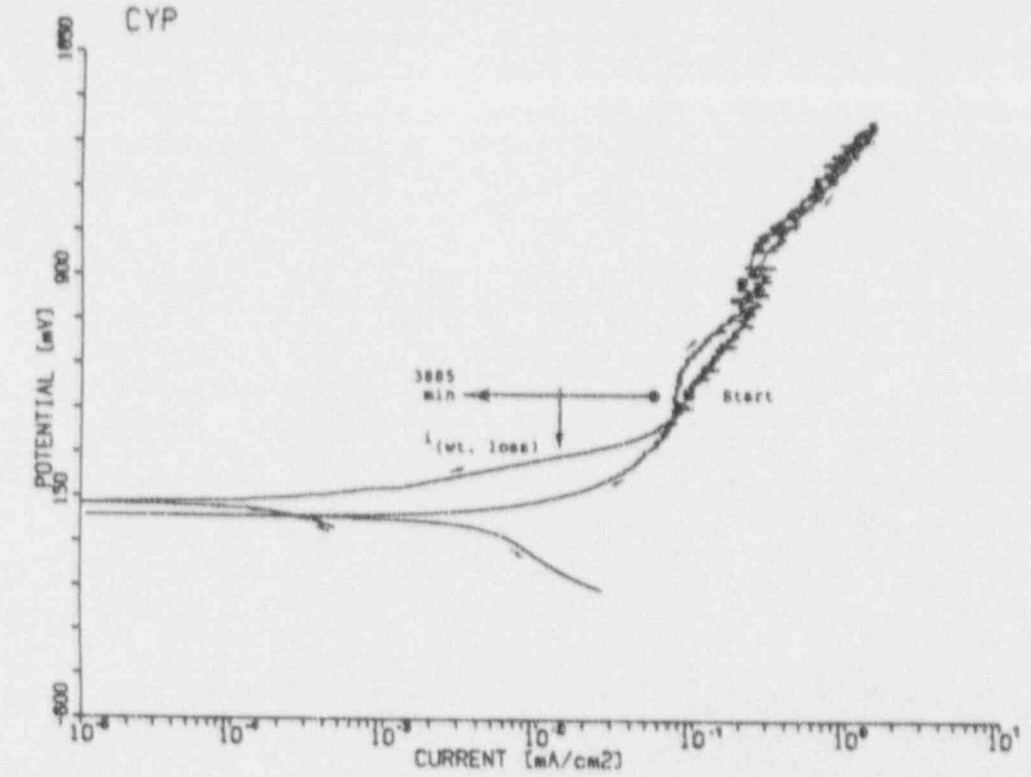

Figure D.3 Cyclic Potentiodynamic Polarization And Potentiostatic Data For Alloy 825 In Solution No. 18 At 90°C Potentiostated On The Forward Scan To +500 mV (SCE) (No Pitting, No Attack In Potentiostatic Test)

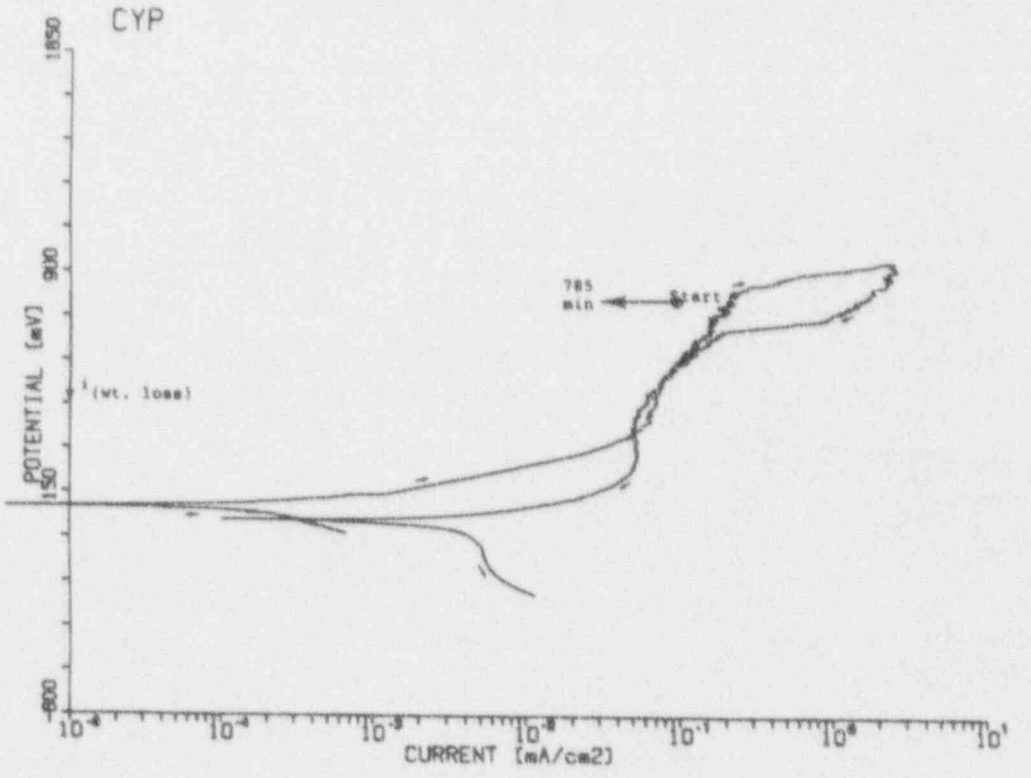

Figure D.4 Cyclic Potentiodynamic Polarization And Potentiostatic Data For Alloy 825 In Test Solution No. 34 At 70°C Potentiostated On The Forward Scan To +800 mV (SCE) (Slight Attack At Crevice In Potentiostatic Test)

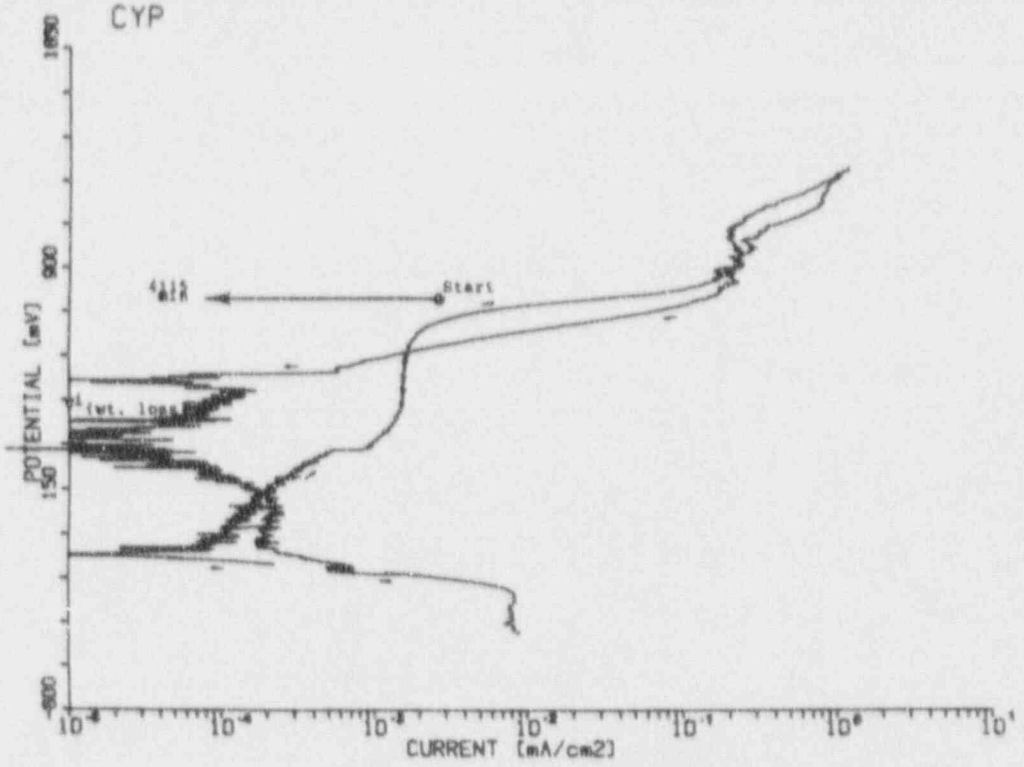

Figure D.5 Cyclic Potentiodynamic Polarization And Potentiostatic Data For Alloy 304L In Solution No. 2 At 50°C Potentiostated On The Forward Scan To +798 mV (SCE) (No Pitting), Slight Tarnishing In Cyclic Potentiodynamic Test)

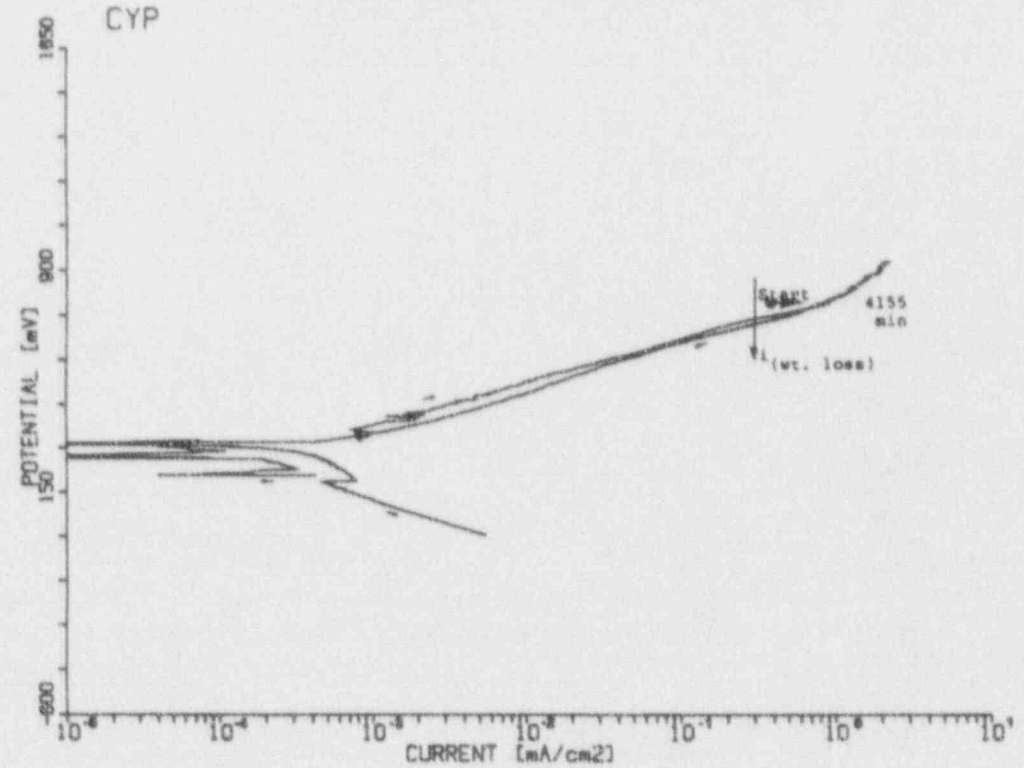

Figure D.6 Cyclic Potentiodynamic Polarization And Potentiostatic Data For Alloy 304L In Solution No. 5 At 50°C Potentiostated On The Forward Scan To +800 mV (SCE) (Severe General Attack In Potentiostatic Test)

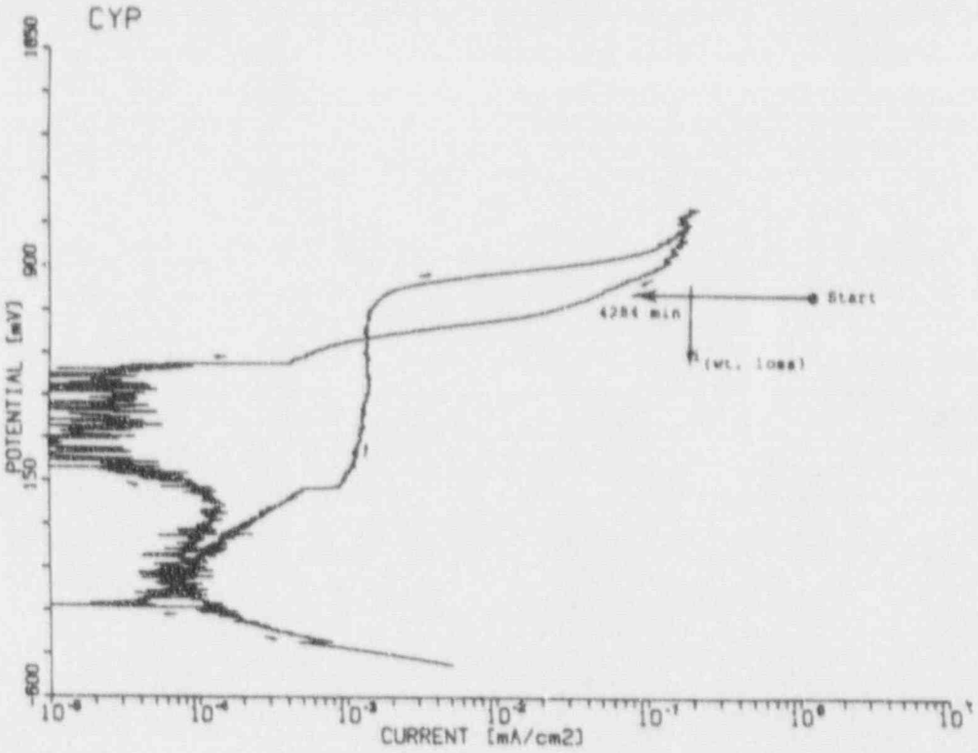

Figure D.7 Cyclic Potentiodynamic Polarization And Potentiostatic Data For Alloy 304L In Solution No. 15 At 50°C Potentiostated On The Reverse Scan To +800 mV (SCE) (Severe Pitting And Crevice Attack In Potentiostatic Test)

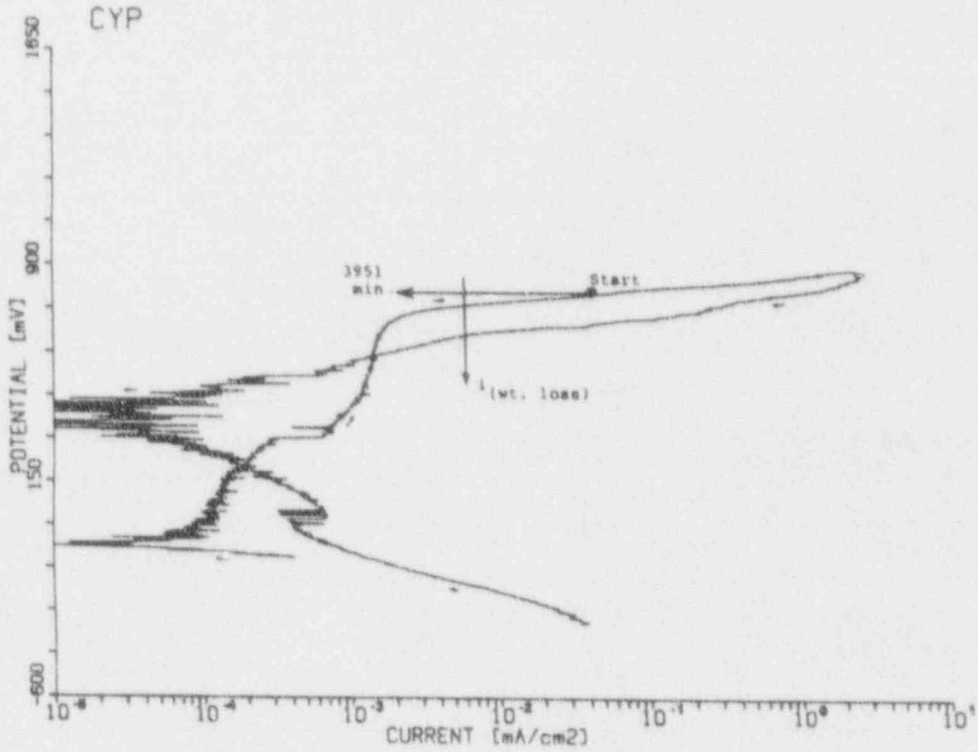

Figure D.8 Cyclic Potentiodynamic Polarization And Potentiostatic Data For Alloy 304L In Solution No. 24 At 90°C Potentiostated On The Forward Scan To +800 mV (SCE) (No Pitting, No Attack in Potentiostatic Test)

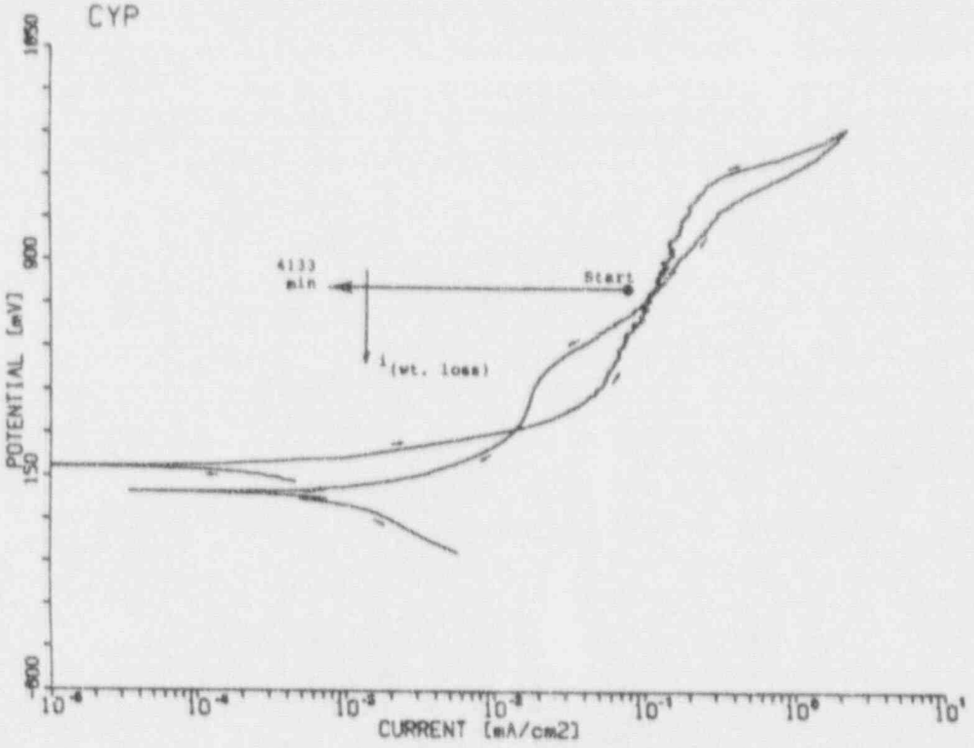

Figure D.9 Cyclic Potentiodynamic Polartzation And Potentiostatic Data For Alloy 304L In Solution No. 27 At 50°C Potentiostated On The Forward Scan To +800 mV (SCE) (No Pitting, No Attack In Potentiostatic Test)

APPENDIX E

POLARIZATION CURVES FOR ALLOY-ENVIRONMENT SYSTEMS USED IN GALVANIC-CORROSION STUDIES

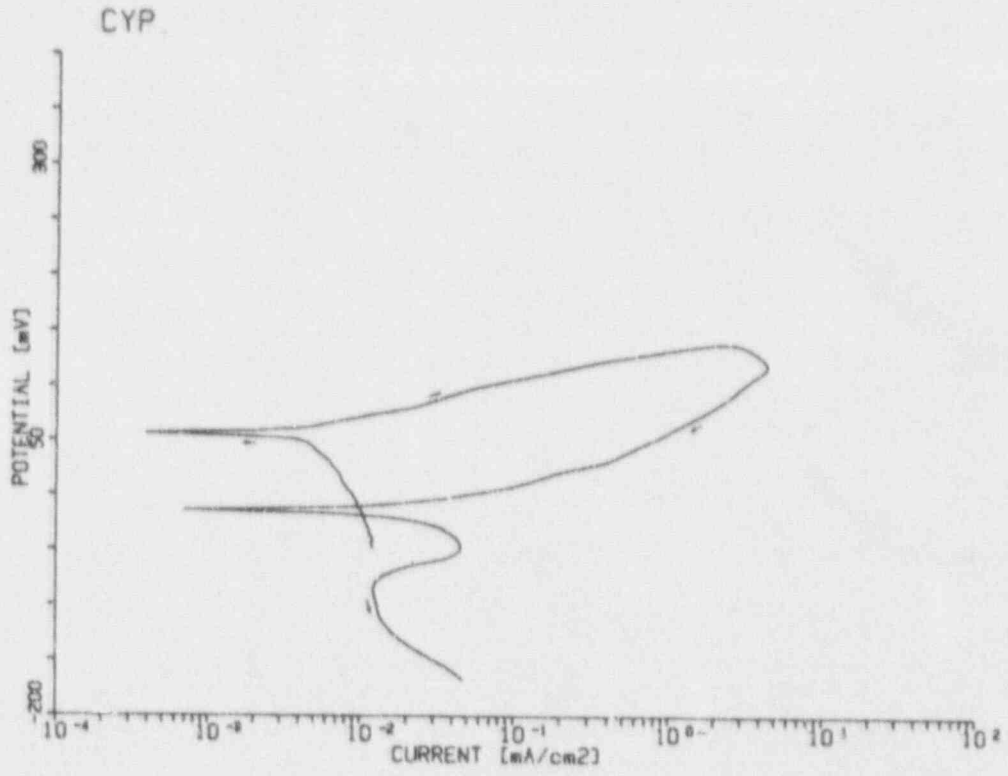

Figure E.1 Cyclic Potentiodynamic Polarization Curve For Alloy CDA 102 In Test Solution No. 22 At 50°C.

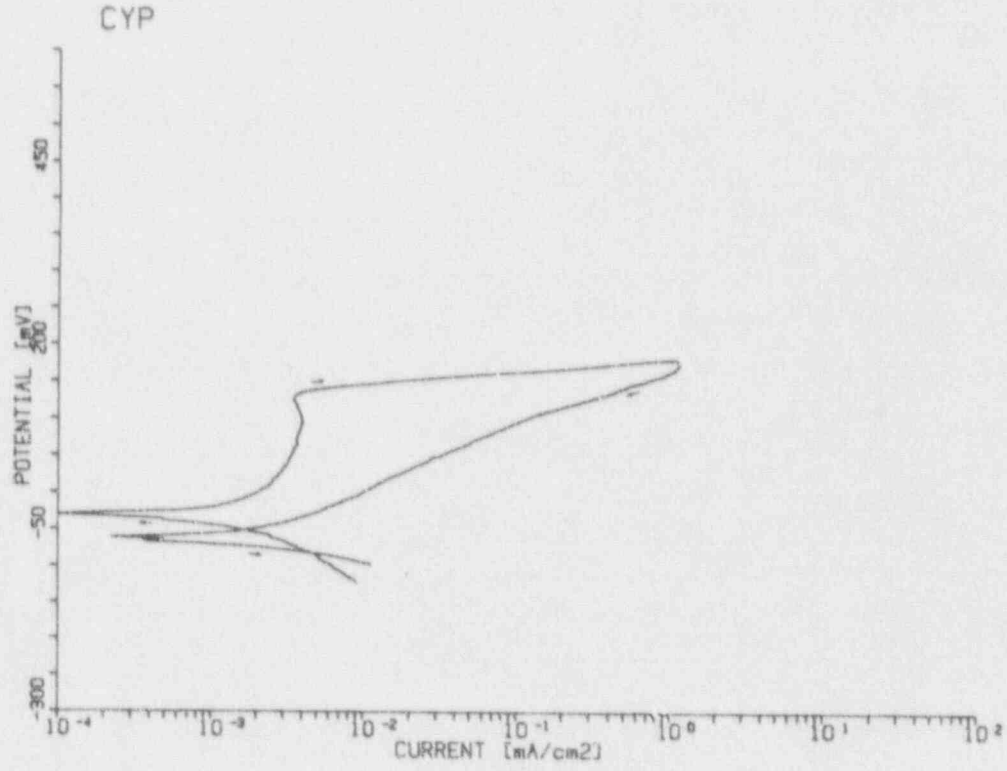

Figure E.2 Cyclic Potentiodynamic Polarization Curve For Alloy CDA 102 In Simulated J-13 Well Water At 90°C.

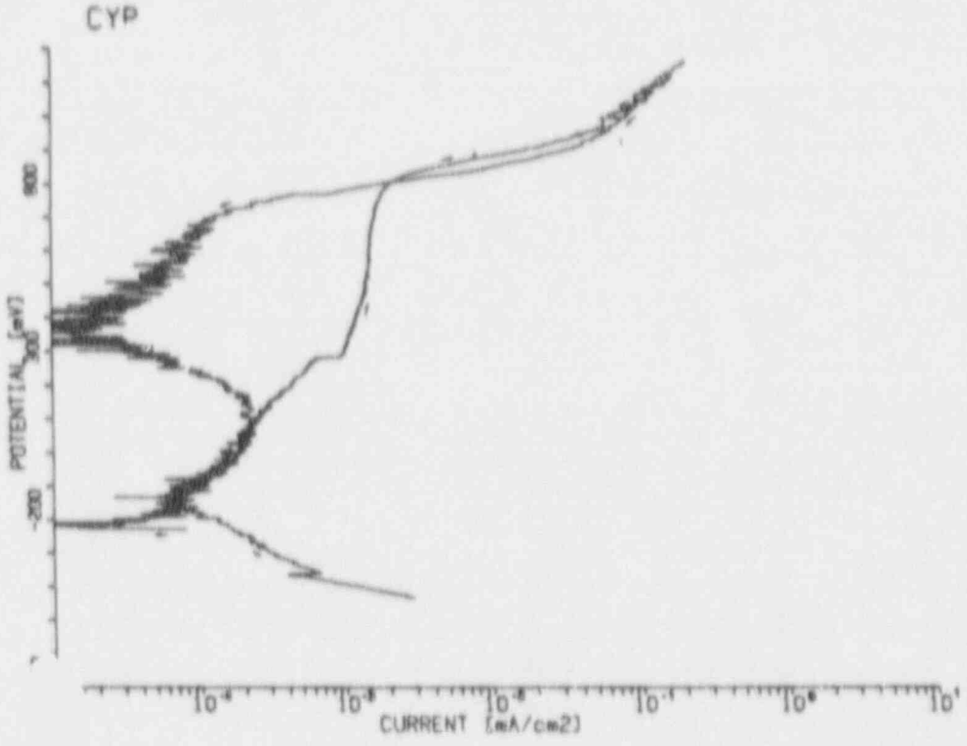

Figure E.3 Cyclic Potentiodynamic Polarization Curve For Alloy 304L in Simulated J-13 Well Water At 90°C.

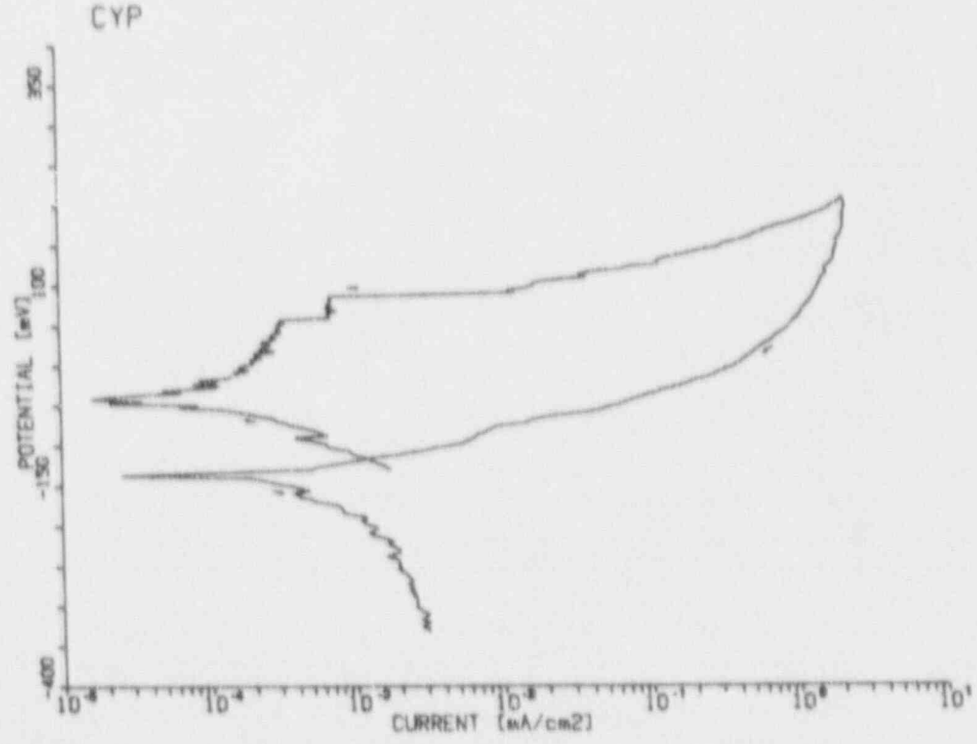

Figure E.4 Cyclic Potentiodynamic Polarization Curve For Alloy 304L in Test Solution No. 7 At 90°C.

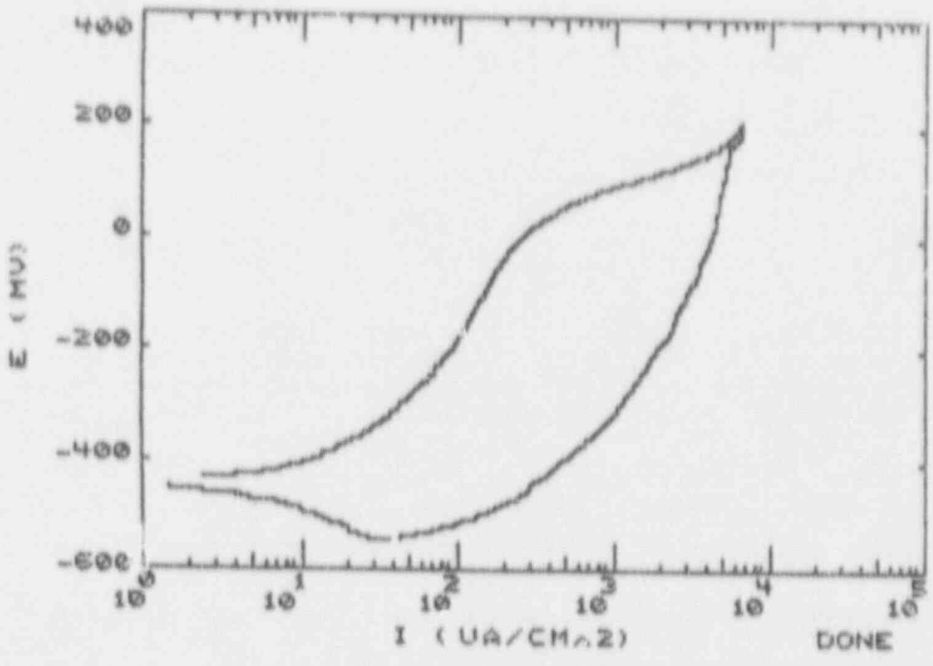

Figure E.5 Cyclic Potentiodynamic Polarization Curve For C1018 Carbon Steel In Simulated J-13 Well Water At 90°C.

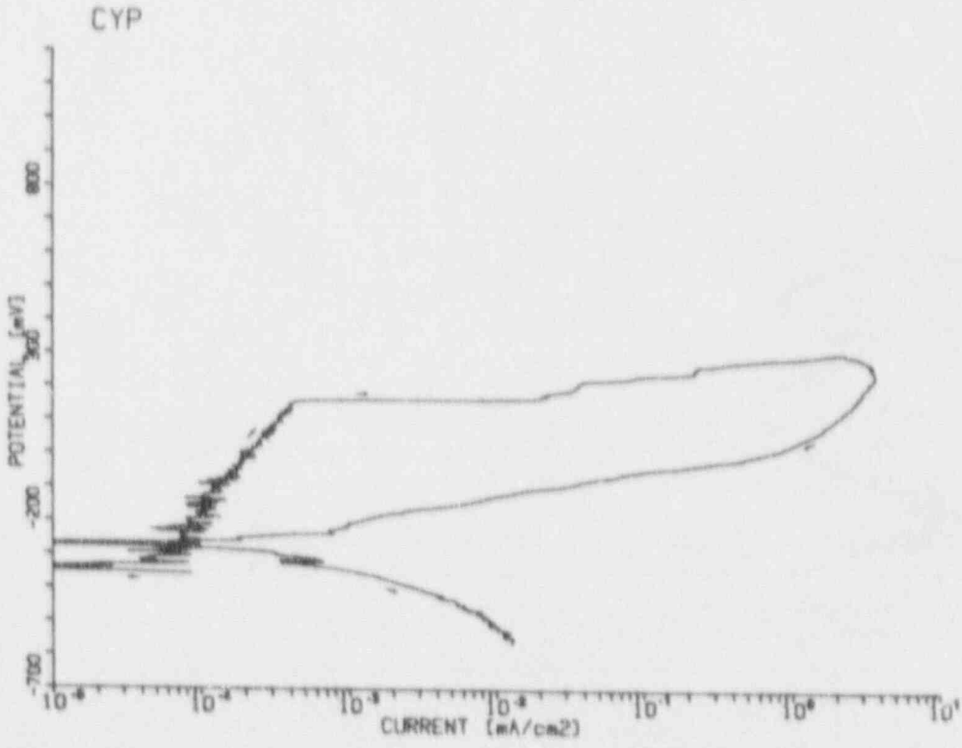

Figure E.6 Cyclic Potentiodynamic Polarization Curve For Alloy 304L In 90°C Simulated J-13 Well Water Containing 1000 ppm Chloride As Sodium Chloride.

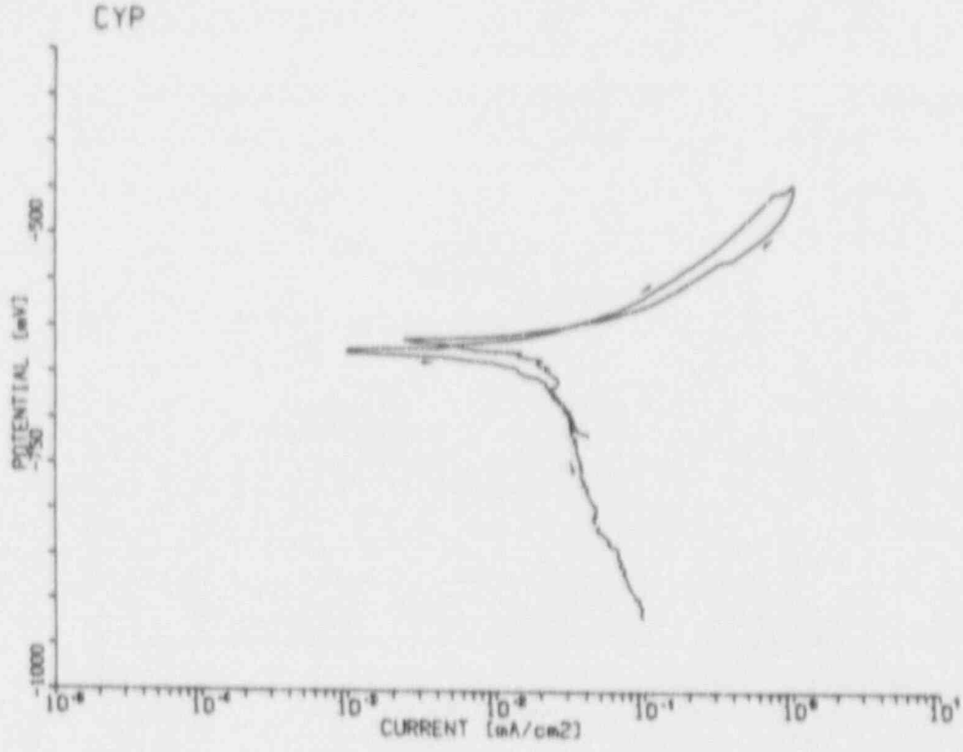

Figure E.7 Cyclic Potentiodynamic Polarization Curve For C1018 Carbon Steel In 90°C Simulated J-13 Well Water Containing 1000 ppm Chloride As Sodium Chloride.

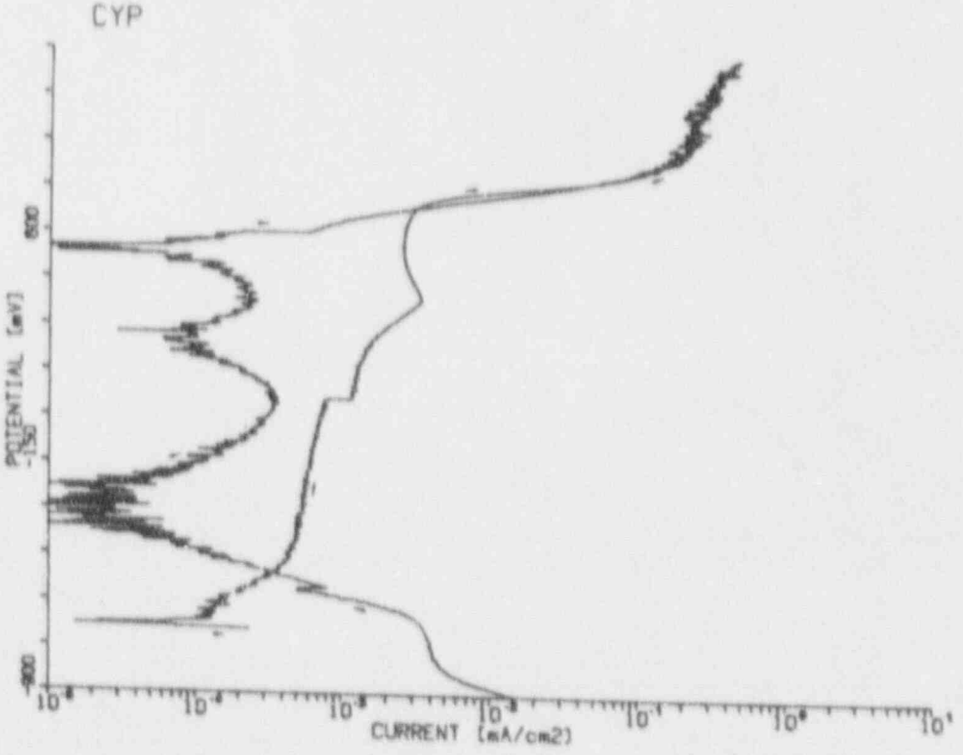

Figure E.8 Cyclic Potentiodynamic Polarization Curve For Alloy 825 In Simulated J-13 Well Water At 90°C.

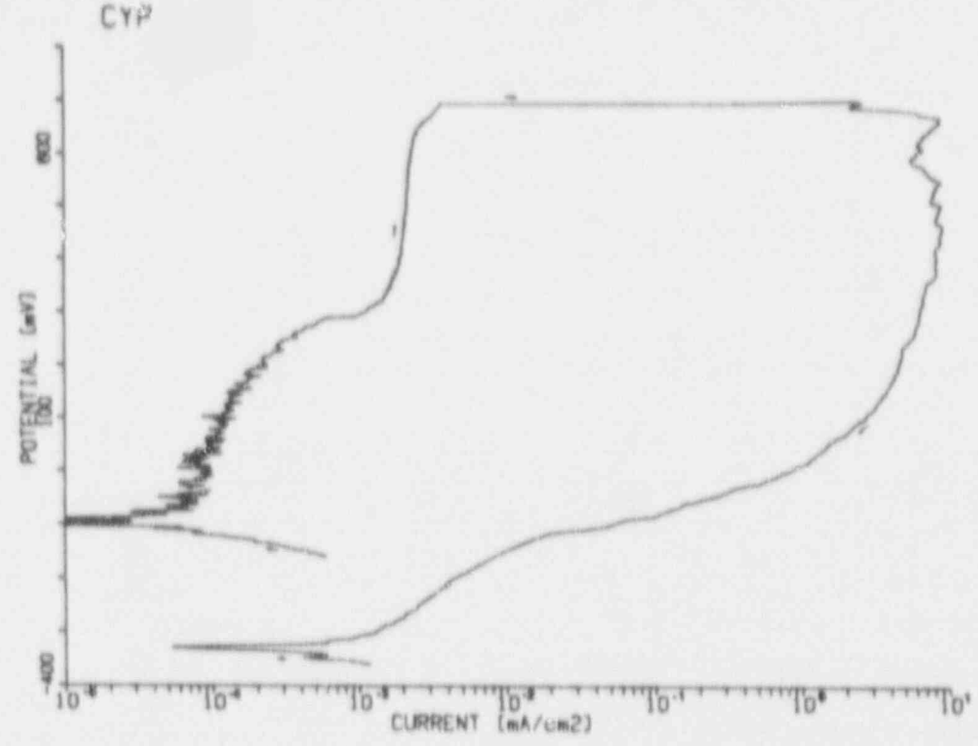

Figure E.9 Cyclic Potentiodynamic Polarization Curve For Alloy 304L In Test Solution No. 10 At 90°C.

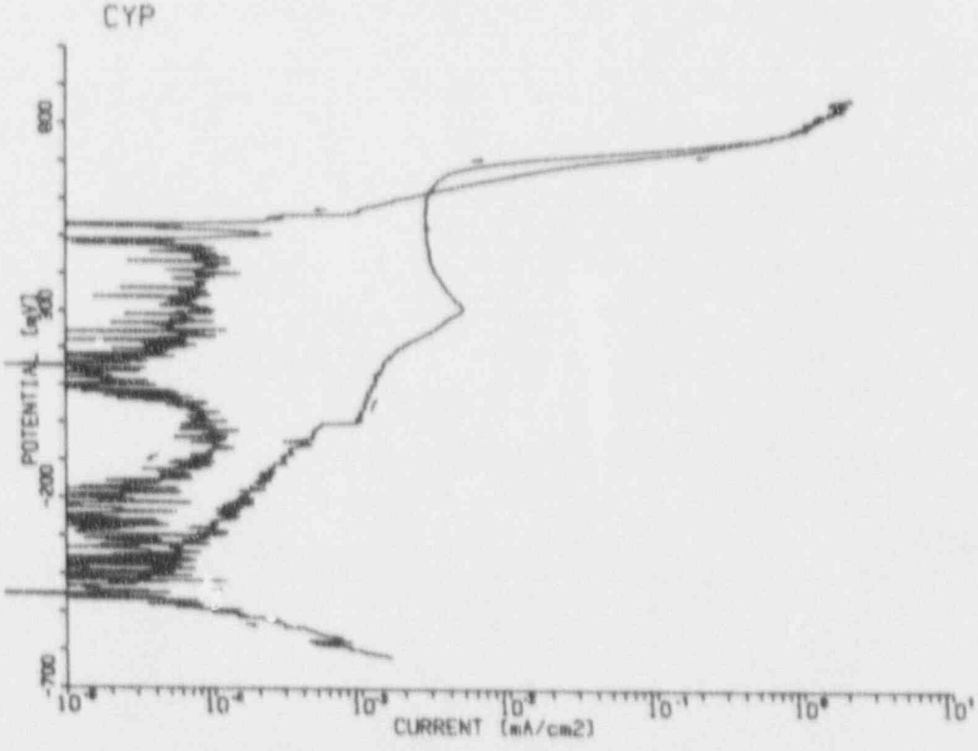

Figure E.10 Cyclic Potentiodynamic Polarization Curve For Alloy 825 In Test Solution No. 10 At 90°C.

APPENDIX F

POLARIZATION CURVES FOR ALLOY-ENVIRONMENT SYSTEMS USED IN THE LONG-TERM STUDIES

Table F.1 Comparison Of Polarization Parameters For Alloy 304L In 90°C Simulated J-13 Well Water Containing Various Types And Concentrations Of Salt.

Chloride Concentration ppm	Chloride Type	E_{cor} V, SCE	I_{cor} μA/cm²	E_{pp} V, SCE	E_{prot} V, SCE	Comments
1 000	NaCl	-.231	0.11	+0.300	-0.059	Pitting, iridescent film, and and crevice attack.
10 000	NaCl	-.241	0.13	+0.163	-0.122	Pitting, iridescent film, and crevice attack.
100 000	NaCl	-.224	0.20	-0.224	-0.330	Pitting and crevice attack.
10 000	$CaCl_2$	-.163	0.05	+0.026	-0.140	Pitting and crevice attack.

Table F.2 Comparison Of Polarization Parameters For Alloy 825 In 90°C Simulated J-13 Well Water Containing Various Concentrations Of Salt.

Chloride Concentration ppm	Chloride Type	E_{cor} V, SCE	I_{cor} µA/cm²	E_{pp} V, SCE	E_{prot} V, SCE	Comments
1 000	NaCl	+0.083	0.30	+0.355	-0.190	Iridescent oxide, pitting and etching, crevice attack.
10 000	NaCl	-0.041	0.60	+0.205	-0.068	Iridescent oxide, pitting and crevice attack.
100 000	NaCl	-0.300	0.10	-0.044	-0.250	Pitting and crevice attack.
10 000	$CaCl_2$	-0.241	0.12	+0.242	-0.150	Pitting and crevice attack.

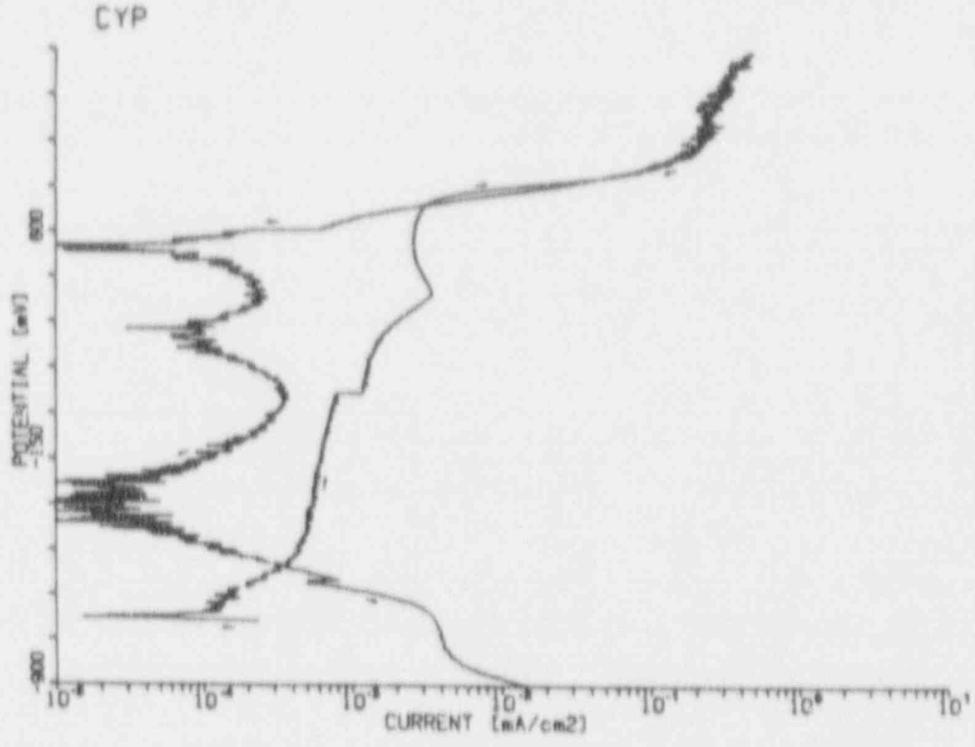

Figure F.1 Cyclic Potentiodynamic Polarization Curve For Alloy 825 In Simulated J-13 Well Water At 90°C.

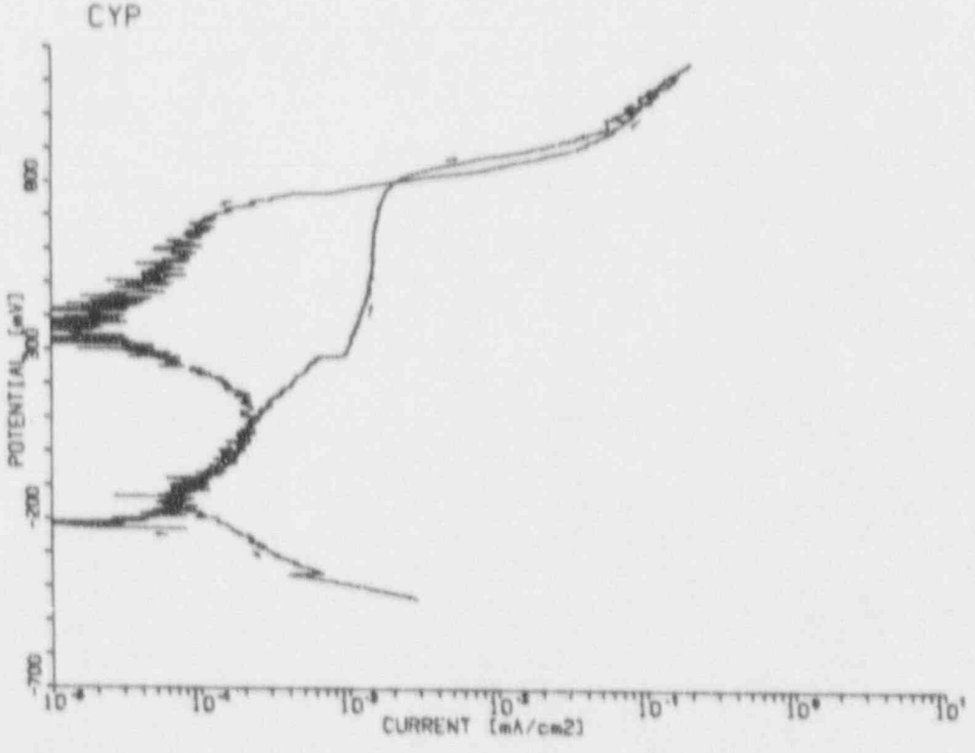

Figure F.2 Cyclic Potentiodynamic Polarization Curve For Alloy 304L In Simulated J-13 Well Water At 90°C.

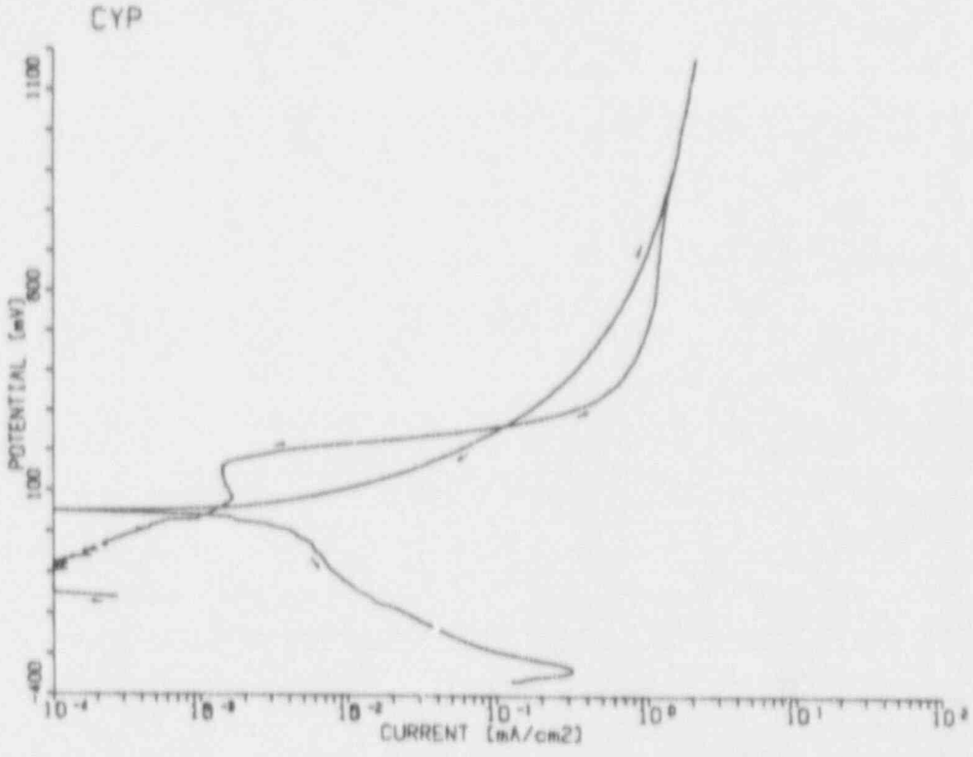

Figure F.3 Cyclic Potentiodynamic Polarization Curve For Alloy CDA 715 In Simulated J-13 Well Water At 90°C.

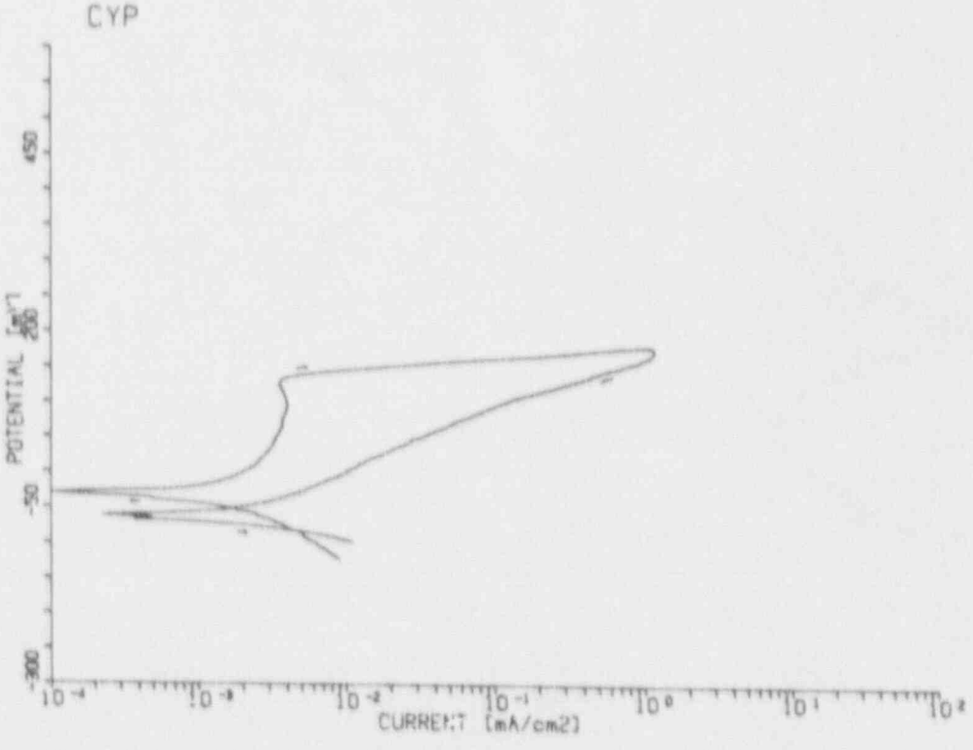

Figure F.4 Cyclic Potentiodynamic Polarization Curve For Alloy CDA 102 In Simulated J-13 Well Water At 90°C.

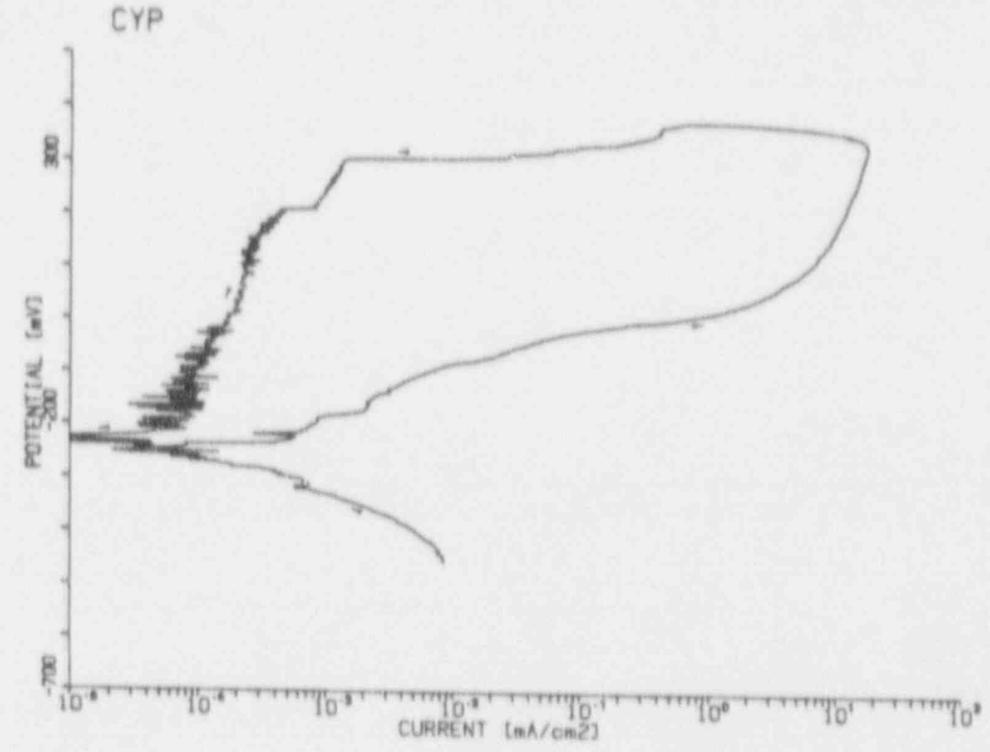

Figure F.5 Cyclic Potentiodynamic Polarization Curve For Alloy 304L In 90°C Simulated J-13 Well Water Containing 1000 ppm Chlorides As NaCl.

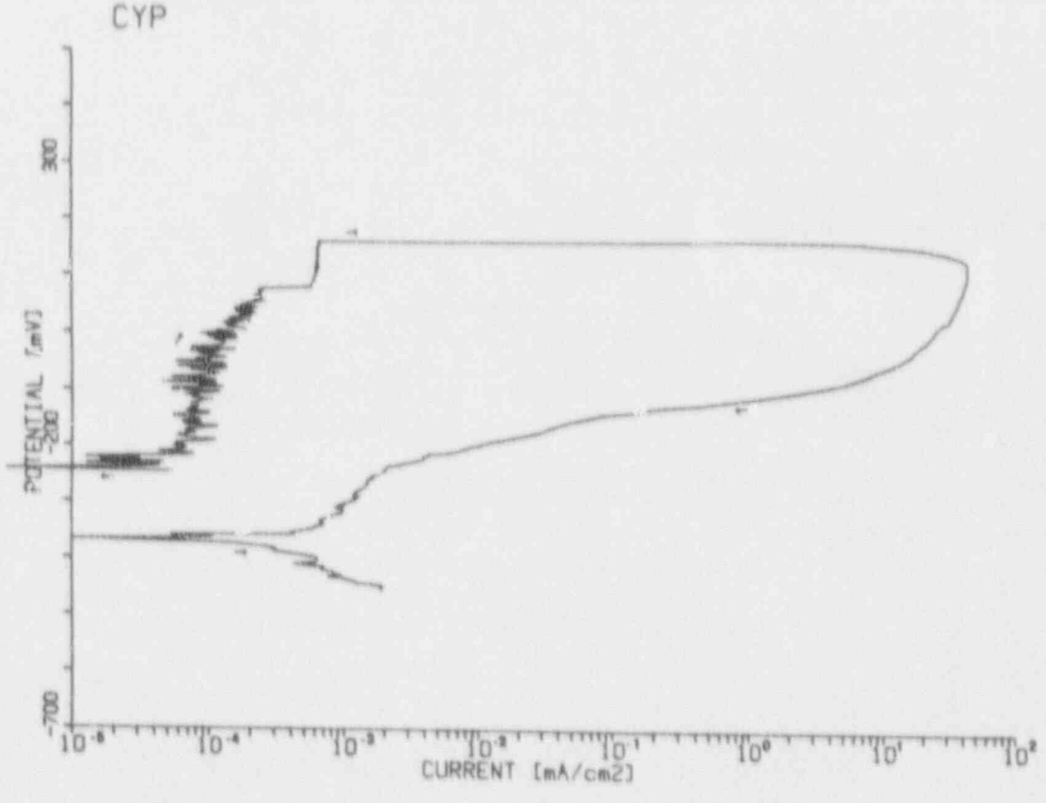

Figure F.6 Cyclic Potentiodynamic Polarization Curve For Alloy 304L In 90°C Simulated J-13 Well Water Containing 10 000 ppm Chlorides As NaCl.

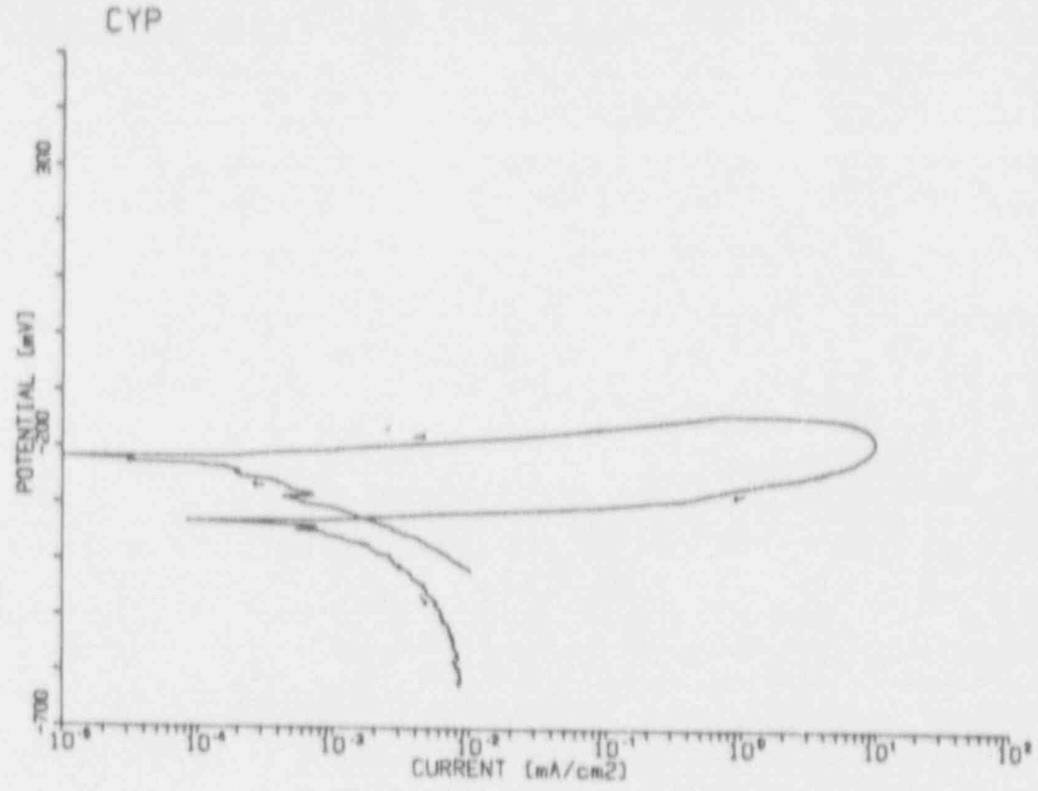

Figure F.7 Cyclic Potentiodynamic Polarization Curve For Alloy 304L In 90°C Simulated J-13 Well Water Containing 100 000 ppm Chlorides As NaCl.

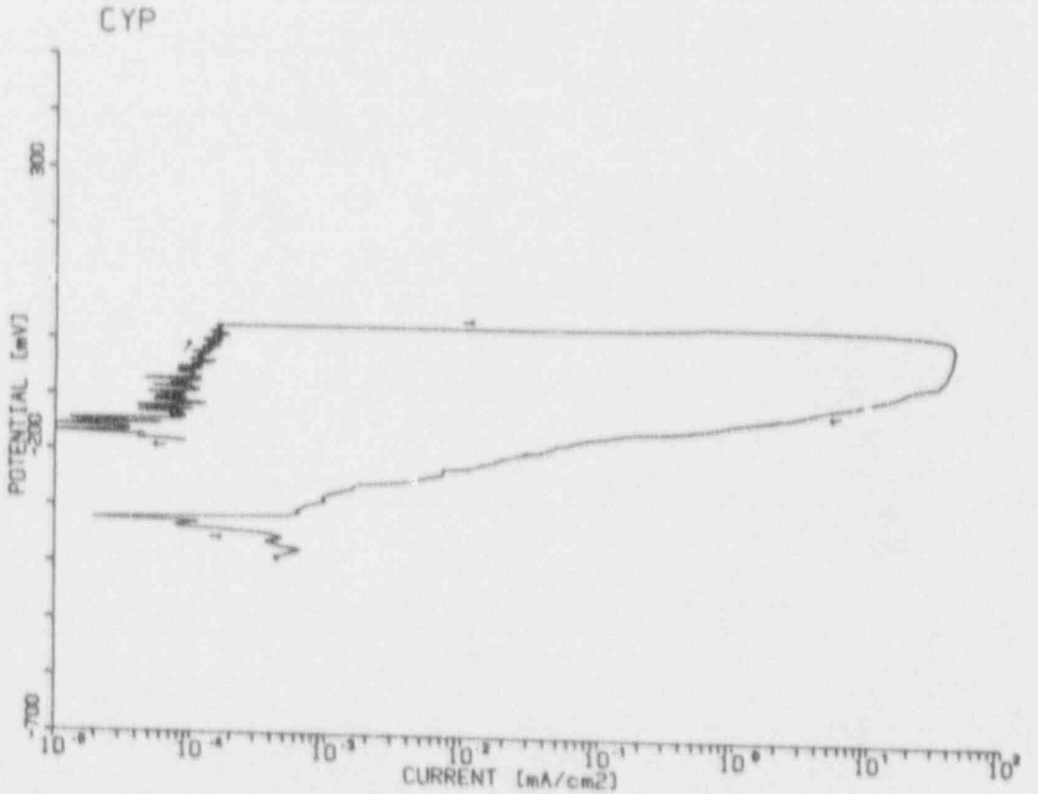

Figure F.8 Cyclic Potentiodynamic Polarization Curve For Alloy 304L In 90°C Simulated J-13 Well Water Containing 10 000 ppm Chlorides As $CaCl_2$

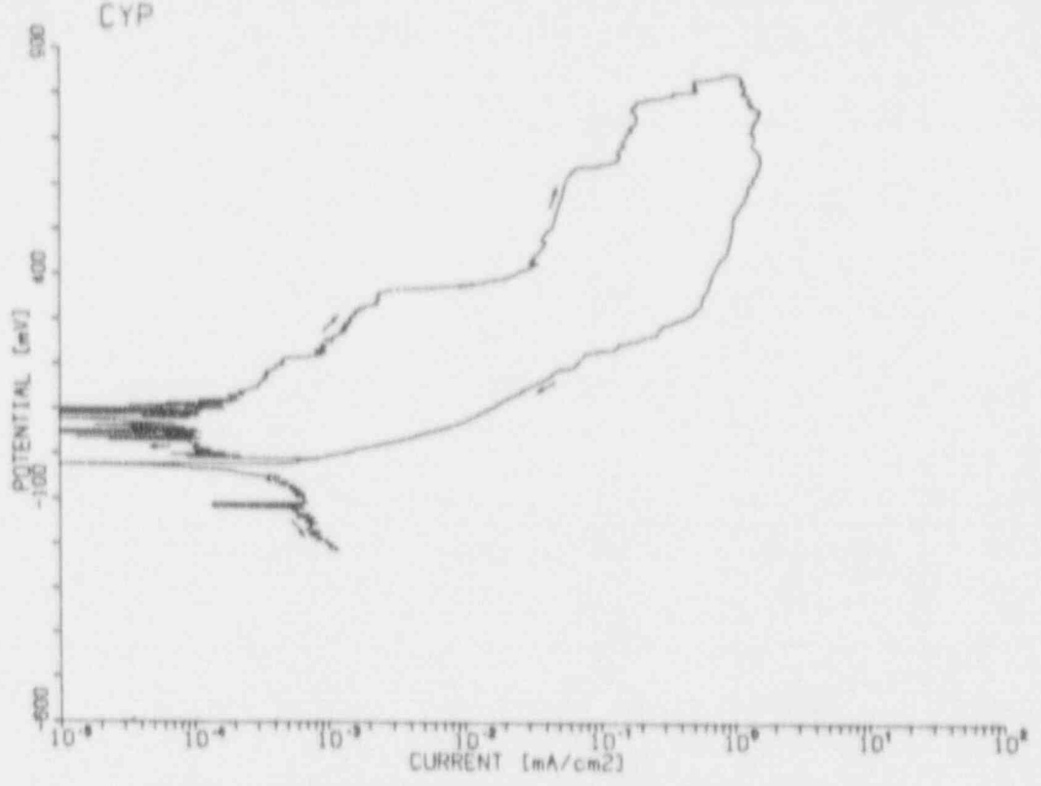

Figure F.9 Cyclic Potentiodynamic Polarization Curve For Alloy 825 In 90°C Simulated J-13 Well Water Containing 1000 ppm Chlorides As NaCl.

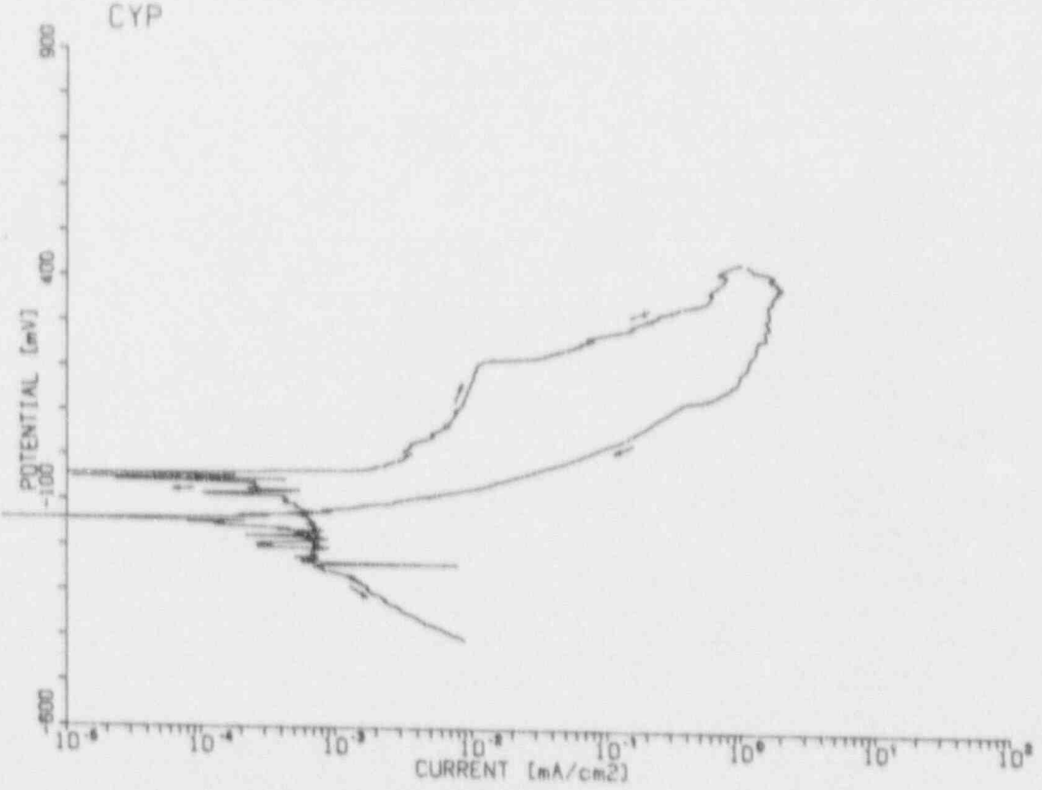

Figure F.10 Cyclic Potentiodynamic Polarization Curve For Alloy 825 In 90°C Simulated J-13 Well Water Containing 10 000 ppm Chlorides As NaCl.

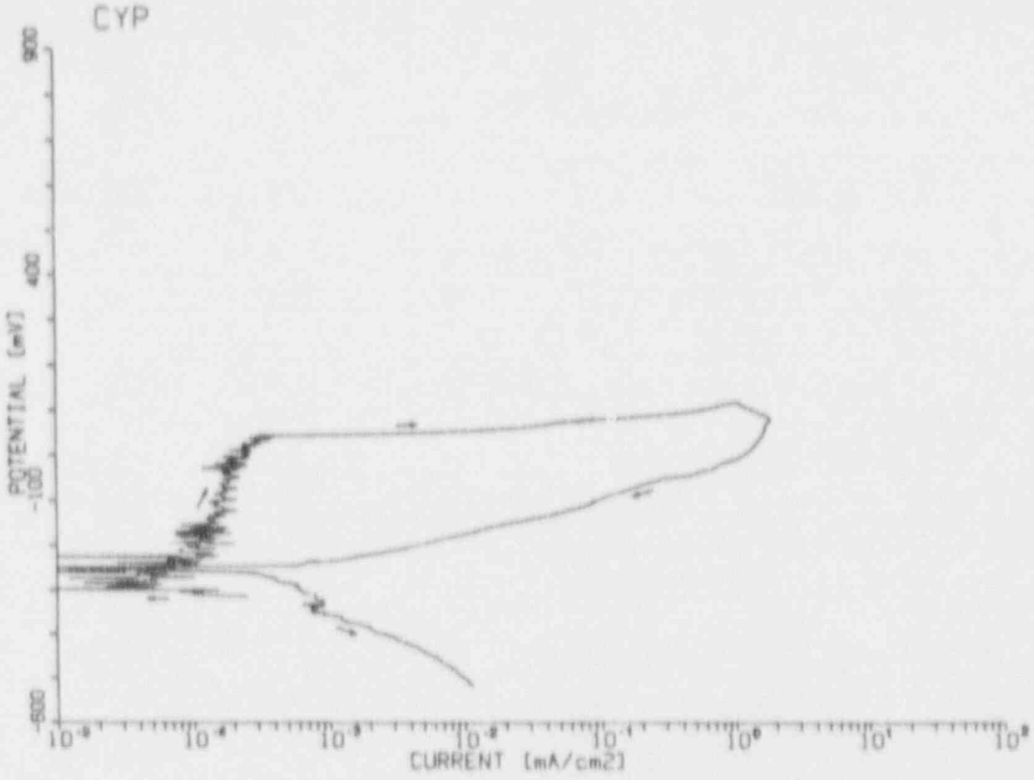

Figure F.11 Cyclic Potentiodynamic Polarization Curve For Alloy 825 In 90°C Simulated J-13 Well Water Containing 100 000 ppm Chlorides As NaCl.

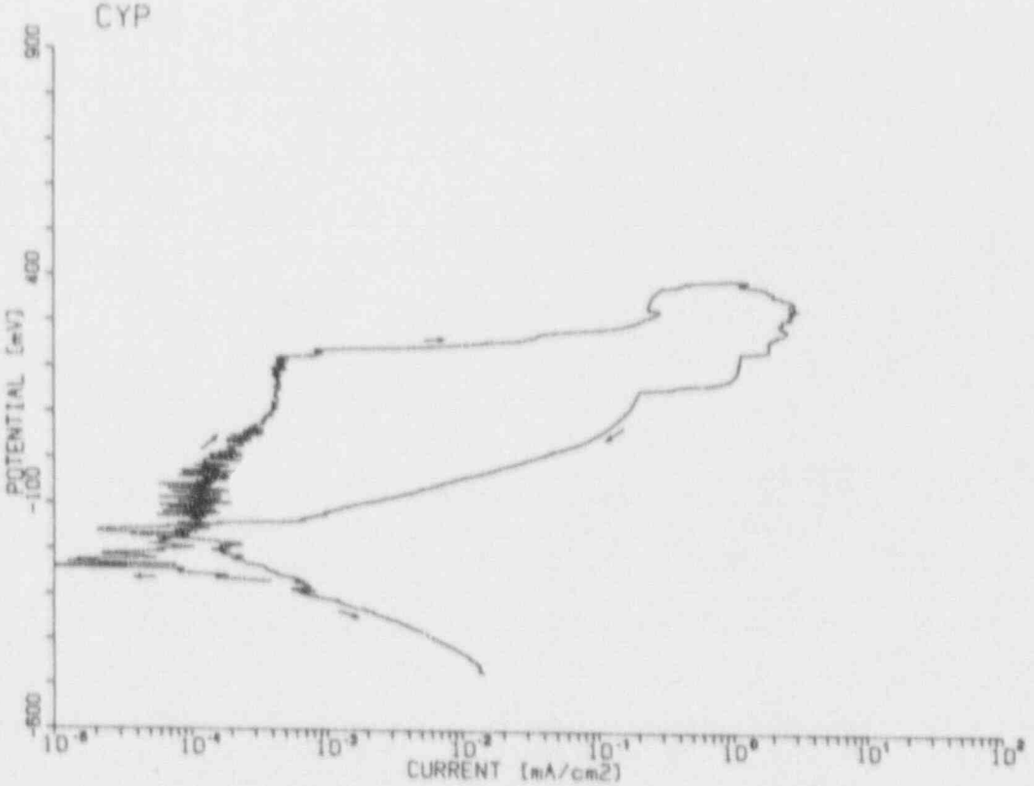

Figure F.12 Cyclic Potentiodynamic Polarization Curve For Alloy 825 In 90°C Simulated J-13 Well Water Containing 10 000 ppm Chlorides As $CaCl_2$

APPENDIX G

CANDIDATE ALLOY COMPOSITIONS

Table G.1 Candidate Alloy Compositions Of Specimens Used For The Pit-Initiation Studies.

ELEMENT	CDA 102	CDA 715	I825	304L
Cu	99.99%	67.17%	1.90%	0.190%
Ni	—	31.78%	43.98%	8.87%
Fe	—	0.46%	26.90%	Balance
Cr	—	—	22.70%	18.22%
Mo	—	—	2.92%	0.170%
Mn	—	0.01%	0.37%	1.21%
C	—	<0.01%	0.02%	0.021%
S	—	<0.01%	0.004%	0.023%
Zn	—	0.01%	—	—
P	—	<0.01%	—	0.026%
Pb	—	<0.01%	—	—
Si	—	—	0.08%	0.520%
Al	—	—	0.06%	—
Ti	—	—	1.07%	—
Co	—	—	—	—
N	—	—	—	0.066%

Table G.2 Candidate Alloy Compositions Of Specimens Used For The Pit-Propagation Studies.

ELEMENT	CDA 102
Cu	99.99%
Ni	—
Fe	—
Cr	—
Mo	—
Mn	—
C	—
S	—
Zn	<1 ppm
P	2 ppm
Pb	4 ppm
Si	—
Al	—
Ti	—
Co	--
N	—

Table G.3 Candidate Alloy Compositions Of Specimens Used For The Thermogalvanic-Couples Experiments.

ELEMENT	CDA 102	304L
Cu	99.99%	0.41%
Ni	—	9.21%
Fe	—	Balance
Cr	—	18.51%
Mo	—	0.30%
Mn	—	1.45%
C	—	0.017%
S	—	0.004%
Zn	<1 ppm	—
P	1 ppm	0.026%
Pb	2 ppm	—
Si	—	0.68%
Al	—	—
Ti	—	—
Co	—	—
N	—	0.034%

Table G.4 Candidate Alloy Compositions Of Specimens Used For The Borehole Liner-Container Interaction Studies.

ELEMENT	C1010	I825	304L
Cu	—	1.71%	0.33%
Ni	—	42.03%	8.86%
Fe	Balance	29.84%	Balance
Cr	—	21.96%	18.18%
Mo	—	3.17%	0.24%
Mn	0.38%	0.41%	1.68%
C	0.08%	0.01%	0.03%
S	0.012%	<0.001%	0.018%
Zn	—	—	—
P	0.022%	—	0.026%
Pb	—	—	—
Si	—	0.17%	0.54%
Al	—	0.05%	—
Ti	—	0.65%	—
Co	—	—	0.15%
N	—	—	0.066%

Table G.5 Candidate Alloy Compositions Of Specimens Used For The Long-Term Boil-Down Tests.

Element	CDA 102		CDA 715		I825		304L	
	Coupons	U-Bends	Coupons	U-Bends	Coupons	U-Bends	Coupons	U-Bends
Cu	99.99	99.95	68.55	Balance	1.97	1.71	0.33	0.47
Ni	—	—	30.00	29.42	44.83	42.20	8.86	9.44
Fe	—	—	0.548	0.60	26.98	29.06	Balance	Balance
Cr	—	—	—	—	21.93	22.56	18.18	18.27
Mo	—	—	—	—	2.73	2.74	0.24	0.10
Mn	—	—	0.617	0.6	0.45	0.51	1.68	1.39
C	—	—	0.035	0.015	0 02	0.02	0.03	0.020
S	—	—	0.007	0.006	0.002	0.003	0.018	0.015
Zn	—	—	0.109	0.05	—	—	—	—
P	—	.0003	0.006	0.004	—	—	0.026	0.022
Pb	—	—	0.008	0.01	—	—	—	—
Si	—	—	—	—	0.31	0.33	0.54	0.54
Al	—	—	—	—	0.04	0.06	—	—
Ti	—	—	—	—	0.74	0.81	—	—
Co	—	—	—	—	—	—	0.15	0.18
N	—	—	—	—	—	—	0.066	0.023

Table G.6 Candidate Alloy Compositions Of U-Bend Specimens Used For The Long-Term SCC Tests.

ELEMENT	I825	304L
Cu	1.82	0.47
Ni	42.89	9.44
Fe	27.72	Balance
Cr	22.78	18.27
Mo	2.74	0.10
Mn	0.45	1.39
C	0.01	0.020
S	0.001	0.015
Zn	—	—
P	—	0.022
Pb	—	—
Si	0.40	0.54
Al	0.11	—
Ti	1.08	—
Co	—	0.18
N	—	0.023

NRC FORM 335 (2-89) NRCM 1102, 3201, 3202

U.S. NUCLEAR REGULATORY COMMISSION

BIBLIOGRAPHIC DATA SHEET

(See instructions on the reverse)

1. REPORT NUMBER (Assigned by NRC, Add Vol., Supp., Rev., and Addendum Numbers, If any.)

NUREG / CR-5709

2. TITLE AND SUBTITLE

Pitting, Galvanic, And Long-Term Corrosion Studies On Candidate Container Alloys For The Tuff Repository

3. DATE REPORT PUBLISHED

MONTH: January | YEAR: 1992

4. FIN OR GRANT NUMBER

FIN D1692

5. AUTHOR(S)

J. A. Beavers, N. G. Thompson, and C. L. Durr

6. TYPE OF REPORT

Technical

7. PERIOD COVERED (Inclusive Dates)

12/87 - 12/91

8. PERFORMING ORGANIZATION – NAME AND ADDRESS (If NRC, provide Division, Office or Region, U.S. Nuclear Regulatory Commission, and mailing address; if contractor, provide name and mailing address.)

Cortest Columbus Technologies, Inc.
2704 Sawbury Boulevard
Columbus, Ohio 43235

9. SPONSORING ORGANIZATION – NAME AND ADDRESS (If NRC, type "Same as above"; if contractor, provide NRC Division, Office or Region, U.S. Nuclear Regulatory Commission, and mailing address.)

Division of Regulatory Applications
Office of Nuclear Regulatory Research
U.S. Nuclear Regulatory Commission
Washington, DC 20555

10. SUPPLEMENTARY NOTES

11. ABSTRACT (200 words or less)

Cortest Columbus Technologies, Inc. (CC Technologies) investigated the long-term performance of container materials for high-level radioactive waste packages for the Tuff Repository. This report summarizes the results of Task 4 (Pitting Studies), Task 6 (Other Failure Modes) and Task 7 (Long-Term Exposures) of the program. Fe-Cr-Ni alloys (Alloy 304L and Alloy 825) and copper-base alloys (CDA 102 and CDA 715) were evaluated in a simulated J-13 well water and in solutions selected from Task 2 of the program.

Pit-initiation studies of the copper-base alloys confirmed that standard interpretations of CPP tests are not always appropriate in the presence of thick oxide layers. Hysteresis in CPP tests may not always be indicative of pitting. Pit-propagation studies with Alloy CDA 102 showed that, if pits initiate, their propagation may be limited by the concentration of oxidizing species such as hydrogen peroxide (H_2O_2).

Thermogalvanic effects on corrosion were found to be, in general, minor in comparison to the deleterious effect of increasing temperature on corrosion rate. In borehole liner-container interaction studies, performed with Alloy 304L - C1010 and Alloy 825 - Alloy 304L galvanic couples, the active member of the couple consistently experienced accelerated corrosion.

Long-term, boil-down studies showed negligible general corrosion rates for Alloys 825, 304L, and CDA 715 following eighty weeks of exposure in concentrated simulated J-13 well water at 90°C. Alloy CDA 102 experienced a general corrosion rate of 0.45 µm/yr in this environment. No SCC of U-bend specimens of any of the four alloys occurred. Alloy 304L and Alloy 825 exhibited no evidence of localized corrosion but some localized corrosion was evident on specimens of Alloy CDA 102 and Alloy CDA 715.

12. KEY WORDS/DESCRIPTORS (List words or phrases that will assist researchers in locating the report.)

Corrosion
Container Materials
General Corrosion
Thermogalvanic Corrosion
Galvanic Corrosion
Pitting Corrosion
Copper-Base Alloys
Fe-Cr-Ni Alloys
Environmental Effects
High Level Nuclear Waste Disposal
Tuff Repository

13. AVAILABILITY STATEMENT

Unlimited

14. SECURITY CLASSIFICATION

(This Page) Unclassified

(This Report) Unclassified

15. NUMBER OF PAGES

16. PRICE

THIS DOCUMENT WAS PRINTED USING RECYCLED PAPER

UNITED STATES
NUCLEAR REGULATORY COMMISSION
WASHINGTON, D.C. 20555

OFFICIAL BUSINESS
PENALTY FOR PRIVATE USE, $300

SPECIAL FOURTH CLASS RATE
POSTAGE & FEES PAID
USNRC
PERMIT No. G-67